Advances in High-Resolution Probes for Scanning Probe Microscopy

Thesis by Marc A. Unger

In partial fulfillment of the requirements for the degree
of Doctor of Philosophy

California Institute of Technology
Pasadena, California
1999
(Submitted March 17, 1999)

For Kim – the best of all possible women.

Acknowledgement

Joining the Baldeschwieler group was a far better choice than I realized at the time. I joined for good reasons: not only was the research going on in the group as a whole interesting, but my project, in particular, was worthy of my best efforts (and then some!). But it turned out to be a good choice for other reasons too, including some that I did not have any conception of at the time. My first acknowledgement, therefore, is to Fortune, for smiling on me. Fortune's smile is like the Mona Lisa's: it isn't simple happiness, but rather a promise of what can be.

I was exceptionally fortunate to have John Baldeschwieler as my advisor. John allowed me a great deal of latitude in pursuing my research, and was very tolerant of my early attempts at self-guidance. The path I followed through my research was far from a straight line, and I certainly took some false turns, but I also found myself in some very interesting territory which I otherwise might never have suspected to exist... and, more importantly, I learned to navigate on my own. Throughout this experience John led me by example, and was always a great source of guidance, of optimism and encouragement, and of genuine scientific curiosity. He was also a tremendous source of knowledge on the interface between science and the rest of the world, and his entrepreneurial spirit proved quite contagious. I count myself very lucky to have earned my doctorate under him.

Steve O'Connor was my mentor for the early years of my time here, and a friend since the beginning. If intelligence is measured by the product of raw IQ and how well it is applied to real problems, Steve is one of the most intelligent people I have ever met. In addition to teaching me about atomic force microscopes and research, he's also taught me a lot about life and how to enjoy it. I thank him for the advice, the honesty, and the friendship.

I thank Steve and all my other labmates (Tom Theriault, Kim Mislick, and Dmitri Kossakovski) for making life as a graduate student better than just work... especially the bouts of Doom (and the occasional brouhaha) that could be heard all the way down the hall.

Thanks to Sean Elliot and Seth Miller, good friends and comrades in arms.

Thanks to the Tai group in Electrical Engineering, especially John Wright and Tom Tsao, for teaching me about MEMS and for patterning photoresist for chemically patterned surfaces (Chapter 3). Dave Preston spent an arduous but rewarding summer with me optimizing our silanization protocol (Chapter 4). Dmitri Kossakovski first interested me in optical fiber etching, and he and Rajat Kongovi helped me learn how to etch IR fibers (Chapter 5). Thanks to the Smalley group at Rice University in Houston, for figuring out

how to mount carbon nanotubes on AFM probes and for teaching me the technique. My nanotube research could not have been carried out without the expertise and patience of Pat Koen, who taught me how to use the transmission electron microscope.

My wife, Kim, deserves more thanks than I can adequately express here for her support, her patience with me when research was going badly, her happiness when research was going well, her love, and the tremendous fun we've had together ever since our first date. I also owe her a great debt for assistance well above and beyond the call of duty in preparing this thesis.

Finally, I would like to thank the National Science Foundation and Lucent for their financial support.

Abstract

This thesis describes work designed to improve the resolution of Scanned Probe Microscopy (SPM). The work falls into three main sections. Sections I and III are both aimed towards making scanned probes with atomic resolution by attaching a single sharp molecule to the end of a tip. Section II is aimed towards making a near-field "optical" probe in the infrared wavelengths.

The first section centers on the Touchdown Scheme, a path towards attachment of a single sharp molecule at the end of a conventional atomic force microscope (AFM) tip. The ability to derivatize the tip with a good monolayer was required. Chapters 2 and 3 describe the development and optimization of surface chemistry for this purpose. Included in this development were methods for making chemically patterned surfaces with simple photolithography techniques. Chapter 1 describes mathematical methods to extract intermolecular pair potentials from AFM force measurements.

The second section describes a technique for etching infrared-transmitting fibers to very sharp points. These sharpened fibers serve as probes in a Near-field Scanning Infrared Microscope (NSIM). Making tips by chemical etching is far easier than heat-pulling, and the etched probes have a power throughput several orders of magnitude higher than pulled probes.

The third section centers on attempts to attach a single molecule to the end of a single carbon nanotube for use as an ultrasharp AFM tip. Bulk derivatization and labeling chemistry of carbon nanotubes was developed and successfully applied to single mounted nanotubes. Along the way, several new methods for handling nanotubes were developed. These include methods for non-oxidative cleaning, making stable suspensions, fluorescence staining, and removal from solution without coalescence.

Table of Contents

Table of Contents

CHAPTER ONE

Introduction

I. Introduction

The ability to sense and manipulate matter reliably and precisely at the atom-by-atom level is the ultimate goal of chemistry. This capability would have a tremendous impact on humanity. It would put mankind in command of machines capable of producing any thermodynamically stable configuration of matter - including more copies of the machines themselves. Our ability to deal with matter would expand in the same manner that computers have expanded our ability to process information. Matter would then be able to process matter atom by atom, in the same way that a computer allows information to process information bit by bit. The computer revolution is limited by the necessity of physically creating the computers. Matter processing matter would have no such limitations.

Our ability to control and manipulate matter, however, is contingent on our ability to analyze the results; in order to *manipulate* with atomic precision, we must be able to *see* with atomic precision. We must develop the ability to see atoms well. This is a high goal, and it will require much work before it can be achieved. However, we are most of the way there. To put our capabilities in perspective, it is useful to consider the different kinds of microscopes and their limitations.

A. Optical Microscopy

Conventional optical microscopes use solid lenses to bend electromagnetic radiation (light) and magnify the subject under investigation. Diffraction limits the maximum achievable resolution to approximately half the wavelength of the light employed – the Abbe diffraction limit[1]. In optical wavelengths, the wavelength is approximately 500 nm, giving a maximum achievable resolution of approximately 250 nm - ¼ micron. This is already quite small – 1/200th the width of a human hair – but falls short of seeing atoms by a factor of approximately 1500x.

B. Electron Microscopy

The resolution of a microscope can be improved by using radiation with a shorter wavelength. With Davisson and Germer's discovery that electrons also have a wavelength, the stage was set for the invention of the electron microscope, which uses accelerated electrons as its imaging medium. The shorter wavelength of the accelerated electrons allows imaging with down to ~ 1.5 A resolution, some 1600 times better than optical microscopy. However, this high resolution comes with a price: imaging must be done under high vacuum conditions, and the contrast of the image depends on the electron density of the material imaged. Essentially, the heavier the atoms, the better they scatter electrons, and the better the image contrast. Light atoms of the kind that comprise biological molecules (i.e., proteins, nucleic acids, carbohydrates, composed of C, H, O, N, and P) scatter poorly. High vacuum conditions are also antithetical to living biological systems, so samples must be removed from their natural state before imaging. Since electrons interact strongly with matter, only very thin (< 300 nm) samples can be imaged at such high resolution.

Finally, highly accelerated electrons can damage the sample.

C. Scanning Probe Microscopy

Scanning Probe Microscopy (SPM) provides a way of getting around the diffraction limit. In essence, SPM images a sample by "touch" – that is, by sensing a very short-range interaction between a probe and the sample.

1. STM

The first probe microscope was the Scanning Tunneling Microscope, invented by Binnig and Rohrer[2] in 1982. The STM senses the tunneling current between a sharp conductive tip – the probe – and a conductive sample as the tip is scanned over the sample.

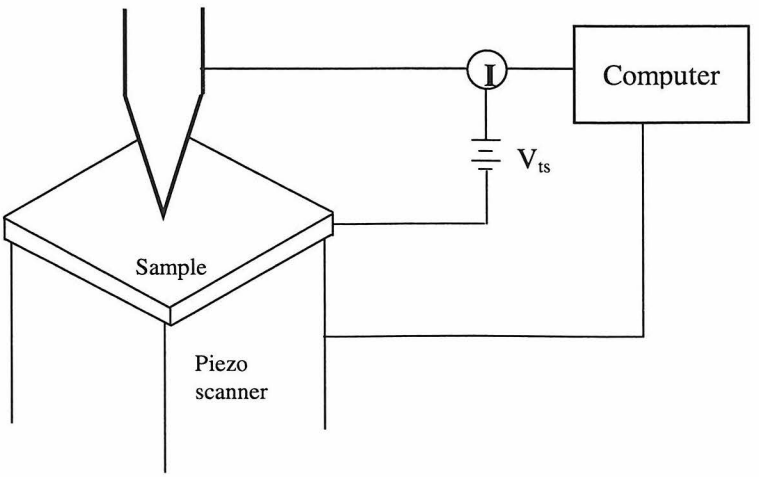

Figure 1: STM schematic

The voltage applied between tip and sample is insufficient to allow the electrons to travel classically through the space between the tip and the sample. To do this they would have to have enough energy to pay the energetic price of leaving their home metal – i.e., the work function. However, they can *tunnel* from tip to sample. This is a quantum mechanical process, which occurs because the wave function of an electron in the tip extends out to the substrate. The wave function of an electron extending into a classically forbidden energy region decays exponentially, so the chance of electron tunneling depends exponentially on the distance between the tip and sample (with a decay length of ~1 A). This exponential dependence of the tunneling current on tip-sample distance is the "short-range interaction" in STM.

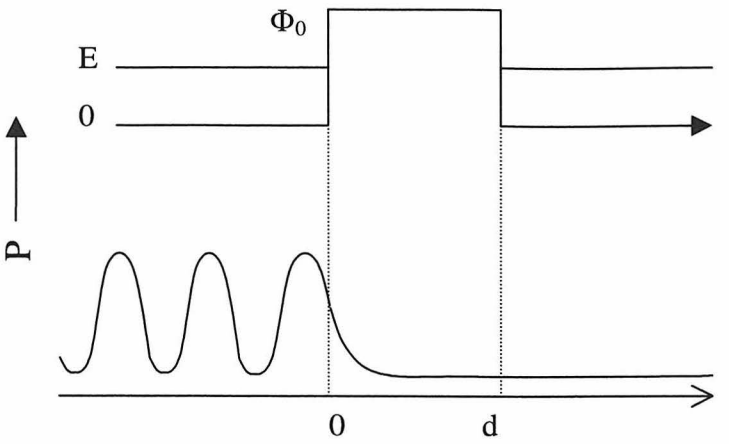

Figure 2: Decay of tip electron wavefunction to sample

Typically, the STM is operated in "constant current" mode: the probe tip is scanned over the surface, and its height is continually adjusted (with a feedback loop) to maintain the current at a constant value. The height values then represent the sample topography. The exquisite fine response of the piezoceramic scanners used gives the STM a vertical resolution of .01 A, and STM is easily capable of imaging atoms on a flat conductive sample. Its resolution on more 3D samples depends on the shape of the probe tip, but may be estimated at several nanometers.

Observation of variations in the current as the probe-sample voltage is varied (I-V curves) also gives the STM the ability to probe the local electronic properties of the substrate.

2. AFM

Atomic Force Microscopy (also known as Scanning Force Microscopy) employs the local repulsive forces between the sample and a probe tip as its short-range interaction. A cantilever with a sharp probe tip at the end is held over the sample surface. The probe is lowered into contact with the surface, and the repulsion between the probe and the

surface perturbs the cantilever from its normal equilibrium position. The deflection of the probe measures the force exerted on the cantilever (by F = -kx).

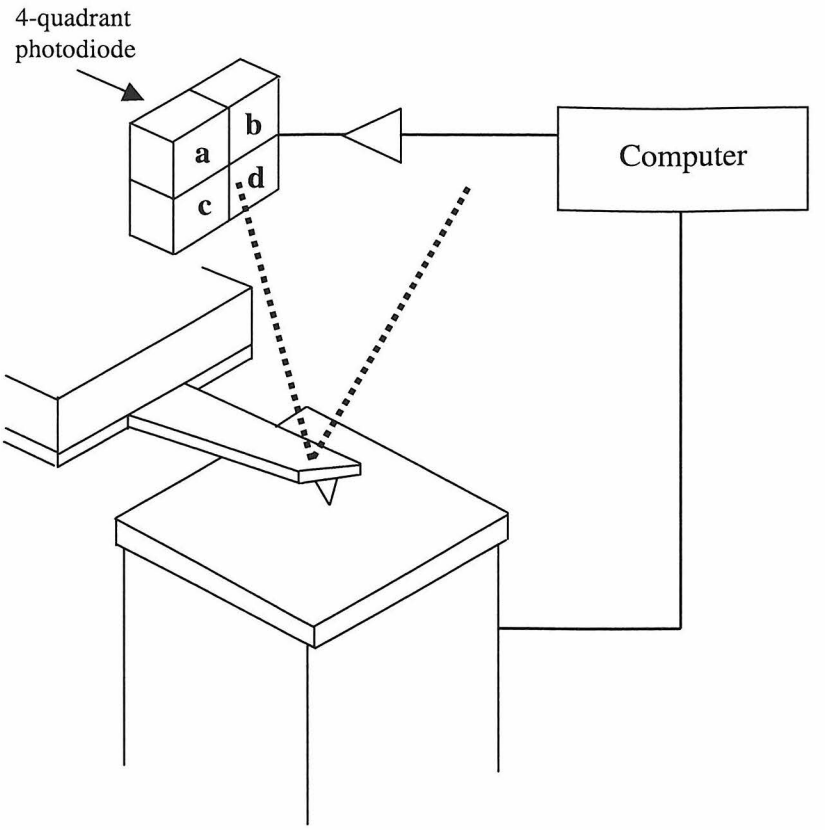

Figure 3: AFM schematic – optical lever configuration

Just as with STM, AFM is typically done in "constant deflection" mode: the probe tip is scanned over the surface, and its height is continually adjusted via a feedback loop to maintain a constant cantilever deflection. The height values then represent the sample topography. The AFM also has exquisite vertical resolution (0.1 A), and is capable of discerning atoms on flat surfaces. Its resolution on more 3D samples, as with STM, depends on the shape of the probe tip, but may be estimated at 5 – 10 nm. AFM has the advantage that it is capable of imaging under a larger variety of conditions than STM (from ultra-high vacuum to biological buffer solutions). Because it is force-based, it is also the basis for other imaging techniques where the interaction to be measured may be transduced into force, including magnetic force[3], electrostatic force[4], magnetic resonance[5], capacitance[6], and ultrasonic modulation[7].

3. NSOM

Near-Field Scanning Optical Microscopy (also known as SNOM or Photon Scanning Tunneling Microscopy) uses evanescent wave coupling as its short-range interaction.

surface perturbs the cantilever from its normal equilibrium position. The deflection of the probe measures the force exerted on the cantilever (by F = -kx).

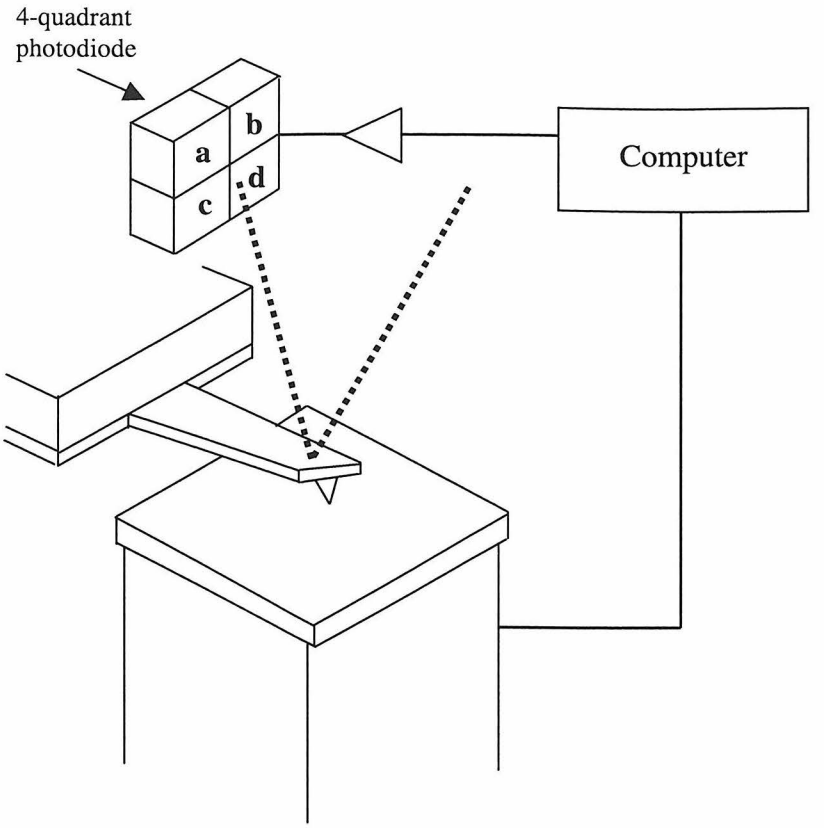

Figure 3: AFM schematic – optical lever configuration

Just as with STM, AFM is typically done in "constant deflection" mode: the probe tip is scanned over the surface, and its height is continually adjusted via a feedback loop to maintain a constant cantilever deflection. The height values then represent the sample topography. The AFM also has exquisite vertical resolution (0.1 A), and is capable of discerning atoms on flat surfaces. Its resolution on more 3D samples, as with STM, depends on the shape of the probe tip, but may be estimated at 5 – 10 nm. AFM has the advantage that it is capable of imaging under a larger variety of conditions than STM (from ultra-high vacuum to biological buffer solutions). Because it is force-based, it is also the basis for other imaging techniques where the interaction to be measured may be transduced into force, including magnetic force[3], electrostatic force[4], magnetic resonance[5], capacitance[6], and ultrasonic modulation[7].

3. NSOM

Near-Field Scanning Optical Microscopy (also known as SNOM or Photon Scanning Tunneling Microscopy) uses evanescent wave coupling as its short-range interaction.

When electromagnetic radiation passes through a hole smaller than its wavelength, it forms a diffraction pattern in the far field – "far" meaning any distance large comparable to the wavelength of light. Near the hole, however, the radiation is collimated to approximately the width of the hole. Thus, it is possible to illuminate an area far smaller than the wavelength of light – beating the diffraction limit – as long as we stay in the "near field" of the aperture.

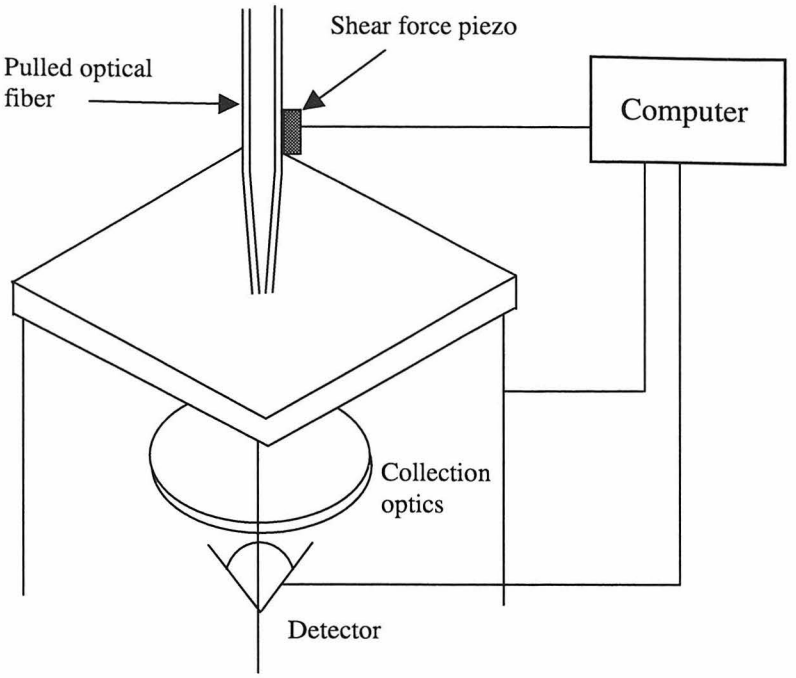

Figure 4: NSOM schematic

NSOM is capable of simultaneous topographical ("shear force") and optical imaging. The optical resolution is very strongly dependent on the construction of the probe; a typical value is ~50 nm, while the theoretical limit for a pulled fiber probe is ~12 nm. NSOM is capable of measuring many different optical properties, including fluorescence, absorption, polarization, refractive index, and even fluorescence lifetime.

II. Limitations

A. Convolution

Since STM, AFM, and NSOM all rely on short-range interactions, they are all limited by convolution of the shape of the probe with the shape of the sample:

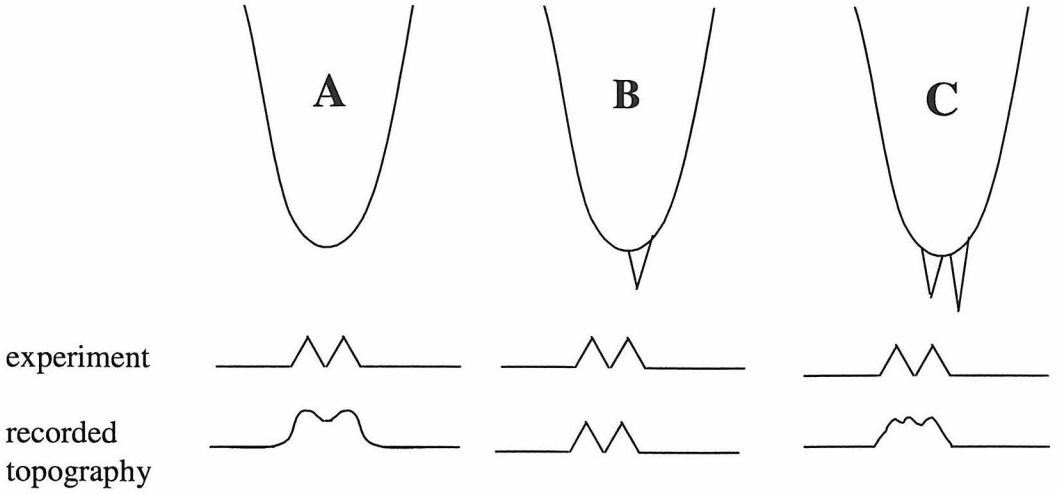

Figure 5: Image convolution from tip-sample interaction

In STM, the tunneling current is the sum of the tunneling current through all paths from tip to sample. Since the tunneling current is exponentially dependent on distance, it is often a good approximation to think of it as passing only through the pair of atoms on tip and sample. As the diagram suggests, if there is sufficient relief in the sample, tunneling can also occur from atoms on the sides of the tip, rather than just the apex. This results in a broadening of small sample features; mathematically, this broadening is referred to as a "dilation" of the shape of the sample with the shape of the tip.
A similar phenomenon occurs with AFM, except that it is short-range Van der Waals repulsion instead of tunneling current that is sensed. Since this force decays as $\sim 1/r^6$ rather than exponentially, the force does not have as sharp of a "cutoff" as STM, and imaging will most often involve multiple atoms on both tip and sample. This degrades the resolution of AFM relative to STM.

In NSOM, topographical resolution is governed by the physical size of the probe, while optical resolution is governed by the size of the aperture through which light is emitted or collected. The probes are physically larger than AFM probes, so their topographical resolution is blurred even more strongly. The optical signal is a literal convolution of the shape of the optical near-field with the optical response of the sample.

III. Probes

A. STM

STM probes are most often made of tungsten or a platinum/iridium alloy wire. Tungsten tips are typically created by either electrochemical etching or mechanical shearing. Electrochemical etching[8] produces tips that are – at least on a gross scale – more reproducible. Mechanical shearing (clipping with a pair of cutters) produces a highly irreproducible tungsten tip that nevertheless may have atomically sharp features. Compared to mechanically sheared tips, electrochemically etched tips are more reproducible but (in general) less sharp at the tip apex. Almost all probes are capable of atomic resolution on a flat surface; getting a probe that gives good resolution on a surface with higher relief is much harder. Despite the fact that STM is the oldest form of probe microscopy, getting a good probe remains a matter of art and luck rather than science.

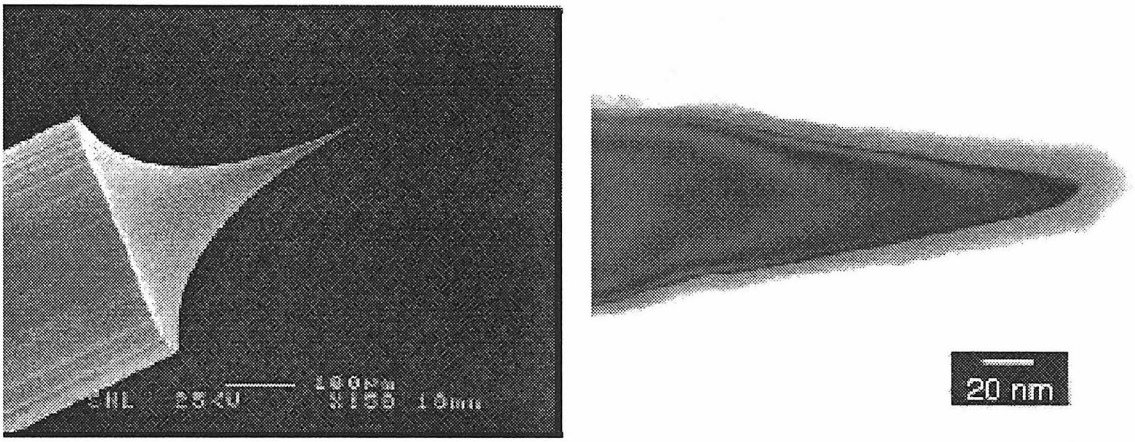

a b

Figure 6: a: SEM and b: TEM images of electrochemically etched W STM tip[9]

B. AFM

AFM probes have benefited far more from technological innovation than STM probes. The first AFM probe was a strip of aluminum foil; AFM probes are now micromachined[10] from silicon and silicon nitride, using techniques adopted from the semiconductor industry. Typical tips are triangular in shape (for mechanical stability), approximately 100 μm in length, and have an integrated pyramidal tip at the end. The pyramidal tip is the part that interacts with the sample, and remains the greatest weakness of the technique. Despite many attempts to improve it, this pyramid remains dull on the atomic scale, with a radius of curvature of ~5 nm or larger.

Figure 7: SEM images of AFM cantilevers. a,b,c: Si_3N_4 contact mode tips. **d,e:** Si tapping mode tips. (**a-d** from Digital Instruments, Inc.[11]; **e** from Nanosensors, Inc.[12])

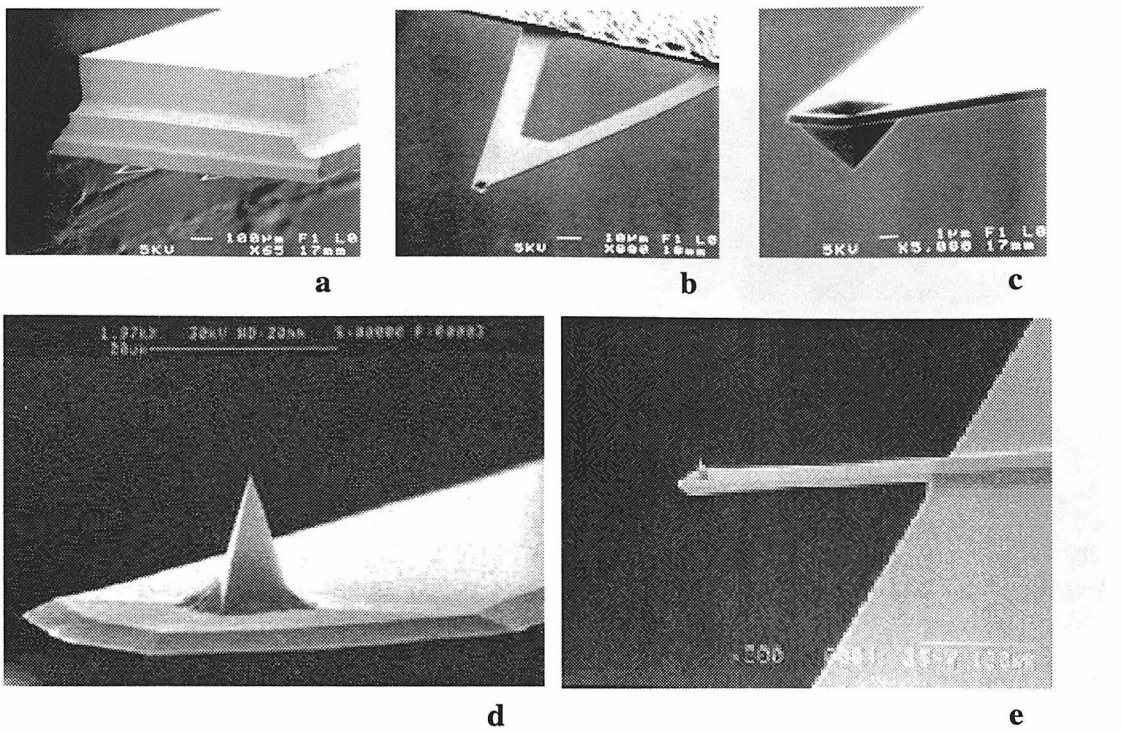

C. NSOM

NSOM probes are most often fabricated by heat-pulling optical fibers[13], although the popularity of chemical etching[14,15] is growing. Heat-pulled fibers are pulled to a very sharp tip (typically with a laser capillary puller), followed by evaporation of a highly reflective metal (i.e., aluminum) on the sides of the probe to minimize losses. The size of the aperture controls the size of the near-field zone; the size of the aperture is controlled by the final diameter to which the fiber is pulled and the way in which the metal is applied. Making NSOM tips is, again, more of an art than a science. The optical resolution is ultimately limited by the fact that even the most reflective metal still allows the passage of photons through a very thin layer; even Al has a non-zero skin depth.

Figure 8: SEM images of heat-pulled Al-coated NSOM tips. a,b: first tip; **c,d:** second tip. Note the grain structure in the Al coating in d. Images provided by Dmitri Kossakovski, Caltech

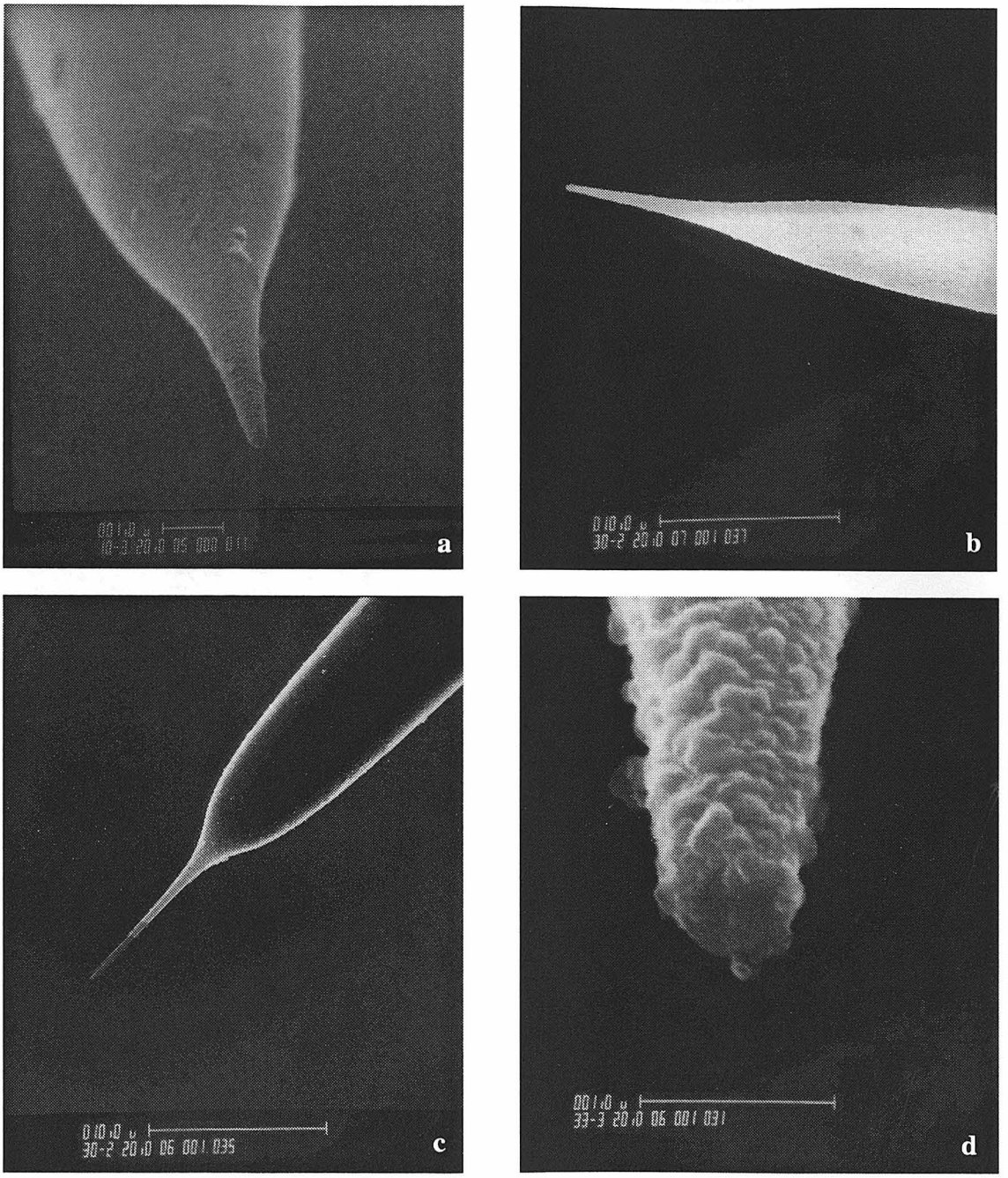

IV. This Work

It is clear that SPM is primarily limited by the difficulty in creating sufficiently sharp probes. The inspiration for this thesis came from a singular, unreproduced result that showed that this limitation is technical, rather than fundamental: the atomic resolution images of DNA on graphite[16].

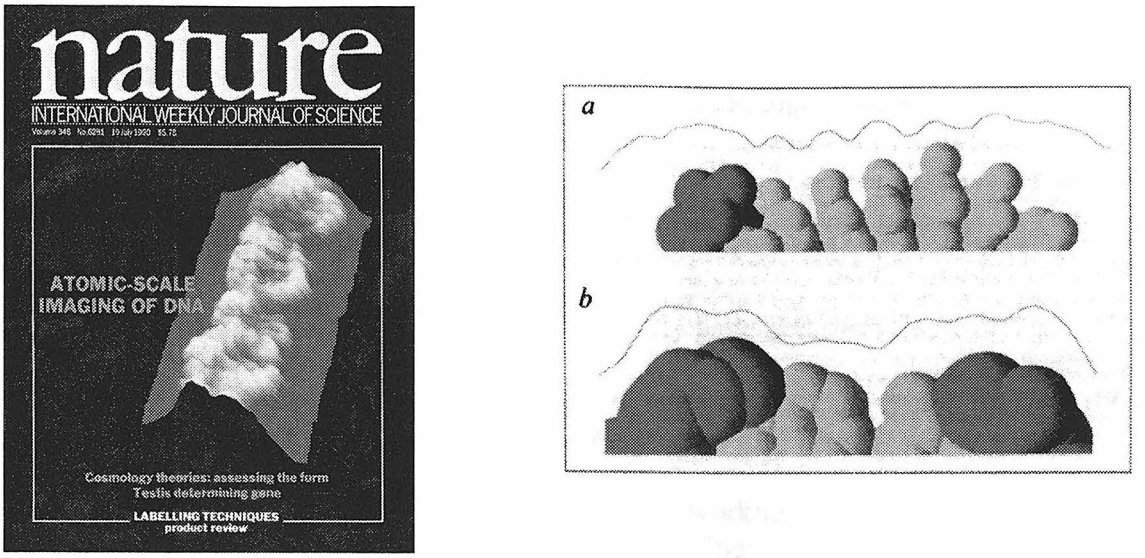

Figure 9. Right, traces of STM topography overlying a computer model of DNA

This set of images demonstrated that atomic resolution of highly three-dimensional structures was possible. My work here was in the service of making probes to reproduce this result – more specifically, to attach a single molecule to an SPM tip and use it to achieve atomic resolution.

Our initial working plan was the Touchdown Scheme, as seen in Figure 10:

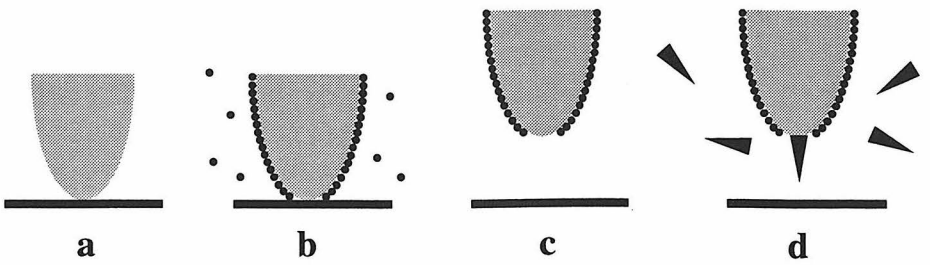

Figure 10: The touchdown scheme. a: touchdown, **b:** passivate, **c:** retract, **d:** functionalize

The essential idea was to protect a small area at the apex of the tip by bringing it into close proximity with a substrate surface, so that the molecules of the passivating agent are sterically impeded from contact with the small area at the apex of the tip. Simply withdrawing the tip from the substrate would deprotect the apex area, allowing the area to be functionalized. Proper control of experimental conditions would allow the size of the functionalized area to be small enough so that only one molecule could be attached. For more detail, see our Patent in the Appendix ("Probes for Sensing and Manipulating Microscopic Environments and Structures").

Development of the idea and chemistry of the Touchdown scheme led to consideration of what would happen when fully-derivatized tips came into contact with a surface. This led to the development of a theory for deriving true tip-sample potentials from AFM force-distance curves and for deriving intermolecular pair potentials from tip-sample potentials and knowledge of the shape of the tip (**Chapter 2**).

Chapters 3 and 4 describe the creation of chemically patterned surfaces (useful analytical tools for surface functionalization chemistry, as well as interesting in their own right) and our work in optimizing the silanization reaction (which we planned to use for functionalizing surfaces in the Touchdown scheme).

As a side project, Dmitri Kossakovski and I had been working on a method to etch infrared transmitting fibers – the IR cousins of optical fibers. **Chapter 5** describes the method we developed to chemically etch the fibers to a highly smooth and reproducible sharp point. This work extends NSOM into the infrared range, allowing chemical information to be accessed with nanometer resolution.

Our work on the Touchdown scheme was interrupted by the arrival of two important facts from outside our lab. The first, from another group at Caltech[17] was the discovery that the pyramids of AFM cantilevers - in spite of their high hardness (silicon or silicon nitride) – were damaged and worn down by contact with the surface. This cast doubt on the chances for survival of a molecule put in place by the Touchdown scheme. The other discovery, by the Smalley group at Rice University[18], was a method to attach a single multi-walled carbon nanotube to an AFM tip. Although the resolution of nanotube tips was only as good as that of a sharp conventional AFM tip, carbon nanotubes proved nearly indestructible, and their resolution did not degrade (while that of conventional tips did). Carbon nanotubes, being essentially sheets of graphite (and unreactive) on the sides while having potentially reactive ends, presented a tempting target for single-molecule functionalization.

Chapter 6 describes the technique used for mounting carbon nanotubes on SPM probes, as learned at Rice University and adapted at Caltech. **Chapter 7** describes experiments on the bulk chemistry of carbon nanotubes, undertaken in preparation for its application to mounted single tubes. **Chapter 8** describes the successful application of this chemistry to mounted single multiwalled carbon nanotubes.

The appendices contain the patent applications filed during my tenure as a graduate student, and also Marc's Rules of Research.

---

[1] Hecht, E. Optics, 3rd Ed. Reading, Mass.: Addison-Wesley, 1998

[2] Binnig, G., Rohrer, H., Gerber, C., Weibel, E. (1982) *Phys. Rev. Lett.* **49**, 57-61

[3] Matin, Y., Wickramasinghe, H.K. (1987). Magnetic Imagine by Force Microscopy with a 1000-A Resolution. *Applied Physics Letters* **50**: (20) 1455-1457

[4] Stern, J.E., Terris, B.D., Mamin, H.J., Rugar, D. (1988). Deposition and Imaging of Localized Charge on Insulator Surfaces Using Force Microscope. *Applied Physics Letters,* **53**: (26) 2717-2719

[5] Zuger, O., Rugar, D. (1994). Magnetic-Resonance Detection and Imaging Using Force Microscope Techniques. *Journal of Applied Physics*, **75**: (10) 6211-6216, Part 2A

[6] Martin, Y., Abraham, D.W., Wickramasinghe, H.K. (1988). High-Resolution Capacitance Measurement and Potentiometry by Force Microscopy. *Applied Physics Letters*, **52**: (13) 1103-1105

[7] Kolosov, O., Yamanaka, K. (1993). Nonlinear Detection of Ultrasonic Vibrations in an Atomic-Force Microscope. *Japanese Journal of Applied Physics: Part 2 – Letters*, **32**: (8A) L1095-L1098

[8] Ekvall, I., Wahlstrom, E., Claesson, D., Olin, A., Olsson, E. (1999). Preparation and Characterization of Electrochemically Etched W Tips for STM. *Measurement Science and Technology*, **10**: (1)

[9] Ibid

[10] Albrecht, T.R., Akamine, S., Carver, T.E., Quate, C.F. (1990). Microfabrication of Cantilever Styli for the Atomic Force Microscope. *Journal of Vacuum Science & Technology: A-Vacuum Surfaces and Films*, **8**: (4) 3386-3396

[11] http://www.di.com/Products/TipGuide.html

[12] http://www.molec.com/nanosensors/index.html. PointProbe etched Si probe; reported typical end-radius of curvature of 10 nm or less.

[13] Betzig, E., Trautman, J., Harris, T., Weiner, J. and Kostelak, R. (1991). Breaking the Diffraction Barrier – Optical Microscopy on a Nanometric Scale. *Science* **251**, 1468

[14] Zeisel, D., Nettesheim, S., Dutoit, B., Zenobi, R. (1996). Pulsed Laser-induced Desorption and Optical Imaging on a Nanometer Scale with Scanning Near-field Microscopy Using Chemically Etched Fiber Tips. *Applied Physics Letters*, **68**: (18) 2491-2492

[15] US Patent US4469554: Etch procedure for optical fibers, Turner, Dennis R., Issued Sept. 4, 1984

[16] Driscoll, R.J., Youngquist, M.G., Baldeschwieler, J.D. (1990). Atomic-scale Imaging of DNA Using Scanning Tunneling Microscopy; *Nature* **346**: (6281) 294-296

[17] DeRose, J.A., Revel, J.P. (1997). Examination of Atomic (scanning) Force Microscopy Probe Tips with the Transmission Electron Microscope. *Microscopy and Analysis,* **3**: (3) 203-213

[18] Dai, H.J., Hafner, J.H., Rinzler, A.G., Colbert, D.T., Smalley, R.E. (1996). Nanotubes as Nanoprobes in Scanning Probe Microscopy. *Nature*; **384**: (6605) 147-150

CHAPTER TWO

Tip-Sample Interactions: Extraction of Single Molecular Pair Potentials from Force Curves

This chapter describes a method for extracting true tip-sample potentials from force curves in atomic force microscopy. These potentials are not the negative integrals of the observed force curve. Rather, the potential is a function of the cantilever deflection and cantilever spring constant. If information about the shape of the tip is known, a decorrelation may be performed to extract molecular pair potentials from the total tip-sample potential. Applications and limitations of this method are discussed.

I. Introduction

Accurate determination of molecular pair potentials is of great interest for molecular design and eventually nanotechnological applications. Atomic Force Microscopy (AFM) is capable of imaging surfaces with high resolution in a non-invasive manner[1,2,3]. To perform an AFM experiment, a flexible cantilever with a small protruding tip is brought into contact with a surface; as the tip is scanned, the interaction forces between the electron clouds of the atoms of the tip and the sample perturb the cantilever from its equilibrium position.

In addition to its imaging capability, AFM is also capable of measuring the force between the tip and sample as a function of tip-sample separation[4]. This "force curve" is completely analogous to Israchevilli's surface force experiments with a smaller contact area[5].

Several models have been proposed to explain observed AFM force curves[6,7,8]. These models show poor agreement with experimental data. One error that is inherent in these models is that they assume that the force curve is related to the interaction potential by:

$$[1] \qquad F_{meas}(r) = -\frac{d}{dr}V(r),$$

where r is tip-sample separation and V(r) is the potential. However, a force curve does not record the force as a function of tip-sample distance. Rather, it monitors the force versus the separation of the cantilever base and the sample. Equation [1] is only correct when the cantilever base and the tip do not move with respect to each other, which is true only in the limit of an infinite cantilever spring constant.

The chemical nature of the tip and sample must also be considered when interpreting force curves. The potential between tip and sample will be primarily due to the interactions of the surface atoms[9]. Controlled experiments confirm that the surface chemistry dominates the shape of the force curves[9,10,11].

In this chapter, a thorough analysis of the AFM sample-tip-cantilever system will be presented. An accurate expression for the relationship between the force curve and the actual tip-sample potential will be derived. These results will be compared to the standard method of force curve interpretation by numerical simulation.

A chemical model of AFM tip-sample interaction will also be developed. This model analyzes the relation between the tip shape, intermolecular potential, and the total potential between tip and sample. Single intermolecular pair-potentials will be extracted from the total tip-sample potential, and the applications and limitations of applying this method to real experimental data are discussed.

II. Extraction of Accurate Tip-Sample Potentials From Force Curves

A. Theoretical Model (Analytical)

The sample-tip-cantilever system will be modeled by replacing the cantilever with a spring of spring constant k. In Figure 1, the cantilever deflection is (z - D - c_{eq}), where c_{eq} is the equilibrium length of the spring.

To perform a force curve, the cantilever deflection is monitored as the base is withdrawn from the sample; z is being controlled, not D. Since a force curve does not accurately describe the force vs. distance behavior of the tip vs. the sample, we will use the terminology "deflection vs. distance (DVD) curve."

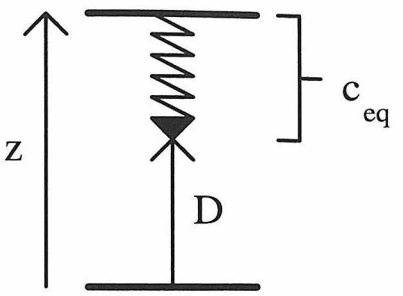

Figure 1: The tip-sample-cantilever system

The relationship between D and z will be used to relate the DVD curve (which is denoted $\beta(z)$) to the tip-sample potential. To find the relationship between D and z, an equation for force balance is used:

[2] $$k(z - D - c_{eq}) + -\tfrac{d}{dD}V_{ts}(D) = 0.$$

The first term is the force from the cantilever spring; the second term is the force due to the tip-sample potential. When the cantilever is in contact (a compressed state), the cantilever force is negative. The compressed position is in a repulsive regime of the tip-sample potential, so the negative derivative will be positive. The total force will be zero at equilibrium.

As the cantilever base is moved, the change in the tip sample distance (dD/dz) is:

[3] $$\frac{dD}{dz} = \frac{k}{k + \frac{d^2}{dD^2}V_{ts}(D)} \quad .$$

For the limiting case where $k >> d^2V_{ts}/dD^2$, the cantilever is not bent by the tip-sample potential, and D changes exactly the same amount as z. For $k << d^2V_{ts}/dD^2$, the tip-sample potential is very stiff and the tip remains fixed relative to the sample regardless of how the cantilever base is moved.

Experimentally, the change in cantilever deflection with respect to z is measured when a force curve is performed:

[4] $$\beta'(z) = \frac{d\beta(z)}{dz} = \frac{d}{dz}(z - D - c_{eq}) = 1 - \frac{dD}{dz} = \frac{\frac{d^2}{dD^2}V_{ts}(D)}{k + \frac{d^2}{dD^2}V_{ts}(D)},$$

which becomes:

[5] $$V_{ts}(D) = \iint \frac{k(\beta'(z))}{(1-\beta'(z))} dDdD .$$

Since the function is integrated with respect to D, not z, Equation [5] must first be written as a function of D:

[6] $$\beta'(z) = \beta'(D(z)),$$

and from Equation [4]:

[7] $$D(z) = \int 1 - \beta'(z) dz .$$

1. Numerical Simulation

Computer code has been developed to convert the DVD curve to the tip-sample potential (Equation 5). Figure 2 presents a hypothetical "hard-wall" potential. The DVD curve that would actually be measured due to this potential was calculated; from this DVD curve, the potential was "reconstructed" by the negative integral method and our method (Equation 5). The zero point on the numerical integration was determined by assuming that the force on the cantilever is zero at maximal distance from the sample. Figure 3 is the same simulation for a Morse potential.

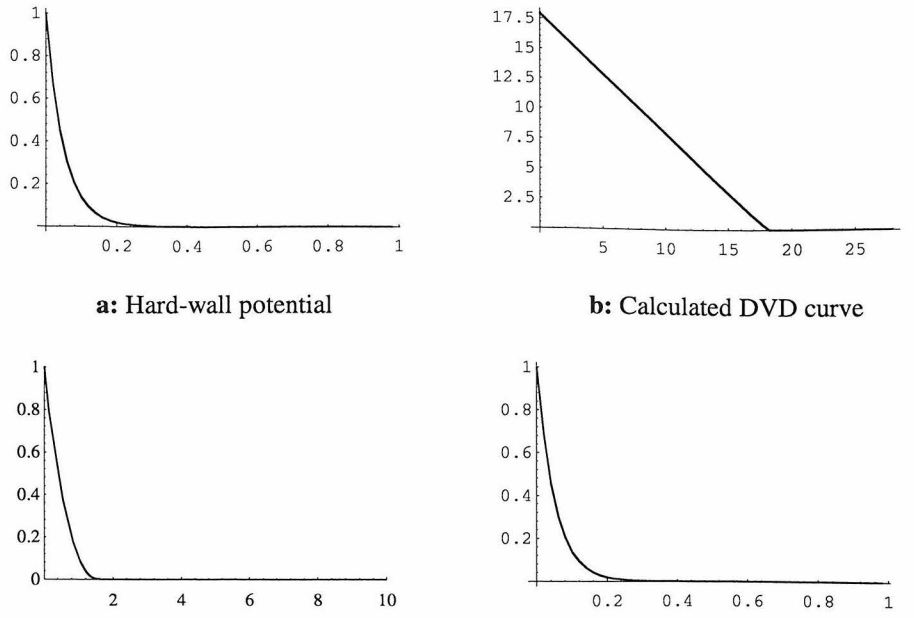

a: Hard-wall potential

b: Calculated DVD curve

c: Potential from negative integral method

d: Potential from Equation [5] method

Figure 2: Hard Wall Potential Simulation. The cantilever spring constant = 1 N/m. All the DVD curves have been multiplied by -1 to show deflection away from the surface as positive. The potential derived with the negative integral method has been truncated at 1 nJ for comparison. Notice the difference in length scale.

AFM systems experience noise from several sources, including thermal cantilever oscillations, electronics noise, and ambient acoustic coupling. The AFM system in our laboratory has a total noise level corresponding to approximately 0.1 nm with a 10μm scan piezo.

Simulations show that the DVD-to-potential transformation is highly sensitive to noise. The effects of the addition of random noise are shown in Figures 4 and 5. This sensitivity is most likely a manifestation of the non-linearity of the algorithm used to perform the conversion.

Application of a smoothing algorithm to the DVD curve corrects this problem. The smoothing algorithm employed was a simple, three-point moving window: the new value at each point is the average of the point and its two nearest neighbors. For 0.1 nm of noise and a cantilever with a 0.1 N/m spring constant, 5 passes of this smoothing algorithm are usually sufficient. For 0.25 nm of noise, 10 passes are sufficient. The smoothing is considered complete when the conversion results are reproducible.

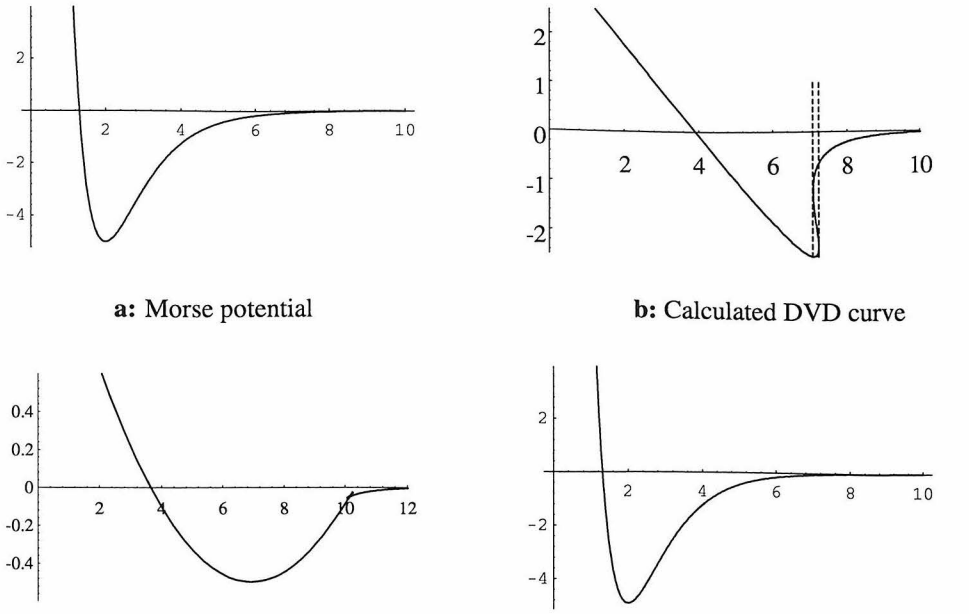

a: Morse potential

b: Calculated DVD curve

c: Potential from negative integral method

d: Potential from Equation [5] Method

Figure 3: Morse Potential Simulation. The cantilever spring constant = 0.1 N/m. The distance origin is arbitrary. Note the "loopback" in the DVD curve. The dotted lines denote the "points of instability" which manifest themselves in the "jump to contact" and "snap-off" commonly seen in force curves.

Two other factors may contribute to the inaccuracy of force curves: scanner calibration and spring constant uncertainty. An AFM tube piezoceramic is used to alter the cantilever base-sample distance (z) in a quantitative manner. For most commercially available systems, these scanners are calibrated by the manufacturer. However, hysteresis and repolling may cause these calibrations to be inaccurate. It is preferential to monitor the sample position simultaneously with an alternative mechanism (such as interferometry or capacitance) while the force curve is being performed.

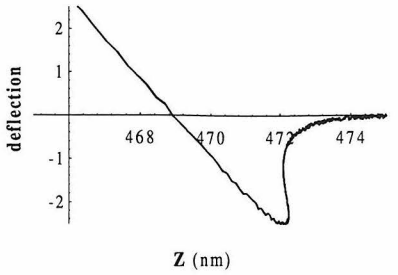

a: DVD curve with 0.1 nm of noise

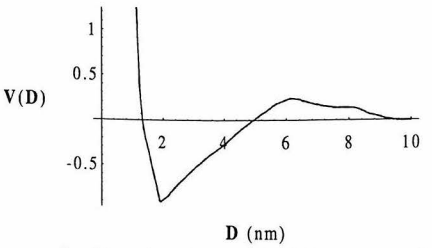

b: Resultant potential (no smoothing)

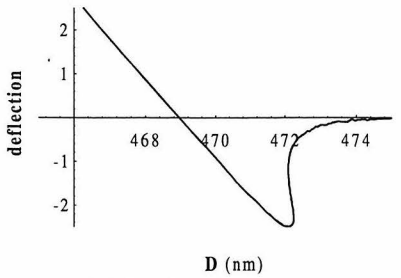

c: DVD after 5 smoothing passes

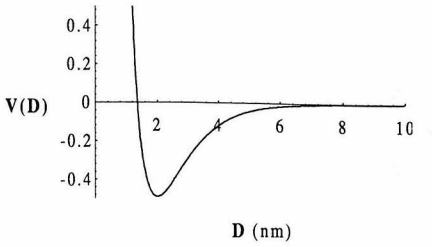

d: Resultant potential (5 passes)

Figure 4: Simulation with 0.1 nm of noise

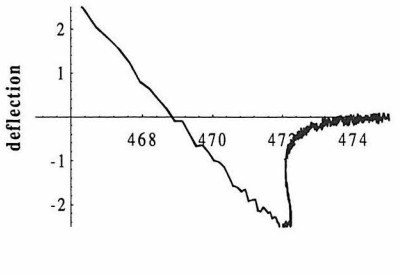

a: DVD curve with 0.25 nm of noise

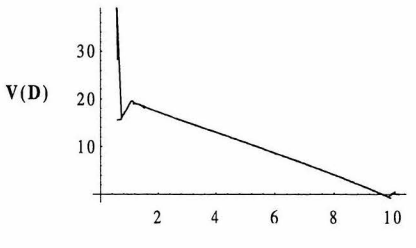

b: Resultant potential (no smoothing)

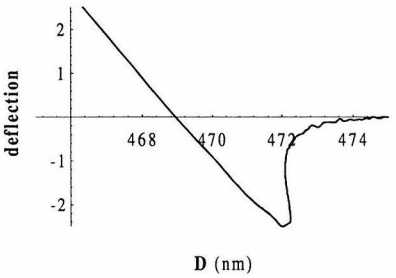

c: DVD after 10 smoothing passes

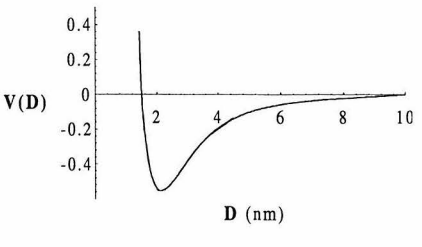

d: Resultant potential (10 passes)

Figure 5: Simulation with 0.25 nm of noise

Equation 5 is also dependent upon the cantilever spring constant. Manufacturer specifications can be very inaccurate[12]. A number of highly accurate methods have been developed to determine the cantilever spring constant experimentally[12,13,14].

III. Extraction of Intermolecular Pair Potentials From Tip-Sample Potentials

A. Theoretical Model (Analytical)

In this section, the relationship between intermolecular pair potentials, tip geometry, and total tip-sample potential will be analyzed. It will be shown that tip-sample potential can be modeled as the potential between rigidly bound head groups on the tip and sample, *i.e.*, $V_{ts}(D) = V_{mol}(D)$. Finally, the tip-sample interaction will be represented by the summation of all the pairwise interactions of chemical "head groups."

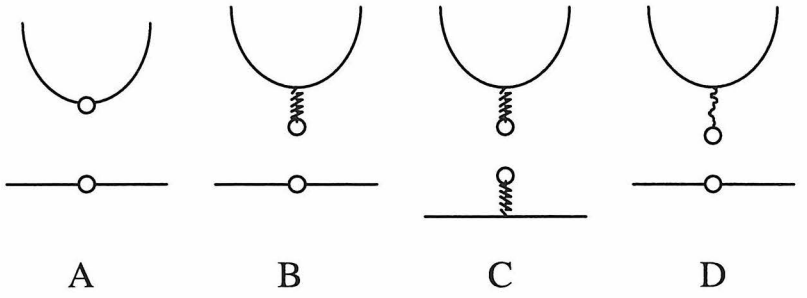

Figure 6: a: rigid-rigid model, **b:** rigid-bond, **c:** bond-bond, **d:** molecular tether

1. Single Interacting Pair

a. Rigid - Rigid

In the case of two interacting headgroups rigidly bound to the tip and sample, the headgroup-headgroup distance D is completely controlled by the relative position of the tip with respect to the sample. In this case, the tip-sample distance and the headgroup-headgroup distance are equal (D). The potential between tip and sample ($V_{ts}(D)$) is equal to the intermolecular pair potential ($V_{mol}(D)$) between the two head groups: $V_{ts}(D) = V_{mol}(D)$.

b. Rigid - Bond

If one of the head groups is at the end of a covalent bond, the situation is more complex. The potential in the rigid-rigid case was strictly one-dimensional: $V_{ts} = V_{mol}(D)$. With a covalent bond added, the potential is now a two variable function: $V_{ts}=V_{mol}(D,x)$.

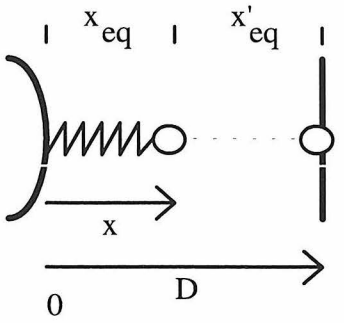

Figure 7: Rigid - bond model. The spring represents a covalent bond; the dotted line represents the headgroup-headgroup interaction. x_{eq} and x'_{eq} are the equilibrium bond lengths of the covalent and non-covalent (measured) interactions, respectively.

A few simple approximations are used:

1. The total potential is the sum of the potentials of the covalent bond and the interaction potential: $V_{ts} = V_{cov}(x) + V_{mol}(D-x)$.
2. The covalent bond doesn't break in the process of pulling the tip away from the sample.
3. The covalent bond may be assumed to be fixed at its equilibrium length.

The first approximation will fail only if V_{cov} and V_{mol} have a significant amount of "crosstalk" (*i.e.*, if the true potential differs from $V_{cov} + V_{mol}$ by a large amount). Figure 8a is a contour plot of the total potential for a covalent bond (C-C) and a hydrogen bond, both approximated by morse potentials.

The second approximation can be tested by applying the Boltzmann distribution to the 2D potential. As the tip is retracted from the sample, the tip head-group will enter the "deep" trough (*i.e.*, break the V_{mol} bond) or the "shallow" trough (*i.e.*, break the covalent bond). Since D changes slowly compared to molecular vibrations ($< 10^7$ nm/sec for a force curve, versus ~ 10^{12} nm/sec for a molecular vibration), the head group is effectively in thermal equilibrium with its surroundings. Therefore, it is reasonable to consider the two troughs as "states" that will be populated in accordance with the Boltzmann distribution. The ratio of probabilities of occupation of these two states (and therefore the ratio of probabilities of breakage of each bond) is:

[8] $$\frac{P_{shallow}}{P_{deep}} = \frac{P_{break,\mathrm{cov}}}{P_{break,mol}} = \frac{e^{-D_{e;\mathrm{cov}}/k_bT}}{e^{-D_{e;mol}/k_bT}} = e^{(D_{e;mol}-D_{e;\mathrm{cov}})/k_bT},$$

where $D_{e;cov}$ and $D_{e;mol}$ are the dissociation energies of the covalent interaction and the headgroup-headgroup interaction, respectively. For a very weak covalent bond (*e.g.*, an oxygen-oxygen peroxide bond, $D_{e;cov} = 2.7 \times 10^{-19}$ J) and a very strong hydrogen bond, ($D_{e;mol} = 5 \times 10^{-20}$ J) the probability of breaking the covalent bond is 6×10^{-24}. For more reasonable bonds strengths (*e.g.*, a C-C bond, $D_{e;cov} = 5.6 \times 10^{-19}$ J), this probability would be even lower.

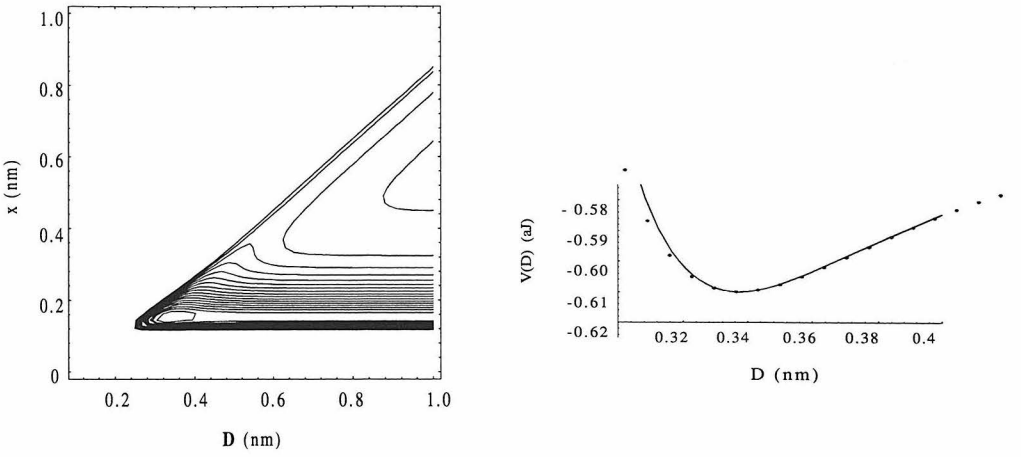

a **b**

Figure 8: Two-dimensional rigid–bond potential

The final assumption is to fix the covalent bond at its equilibrium length. Effectively, this means that $V_{ts}(D)$ is a linecut of $V_{mol}(D,x)$ along $x = x_{eq}$. From the first assumption:

[9] $$V_{ts}(D) = V_{\mathrm{cov}}(x_{eq}) + V_{mol}(D - x_{eq}) = b + V_{mol}(D - x_{eq}).$$

$V_{ts}(D)$ is $V_{mol}(D)$ with an offset in D (x_{eq}) and a constant added to the potential. Since the force is measured (-dV/dD), the added constant has no effect and:

[10] $$V_{ts}(D) = V_{mol}(D - x_{eq}).$$

This approximation will only fail if the path of the head group in the potential deviates significantly from a straight line. For example, this deviation may occur in situations where the gradient of V_{mol} approaches the order of the gradient of V_{cov}. Since most intermolecular forces are weaker and vary more slowly than covalent bond forces, this approximation should be accurate. Figure 8b shows a linecut along $x = x_{eq}$ (solid line) and the actual minimum potential vs D (dotted line). Since the covalent bond vibrates

rapidly with respect to the change in D, the true path is effectively averaged over the bottom of the deeper trench.

c. Bond-Bond

In the case where each head group is at the end of a covalent bond, the potential is three-dimensional. This potential can be reduced to a one-dimensional problem by the same method as before.

2. Multiple Groups

In order to derive single molecular potentials from the total tip-sample potential, analytical correlations with a number of tip shapes and a wide variety of intermolecular potentials have been performed. (See Table 1.) Further, computer algorithms have been developed to perform numerical correlations and decorrelations.

a. Sum → Correlation

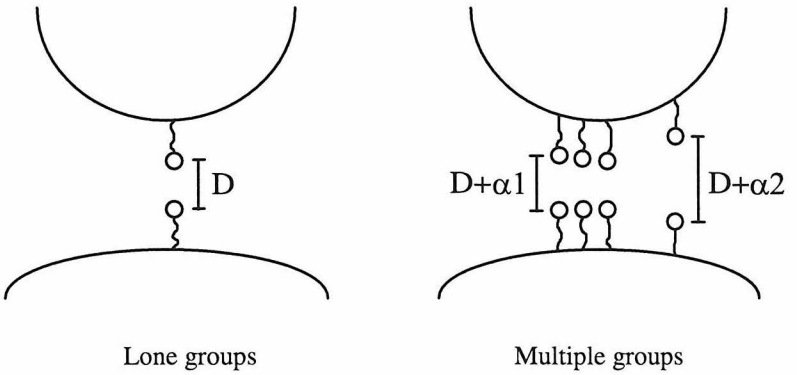

Figure 9: Multiple group model

The total tip-sample potential can be written as a sum of the single potentials at variable distances (α) (see Figure 9):

$$[11] \qquad V_{ts}(D) = V_{mol}(D+\alpha_1) + V_{mol}(D+\alpha_2) + V_{mol}(D+\alpha_3) + \ldots;$$

and for n groups:

$$[12] \qquad V_{ts}(D) = \sum_{i=1}^{n} V_{mol}(D+\alpha_i).$$

This model assumes no cooperative interaction between the chemical groups. As the limit of a continuum of α_i's is approached:

[13] $$V_{ts}(D) = \int_{-\infty}^{\infty} V_{mol}(D+\alpha)\rho(\alpha)d\alpha,$$

where ρ is the distribution of distances. This integral is a cross-correlation of $V_{mol}(D)$ and $\rho(D)$, a close mathematical relative of the convolution:

[14] $$f(x) * g(x) = \int_{-\infty}^{\infty} f(x-\alpha)g(\alpha)d\alpha \qquad \text{Convolution}$$

[15] $$f(x) \otimes g(x) = \int_{-\infty}^{\infty} f(x+\alpha)g(\alpha)d\alpha \qquad \text{Cross - correlation}$$

[16] $$V_{mol}(D) \otimes \rho(D) = \int_{-\infty}^{\infty} V_{mol}(D+\alpha)\rho(\alpha)d\alpha \qquad \text{Tip - Sample cross - correlation}$$

therefore:

[17] $$V_{ts}(D) = V_{mol}(D) \otimes \rho(D).$$

This mathematical model is very useful since:

- the correlation may be found by a Fourier transform method if the integral cannot be performed analytically,
- the Fourier transform method can be used to perform a decorrelation, allowing us to find V_{mol} if we know ρ and V_{ts}, and
- numerical methods for performing correlations and decorrelations are readily available.

The Fourier transform method of performing convolutions can be derived by application of the definition of the Fourier transform to the convolution integral. The corresponding method for performing correlations can be derived analogously:

V_{ts} / $\rho(D)$	planar $\delta(\alpha)$	tilted square $\begin{cases}1, & 0 \le \alpha \le l\sin\theta \\ 0, & \text{elsewhere}\end{cases}$	sphere πd	cone $\alpha\pi\sin\theta$	gaussian $\frac{e^{-\alpha^2/2\lambda^2}}{\lambda\sqrt{2\pi}}$
lennard jones $4D_e\left(\left(\frac{\sigma}{r}\right)^{12}-\left(\frac{\sigma}{r}\right)^{6}\right)$	$4D_e\left(\left(\frac{\sigma}{r}\right)^{12}-\left(\frac{\sigma}{r}\right)^{6}\right)$	$4D_e\left(\frac{\sigma^{12}}{11r^{11}}-\frac{\sigma^{12}}{11(r+l\sin\theta)^{11}}-\frac{\sigma^6}{5r^5}+\frac{\sigma^6}{5(r+l\sin\theta)^5}\right)$	$\pi d 4D_e\frac{\sigma^6\left(-11r^6+5\sigma^6\right)}{55r^{11}}$	$\pi\sin\theta 4D_e\sigma^6\frac{\left(2\sigma^6-11r^6\right)}{55r^{10}}$	$D_e\left(\frac{-\pi\sigma^{12}\lambda^{10}L_{\frac{1}{2}}^{\frac{1}{2}}\left(\frac{r^2\lambda^2}{2}\right)+480\pi\sigma^6\lambda^4L_{\frac{1}{2}}^{\frac{1}{2}}\left(\frac{r^2\lambda^2}{2}\right)}{1920e^{r^2\lambda^2/2}}\right)$
morse $D_e\left(\left(1-e^{-\beta(r-r_0)}\right)^2-1\right)$	$D_e\left(\left(1-e^{-\beta(r-r_0)}\right)^2-1\right)$	$\frac{D_e}{2\beta}\left[\begin{matrix}-\left(e^{\beta(r_0-(r+l\sin\theta))}-2\right)^2+4\\+\left(e^{\beta(r_0-r)}-2\right)^2-4\end{matrix}\right]$	$\pi d\frac{D_e}{2\beta}e^{\beta(r_0-r)}\left(e^{\beta(r_0-r)}-4\right)$	$\pi\sin\theta D_e\left[\frac{e^{-2\beta(r-r_0)}}{(2\beta)^2}-\frac{2e^{-\beta(r-r_0)}}{\beta^2}\right]$	$D_e\left[e^{2\beta\left(r_0-r+\beta\lambda^2\right)}-2e^{\beta\left(r_0-r+\beta\lambda^2/2\right)}\right]$
power law $\left(\frac{\sigma}{r}\right)^n$	$\left(\frac{\sigma}{r}\right)^n$	$\frac{\sigma^n}{(n-1)r^{n-1}}-\frac{\sigma^n}{(n-1)(r+l\sin\theta)^{n-1}}$	$\pi d\left(\frac{\sigma^n}{n-1}\right)\frac{1}{r^{n-1}}$	$\pi\sin\theta\sigma^n\frac{1}{n^2-3n+2}\frac{1}{r^{n-2}}$	$\frac{\left(\frac{1}{2}\right)^{\frac{n}{2}}\lambda^{-n}}{2^{n+1}(-1)^n\left(\frac{1}{4}\right)^{\frac{n}{2}}\sqrt{\pi}\lambda e^{r^2\lambda^2/2}}\left[\begin{matrix}\left(4+(-1)^n\right)\left(\frac{1-n}{2}\right)_1F_1\left(\frac{1-n}{2},\frac{1}{2},\frac{r^2\lambda^2}{2}\right)\\+\left(-1+(-1)^n\right)\lambda\sqrt{2\pi}\left(1-\frac{n}{2}\right)_1F_1\left(1-\frac{n}{2},\frac{3}{2},\frac{r^2\lambda^2}{2}\right)\end{matrix}\right]$
exponential ce^{-r/σ_0}	ce^{-r/σ_0}	$-c\sigma_0\left(e^{-(r+l\sin\theta)/\sigma_0}-e^{-r/\sigma_0}\right)$	$\pi dc\sigma_0e^{-r/\sigma_0}$	$\pi\sin\theta c\sigma_0^2e^{-r/\sigma_0}$	$\frac{c}{2\lambda^2}e^{\lambda^2\sigma_0^2/2-r/\sigma_0}$
coulomb $\frac{q_1q_2}{4\pi\varepsilon}\frac{1}{r}$	$C_c\frac{1}{r}$	$C_c\left(\ln(r+l\sin\theta)-\ln(r)\right)$	does not converge	does not converge	$C_c\frac{\sqrt{\pi/2}Erfi\left(r\lambda/\sqrt{2}\right)}{\lambda e^{r^2\lambda^2/2}}$
charge-dipole $-\frac{q\mu\cos\theta}{4\pi\varepsilon}\frac{1}{r^2}$	$-C_{cd}\frac{1}{r^2}$	$-C_{cd}\left(\frac{1}{r}-\frac{1}{r+l\sin\theta}\right)$	$-d\pi C_{cd}\frac{1}{r}$	does not converge	$C_{cd}\frac{\pi\lambda L_{\frac{1}{2}}^{-\frac{1}{2}}\left(\frac{r^2\lambda^2}{2}\right)}{2\lambda e^{r^2\lambda^2/2}}$
dipole-dipole $-\frac{\mu_1\mu_2\left(\begin{matrix}2\cos\theta_1\cos\theta_2\\-\sin\theta_1\sin\theta_2\cos\phi\end{matrix}\right)}{4\pi\varepsilon}\frac{1}{r^3}$	$-C_{dd}\frac{1}{r^3}$	$-\frac{C_{dd}}{2}\left(\frac{1}{r^2}-\frac{1}{(r+l\sin\theta)^2}\right)$	$-d\pi C_{dd}\frac{1}{r^2}$	$-\pi^2\sin\theta C_{dd}\frac{1}{2r}$	$\pi C_{dd}\frac{\pi\lambda^2rL_{\frac{1}{2}}^{\frac{1}{2}}\left(\frac{r^2\lambda^2}{2}\right)}{4e^{r^2\lambda^2/2}}$
charge-nonpolar $-\frac{q^2\alpha}{2(4\pi\varepsilon)^2}\frac{1}{r^4}$	$-C_{cn}\frac{1}{r^4}$	$-\frac{C_{cn}}{3}\left(\frac{1}{r^3}-\frac{1}{(r+l\sin\theta)^3}\right)$	$-\pi dC_{cn}\frac{1}{r^3}$	$-\pi\sin\theta C_{cn}\frac{1}{6r^2}$	$C_{cn}\frac{\pi\lambda^2L_{\frac{3}{2}}^{\frac{1}{2}}\left(\frac{r^2\lambda^2}{2}\right)}{4e^{r^2\lambda^2/2}}$
dipole-nonpolar $-\frac{\mu^2\left(1+3(\cos\theta)^2\right)}{2(4\pi\varepsilon)^2}\frac{1}{r^6}$	$-C_{dn}\frac{1}{r^6}$	$-\frac{C_{dn}}{5}\left(\frac{1}{r^5}-\frac{1}{(r+l\sin\theta)^5}\right)$	$-\pi dC_{dn}\frac{1}{r^5}$	$-\pi\sin\theta C_{dn}\frac{1}{20r^4}$	$C_{dn}\frac{\pi\lambda^4L_{\frac{5}{2}}^{-\frac{1}{2}}\left(\frac{r^2\lambda^2}{2}\right)}{16e^{r^2\lambda^2/2}}$
nonpolar-nonpolar $-\frac{3h\nu\alpha^3}{4(4\pi\varepsilon)^2}\frac{1}{r^6}$	$-C_{nn}\frac{1}{r^6}$	$-\frac{C_{nn}}{5}\left(\frac{1}{r^5}-\frac{1}{(r+l\sin\theta)^5}\right)$	$-\pi dC_{nn}\frac{1}{r^5}$	$-\pi\sin\theta C_{nn}\frac{1}{20r^4}$	$C_{nn}\frac{\pi\lambda^4L_{\frac{1}{2}}^{-\frac{1}{2}}\left(\frac{r^2\lambda^2}{2}\right)}{16e^{r^2\lambda^2/2}}$

Table 1: Analytical correlations

[18] $f(x) * g(x) = F^{-1}[F[f(x)] \cdot F[g(x)]]$ Convolution

[19] $f(x) \otimes g(x) = F^{-1}[F[f(x)] \cdot F[g(-x)]]$ Correlation

[20] $V_{mol}(D) \otimes \rho(D) = F^{-1}[F[V_{mol}(D)] \cdot F[\rho(-D)]]$ Tip - Sample Correlation

F and F^{-1} represent the Fourier transform and inverse Fourier transform, respectively.

b. Numerical Decorrelation

1. Used to Find Intermolecular Pair Potential:

Straightforward manipulation of the correlation Equations [17] and [20] gives:

[21] $$V_{mol}(D) = F^{-1}\left[\frac{F[V_{ts}(D)]}{F[\rho(-D)]}\right].$$

If $V_{ts}(D)$ and $\rho(D)$ are known, it is in principle possible to extract the intermolecular pair potential of the head groups ($V_{mol}(D)$).

There are several intrinsic limitations to the decorrelation method. Since $V_{ts}(D)$ is averaged over x and y, the extracted $V_{mol}(D)$ is also averaged in x and y. A smooth $\rho(D)$ is a good approximation for a reasonably large number of head groups (n > 200 or more).

The correlation method makes the assumption that all interactions are pairwise and molecules only interact with other molecules that are directly opposite them. No account is made for cooperatively between neighboring head groups. If necessary, an appropriately weighted $\rho(D)$ could be chosen to include these cooperative interactions before decorrelating.

2. Used to Find ρ:

The correlation Equations [17] and [20] can also be rearranged to give:

[22] $$\rho(-D) = F^{-1}\left[\frac{F[V_{ts}(D)]}{F[V_{mol}(D)]}\right].$$

Therefore, if $V_{ts}(D)$ and $V_{mol}(D)$ are known, it is in principle possible to extract $\rho(D)$, the head-group distribution function. However, this method has limitations similar to those discussed above. Also, $\rho(D)$ does not uniquely determine the actual geometry (see Figure 10). However, the distribution itself is a valuable piece of information because it

allows the radius of curvature at the apex of the probe to be estimated. A distribution which has a large value close to D = 0 must have a large radius of curvature; a distribution which is near zero at D = 0 has a small radius of curvature.

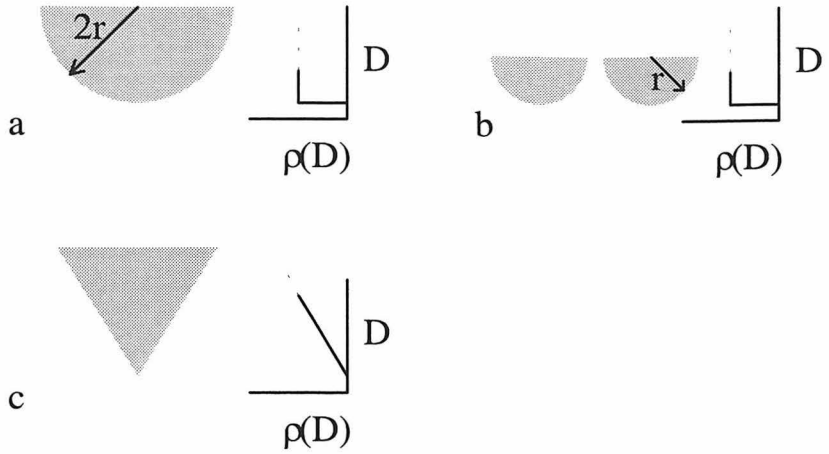

Figure 10: The sphere in **a** and the two spheres in **c** have an identical ρ(D), despite having radically different geometries. Comparison of **a** and **c** shows how ρ(D) differs for dull and sharp tip apex shapes.

IV. Applications

Both of the decorrelation methods above assume that $V_{ts}(D)$ has been extracted from the DVD curve. In practice, instrumental limitations restrict the measurement to a finite segment of the DVD curve and thus a finite segment or "envelope" of the potential. Effectively, $V_{ts}(D)$ is being multiplied by a window function (w(D)); w(D) = 1 where $V_{ts}(D)$ is known; w(D) = 0 elsewhere. Therefore, in the Fourier domain, $F[V_{ts}(D)]$ must be replaced with $F[V_{ts}(D)] * F[w(D)]$ (Equations [20] and [21]). This limitation makes the numerical decorrelation possible only under certain conditions.

If $V_{ts}(D)$ is zero outside the envelope, the decorrelation is correct and the information outside the envelope does not corrupt the data. For example, at the right cutoff (i.e., large D), $V_{ts}(D)$ approaches zero. However, most potentials become strongly repulsive as D approaches zero. The left cutoff will be in the repulsive regime, where $V_{ts}(D)$ is large outside the envelope and may distort the results.

If the portion of $V_{ts}(D)$ that lies outside the envelope contributes to the value of the correlation at a particular point, the decorrelation of the envelope-limited $V_{ts}(D)$ at that

point will be inaccurate. $V_{ts}(D)$ beyond the left cutoff will be large and will contribute to the value of the correlation within the width of the window. For example, if $\rho(D)$ is non-zero at 1 nm, then the leftmost 1 nm of the decorrelation of the envelope-limited $V_{ts}(D)$ will be inaccurate and must be discarded. Therefore, this method is limited to cases where the width of the correlating function is less than the width of the potential, $V_{ts}(D)$. Practically, a narrow $\rho(D)$ is required, such as planar, tilted square (with a small angle), narrow gaussians, *etc.*

A more flexible way of doing decorrelations is to use an analytical correlation as given in Table [1]. A functional form, $V_{ff}(D)$, must first be chosen to represent the intermolecular. The correlation $V_{ff}(D) \otimes \rho(D)$ is then fit to the experimentally determined $V_{ts}(D)$. This method avoids envelope-limited potentials and is less sensitive to noise than the decorrelation method. Unfortunately, this method limits the functional form of the potential.

V. Conclusion

An accurate method for deriving tip-sample potentials from AFM force curves has been developed. Also, a mathematical technique for determining single molecular pair potentials from these tip-sample potentials has been developed. In practice, these algorithms may be used by an experimental microscopist in two manners.

First, if the surface chemistry of the AFM tip is carefully controlled, it should be possible to determine an accurate $\rho(D)$ from the measured force curve, since the molecular pair potentials can be estimated. As noted above, many complicated tip geometries may possess similar $\rho(D)$. However, for typical AFM tips, it should be possible to accurately estimate the radius of curvature of the apex with this method.

Second, an accurate determination of the tip apex shape will produce an accurate $\rho(D)$. Therefore, if a chemical moiety with an unknown pair potential is attached to the tip, the pair potential can be extracted from the force curve.

---

[1] Binnig G., Quate C., Gerber C. (1986). Atomic Force Microscope *Phys. Rev. Lett.* **56**, 930

[2] Albrecht T., Quate C., (1987). Atomic Resolution Imaging of a Nonconductor by Atomic Force Microscopy. *J. Appl. Phys.* **62**, 2599

[3] Hansma P., et. al., (1994). Tapping Mode Atomic Force Microscopy in Liquids. *Appl. Phys. Lett.* **64**, 1738

[4] Burnham N., Colton R., Pollock M. (1993). Interpretation of Force Curves in Force Microscopy. *Nanotechnology* **4**, 64

[5] Israelachivili J. (1992). *Intermolecular and Surface Forces*, Academic Press, New York, NY.

[6] Hartmann U. (1991). Theory of Van der Waals Microscopy. *JVSTB* **9**, 465

[7] Burnham N., Colton R., Pollock H. (1992). Work-function Anisotropies as an Origin of Long-range Surface Forces. *Phys. Rev. Lett.* **69**, 144

[8] Kotomin E., Shluger A., Causa M., Dovesi R., Ricca F. (1990). The Adsorption of SiO Molecules on MgO Surfaces as a Model for the Silicon Lever Atomic Force Microscope (AFM). *Surf. Sci.* **232,** 399

[9] Frisbie C., Rozsnyai L., Noy A., Wrighton M., Lieber C. (1994). Functional-Group Imaging by Chemical Force Microscopy. *Science* **265,** 2071

[10] Lee G., Chrisey L., Colton R. (1994). Direct Measurement of the Forces Between Complementary Strands of DNA. *Science* **266,** 771

[11] Lee G., Kidwell D., Colton R. (1994). Sensing Discrete Streptavidin Biotin Interactions with Atomic Force Microscopy. *Langmuir* **10**, 354

[12] Senden T., Ducker W. (1994). Experimental Determination of Spring Constants in Atomic Force Microscopy. *Langmuir* **10**, 1003

[13] Cleveland J., Manne S., Bocek D., Hansma P., (1993). A Nondestructive Method for Determining the Spring Constant of Cantilevers for Scanning Force Microscopy. *Rev. Sci. Inst.* **64**, 403

[14] Hutter J., Bechhoefer J. (1993). Calibration of Atomic Force Microscope Tips. *Rev. Sci. Inst.* **64**, 1868

CHAPTER THREE

Chemically Patterned Surfaces

This chapter describes the use of simple masking methods from the semiconductor industry to create chemically patterned surfaces. Both novolac photoresist and gold are employed as chemical masks for subsequent silanization. Both create chemically patterned surfaces with good contrast in frictional force microscopy images, but photoresist is found to catalyze the polymerization of aminopropyltriethoxy silane due to its acid content. Gold masks are easy to create, easy to remove as photoresist, but do not catalyze aminosilane polymerization. Fluorescent labeling of surface amines is found to be a useful method to analyze aminosilanization quality, but fluorescence quenching of fluorophores by proximity of a semiconductor surface limits its general applicability to insulator surfaces.

I. Introduction

A. Background

1. Diagnostic for Surface Derivatization Chemistry

The primary motivation for developing a method to produce chemically patterned surfaces was the Touchdown scheme: a method was needed to evaluate the success of the surface derivatization chemistry. Most of the techniques used by organic and inorganic chemists – IR and NMR spectroscopy, Mass Spectrometry, and chromatography, among others – require a large number of molecules, and cannot be used to evaluate reactions on flat surfaces. Attempts were made at using IR and NMR spectroscopy on high-surface area silica particles in our laboratory, but these were unsuccessful.

A chemically patterned surface (with some areas derivatized and some left bare) can provide contrast for microscopic imaging. This provides a method for debugging the surface chemistry: if the pattern can be seen, then the derivatization must have been successful. As long as we choose a substrate of the same chemical nature as the AFM probes, this is a useful method to analyze and debug the probe derivatization chemistry.

Analyzing the surface chemistry results was particularly critical for the refinement of the surface chemistry for the Touchdown Scheme (see Figure 1).

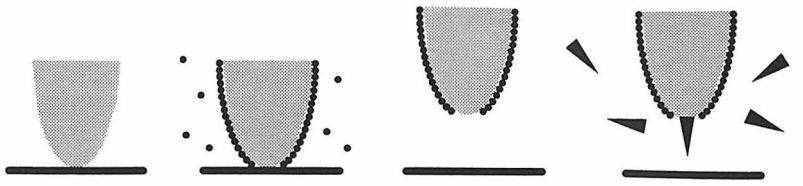

Figure 1: Touchdown Scheme. a: touchdown, **b:** passivate, **c:** retract, **d:** functionalize.

For the Touchdown scheme to work, it was clearly necessary to have a functionalization chemistry that resulted in a high-quality monolayer. With the passivation scheme, a faulty monolayer would result in molecules being attached at multiple points on the tip. With the activation scheme, a faulty monolayer would reduce the chance that a molecule with the correct functional group was at the tip apex to be activated. With either scheme, monolayer chemistry that didn't work reliably or efficiently would reduce the chances of a molecule being attached at the desired site.

2. Substrates for Chemical Microscopy

There was also another motivation for the production of chemically patterned surfaces in our laboratory: a chemically patterned surface also serves as a substrate to analyze with a chemically derivatized probe.

One method to analyze chemical patterns on surfaces is Frictional Force Microscopy, illustrated in Figure 2. As an AFM cantilever is scanned across the surface in contact mode, the strength of the tip-surface interaction varies with the chemistry on the surface. In regions where the chemistry on the surface is more attractive to the tip surface, the tip "sticks" more to the surface – an effect similar to dragging one's finger across a smooth tabletop and through a region where someone spilled grape juice[1]. This sticking retards the tip compared to the cantilever base, creating a torsion in the cantilever and moving the reflected beam to the left or right on the four-quadrant photodiode. This is recorded as the "friction" signal in commercial AFM instruments.

For instance, suppose we have a surface patterned with a fluorinated compound. A probe derivatized with NH_2 groups (which can form hydrogen bonds) would be expected to stick more strongly to the underivatized areas (which have surface –OH groups) than to the fluorinated areas.

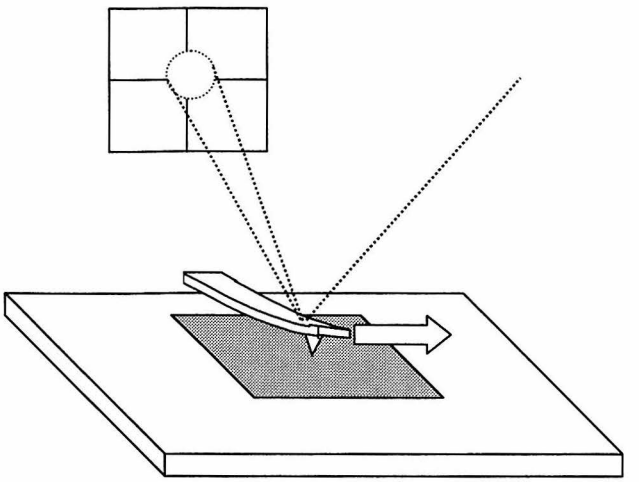

Figure 2: Frictional force microscopy

Microscopy using this contrast mechanism also holds the promise of revealing information about the surface chemistry of biological substrates. However, in order to obtain useful information, it is first necessary to evaluate the contrast on a substrate of well-defined chemistry. A chemically patterned surface serves as a "test pattern" to image with a fully-derivatized probe.

As mentioned in Chapters 1 and 2, if the chemistry of the probe and surface can be controlled and the shape of the tip is known, the intermolecular pair potential can be extracted from the AFM force curve. Thus, the production of chemically patterned surfaces was also a route to experimental measurement of intermolecular pair potentials.

3. Other Uses of Chemical Patterning

Chemical patterning of surfaces has also proved its utility in other areas, most of them developed since this work was undertaken.

DNA patterns[2] have been created by surface silanization with photolabile reactive silane followed by patterned light exposure and DNA attachment.

Chemical patterning is also proving useful for high-resolution lithography. Motivated by the promise of photoresists with truly molecular resolution, Calvert et al. have developed a pattern transfer technique based on silanes with metal chelating ligands[3]. The metal chelating ligands bind metal catalyst molecules (i.e., $PdCl_4^{2-}$), which serve as a seed layer for electroless metal deposition. The metal then serves as a resist in a reactive ion etch (RIE) step, producing linewidths[4] down to 35 nm. Whitesides et al. have used microcontact printing to transfer patterns to Au, Ag, Cu, and GaAs (with alkanethiolates[5]) and Si/SiO_2 and glass[6] (with alkoxysilanes).

Chemically patterned surfaces have also been used to guide biological processes; axons of nerve cells growing in culture, for instance, preferentially adhere to regions of a surface patterned with n-(2-aminoethyl-3-aminopropyl) groups[7], and influence of cell shape on the cell cycle was demonstrated with patterned alkanethiolates microcontact printed on gold[8].

Another use, recently developed, is in flow control in microfluidic systems[9]. Burns et al. have taken advantage of the fact that aqueous solutions will wet surfaces functionalized with groups capable of forming hydrogen bonds, but not those functionalized with hydrophobic groups to provide a "flow stop" in a microfabricated DNA analysis device.

B. Organosilane Chemistry

Organosilanes are compounds of the formula SiR_nX_{4-n}, where R stands for an alkyl group (often supporting a functional group) and X stands for a halogen atom (i.e., Cl), an alkoxy group (i.e., methoxy, $-OCH_3$), or an –OH group. Both halogens and alkoxy group are hydrolyzed by water, yielding OH groups. The salient characteristic of organosilanes is that they can form covalent bonds with molecules – and surfaces – that contain free -OH groups[10].

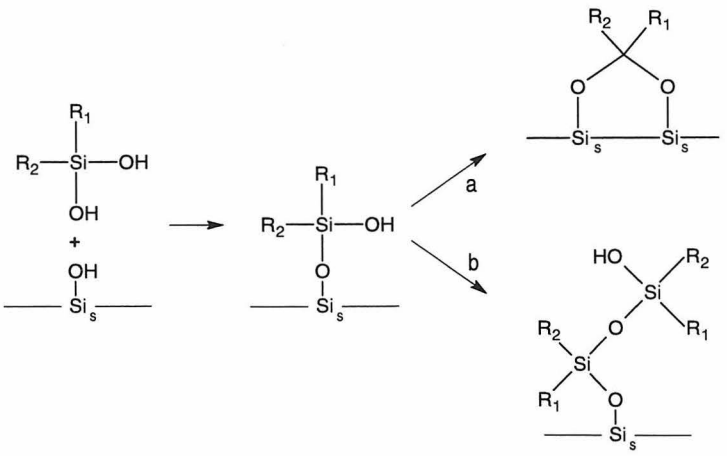

Figure 3: Silane reactions. a: formation of multiple bonds with the substrate, **b:** formation of a siloxane polymer

Such surfaces include metal oxides[11,12,13], and (more importantly) silicon dioxide. The surface of pure silicon quickly forms a thin layer of oxide if exposed to air or water. Silicon nitride – from which most contact-mode AFM cantilevers are made – quickly develops a surface layer of silicon-oxy-nitride. Both of these "native oxides" are terminated with –OH groups[14].

The silanization reaction is catalyzed by both acid and base. With n < 3, there is the additional danger that the organosilane molecule can form a bond with the –OH on another organosilane molecule (Figure 4), rather than an –OH supported by the native surface (Figure 5). Only the latter reaction leads to the formation of a good monolayer.

Strong infrared evidence[15] indicates that the tendency of *methyl*silanols to condense with surface Si_s-OH groups follows the order

$$(CH_3)_3SiOH > (CH_3)_2Si(OH)_2 > CH_3Si(OH)_3.$$

This is consistent with a mechanism involving nucleophilic attack on the organosilane Si by the surface silanol oxygen lone pair:

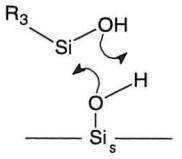

Figure 4. Silanization mechanism

The surface silanol is more acidic than the alkylsilanol[16] (pKa 7.1 vs 11), so it is much more likely to perform nucleophilic attack. Electronic structure calculations indicate that the Si-O bond length decreases in the order

$$(CH_3)_3SiOH > (CH_3)_2Si(OH)_2 > CH_3Si(OH)_3.$$

Since a longer bond length generally indicates a weaker bond, the capacity of the hydroxyl group to function as a leaving group probably follows the same trend, giving rise to the observed behavior.

Since attachments to the surface with multi-alkoxy silanes are (in general) empirically more stable than attachments with mono-alkoxy silanes, this might seem an odd result. However, it is important to keep in mind that this result was obtained with *methyl*silanols. Consistent with the above mechanism, addition of bases to the surface before the organosilane causes even the trisilanol to fully condense with surface silanols[17]. This is because the base forms a strong hydrogen bond with the surface silanol hydrogen, increasing the nucleophilicity of the surface silanol oxygen as shown in Figure 5.

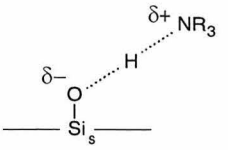

Figure 5: Nucleophilicity enhancement with a trialkylamine

The anomalous stability of aminofunctional silanes may be based on a similar mechanism, with the amino group of the organosilane forming a hydrogen bond with the surface silanol.

Aminofunctional silanes were among the first silanes used as adhesion promoters between polymer resins and glass fibers, and the literature on them is very extensive[18]. Several groups[19,20] had generated good results (indicating monolayers covalently bonded to the surface) with these compounds, and this formed the starting point for the chemical development of the Touchdown scheme.

II. Experimental

A. Materials

Two different Si wafers were employed for data presented here. One was a (100)-oriented Si wafer n-doped with P to 0.410-0.510 ohm-cm. The other was a (111)-oriented Si wafer n-doped with Sb to < 0.010 ohm-cm. The SiO_2 substrate was SiO_2 field oxide grown (several thousand A thick) on an Si wafer of unknown composition. Wafers were scribed with a diamond-tipped stylus and broken into approximately 5 x 5 mm chips. Experiments with differently-doped Si chips (highly p-doped to highly n-doped) revealed no differences in derivatization behavior (data not shown).

Tridecafluoro-1,1,2,2, tetrahydrooctyldimethylchlorosilane ("fluorosilane") was obtained from Gelest, Tullytown PA and was 98% pure; 3-mercaptopropyltrimethoxysilane ("mercaptosilane") was obtained from Sigma (97% pure), and 3-aminopropyltriethoxysilane (APTES) was obtained from Aldrich (98% pure).

B. Cleaning/Derivatization Protocols

Chips were typically cleaned by stirring in 50:50 HCl/MeOH solution at room temperature for 20 minutes, and dried with a dry N_2 stream. Silane derivatization was carried out by stirring in a 1% solution of silane in toluene for 20 minutes, then rinsing with toluene.

C. Apparatus

Chips were mounted in a pipette-tip-based apparatus for treatments in liquid, as shown in Figure 6. This apparatus has the advantage of being both inexpensive and inert.

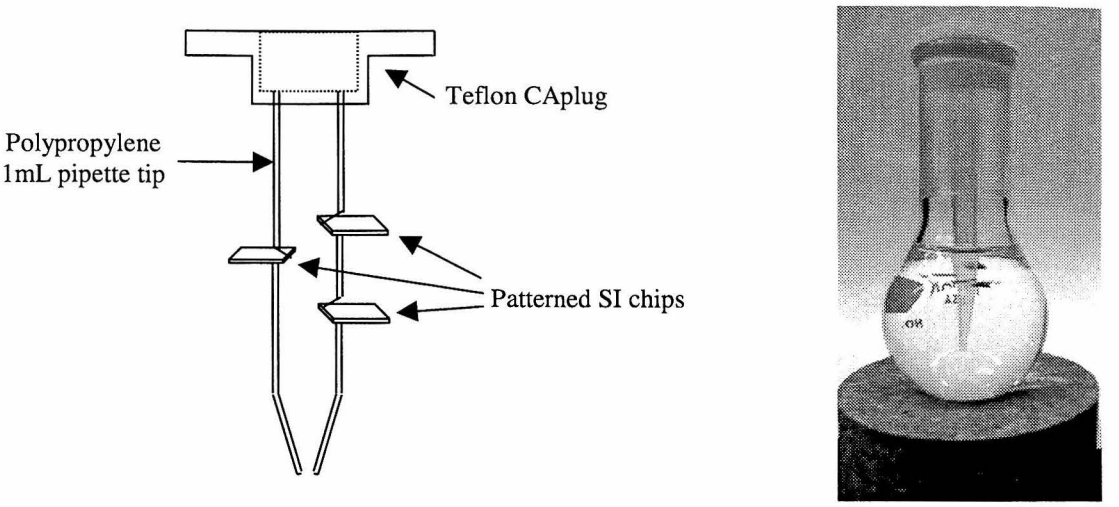

Figure 6: Chip-holder apparatus

D. Analysis

SEM images were acquired on an Etec AutoScan Scanning Electron Microscope and a Camscan Series II Scanning Electron Microscope. AFM images were acquired with a Topometrix Discoverer Atomic Force Microscope operating in contact mode in air or water. Confocal microscope images were acquired with a BioRad 600 Confocal Microscope using a fluorescein filter set.

III. Results and Discussion

A. Lithographic Patterning

The semiconductor industry has spent a great deal of effort creating micron-scale, spatially defined patterns on flat substrates – particularly silicon and silicon dioxide. This size of pattern turned out to be both necessary and desirable for the microscopes that would be used to image the results.

The basic paradigm of lithographic patterning is the patterning of photoresist with light, with subsequent pattern transfer to the substrate. The first step is the creation of a mask – typically chrome on quartz – which blocks light in some areas and transmits in others. The photoresist is a layer of photosensitive polymer, typically spun onto a flat surface. The photoresist is exposed to light through the mask. As the photoresist is exposed to light, it changes its solubility in the developer. The most typical photoresist – *positive*

photoresist – becomes more soluble in developer when exposed to light. After exposure, the exposed photoresist is dissolved away with developer, leaving the corresponding area of the substrate exposed (see Figure 7).

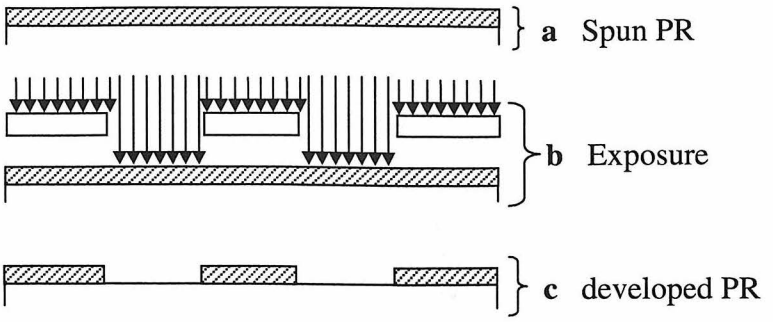

Figure 7: Basic lithographic mechanism

B. Silicon Wafers with Photoresist Masks

The first attempt at chemical patterning of surfaces in this laboratory used the photoresist itself as a chemical mask. After patterning of the photoresist, the wafer was cleaned to remove surface contamination of the exposed areas. Then the wafer was immersed in a derivatization bath of organosilane (generally in toluene). After rinsing, the remaining photoresist was removed with acetone as seen in Figure 8. SEM and AFM images of our PR patterns are shown in Figure 9.

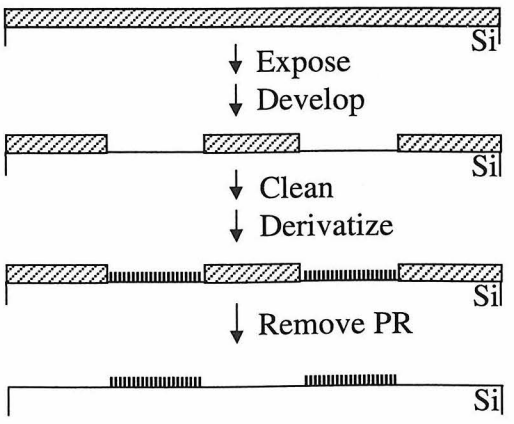

Figure 8: Silanization with a PR mask

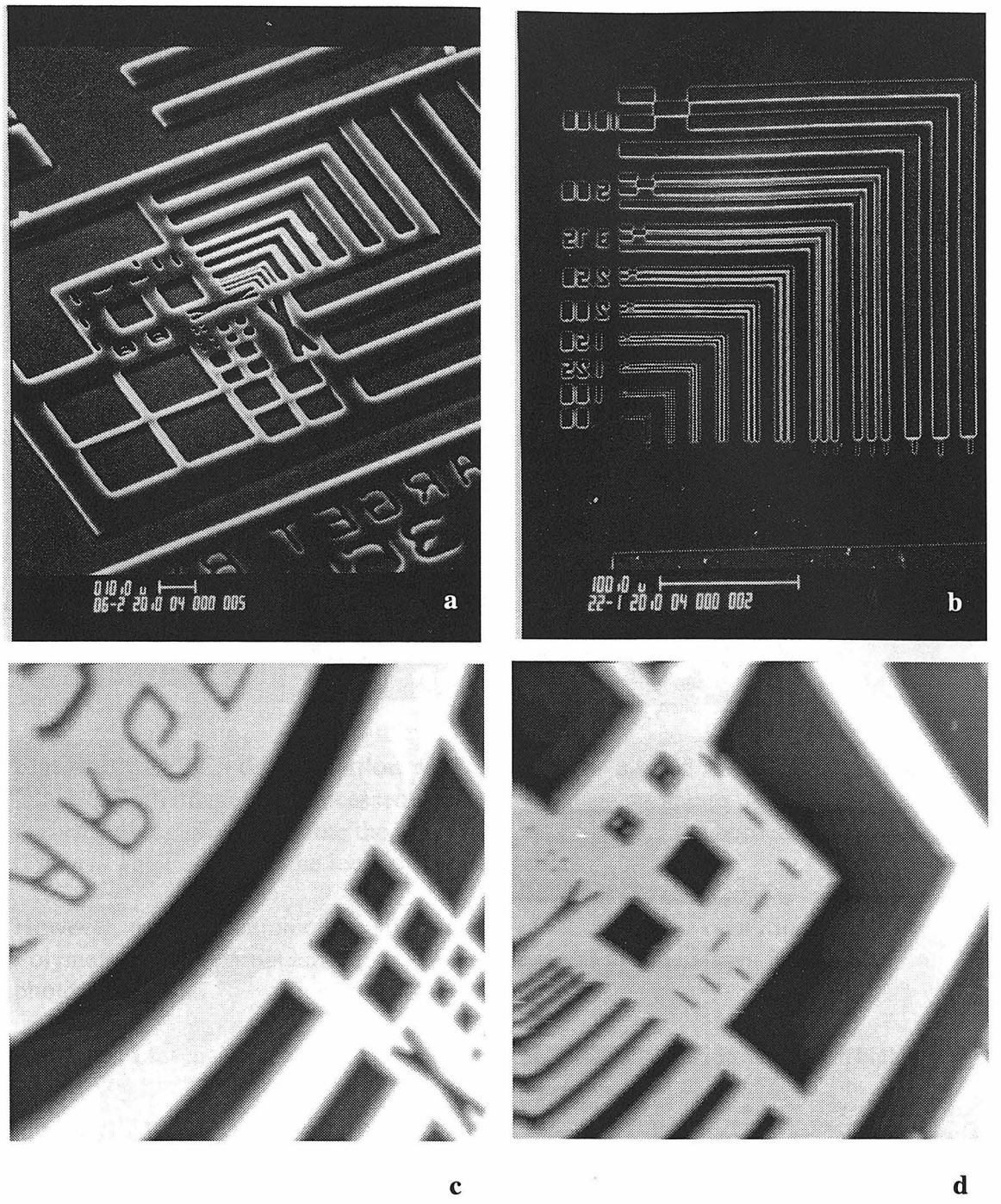

Figure 9: Photoresist test patterns. a,b: SEM images of patterned PR chips. **c,d:** 75x75 μm AFM images of patterned PR chips. Higher topography is displayed as bright. The photoresist is 2.46 μm high. At the edges of the photoresist, the slope of the cantilever is visible, and is measured to be 38°.

Photoresist proves to be suprisingly durable as a chemical mask. Although not very resistant to polar organics, it survives many other chemical compounds useful in

synthesis quite well, including HCl/MeOH (our cleaning solution) and toluene (our silanization solvent). Appendix A is a table of photoresist durability. A control experiment showed no trace of the photoresist remaining after removal with acetone.

After debugging some interesting static charging problems[21], AFM analysis of the chemically patterned surfaces clearly shows derivatization.

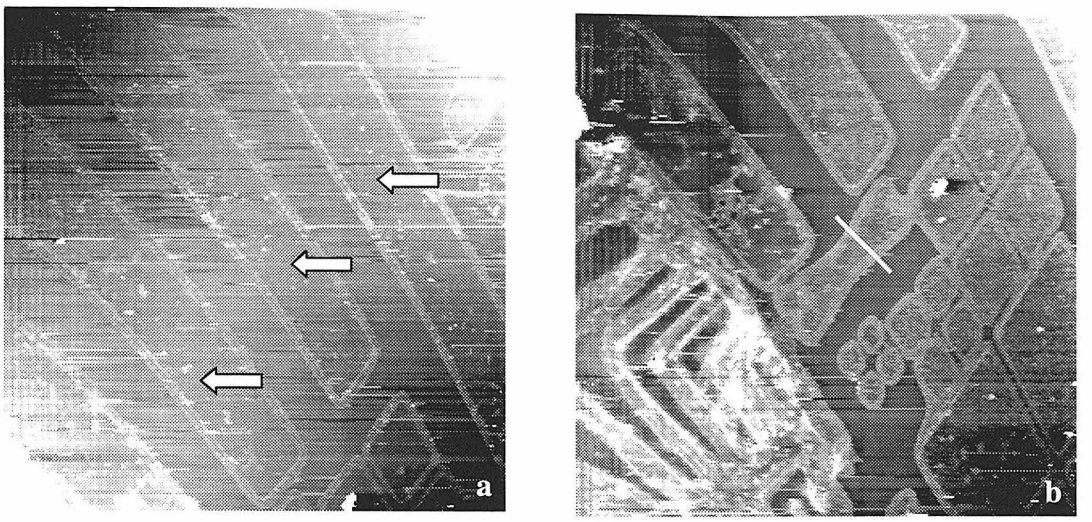

Figure 10: APTES derivatization with a PR mask. a,b: 75 x 75 μm AFM height images. Both images are processed[22] to remove image curvature. Arrows mark the derivatized regions in **a**. Note the wide, high edge beads at the borders of the derivatized regions. The line marks the location of the linecut.

However, polymerization of the silane is substantial under the conditions used. Polymerization is particularly noticeable at the edges of the pattern, next to the photoresist mask.

Figure 11: Linecut from Figure 9b. The edge bead is ~2500 μm wide and 70 nm high.

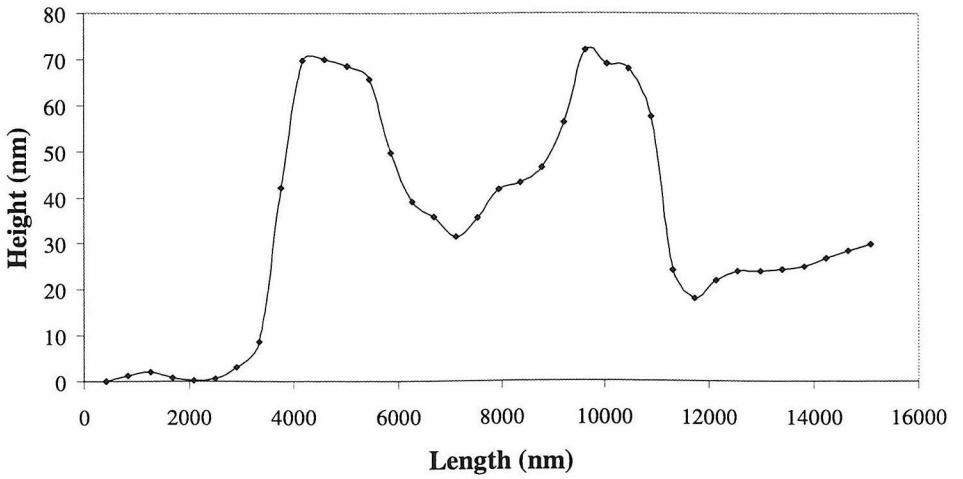

This polymerization is most likely due to an interaction between the chemistry of the aminosilane and the photoresist. Photoresist contains approximately 50% diazonapthoquinonesulfonic ester (sensitizer). In its native form the sensitizer is base-insoluble. Once exposed to light, however, it reacts to form a base-soluble carboxylic acid (as shown in Figure 12) and renders the resist sufficiently soluble to dissolve in aqueous base (the developer).

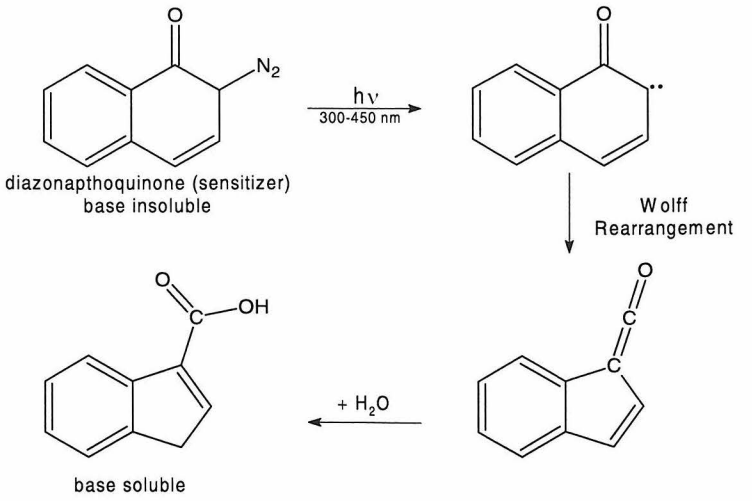

Figure 12: Photoresist sensitizer chemistry

In our case, the remaining photoresist, which was being used as our chemical mask, had also been exposed to sufficient light to convert a large portion of the sensitizer to its acid form: developer removed all photoresist from a test piece of wafer. Since organosilane deposition is acid catalyzed, the excessive polymerization at the edges was almost certainly a result of catalysis by the sensitizer in its light-exposed, acid form. Clearly, another chemical mask was necessary.

C. Silicon Wafers with Gold Masks

The answer to this dilemma was to use gold as a chemical mask. Gold is exceptionally inert. Surprisingly, it is also relatively easy to remove: Iodide etch, a simple mixture of I_2 and KI in water (4g KI : 2g I_2 : 10mL H_2O), dissolves gold extremely rapidly by the formation of a gold-iodine complex[23]. A gold pattern can be created by using a "liftoff" procedure, also adopted from the arsenal of semiconductor technology (see Figure 13):

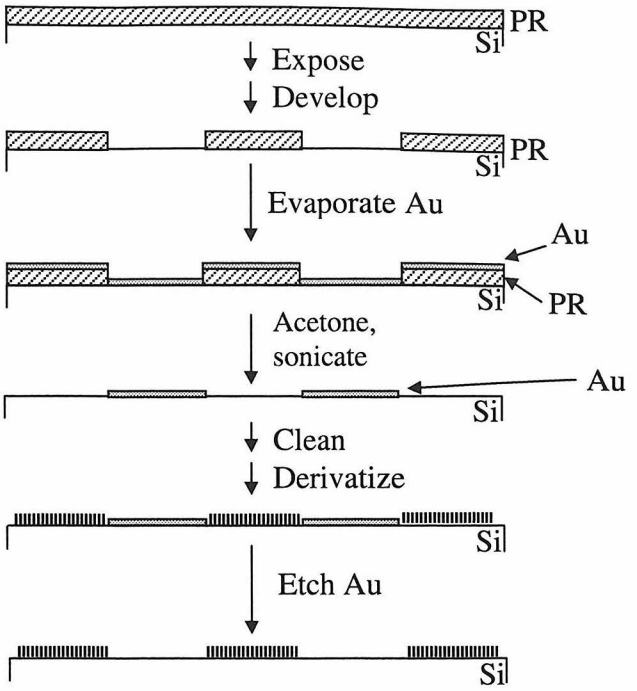

Figure 13: Silanization with a gold mask

After the gold is patterned, the wafer is cleaned and derivatized as previously. A control experiment shows that no trace of the gold remains on the chip after gold etching.

AFM analysis of the aminosilane patterned chips produced by this method show a dramatic improvement. Refinement of the protocol has dramatically reduced the amount of polymerization. Most importantly, the gold chemical mask does not catalyze organosilane polymerization, dramatically reducing the "edge bead" observed with photoresist as a chemical mask.

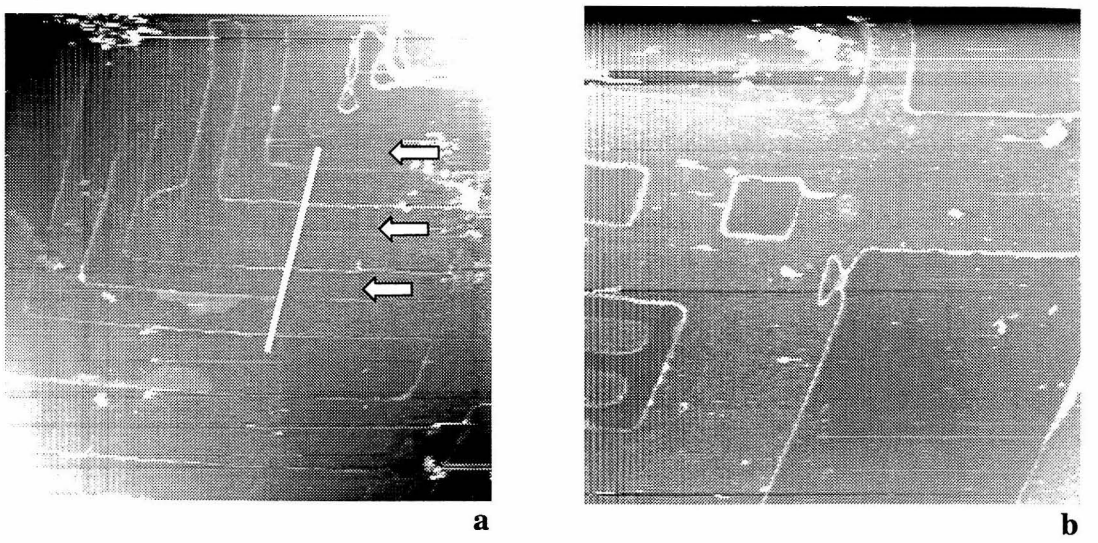

Figure 14: APTES derivatization with an Au mask. a,b: 37.5 x 37.5 μm AFM height images. The arrows in a point to the areas previously masked by Au. The line indicates the linecut. In **b**, the derivatized area is slightly higher (brighter).

The height of the organosilane layer has been reduced from approximately 25 nm to 2-3 nm; this is greater than the expected value for a monolayer (~1.5 nm) by a factor of approximately 1.7.

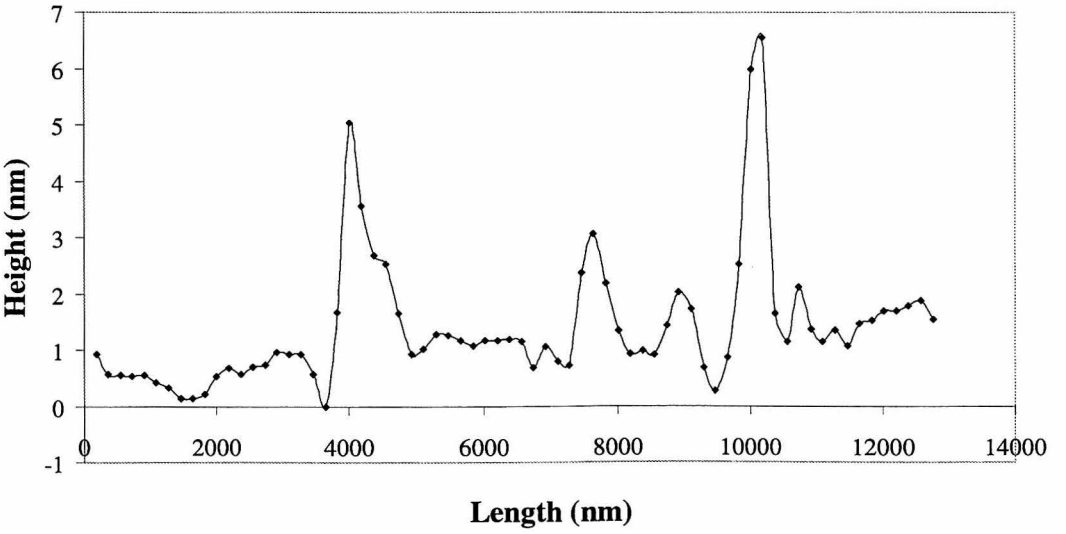

Figure 15. Linecut from Figure 4. The edge bead is approximately 500 nm wide and 5 nm high.

The reduction in edge bead width and height, as well as the reduction in the thickness of the derivatized layer, both indicate that the use of Au as a mask is superior to photoresist.

Frictional force images clearly show chemical contrast, demonstrating that the basis of Scanning Chemical Microscopy is sound.

Figure 16: AFM height/friction pairs for different chips derivatized with different silanes. a,b: 37.5 x 37.5 μm images[24] of a fluorosilanized surface. Essentially no topography is visible, but the friction signal is very clear. The derivatized area is bright, corresponding to higher friction. **c,d**: 75 x 75 μm images of a mercaptosilanized surface[25]. The derivatized area is clearly lower friction.

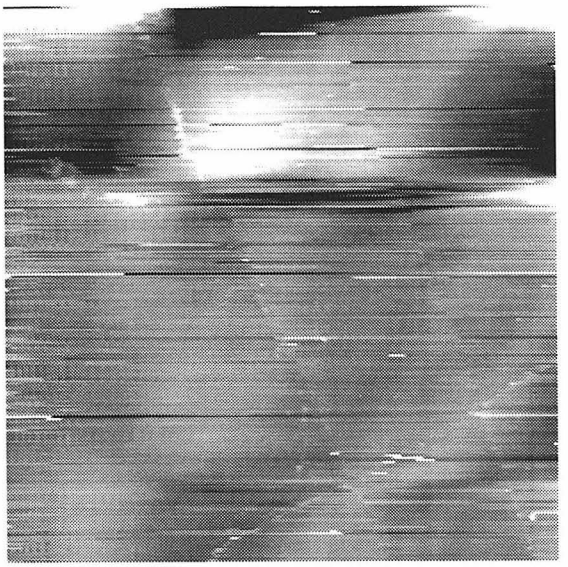

a. Fluorosilane height

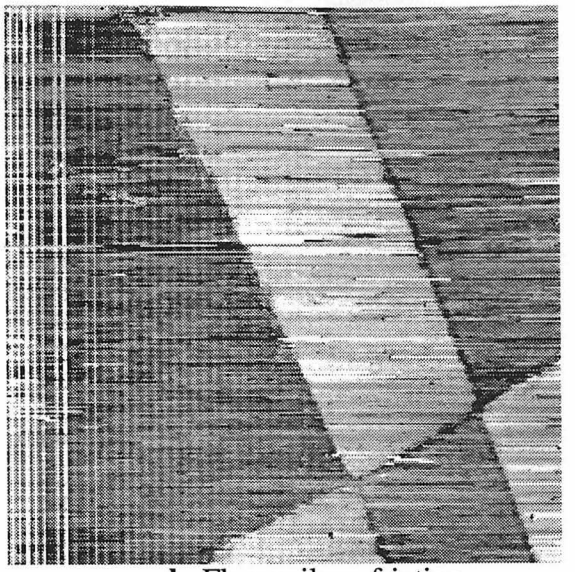

b. Fluorosilane friction

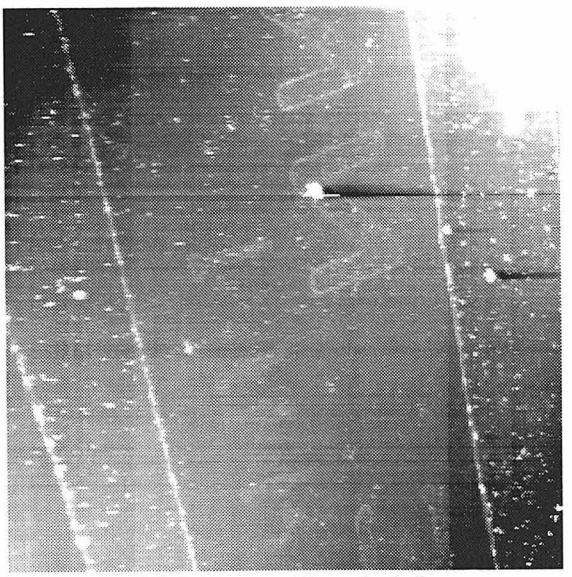

c. Mercaptosilane height

d. Mercaptosilane friction

D. Florescence Labelling

Because AFM analysis proved time-intensive, extensive attempts were also made to analyze the chemical patterns with fluorescence microscopy. The workhorse technique of this effort was to derivatize the $-NH_2$ group with fluorescein isothiocyanate (FITC) as shown in Figure 17.

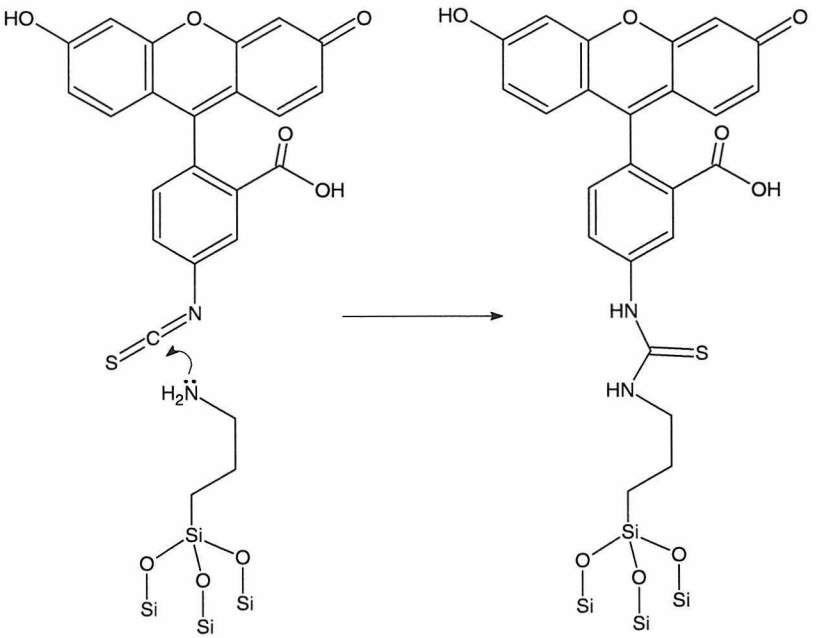

Figure 17: Reaction of APTS with FITC

After an initial optimization of the fluorescence labelling chemistry, results as shown in Figure 18 were reproducibly obtained:

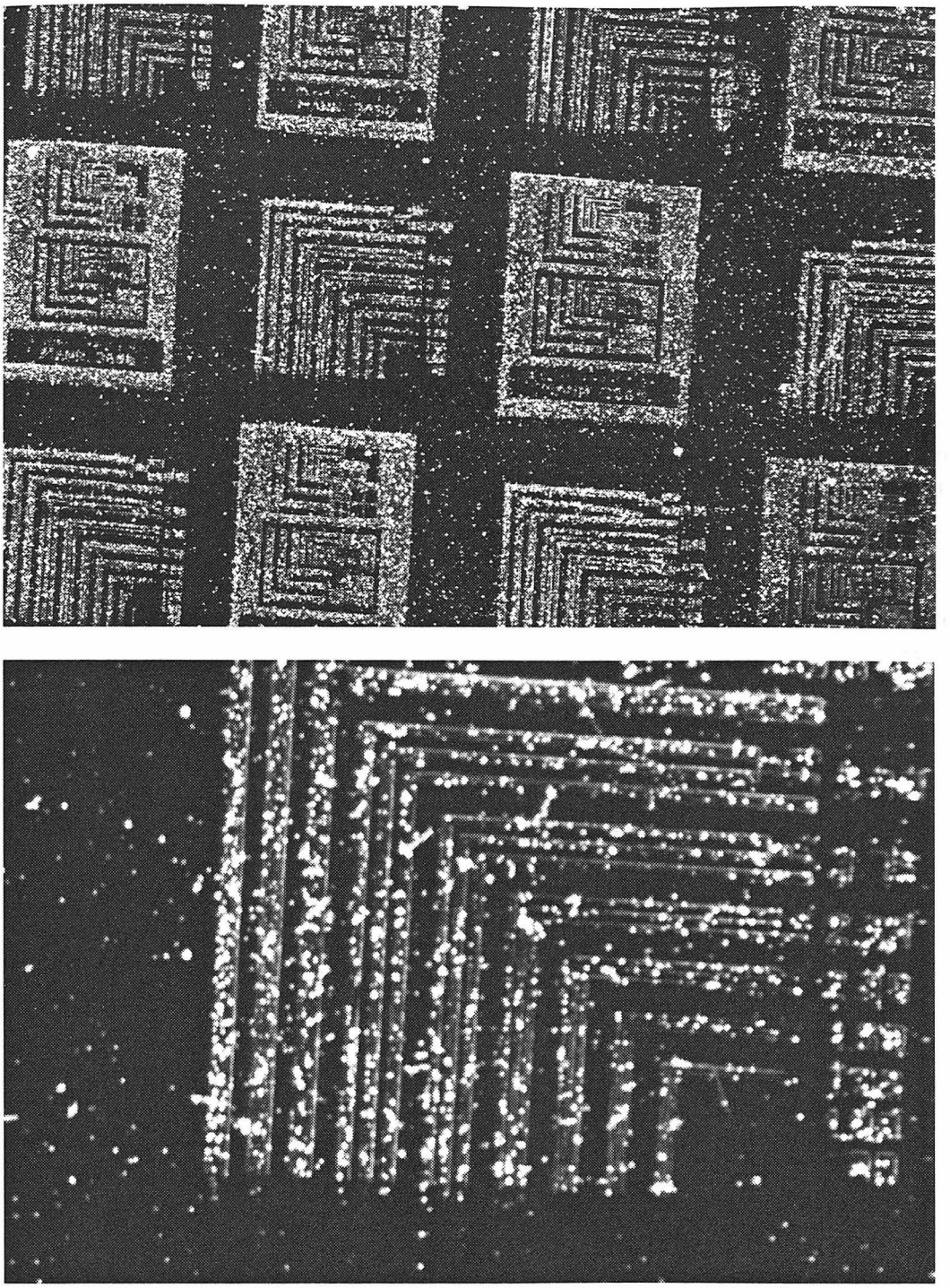

Figure 18: CM picture of Au-masked APTES chip

Several salient features are noticeable. First, the fluorescence is not uniform, but rather occurs in "blobs." These blobs were found to persist despite attempts at optimization of the derivatization and labelling chemistry. Much less obvious at first glance, but far more

important, *the fluorescence shows up where the gold mask was covering the silicon substrate, rather than on the exposed areas of silicon.* The large L-pattern visible in the previous image was originally L-shaped holes in photoresist; after application of Au and liftoff, the gold L's remained on the Si surface.

A control experiment verified that APTS-derivatized *glass* prepared under the same conditions fluoresced brightly and smoothly. Another showed that the fluorescence on the masked areas increased when the gold was removed. The hypothesis that explains this is that the APTS polymerizes across both the silicon substrate and the gold, but the fluorescence of the label is quenched by proximity to the silicon. A search of the literature revealed that this phenomenon has been reported previously[26,27]. The APTS on the gold forms a thin (probably ~2 monolayers in thickness) web or membrane across the gold, which collapses when the gold is removed. Since it does not collapse uniformly, some areas are further away from the silicon surface. The fluorophores attached to these areas are not quenched by proximity to the silicon, and these areas appear as "blobs" in a fluorescent image.

In order to confirm this hypothesis, we prepared patterns of gold on a silicon dioxide layer on a silicon wafer. The process was slightly different; instead of using a liftoff scheme to pattern the gold, we etched our pattern into a uniform gold layer as seen in Figure 19.

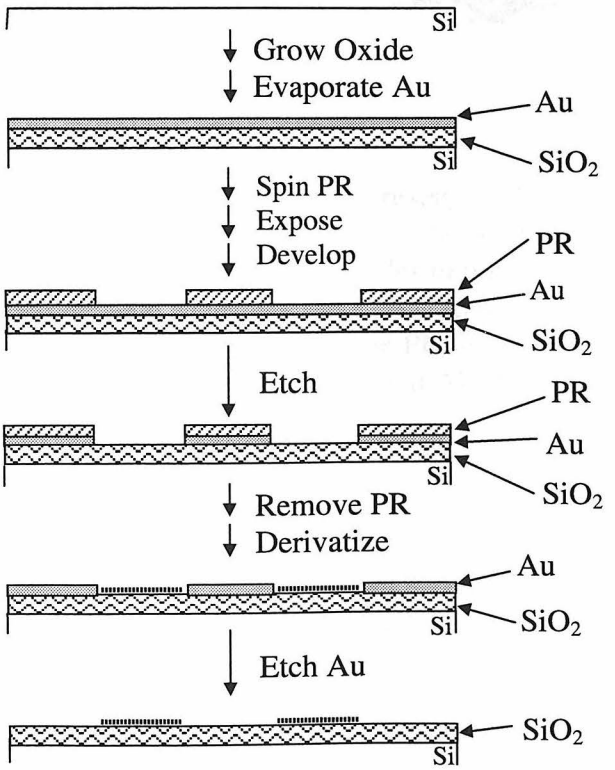

Figure 19. Silanization with an Au mask on silicon dioxide

Derivatization with FITC now produces the expected result – strong fluorescence on the exposed areas:

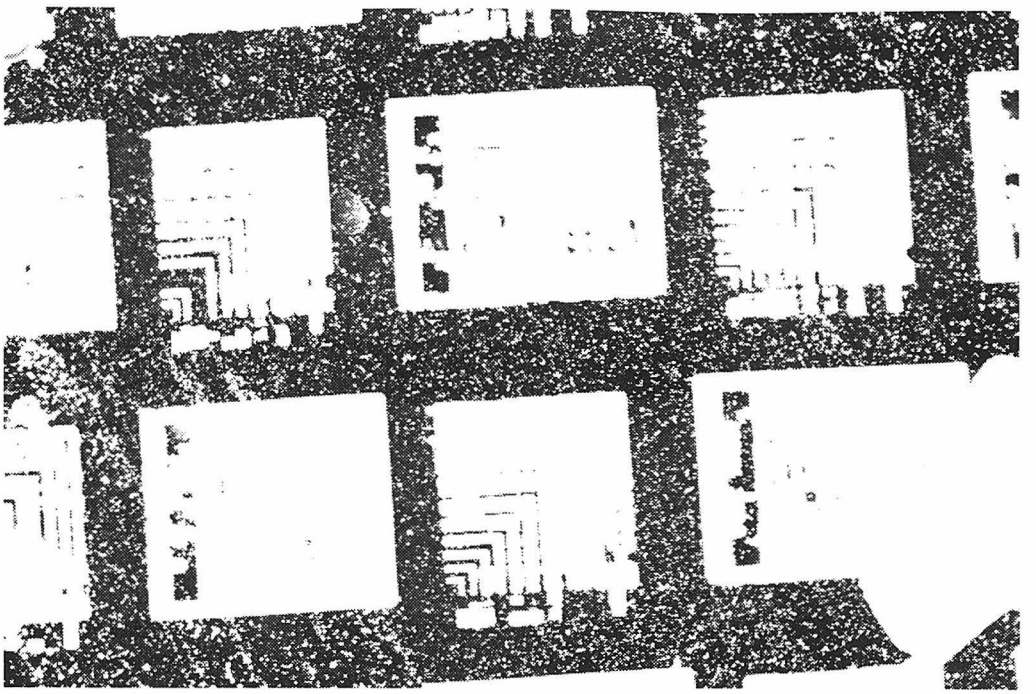

Figure 20: CM picture of Au/SiO2/APTS/FITC chip

The large "L" pattern is L-shaped holes in the photoresist. In the Au/Si case, this yields Au L-shapes on Si: the L's are where the gold was. In the Au/SiO_2 case, the photoresist is on top of the gold. Etching produces L-shaped *holes in the gold* down to the SiO_2 beneath: the L's are where the bare SiO_2 was. The poor resolution of this pattern is due to slight overetching – the etch began to undercut the PR mask, etching excess Au. One can also note that the fluorescence of the FITC-labelled APTS membrane is still present in the regions that were masked by gold.

IV. Conclusion

We have demonstrated that techniques used from the semiconductor industry can be used to produce chemical masks and chemical patterns on surfaces. Photoresist functions as a good chemical mask, but it has some limitations in its durability and catalyzes aminosilane polymerization. Gold makes a much better chemical mask, being substantially more durable and inert while still being very easy to remove.

This set of experiments also demonstrated that our organosilane derivatization technique works on silicon, SiO_2, and glass. AFM analysis was found to give useful information

both through topography and friction images, although it is somewhat time-consuming. Fluorescence labelling and fluorescence microscopy is a quick routine method for analyzing $-NH_2$ patterns, but cannot be applied on silicon surfaces due to quenching of fluorescence by transfer of the excitation energy to the silicon by a non-radiative mechanism.

Although the success of the patterning technique was clear, this set of experiments also showed that our protocol was not giving well-defined monolayers of organosilane. Since high-quality monolayers were necessary for the Touchdown scheme, we had to push the chemistry further. The next chapter describes the optimization of the organosilane derivatization protocol, and the discoveries made during that process.

---

[1] An analogy due to Steve O'Connor. Although inexact, the author has yet to find a better explanation or analogy for the effect in the literature. Most probably, the effect is due to the fact that the bonds which must be broken (at the trailing edge of the tip) for the tip to move forward are aligned nearly parallel to the surface, requiring force parallel to the surface, whereas the bonds which are formed (at the leading edge) are more nearly perpendicular to the surface, generating a force nearly perpendicular to the surface. Since bond formation and breakage are not symmetric, the twisting of the tip increases with the strength of the bonds formed between tip and surface.

[2] Chrisey, L.A., Oferrall, C.E., Spargo, B.J., Dulcey, C.S., Calvert, J.M. (1996). Fabrication of patterned DNA surfaces. *Nucleic Acids Research*; **24**: (15) 3040-3047

[3] Calvert, J.M., (1993). Lithographic Patterning of Self-Assembled Films. *Journal of Vacuum Science and Technology B*, **11**: (6) 2155-2163

[4] Brandow, S.L., Dressick, W.J., Dulcey, C.S., Koloski, T.S., Shirey, L.M., Schmidt, J., Calvert JM., (1997). Nanolithography by displacement of catalytic metal clusters using an atomic force microscope tip. *Journal of Vacuum Science and Technology B*, **15**: (5) 1818-1824

[5] Xia, Y.N., Zhao, X.M., Whitesides, G.M., (1996). Pattern transfer: Self-assembled monolayers as ultrathin resists. *Microelectric Engineering. B*: (1-4) 255-268

[6] Wang, D.W., Thomas, S.G., Wang, K.L., Xia, Y.N., Whitesides, G.M., (1997). Nanometer scale patterning and pattern transfer on amorphous Si, crystalline Si, and SiO2 surfaces using self-assembled monolayers. *Applied Physics Letters*, **70**: (12) 1593-1595

[7] Matsuza, W.A.M., Potember, R.S., Stenger, D.A., Krauthamer, V. (1993). Containment and Growth of Neuroblastoma Cells on Chemically Patterened Substrates. *Journal of Neuroscience Methods*, **50**: (2) 253-260

[8] Chen, C.S., Mrksich, M., Huang, S., Whitesides, G.M., Ingber, D.E. (1998). Micropatterned Surfaces for Control of Cell Shape, Position, and Function. *Biotechnology Progress*, **14**: (3) 356-363

[9] Burns, M.A., Johnson, B.N., Brahmasandra, S.N., Handique, K., Webster, J.R., Krishnan, M., Sammarco, T.S., Man, P.M., Jones, D., Heldsinger, D., Mastrangelo, C.H., Burke, D.T. (1998). An Integrated Nanoliter DNA Analysis Device. *Science*, **282**: (5388) 484-487

[10] Calvert, J.M. (1993). Lithographic Patterning of Self-Assembled Films. *JVSTB* **11**(6), 2155-2163

[11] Moses, P.R., Murray, R.W. (1977). Chemically Modified Electrodes Part VII. Covalent Bonding of a Reversible Electrode Reactant to Pt Electrodes Using an Organosilane. *J. Electroanal. Chem.* **78**, 195-201

[12] Moses, P.R., Murray, R.W. (1977). Chemically Modified Electrodes Part V. Covalent Binding of a Reversible Electrode Reactant to RuO_2 Electrodes. *J. Electroanal. Chem.* **77**, 393-399

[13] Wrighton, M.S., Palazzotto, M.C., Bocarsly, A.B., Bolts, J.M., Fischer, A.B., Nadjo, L. (1978). *J. Amer. Chem. Soc.* **100**(23), 7264-7271

[14] Raider, S.I., Flitsch, R., Aboaf, J.A., Pliskin, W.A. (1976). *J. Electrochem. Soc.* **124**(4), 560-565.

[15] Tripp, C.P., Hair, M.L. (1998). Reaction of Methylsilanols with Hydrated Silica Surfaces – The Hydrolysis of Trichloromethylsilanes, Dichlorormethylsilanes and Monochloromethylsimanes and the Effects of Curing. *Langmuir*, **11**: (1) 149-155

[16] Hair, M.L. Infrared Spectroscopy in Surface Chemistry; Marcel Dekker: New York, 1967.

[17] Tripp, C.P., Hair, M.L. (1993). Chemical Attachment OF Chlorosilanes to Silica - A 2-Step Amine-Promoted Reaction. Journal of Physical Chemistry, **97**: (21) 5693-5698

[18] For a starting point, see Silane Coupling Agents, 2nd edition, Edwin P. Plueddemann, Plenum Publishing, New York, 1991.

[19] Phillips, L.V., Hercules, D.M., (1986). Surface spectroscopic studies of organosilane layers on glass, **p235-265** in Silanes, Surfaces, and Interfaces, edited by D.E. Leyden, Gordon and Breach Science Publishers, New York, 1986

[20]Morrall, S.W., Leyden, D.E. (1986). Modification of siliceous surfaces with alkoxysilanes from a nonaqueous solvent. **p501-524**, also in Silanes, Surfaces, and Interfaces edited by D.E. Leyden, Gordon and Breach Science Publishers, New York, 1986.

[21] Silicon builds up an electrostatic charge with respect to the AFM tip, possibly from electron-hole pairs generated by the optical lever laser. Grounding or imaging in water is necessary to avoid this problem.

[22] Both images are median flattened vertically and horizontally. Median flattening involves line-by-line subtraction of the median value of the height from the entire line. It is useful to remove image curvature in the presence of bumps that create artifacts with average subtraction.

[23] CRC handbook of metal etchants / editors, Perrin Walker, William H. Tarn; Boca Raton : CRC Press, 1991

[24] These images have been line-leveled: the best-fit line is subtracted from each line. Line-leveling is useful to remove image distortion due to piezo nonlinearity.

[25] The height image is median flattened vertically and horizontally; the friction image is unprocessed.

[26] Naturforschung A. (1992). Zeitaufgeloestes Fluoreszenz-Loeschen in ultraduennen Coronen-Schichten auf Silizium-Substraten. *Journal of Physical Sciences*, **47a**, p797-802.

[27] Stavola, M., Dexter, D.L., Knox, R.S., (1985). Electron-hole Pair Excitation in Semiconductors via Energy-transfer from an External Sensitizer. *Physical Review B – Condensed Matter*, **31**: (4) 2277-2289

CHAPTER FOUR
Silanization Optimization

This chapter describes the optimization of a protocol for surface derivatization with reactive aminosilanes. Monolayer quality and number of reactive sites were optimized by systematic variation of experimental conditions, including substrate, precleaning, cleaning, silanization solvent, curing, silane structure, postderivatization treatment, and time. The most important factors are found to be solvent, silane structure, and postderivatization water exposure. The best solvents are toluene and acetonitrile, with toluene providing the lowest slide-to-slide variation. Monoethoxy silane is found to give much less bound silane than di- and triethoxy silane; the kinetics of surface attachment proceed in the order APDES >> APMES > APTES. Replacement of ethoxy groups with methoxy groups results in a nearly tenfold increase in both amount of attached silane and kinetics of attachment, but this is probably due to polymerization.

Silanization is quantified by attachment of fluorescent and radioactive labels to the surface amines. The silanization protocol is developed which gives an average surface density of 51 pmol/cm^2. Fluorescence quenching occurs at fluorophore surface densities typically achieved with this protocol, but surface densities may be measured by absorbance. Fluorescence-and radiolabeling measurements give results in agreement with each other.

I. Introduction

As described in the last chapter, our early silane derivatization techniques were successful in creating chemically patterned surfaces, but were not giving well-defined monolayers of organosilane. The Touchdown scheme required high-quality monolayers. Thus, this study was undertaken in order to learn how to produce reproducible reactive silane monolayers on glass and related substrates, suitable for further derivatization and the attachment of molecules. The work discussed here concentrates on amino-functional silanes, and in particular aminopropyltriethoxysilane (APTES).

In addition to its original use as coupling agents applied to glass fibers to promote the adhesion of polymer resins, APTES derivatized surfaces have been used as synthetic catalysts[1], substrates for making chiral reagents[2], column packings for HPLC[3], and for

extraction and detection of metal ions[4], preparation of immobilized artificial membranes[5], and immobilization of enzymes[6], antibodies[7], and DNA[8].

This work employs post-silanization labeling to measure the silane derivatization. This approach has advantages and disadvantages. This method of measurement has the disadvantage that we are always measuring the combined success of two reactions (silanization followed by labeling) rather than one. This disadvantage can be minimized by carefully controlling the reaction conditions – if the labeling reaction is the same for all samples, then any variation must be due to differences in the silanization reaction. The advantage of this method is that it focuses on a matter of great practical import: how well molecules can be attached to the surface. Spectroscopic techniques which measure only the *presence* of silane (for instance) may not correlate so directly with how well molecules can be attached. Since one of the biggest uses (if not *the* biggest) of silanization chemistry is attaching molecules (often biomolecules) to glass, this work has practical relevance.

Two methods were used to study silanization in this work: labeling with a fluorescent dye and radiolabeling. The attachment of fluorescent dye was analyzed both fluorescence and absorbance. Fluorescence measurements were useful for characterizing variation of bound fluorophore across a substrate surface (i.e., standard deviation). Fluorescence measurements were also useful in the early stages of protocol development, when surface densities of fluorophore were still relatively low. As the derivatization protocol improved, surface densities increased and fluorescence could no longer be used for quantitation due to fluorescence quenching. Fortunately, at such densities, measurement of absorbance becomes practical. Radiolabeling was required for non-transparent substrates.

Many papers in the literature make use of silanization, but the range of protocols is extremely broad. One of the objectives of this work is to evaluate the effect of some of the variations found in the literature – including solvent, curing, and silane structure. Another is to identify the effect of variables that are *not* commonly mentioned in the literature – in particular, substrate, cleaning protocols, and post-silanization handling. An initial evaluation of chemical durability of the silanized surface is also performed.

Labeling with fluorescein isothiocyanate proceeds by nucleophilic attack of the amino group on the isothiocyanate moiety, as shown in Figure 1:

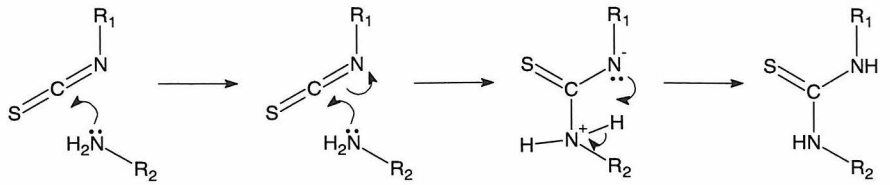

Figure 1: Nucleophilic attack on an isothiocyanate

This reaction is facile under mild conditions, and is the workhorse technique for the work discussed here. The fluorescein is detected by measurement of its absorbance or fluorescence.

Radiolabeling is accomplished by the reaction shown in Figure 2: carbodiimide-mediated linkage of ^{32}P adenosine triphosphate (ATP) to the amine group.

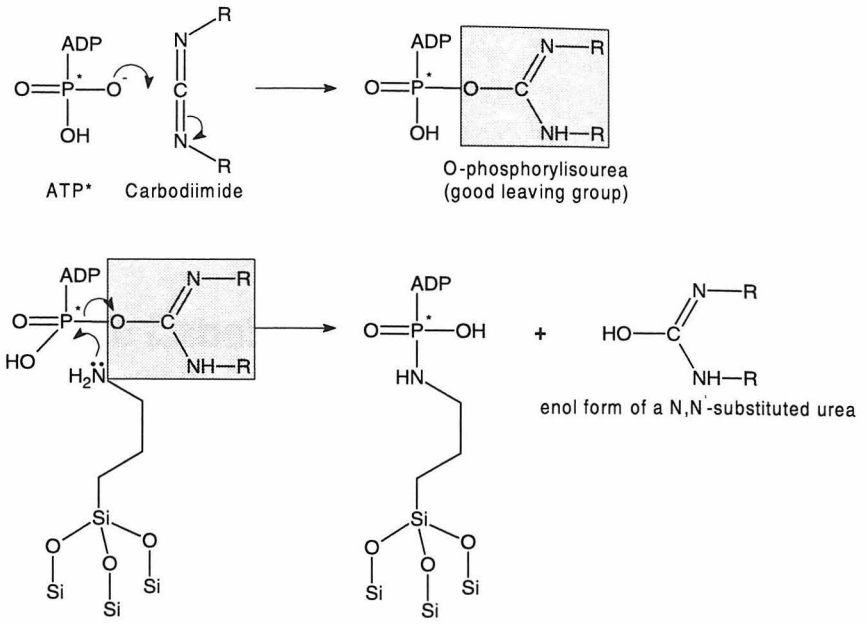

Figure 2: Radiolabelling of APTES

II. Experimental

A. Standard Cleaning and Derivatization Protocol

Standard 1x3" glass microscope slides (VWR, Corning) were handled in glass staining racks in cleaned glass trays. Slides were precleaned by stirring in a 2% detergent solution (Micro, Cole-Parmer Instrument Co.) 20 minutes, rinsed for 3 minutes in DI H_2O, and sprayed with methanol, in order to remove gross contamination.

Slides were then cleaned by stirring in a 50:50 HCl/MeOH solution for 1 hour, rinsed for 5 minutes with DI H_2O, sprayed with acetone, submerged in an acetone bath, and submerged in another acetone bath. They were then dried with dry N_2 for 15 minutes in a parafilm-covered tray to protect from atmospheric contamination.

The slides were then immersed in a bath of 2% APTES in toluene and stirred for 20 minutes. The derivatization is halted by removal from the APTES bath and immersion in two separate baths in toluene, followed by two baths in acetone. The slides are then dried with dry N_2 for 15 minutes in a parafilm-covered tray.

Cleaning and derivatization protocol:

1. HCl/MeOH Clean 1 hr
2. H_2O Rinse 5 min
3. Acetone spray
4. Acetone bath x 2
5. N_2 dry 15 min.
6. 2% APTES/toluene 20 min
7. Toluene bath x 2
8. Acetone bath x 2
9. N_2 dry 15 min.

The reasons for the steps in this protocol will be made clear in the Results and Discussion section.

B. Fluorophore Labeling and Analysis

Slides are derivatized with fluorescein isothiocyanate (FITC) by addition of a freshly prepared 0.1 mg/mL solution of FITC in 0.2 **M** sodium bicarbonate buffer, pH 9.65. The slides are agitated in the solution for 10 minutes in the dark, rinsed for 5 minutes in DI H_2O, sprayed thoroughly with acetone, and transferred to an acetone bath. They were then dried with dry N_2 for 15 minutes in a parafilm-covered tray.

FITC labeling protocol:

1. FITC 0.1 mg/mL in 0.2 **M** NaBicarb buffer pH 9.65, 10 min
2. H_2O rinse 5 min
3. Acetone spray
4. Acetone bath
5. N_2 dry 15 min

FITC labeled slides were analyzed either by absorbance spectrometry or by fluorescence imaging. Absorbance spectra were collected on a Hewlett-Packard 8452 Diode-Array Spectrophotometer. Spectra were acquired for 25 seconds, and the absorbance calculated by subtracting the baseline from the peak value at 500 nm. The baseline was calculated by averaging the absorbance at 400 and 600 nm. The noise in this measurement is approximately .0002 Absorbance units. Absorbance measurements were converted to surface densities of fluorophore using Beer's Law. For fluorescein, 1 absorbance unit = 83.3 molecules/nm^2. (For details of this calculation, see Appendix B).

To evaluate fluorescence (and variation in fluorescence) across a slide, fluorescence imaging was performed with Fluorscan III, a prototype commercial confocal fluoresence scanner[9]. Briefly, slides were raster scanned in the focus (spot size < 15 μm) of a 10 mW Argon-Ion laser and the fluorescence measured with a photomultiplier tube. The data was collected with custom software and analyzed for average and standard deviation.

The high packing density often causes fluorescence quenching (see section H). As a result, fluorescence data alone cannot be used for quantification of bound molecules, although it still provides valid information on homogeneity across the surface.

C. Radiolabeling and Analysis

Silanized substrates were radiolabelled with 1 μL drops of a solution of 1-methylimidazole, 1-(3-dimethylaminopropyl)-3-ethyl carbodiimide (EDC), and ^{32}P-labeled ATP. 1 μL drops were dispensed onto 4 sites on each substrate under test and incubated for 16 hours in a closed container at room temperature, followed by 30 minutes at 37°C. The reaction was quenched with the addition of 2 μL 50 mM β-mercaptoethanol to each spot and allowed to stand for 15 minutes. The substrates were then immersed in TE buffer and stirred for 15 minutes, rinsed with TE buffer, and blown dry with dry N_2.

The spotting solution was a 1:2:7 mixture of 1 M 1-methylimidizole in H_2O, 1 M EDC in H_2O, and 3.33 mM ATP (specific activity of 400 Ci/mol) dissolved in DMSO. The ATP solution was prepared from a 1:2 mixture of 10 mM ATP and 0.33 uM ATP* (specific activity 6 x 10^6 Ci/mol) in water, which was dried under vacuum and redissolved in DMSO.

Radiolabeling protocol:

1. Spot 1 μL ^{32}P solution
2. Incubate 16 hr
3. Quench with 2 μL β-mercaptoethanol solution
4. Incubate 15 min
5. Stir 15 min in TE buffer
6. Rinse TE
7. Blow dry with N_2

The radiolabeled substrates were placed with standards on a phosphor cassette and allowed to expose for approximately 30 minutes. The phosphor cassette was read with a Molecular Dynamics phosphorimager and the counts per spot calculated with the ImageQuant software. The total ATP molecules bound per spot was calculated by comparison with the radioactive standard series.

D. Reagents

All solvents used were reagent grade, and were used without further preparation. APTES was from Sigma and Aldrich (98% pure). APDES and APMES are from Gelest (Tullytown, PA), and were 95% pure. APTMS was from Aldrich (97%). All were used as received.

FITC was from Aldrich or Molecular Probes and was >90% pure. ^{32}P ATP was purchased from Amersham and at a nominal specific activity of 6000 Ci/mmol.

E. Substrates

Standard 1x3" glass microscope slides (VWR, Corning) were employed as glass substrates. The silicon substrate was a single-crystal silicon wafer, <111> orientation, n^{++} doped to < .010 ohm-cm, and was purchased from Silicon Quest International. The SiO_2 substrate was SiO_2 grown on a single-crystal Si wafer by thermal oxidation, several thousand A thick. The Si_3N_4 substrate was Si_3N_4 deposited on a single-crystal silicon wafer by chemical vapor deposition. The gold substrate was 99.99% pure gold evaporated onto a standard glass microscope slide, more than several hundred A thick.

III. Results and Discussion

A. Substrate Comparison

Gold, glass, SiO_2, Si_3N_4, and single crystal Si samples were compared to test their aminosilane binding ability. Samples were cleaned, aminosilanized, radiolabeled, and analyzed according to the protocols described above. The results are shown in Figure 3:

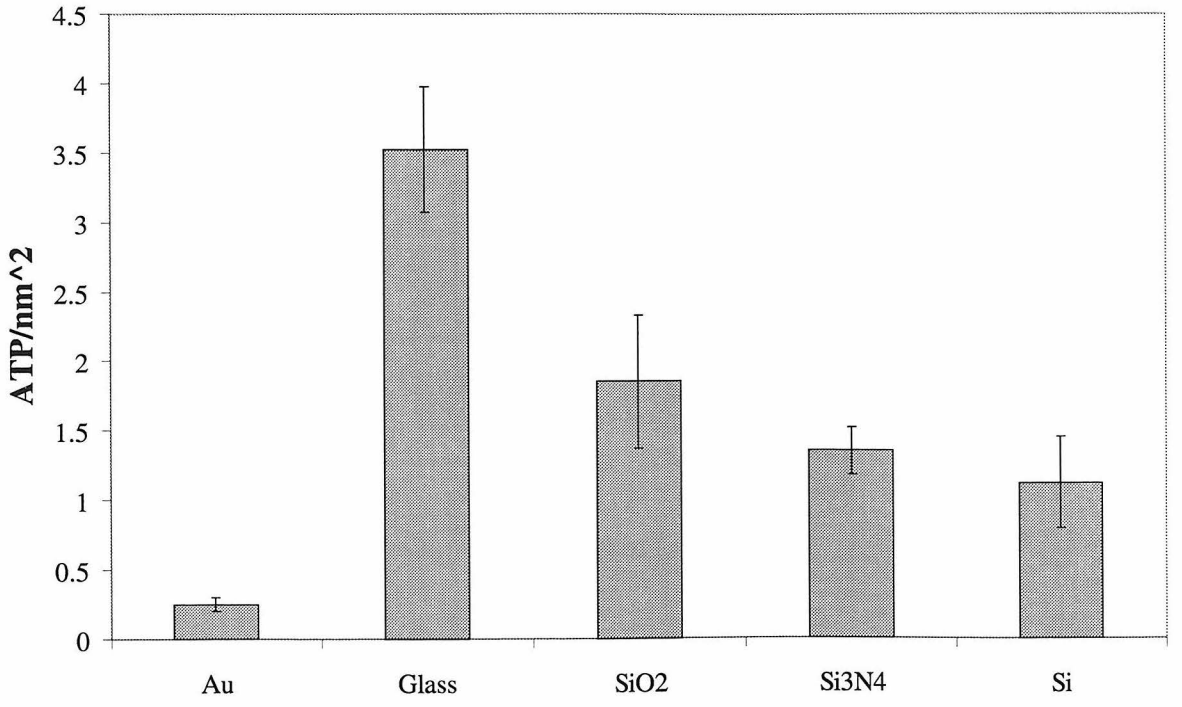

Figure 3: Bound radiolabel vs. substrate. Data is the average of 4 spots. Error bars are 2 standard deviations long in all figures presented.

Since ATP often shows high levels of nonspecific binding, we tested the substrates with DNA hybridization conditions. The radiolabeled substrates were incubated in hybridization buffer (6x SSC, 0.5 % SDS) at 37° C with gentle agitation for 1 hour, then washed twice for 10 minutes with 6 x SSC buffer, rinsed with TE buffer, blown dry, and

the bound radioactivity quantified with a phosphorimager. The results are shown in Figure 4:

These results indicate a ~80-90% loss of radiolabeled ATP during treatment with hybridization solution. Since the purpose of the hybridization solution is to hybridize complementary DNA while preventing nonspecific binding, the ATP that was lost may have been nonspecifically bound or merely chemisorbed, as opposed to covalently bound. It is also possible that the silane is being removed from the surface, but chemical durability studies (see Section J) suggest that removal of silane at pH 7 for 15 minutes should be minimal.

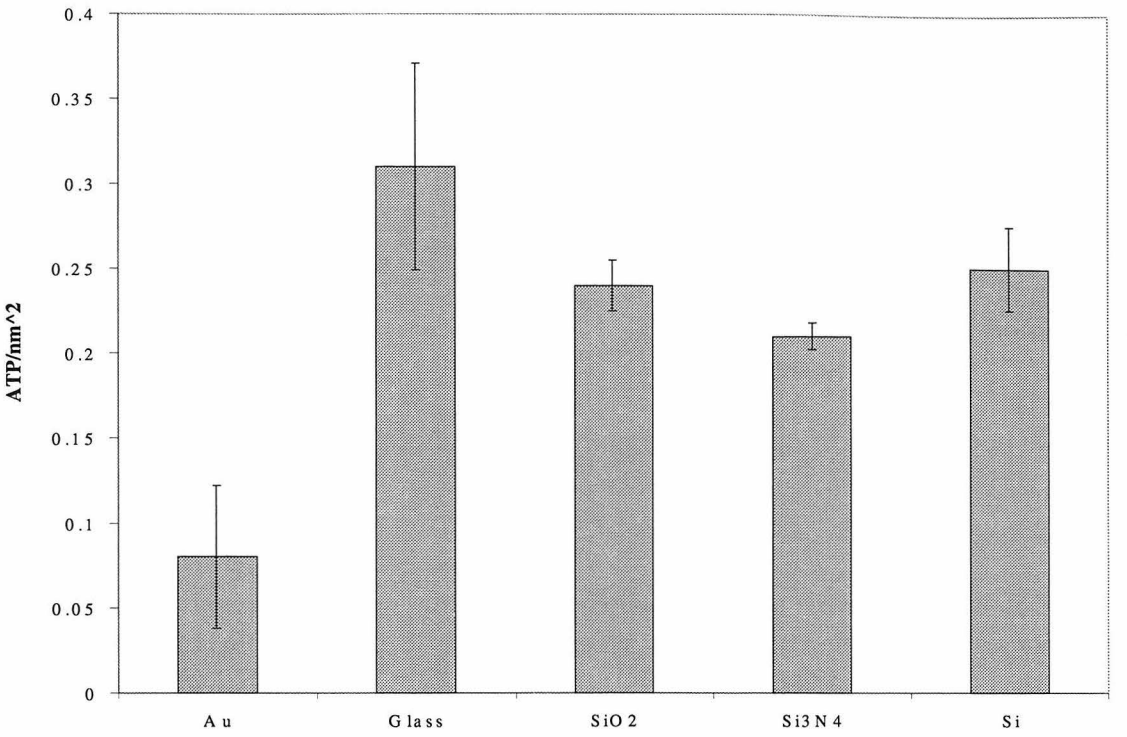

Figure 4: Bound radiolabel after washing

These results correlate reasonably well with the expected density of surface silanols. Glass may be somewhat rougher than the Si-wafer based substrates. SiO_2 is fully oxidized, but depending on its thermal history may have more bridging oxygens than free silanols. Si_3N_4 and Si both have a native oxide layer at the surface, which will bear surface silanols[10].

B. Precleaning

Glass slides as purchased are of very inconsistent cleanliness, ranging from quite clean to visibly encrusted with contaminants. Slides sonicated with detergent (Ivory dishwashing detergent) were compared with slides stirred in 2% detergent (Micro, Cole-Parmer

Instrument Division). Micro was found to be more effective for removing macroscopic contamination.

The effect of precleaning protocol on subsequent silanization and labeling was studied. Slides sonicated with Ivory for 20 minutes were compared with slides stirred in Micro for 20 minutes and slides with no precleaning. Absorbance and fluorescence were measured; the results are shown in Figure 5.

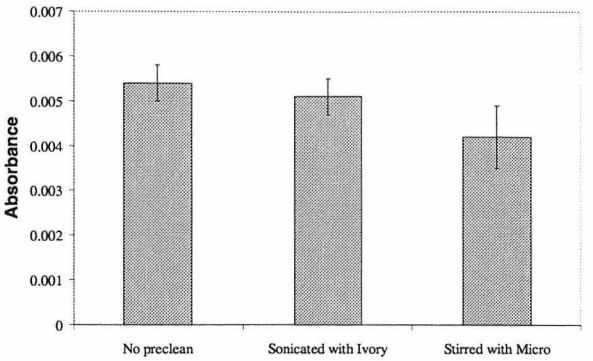

Figure 5a: Absorbance vs. precleaning method

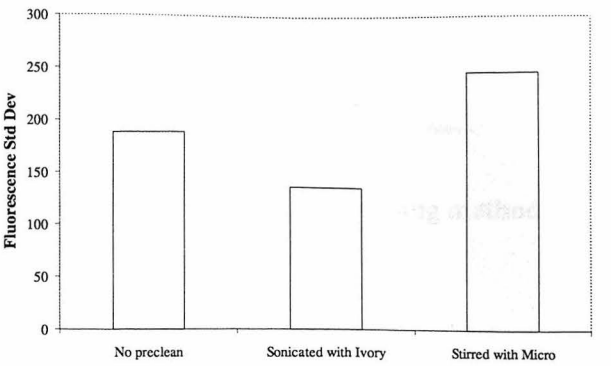

Figure 5b: Fluorescence homogeneity vs. precleaning method

The different methods give similar results. Sonication seems to have the best effect on homogeneity.

C. Cleaning

Slides were cleaned by several different methods, including stirring for 1 hour in concentrated H_2SO_4 at 70°C, 50/50 HCl/MeOH, and piranha solution (70:30 concentrated H_2SO_4 and 30% H_2O_2).

HCl/MeOH is clearly the superior method here, as measured by the higher absorbance. (See Figure 6a.) Quenching may be a factor at the HCl/MeOH absorbance level (see Section H); if so, the HCl/MeOH fluorescence results (Figure 6b) are erroneously low. Since they are already higher than the H_2SO_4 results, the fluorescence results confirm the superiority of HCl/MeOH. (The absorbance levels are low because an early version of the protocol was in use.) Concentrated H_2SO_4 may act as a dehydrating agent, shifting the equilibrium of surface species towards bridging oxygens as illustrated in Figure 7.

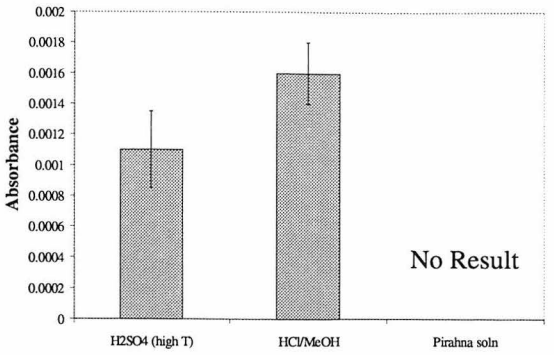

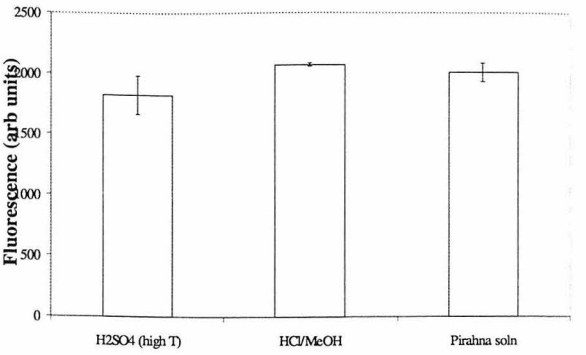

Figure 6a: Absorbance vs. cleaning method **Figure 6b: Fluorescence vs. cleaning method**

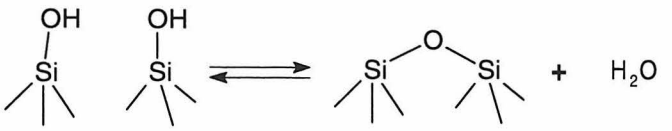

Figure 7: Surface oxygen equilibrium

HCl/MeOH solution can be re-used, but it eventually loses its potency. A comparison of fluorescence data shows that fresh solution has lower slide-to-slide variation and better homogeneity across the slide than solution used to clean ~100 slides:

Method	Slide-to-slide variation	Homogeneity (std dev)
New HCl/MeOH	58	185
Old HCl/MeOH	98	269

D. Drying effects

Whether the slides are dry or wet with solvent before immersion in the aminosilane solution has only a small effect on the outcome. Slides were cleaned with HCl/MeOH, and rinsed with water as per the standard protocol. They were then sprayed with methanol and put in a methanol bath. The "dry" slides were then sprayed with acetone and put in an acetone bath, and then dried with N_2 in a parafilmed tray before immersion in aminosilane solution. The "wet" slides were removed from the methanol and immersed in two subsequent baths of toluene before being put in the aminosilane solution. With APTES, "wet" and "dry" were identical to within experimental error. With APTMS, much more FITC is attached, raising the signal-to-noise level, and the "dry" slides were found to have 5% higher absorbance.

E. Solvent

Of a range of silanization solvents tried (including water, 100% ethanol, acetone, acetonitrile, DMSO, chloroform, toluene, and cyclohexane), toluene gives higher bound FITC than all but acetonitrile, which has a rather high slide-to-slide variability. Figure 8 shows compiled absorbance data from several experiments; the absorbance data has been ratioed to give toluene = 1.0 for ease of comparison.

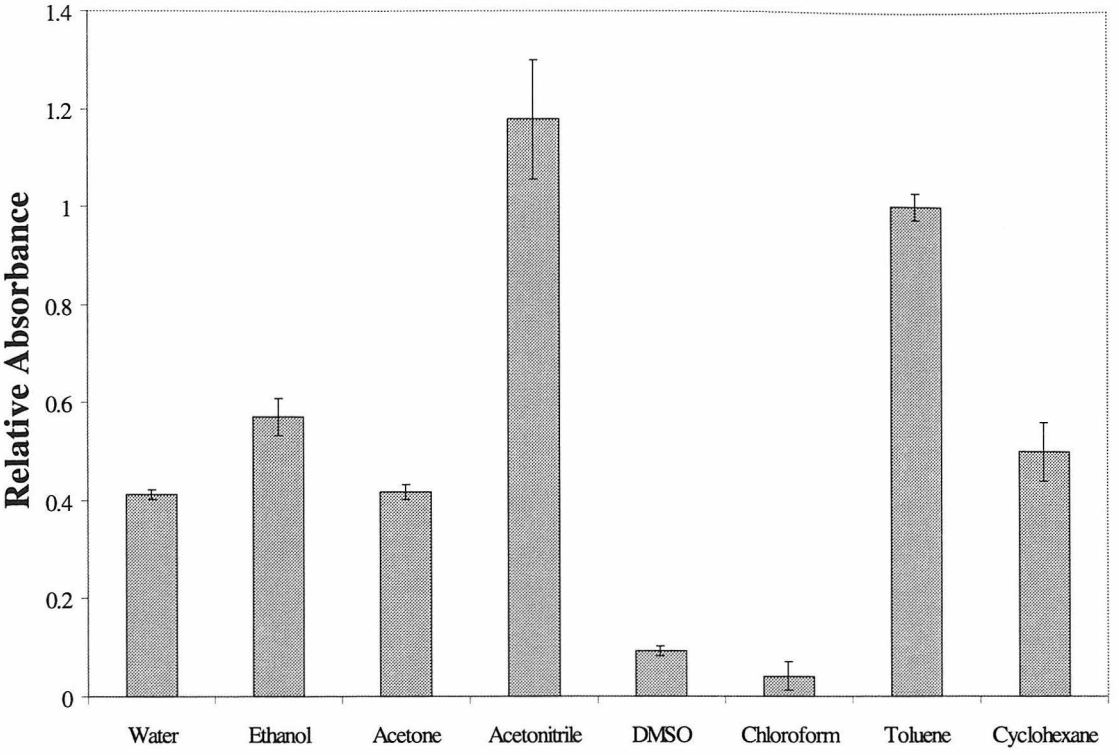

Figure 8: Absorbance vs. silane solvent

F. Variations in Silane

Variation of the aminosilane used can give tremendous variation in the amount of reaction-capable silane attached to the surface. In addition to aminopropyl**triethoxy**silane (AP**TES**), experiments were also run using 3-aminopropylmethyl**diethoxy**silane (AP**DES**), 3-aminopropyldimethyl**ethoxy**silane (AP**MES**, M for monoethoxy), and 3-aminopropyl**trimethoxy**silane (AP**TMS**). Aminosilane structures are shown in Figure 9.

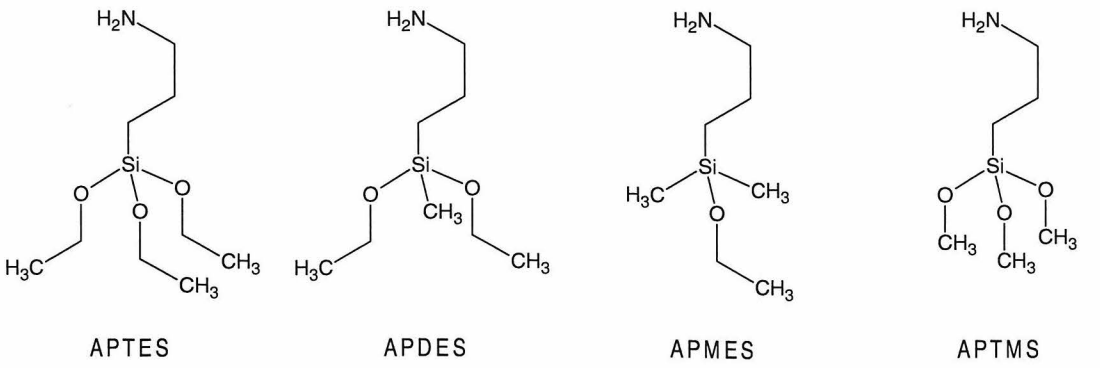

Figure 9. Aminosilane structures.

1. Ethoxy Number

Replacement of ethoxy moieties with methyl groups seems to alter both the kinetics and total amount of silane deposition on the surface. Figure 10 shows time series data of APTES, APDES, and APMES-bound FITC absorbance vs. silanization time.

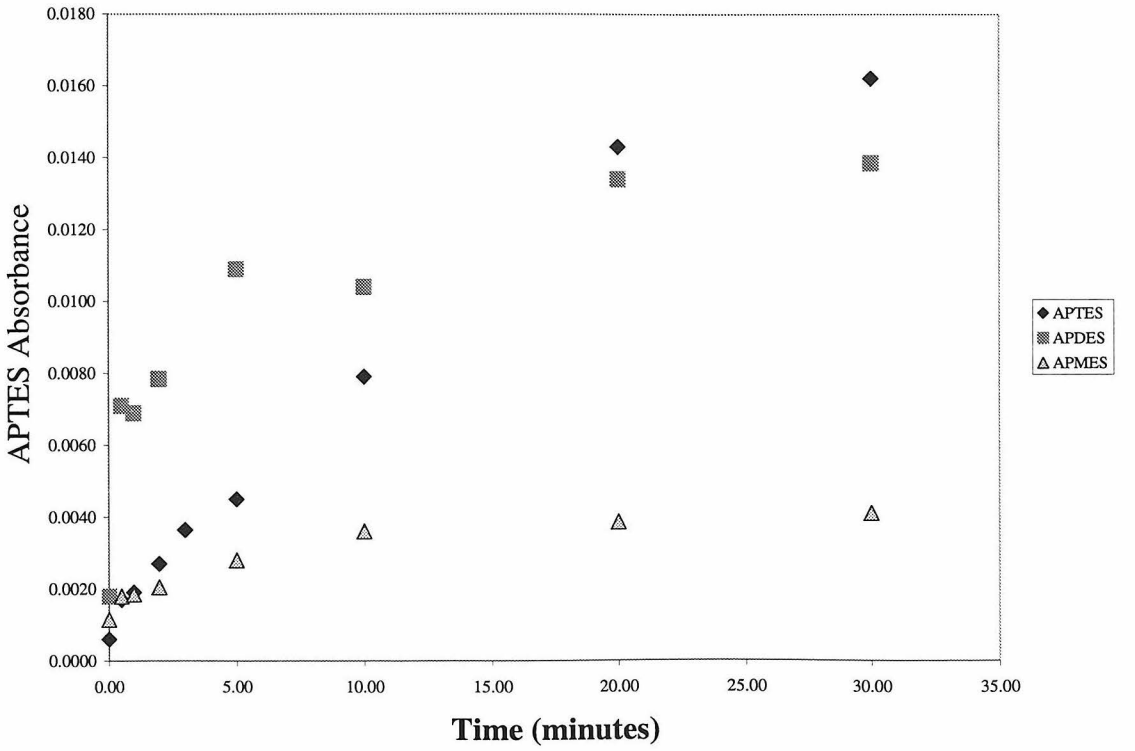

Figure 10: Kinetics variations with ethoxy number. Silane concentration was 4% for APTES and the molar equivalent for APDES and APMES.

APTES and APDES approach nearly the same maximum surface concentration, but APDES appears to bind to the surface much faster. While APTES deposition seems to be approximately linear for the first ~10 minutes, APDES deposition passes the linear range too quickly to be measured by this experiment. APMES seems to have kinetics intermediate between those of APTES and APDES, but approaches a maximum surface concentration that is approximately one-quarter that of APTES. Even taking into account the relatively large run-to-run variations in APTES surface concentration (see Section I.), and assuming that APMES would have similar variations, the difference between APTES and APMES maxima is still statistically significant: APMES clearly gives less reaction-capable silane on the surface.

2. Alkoxy Type

APTMS, on the other hand, gives vastly more reaction-capable silane on the surface than APTES. Figure 11 shows time series data of APTES- and APTMS-bound FITC absorbance vs. silanization time. The silane baths are 1% APTMS and 4% APTES. The APTES absorbance data are multiplied by a factor of 10 for ease of comparison.

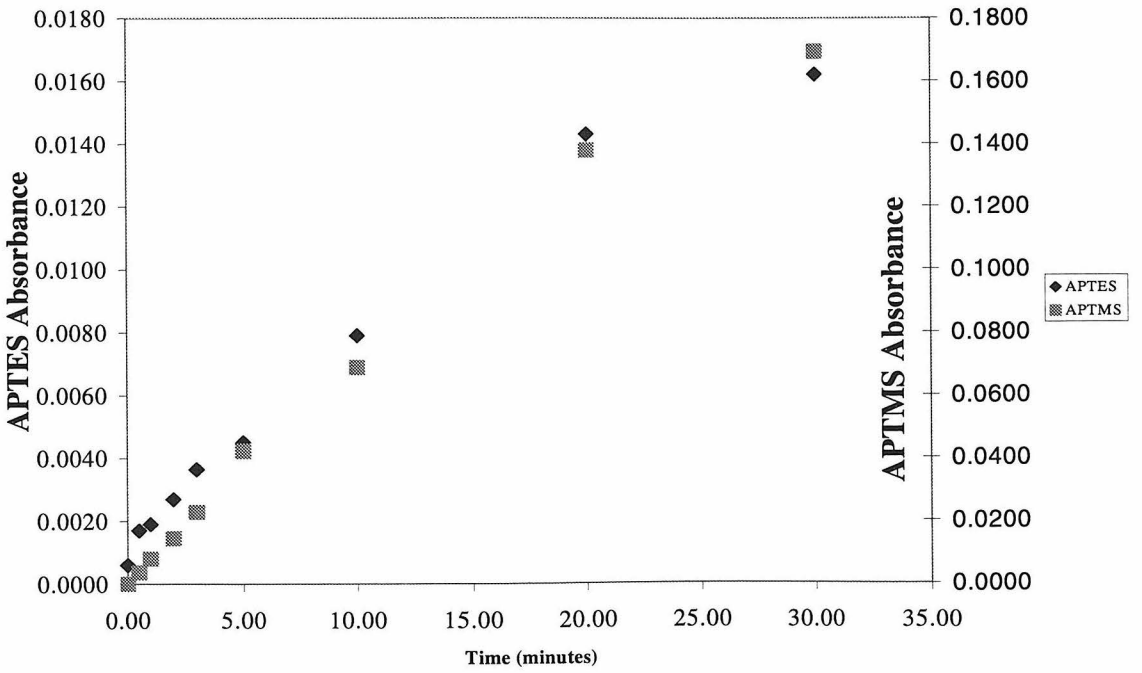

Figure 11: Kinetics variations with alkoxy type

The curves have approximately the same shape, but it is clear that APTMS is being deposited on the surface approximately 10 times faster and is approaching a maximum approximately 10 times as high, even with only one-quarter the silane present in solution. This data also makes it clear that APTMS does not form a monolayer: a FITC absorbance of 0.15 corresponds to a FITC surface density of 5.8 molecules/nm^2, which is physically

impossible for an FITC monolayer. APTMS is probably polymerizing. This is consistent with the more rapid hydrolysis of methoxy groups as compared to ethoxy[11].

G. Postderivatization Treatment (Rinsing, Drying, etc.)

1. Water Exposure

Empirically, aminosilanized slides are very sensitive to water: exposure to water seems to strongly reduce the ability of the aminosilanized surface to bind FITC. Aminosilanized slides prepared by the standard method were either immersed directly into FITC solution (dry), rinsed with DI H_2O and then immersed in FITC solution (wet), or rinsed with DI H_2O, placed in an acetone bath, dried with dry N_2, and then immersed in FITC solution (wet/dry). Figure 12 shows that dry slides have maximal binding and wet slides minimal, while drying the slides after wetting them with water restores less than 50% of the full FITC binding potential.

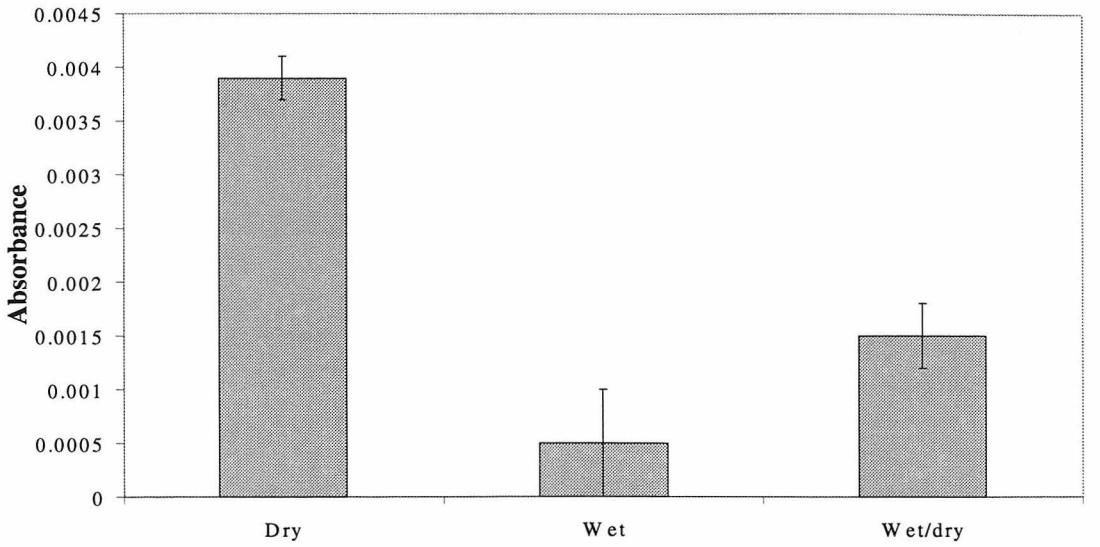

Figure 12: Effects of post-derivatization water exposure

One hypothesis is that the water on the wet slides forms a boundary layer through which the FITC must diffuse, and the reaction time is insufficient to allow effective diffusion to the aminosilane surface. If this is correct, then slides immersed wet into FITC should be incompletely labeled, and it should be possible to finish the labeling with another FITC reaction. "Wet" slides prepared as described above were split into two groups and re-labeled with FITC. One group was immersed dry into the FITC solution, while the other was rinsed with DI H_2O and immersed wet. Figure 13 shows the fluorescence results, with the "dry" slide results as a reference:

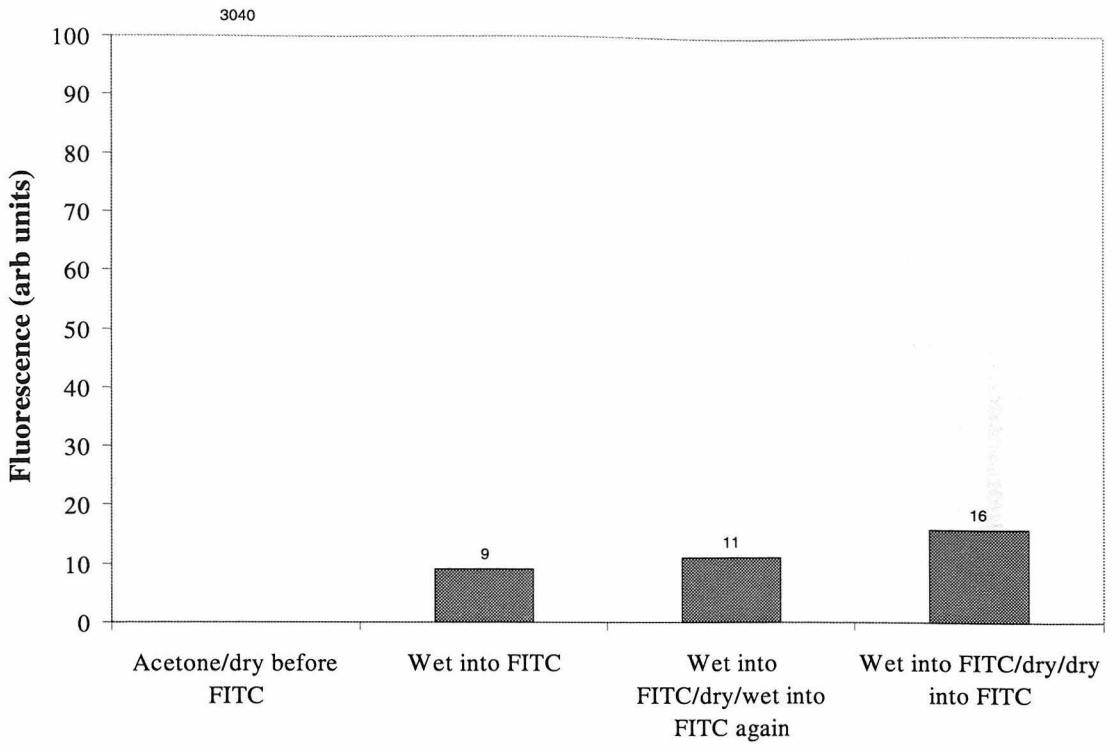

Figure 13: Effects of post-derivatization water exposure - fluorescence

The re-FITC'ed slides have not increased their fluorescence, indicating that the boundary layer hypothesis is incorrect. Exposure to water must chemically alter the NH_2 groups in some fashion.

2. Washing

Thorough post-silanization washing is essential to avoid inadvertent silanization. Anomalously high amounts of FITC were found to bind to blanks that were put back into the same solution as the derivatized slides after only two toluene baths. Apparently, some silane continues to desorb from the slides even after two baths in clean toluene. This problem does not occur with the full washing protocol (two toluene baths, an acetone spray and an acetone bath).

H. Fluorescence Quenching

Successful silanization and labeling can result in a high surface density of fluorophore being present on the substrate surface. Such close proximity of fluorophores can cause

fluorescence quenching, as illustrated in Figure 14, which shows FITC absorbance and fluorescence as a function of silanization time:

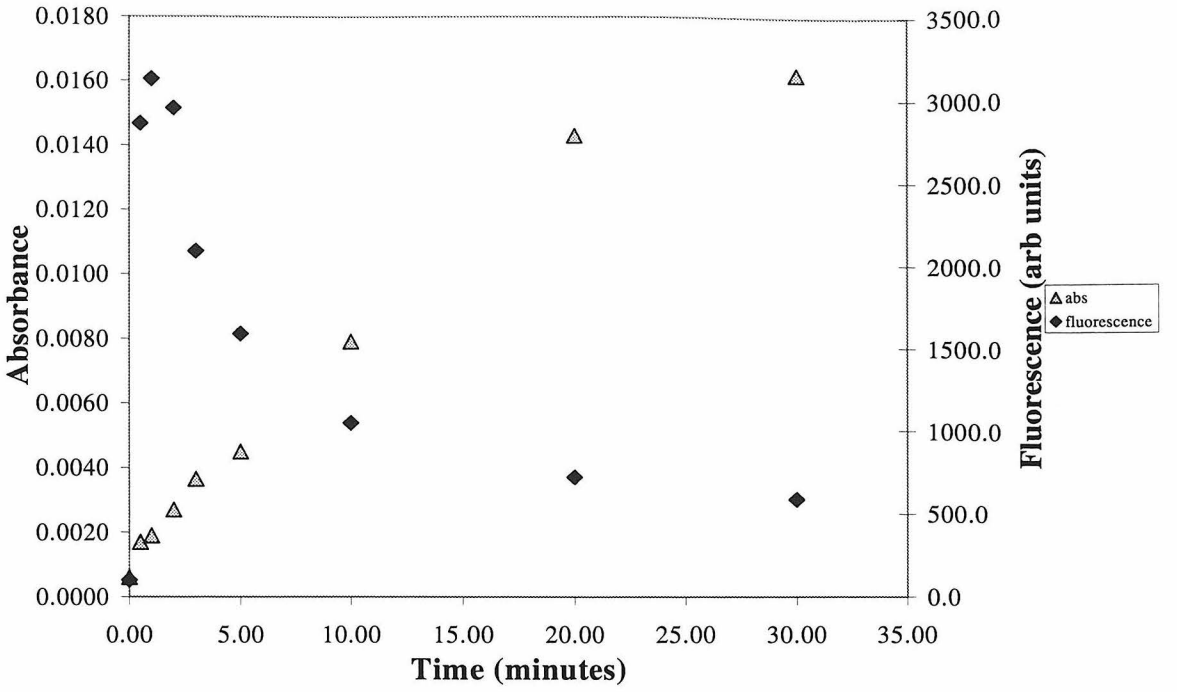

Figure 14: Absorbance and fluorescence vs. silanization time

Several attempts were made to eliminate quenching by diluting the fluorophore on the surface. Methyl isothiocyanate was used in an attempt to consume a fraction of surface amino groups and prevent the attachment of quenching quantities of FITC. Quenching can be reduced this way: the slides treated with MITC have the lowest quenching of any experimental run (data not shown). However, even with 5 mg/mL MITC pretreatment (a 50-fold greater concentration than our normal FITC protocol) for 15 minutes, quenching is not eliminated.

I. Consistency

The standard protocol produces batches of slides with very little variation from slide to slide and good homogeneity across the slide, as illustrated in Figure 15:

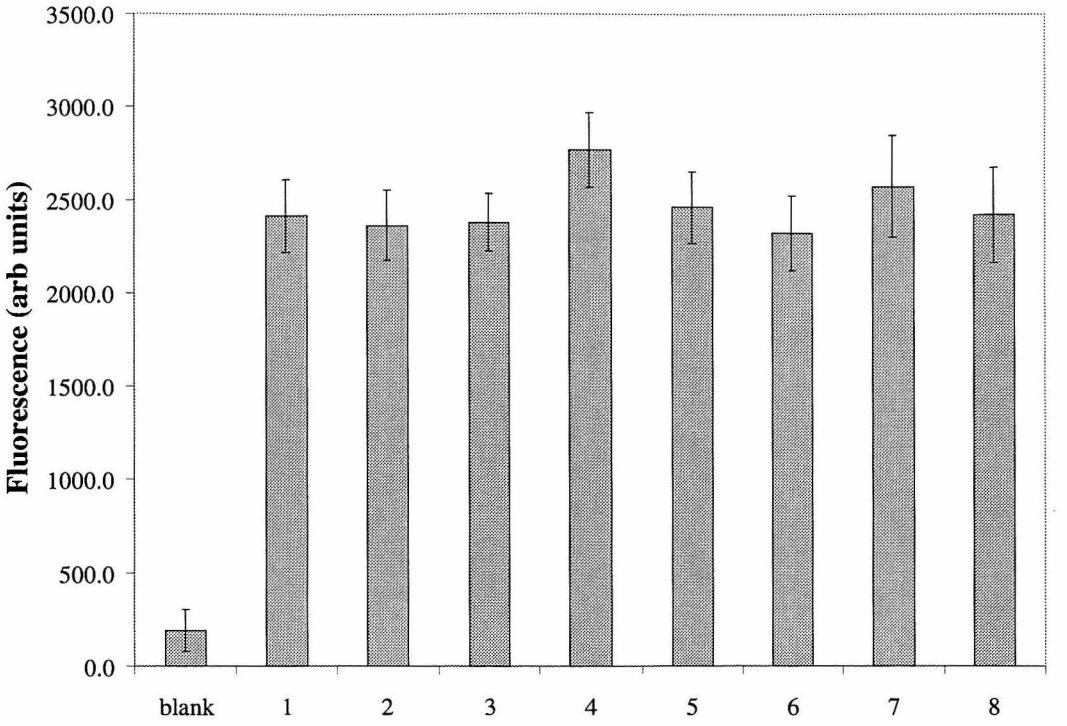

Figure 15: Silanization consistency

The slide-to-slide relative standard deviation is 5.9%. The relative standard deviation of fluorescence values across a slide is 8.5%.

In spite of very careful control of experimental conditions, the batch-to-batch variations are still moderately high. For all slides silanized with the standard protocol, using 4% APTES for 20 minutes, the average absorbance is .0082 +/- .0029, a relative variation of 35%.

J. Chemical Durability

1. Curing

Aminosilanized slides prepared by the standard protocol were tested for FITC binding activity after a number of different treatments, including "curing" at different temperatures, the effects of different pH, and stability under conditions employed in DNA hybridization.

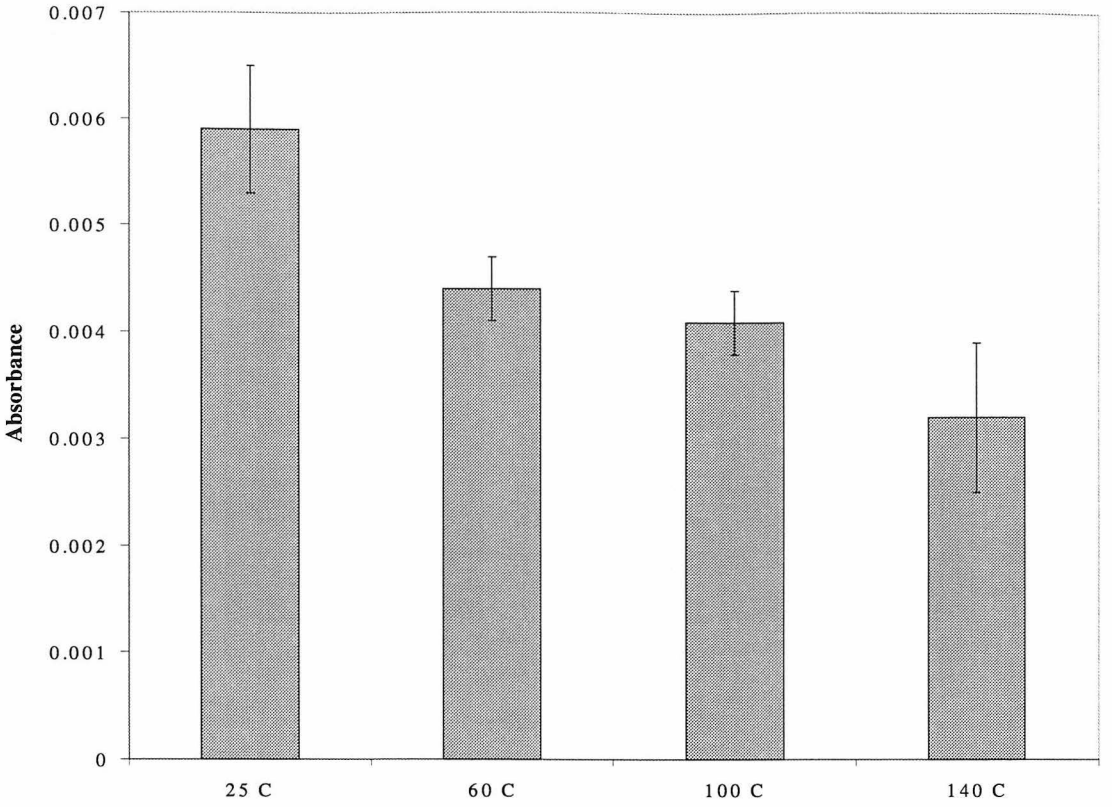

Figure 16: Effects of curing

Curing the aminosilane reduces the FITC binding activity. The higher the curing temperature (for 1 hour), the more the activity is reduced. Figure 16 shows absorbance data for different curing temperatures.

Curing reduces the binding activity over the course of approximately 1 hour (data not shown). Although it does reduce the FITC binding activity, curing is found to improve stability in low pH solutions (see below).

2. pH and Temperature

FITC-labeled slides were incubated in solutions of various pH for 1 hour, then rinsed with DI H_2O, washed twice in acetone, and dried with dry N_2 in a parafilmed tray. The aminosilanized surface is found to be stable at pH 4.8 – 9.5, but not for extremes of pH (6 N HCl or 1 M NaOH). As expected, base attacks the surface more aggressively than acid. At high temperatures, even the more moderate pHs have some deleterious effect:

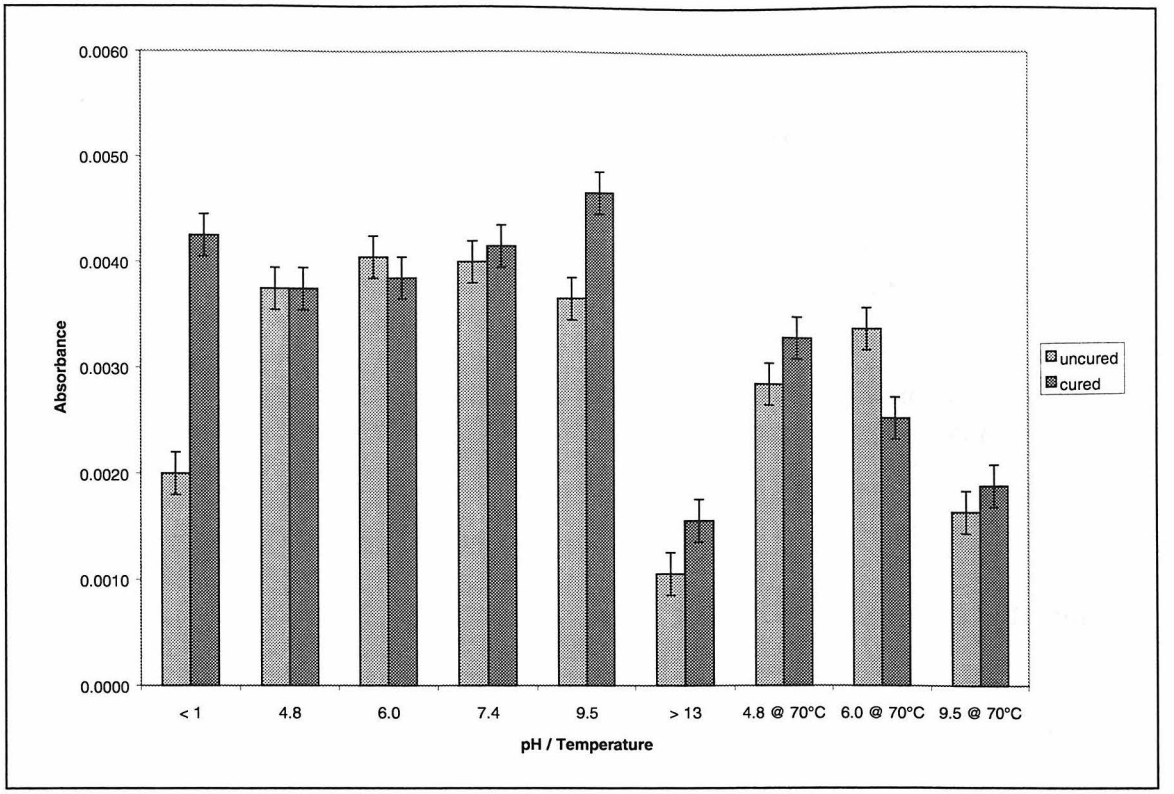

Figure 17: Resistance to pH and temperature for cured and uncured slides

An aminosilane surface cured at 140° C for 1 hour shows improved resistance to acid and base. Figure 17 shows the effects of temperature and pH on cured and uncured slides.

IV. Conclusions

For the silanization protocol, we draw the following conclusions:

Substrate: Glass, SiO2, and Si are equally good substrates within experimental error. Si3N4 is slightly worse, and gold is significantly worse.

Precleaning: Micro works better to remove macroscopic contamination, although it seems to reduce subsequent silanization yield slightly and result in slightly higher variation across the substrate.

Cleaning: HCl/MeOH maximizes silanization while minimizing variation across the substrate. Variation with different methods is moderate.

Pre-drying: Immersing the substrates wet or dry into silanization solution makes no difference.

Solvent: Choice of solvent is critical. Toluene and acetonitrile worked best. Toluene gives less variation from slide to slide.

Ethoxy Number: Variations in ethoxy number have large effects on both endpoint and kinetics. Monoethoxy silane (APMES) yields far less bound silane. Binding speed is APDES >>APMES > APTES.

Alkoxy Type: Variations in alkoxy type also have large effects on both endpoint and kinetics. APTMS yields far more bound silane than APTES (although probably as a result of polymerization).

For the post-silanization experiments, we conclude:

Postderivatization Water Exposure: Exposure to water nearly eliminates FITC binding. Drying the substrates restores <50% of reactivity.

Curing: Curing reduces FITC attachment, but increases stability vs. acid and base.

pH and Temperature: Bound silane is attacked by extremes of pH; increased temperature reduces the margin of stability.

Using the standard method presented here, silanol-bearing surfaces can be aminosilanized with excellent consistency across the surfaces (8.5% variation) and within a batch (5.9% variation), and (nearly) acceptable consistency from batch to batch (35% variation). The number of molecules bound correlates with the expected surface silanol concentration, and is influenced by the nature of the substrate (i.e., Si, Si_3N_4, glass, etc.) and its preparation (i.e., cleaning).

Labeling with fluorophores and radiolabeling (with proper removal of non-specifically bound label) are found to be consistent and accurate methods to measure the surface density of amino groups. Silanization and labeling with dye molecules can easily produce surface densities of fluorophores high enough to cause fluorescence quenching. Hence, measurements of absorbance are much more informative for assessing surface densities. Absorbance and radiolabeling methods agree on an average surface density of 0.31 +/- 0.11 molecules/nm^2 (51 pmol/cm^2) for glass substrates treated with the standard method.

0.31 +/- 0.11 FITC molecules/nm^2 gives a mean FITC-center to FITC-center distance of 1.79 nm. The width[12] of fluorescein is ~1.0 nm. Assuming a planar surface and FITC molecules rotating freely around their central bond, this spacing means that the space between molecules is smaller than a new molecule of fluorescein.

[1] Angeletti, E., Canepa, C., Martinetti, G., Venturello, P. (1988). Silica Gel Functionalized with Amino Groups as a New Catalyst for Knoevenagel Condensation Under Heterogeneous Catalyst Conditions. *Tetrahedron Letters.*, **29**, 2261

[2] Pirkle, W.H., Pochapsky, T.C. (1989). Considerations of Chiral Recognition Relevant to the Liquid Chromatographic Separation of Enantiomers. *Chem. Rev*, **89**, 347

[3] Buszewski, B., Lodkowski, R. J. (1991). Isolation and Determination of Sugars in Nicotian-Tabacum on Aminopropyl Chemically Bonded Phase using SPE and HPLC. *Liquid Chromatography*, **14**, 1185.

[4] Airoldi, C., Alcantara, E.F.L.C., (1989). *Colloids Surf.*, **39**, 291

[5] Markovich, R.J., Qiu, X.X., Nichols, D.E., Pidgeon, C., Invergo, B., Alvarez, F.M. (1991). Silica Subsurface Amine Effect on the Chemical, Stability and Chromatographic Properties of End-capped Immobilized Artificial Membrane Surfaces. *Anal. Chem.* **63**: (17) 1851-1860

[6] Weetall, H.H. (1993). Preparation of Immobilized Proteins Covalently Couples Through Silane Coupling Agents to Inorganic Supports. *Applied Biochemistry and Biotechnology*, **41**: (3) 157-188

[7] Muramatsu, H., Dicks, J.M., Tamiya, E., Karube, I. (1987). Piezoelectric Crystal Biosensor Modified with Protein-A for Determination of Immunoglobins. *Anal. Chem.* **59**: (23) 2760-2763

[8] Chrisey, L.A., Lee, G.U., O'Ferrall, C.E., (1996). Covalent Attachment of Synthetic DNA to Self-Assembled Monolayer Films. *Nucleic Acids Research*, **24**: (15) 3031-3039

[9] Combion, Inc. – since acquired by Incyte Pharmaceuticals.

[10] Raider, S.I., Flitsch, R., Aboaf, J.A., Pliskin, W.A. (1976) *J. Electrochem. Soc.* **124**(4), 560-565

[11] Silane Coupling Agents, 2nd ed. Edwin P. Plueddemann, Plenum Press, New York, 1991

[12] Based on an atom-to-atom measurement on a 3D-optimized model in ACD/3D, software by Advanced Chemistry Development, Inc., Toronto, Canada.

CHAPTER FIVE

Etched Chalcogenide Fibers for Near-Field IR Scanning Microscopy

Typical infrared transmitting fibers comprise a chalcogenide core surrounded by a sulfur-selenide cladding, which is in turn coated with a polymer such as polyamide. For use in a Near-field Scanning Infrared Microscope (NSIM), such infrared-transmitting fibers must be tapered to a sharp point. Sharper points allow smaller apertures, which allow higher resolution. The light throughput of the probe depends on the length of the taper region: the longer the taper length, the further the IR radiation must propagate through a waveguide smaller than its wavelength. Thus, shorter taper lengths should give higher light throughput.

*This chapter describes a method for etching chalcogenide fibers to sub-micron points by simple chemical means. Methods are described for removal of the polyamide coating, stripping of the SSe cladding surrounding the core, and etching the chalcogenide fiber core to a sharp point. Removal of the polyamide coating is most easily accomplished by dissolution in 4-Chloro-1-butanol. The SSe cladding is removed by soaking the fiber in 0.1 **M** NaOH overnight. The chalcogenide core is tapered to a sharp point by immersion in a two-phase etching system, where the top phase is an inert organic solvent, and the bottom phase is a strong oxidant. Fibers both with and without cladding have been tapered. The resulting fibers have a taper length on the order of the core diameter, and terminate with a sub-micron end-radius-of-curvature. The throughput of etched tips is measured, and the potential for use in a near-field scanning IR microscope (NSIM), as well as other uses, is discussed.*

I. Introduction

Near-field Scanning Optical Microscopy (NSOM) allows optical microscopy[1,2,3,4,5] and spectroscopy[4,5,6] with resolution on the order of 10-100 nm, which is far smaller than the far-field diffraction limit ($\lambda/2$). Part of the price for achieving this resolution is the necessity of constructing a probe with an aperture of the size of the desired resolution. As with all scanned probe techniques, the power of the technique depends in large part on the quality of the probe.

Typical NSOM instruments use a pulled optical fiber, coated with metal except for an aperture at the apex, for a probe. They are therefore limited to the wavelength range transmitted by the fiber. With glass (SiO_2) fibers, this is typically[7] 375-850 nm. The throughput (measured in the far field) is typically[8] 10^{-5} - 10^{-6}.

Near-field Scanning Infrared Microscopy (NSIM) is an obvious extrapolation of the NSOM technique. In principle, NSIM has a definite advantage over NSOM: in contrast to the visible region, almost every molecule has an absorption in the IR region. Furthermore, IR absorption bands give direct information about the presence and nature of molecular bonds in the observed region.

High spatial resolution Raman microscopy is another way to extract molecular specific information from a sample. It is known that Raman and IR absorption spectroscopy provide somewhat complementary information due to the nature of IR radiation interaction with the matter. However, NSIM with a tapered fiber probe provides an advantage over Raman imaging: the probe is maintained at constant distance from the sample while scanning which provides topographical information in addition to IR absorption data. As in NSOM, this provides a means to correlate topographical information with spectroscopic data.

Several near-field IR microscope designs have been published[9,10,11,12,13]. To date, however, only two of them[11,12] have made use of IR-transmitting fibers. This is probably because making NSIM probes from IR fibers has been very difficult.

The primary source of difficulty in making NSIM probes from IR fibers is the physical properties of the fiber material. Perhaps the most tractable set of compounds from which IR-transmitting fibers are made is the chalcogenides. Chalcogenide fibers have good chemical stability and are less brittle than the other families of compounds from which IR fibers have been made. Like optical fibers, they are also glasses, so they can be heat-pulled with a capillary puller in a fashion similar to optical fibers. However, heat-pulling chalcogenide fibers is significantly more difficult than heat-pulling glass (SiO_2) fibers. It has been accomplished, to our knowledge, only by Hong[12] *et al.* Pulled IR fibers also have relatively low light throughput (on the order of 10^{-6}, measured in the far field[14]). They also have a very long taper length (several mm - See Figure 1).

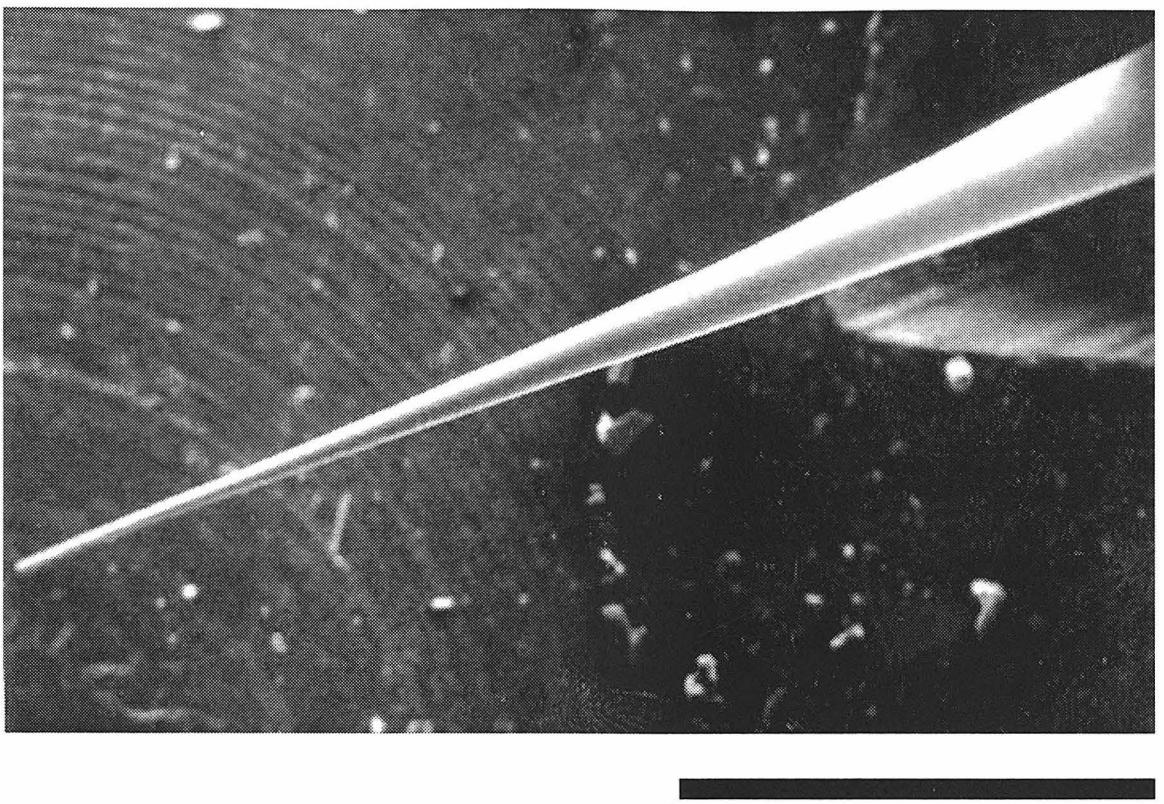

Figure 1: SEM micrograph of heat-pulled chalcogenide fiber. Scale bar = 1 mm. Note the long taper length.

Zeisel *et al.* have reported[15,16] that chemically etched optical fiber probes have far-field light throughput that is 100 - 1000 times greater than pulled fiber probes, probably because the taper region is much shorter. A longer the taper region means a longer region where radiation must propagate in a waveguide narrower than its wavelength. A shorter taper region is thus expected to deliver light more efficiently to the aperture, resulting in higher intensity in both the propagating (far field) and non-propagating (near-field) components. It is thus a reasonable assumption that the increase in far-field throughput mirrors a proportional increase in near-field intensity.

In the present work we describe the application of a simple chemical etching technique to IR-transmitting chalcogenide fibers. The fiber probes etched this way taper to a sharp point ($\leq$ 150 nm end-radius-of-curvature) in approximately one fiber diameter (~ 100 μm). Such sharp probes when scanned in position feedback will easily give spatial topographical resolution of 150nm. One should distinguish topographical resolution

from the spatial resolution of IR imaging, which will be determined by the size of the aperture used.

Simple chemical methods are also described for the removal of the polyamide plastic coating and sulfur-selenide cladding used on these chalcogenide fibers. We also present a preliminary data about the IR radiation throughput measured with etched fibers.

II. Experimental

Chalcogenide fibers were obtained from Amorphous Materials, Inc., 3130 Benton, Garland, TX 75042. Both thin (unclad, but plastic coated) and thick (clad and plastic coated) fibers were used in this study. In both cases the chalcogenide core is an As-Se-Te glass. The cladding is primarily S-Se. Both types of fiber are Plate # 94-131-8, Run # 71395.

Thin fibers have a core diameter of .0058 inch (145 μm) and a polyamide coating .0009 inch (22.5 μm) thick (for a total fiber diameter of .0076 inch (190 μm)).

Thick fibers have a core diameter of .010 inch (250 μm), S-Se cladding .004 inch (100 μm) thick, and a polyamide coating .003 inch (75 μm) thick (for a total fiber diameter of .024 inch (600 μm)).

In the process of creating the fiber probes it was useful to use an optical microscope with an epi-fluorescence / reflectance microscopy attachment. The polyamide coating is slightly fluorescent (under both blue and green light) making it easy to tell if it has been completely removed. Microscopy of the probes under both backlighting and reflected light makes it much easier to determine the shape of the fiber.

The best method for examination of the probe tip is scanning electron microscopy. Chalcogenides are semiconductors, so sputtering the tips with gold is not strictly necessary, although it does improve image clarity at very high magnifications.

III. Results and Discussion

A. Polyamide Coating Removal

The polyamide coating can be easily removed by repeatedly immersing the coated fiber in stirred room-temperature solvent for 1-2 minutes and wiping with a laboratory tissue. Several solvents work for this purpose, including 4-chloro-1-butanol, methanol, and acetone. Properly stripped fibers feel very smooth when wiped with a laboratory tissue; if not all the polymer has been removed, higher friction can be noticed.

B. Cladding Removal

If the fiber is clad, the cladding must be removed before etching. The cladding can be removed by soaking the polyamide-stripped fiber in room-temperature 0.1 **M** NaOH for approximately 18 hours. At the end of this time, the portion of the fiber that was in the NaOH solution generally has lost its reflective sheen. Upon wiping gently with a laboratory tissue, the treated portion of the cladding will come off the core.

If the fiber is removed from the NaOH solution too soon, wiping will not remove the cladding, but the fiber may be safely put back in the solution. We hypothesize that the NaOH must diffuse completely through the cladding before the cladding will come off. If the fiber is left too long in the NaOH solution (> 24 hours), the NaOH will very slowly start to etch the chalcogenide core.

If the polyamide comes into contact with the NaOH solution, the core may become extremely brittle, especially at the point of contact.

C. Chalcogenide Core Etching

Once the core has been exposed, etching the core is straightforward. A container is prepared with a two-phase etching system. The lower phase is the etchant solution, while the upper phase is a protective solvent. (See Figure 2.)

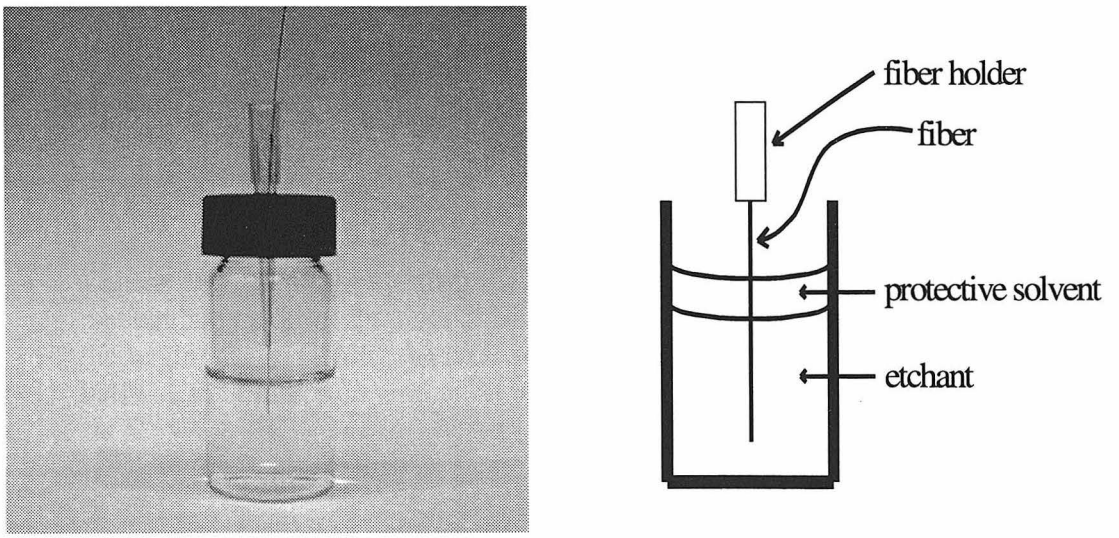

Figure 2: Schematic and photo of the two-phase etching apparatus. Only 1-2 mm of protective solvent are required. The protective solvent serves to keep the meniscus flat at the fiber-etchant interface.

The etchant solution is piranha solution, a 7:3 mixture of concentrated sulfuric acid and 30% hydrogen peroxide. *Caution! Piranha solution may react violently with organic compounds and should not be stored in sealed containers.* Many different organic compounds may serve as the protective solvent. The authors have had the most success with tetramethylpentadecane (TMPD), polydimethylsiloxane (PDMS) and CCl_4, with TMPD having the best long-term stability against piranha solution.

The fiber is immersed in the etching system. At room temperature and without stirring, the fiber will "neck in" approximately one diameter down from the solvent-piranha meniscus. Ultimately, the "neck" will be completely etched through, and the lower piece will fall off. (See Figures 3 and 4)

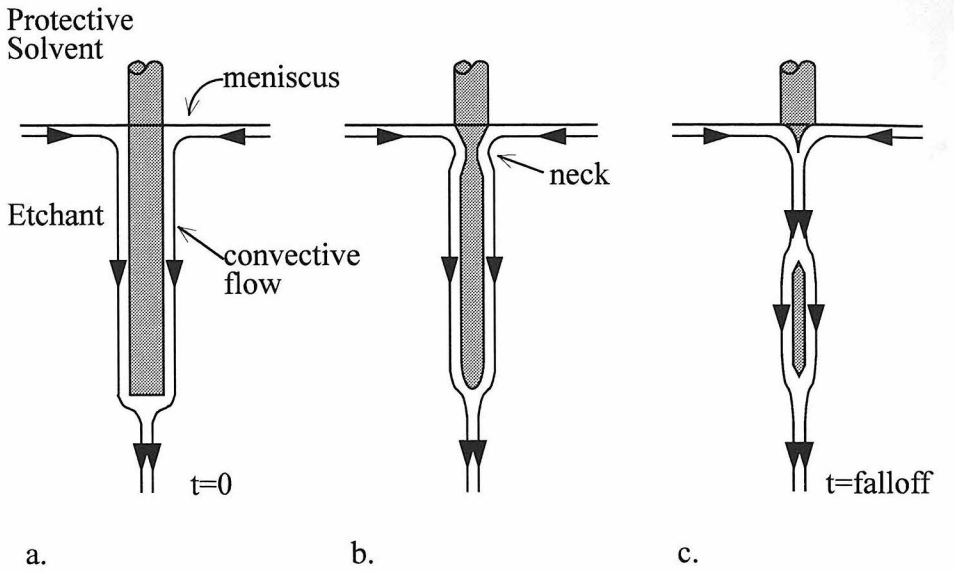

Figure 3: Two-phase etching mechanism. Schematic of etching mechanism under normal conditions (convective control). **a:** The system at the beginning of etching, **b:** after etching has progressed approximately halfway to completion, and **c:** At the falloff point.

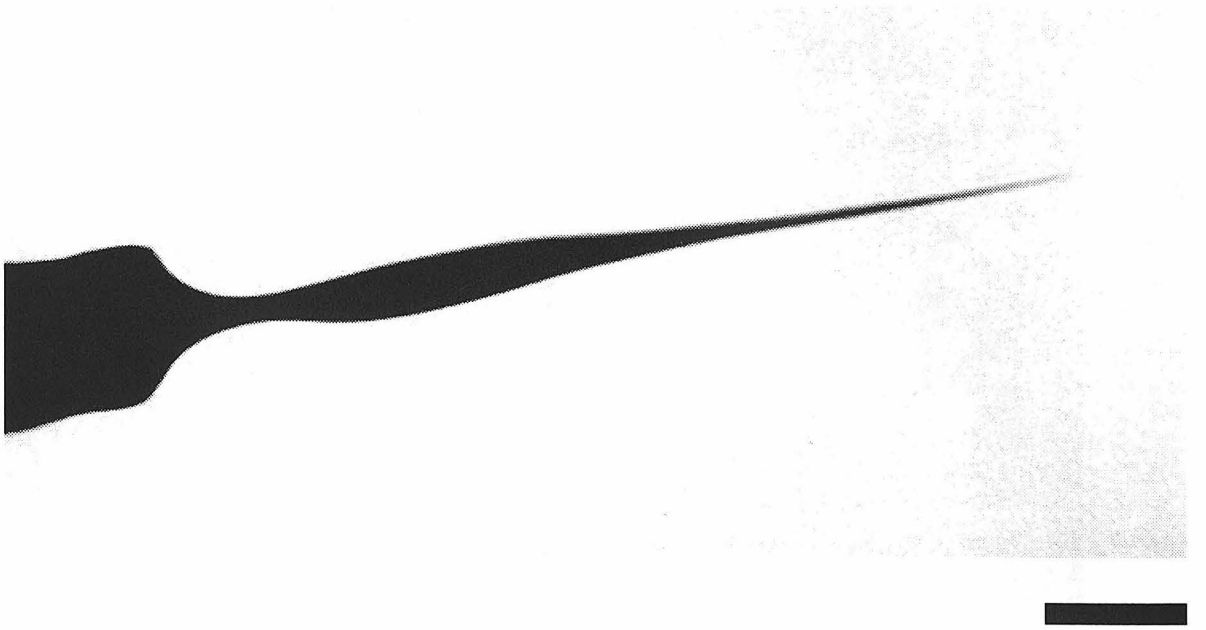

Figure 4: Fiber removed from etching solution before falloff point. Optical micrograph. Scale bar = 150 μm. Note the pronounced "neck."

This is referred to as the "falloff" point. The time it takes to reach "falloff" depends on the age of the piranha solution, its temperature, and the thickness of the chalcogenide core. As a guideline, with freshly made piranha at room temperature, and a 145 μm core, etching takes ~15 minutes. With 2-month old piranha (stored at 5°C), starting slightly below room temperature, and a 250 μm core, etching takes ~50 minutes. Etching times are relatively consistent, but variations of a few minutes must be allowed for.

Approximately 30 seconds after the "falloff," the fiber is withdrawn from the etchant, washed in gently stirred room-temperature methanol, and gently blown dry with N_2 (blowing on-axis onto the tip, rather than from the side).

Figures 5 and 6 show an etched unclad 145 μm fiber. Figures 7, 8, and 9 show an etched, clad fiber with a 250 μm core.

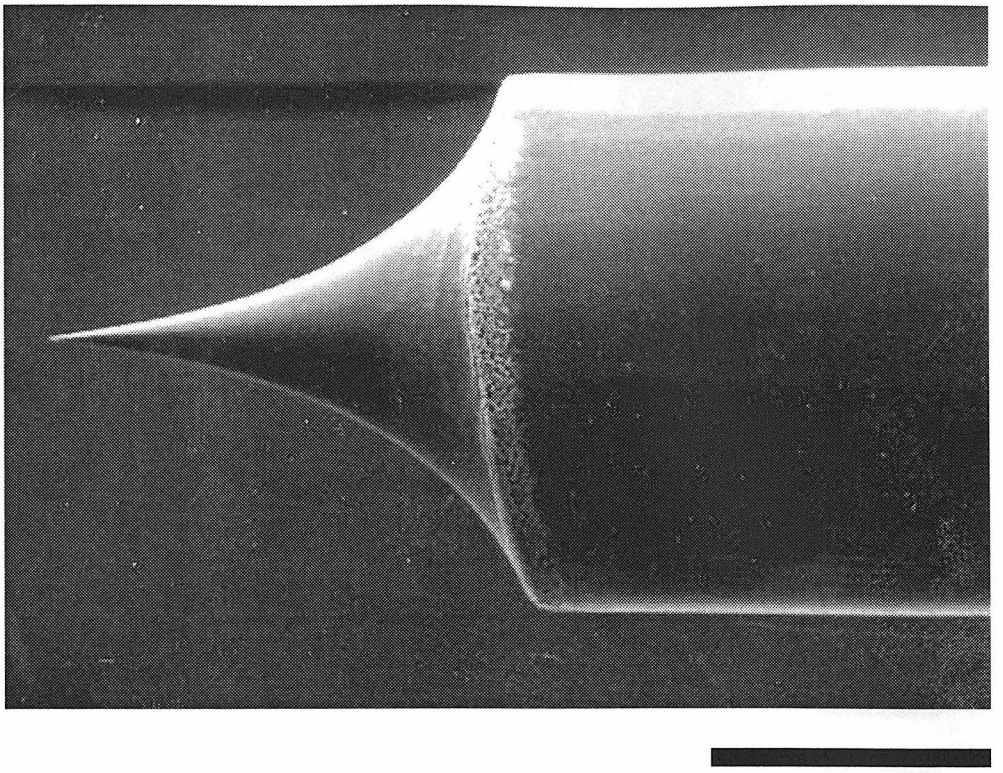

Figure 5: Optical micrograph of a 145 μm diameter core chalcogenide fiber etched by the described method. Scale bar = 100μm.

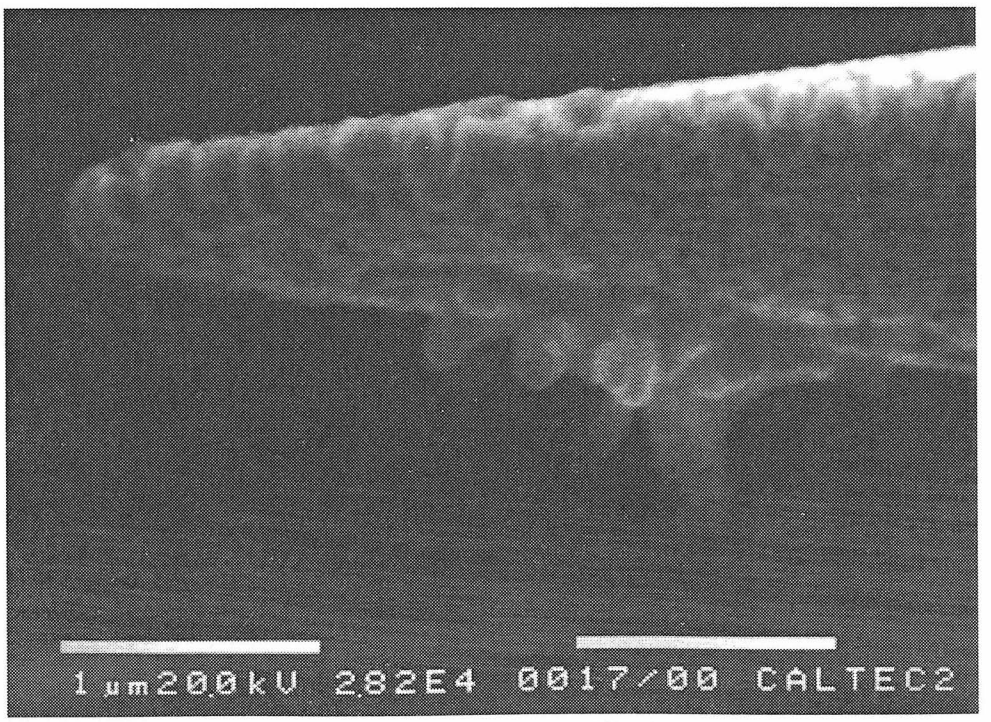

Figure 6: Zoom onto the apex of the tip shown in Figure 5. Scale bar = 1μm. The corrugations and the structure on the underside of the tip are believed to be due to the thin layer of gold applied for SEM imaging.

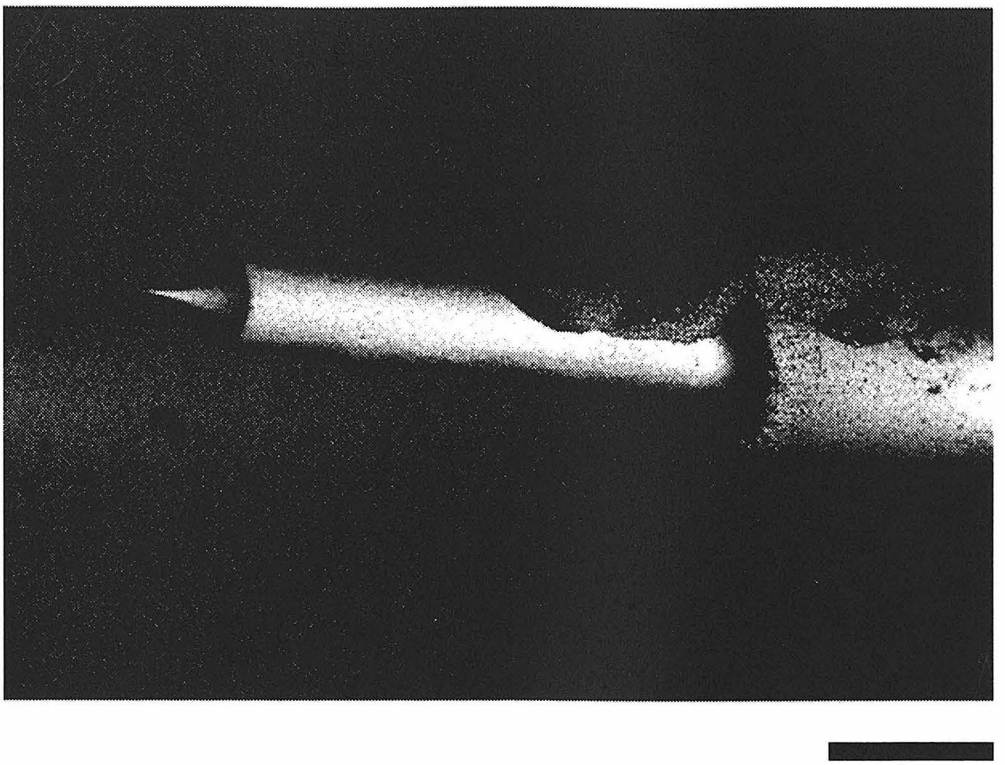

Figure 7: SEM micrograph of a 250 μm diameter core chalcogenide fiber etched by the described method. Scale bar = 500 μm. Removal of the clad and etching of the core are visible. The "blob" at the top is silver paint applied to provide a conductive path to ground for SEM imaging.

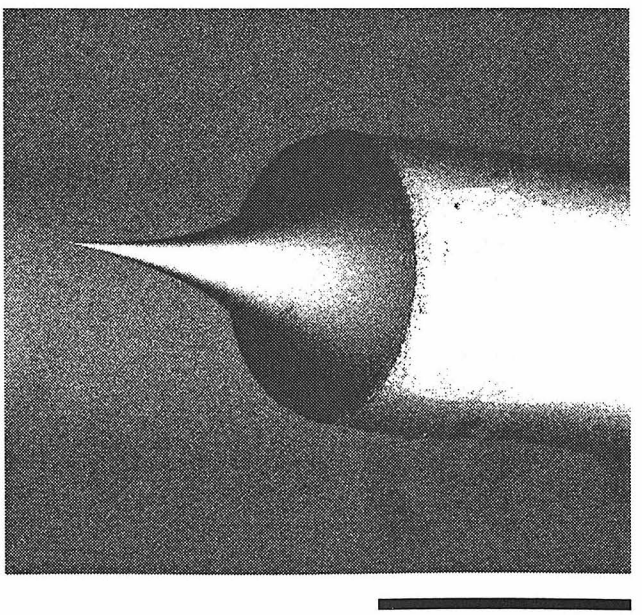

Figure 8: Zoom onto the tip of the fiber shown in Figure 7. Scale bar = 250 μm.

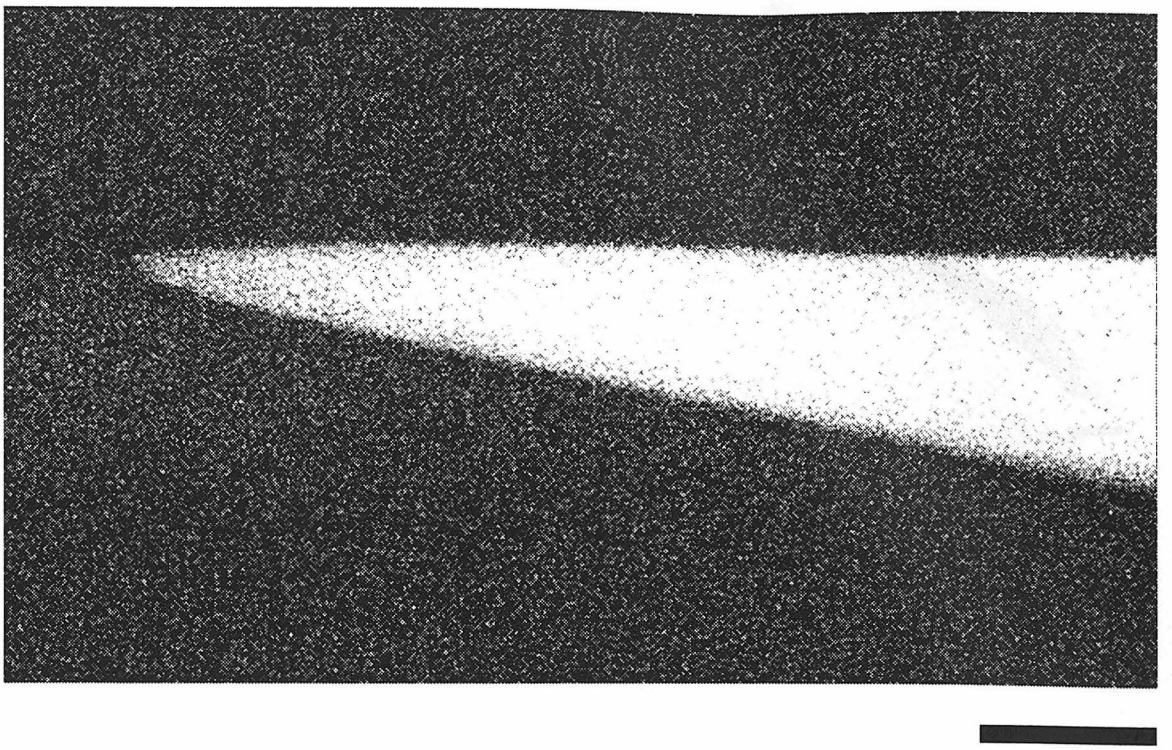

Figure 9: Zoom onto the tip apex of the tip shown in Figure 7. Scale bar = 1μm.

D. Chalcogenide Core Etching Mechanism

The mechanism of tip formation is believed to be convective control of chemical etching. This etching is hypothesized to occur as follows:

As the etching agent dissolves the fiber, the solution density increases next to the fiber surface. Since it is denser than the rest of the solution, it flows down the fiber; under these conditions the flow is laminar. As it flows down the fiber, more etchant solution must move to take its place. Since there is a fluid layer moving parallel to the surface of the fiber everywhere but close to the meniscus (the "top" of where the etchant touches the fiber), new etchant solution enters the convection pattern primarily at the meniscus, as shown in Figure 3. Since the etchant solution contacting the fiber is more reactive (i.e., contains more H_2O_2 and less dissolved chalcogenide) at the meniscus, it etches faster there. This results in a "necking" effect. Eventually the "neck" will be dissolved completely away, and the fiber below the neck will fall.

The protective solvent overlayer serves to make tip shape more smooth and reproducible. Fibers etched without solvent overlayers are typically asymmetric and lack the smooth concave conical shape of fibers etched with solvent overlayers. See Figure 10.

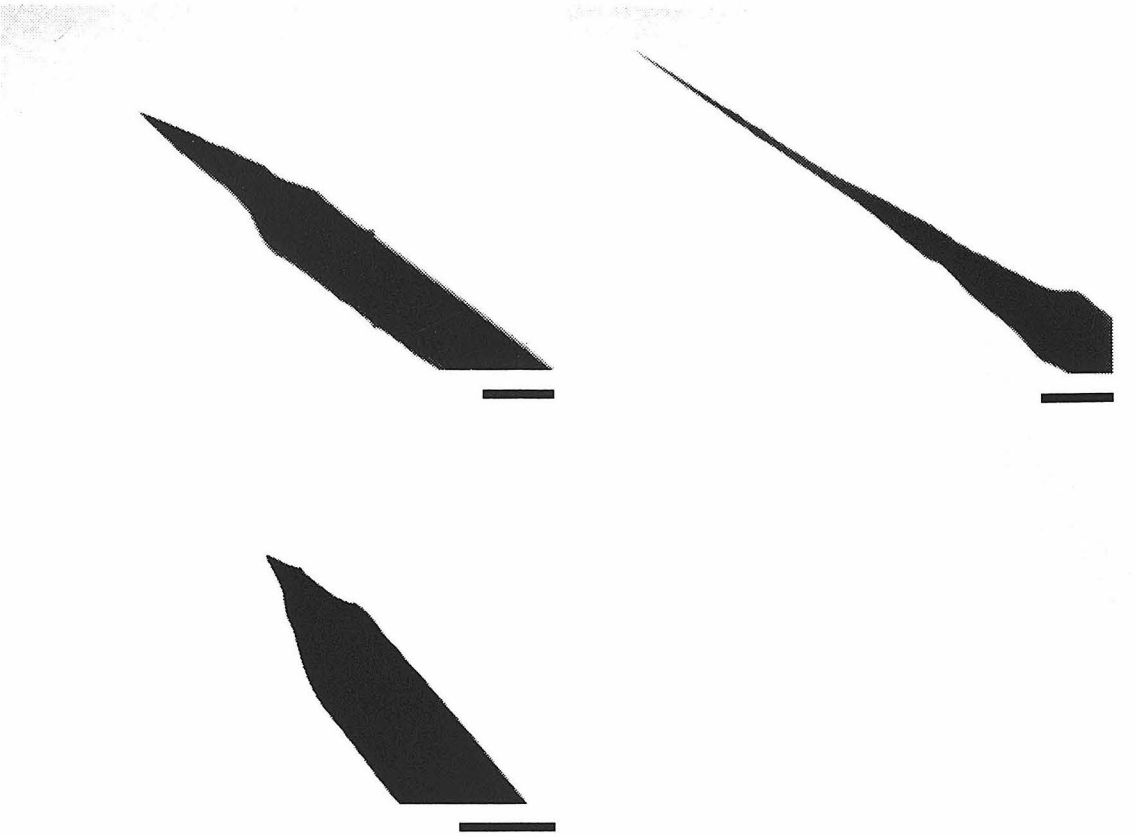

Figure 10: Optical micrographs of tips etched without protective solvent overlayers. Scale bars = 150 μm. Note the asymmetry and large-scale corrugation.

Experimentally, it is observed that without a solvent overlayer, the meniscus of piranha solution at an inserted fiber curves up, whereas with a solvent overlayer the meniscus of the piranha solution at the fiber is flat. This meniscus curvature is believed to disrupt the convection pattern responsible for producing smooth, concave-conical tips.

According to the convective control hypothesis, if the effects of convection are reduced relative to diffusion and reaction, more isotropic etching is expected. See Figure 11.

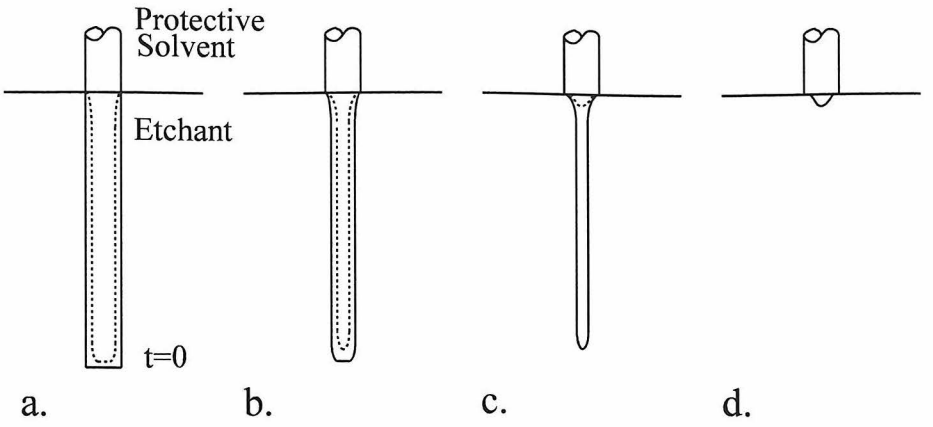

Figure 11: Schematic of the two-phase etching mechanism under conditions of isotropic etching. The dotted lines qualitatively indicate rates of etching, or the new profile of the tip after a discrete time-interval. No "necking" or falloff is expected.

Three different experiments were performed to test this prediction. In the first experiment, etching was performed in the normal apparatus, but at reduced temperature (5° C - see Figure 12).

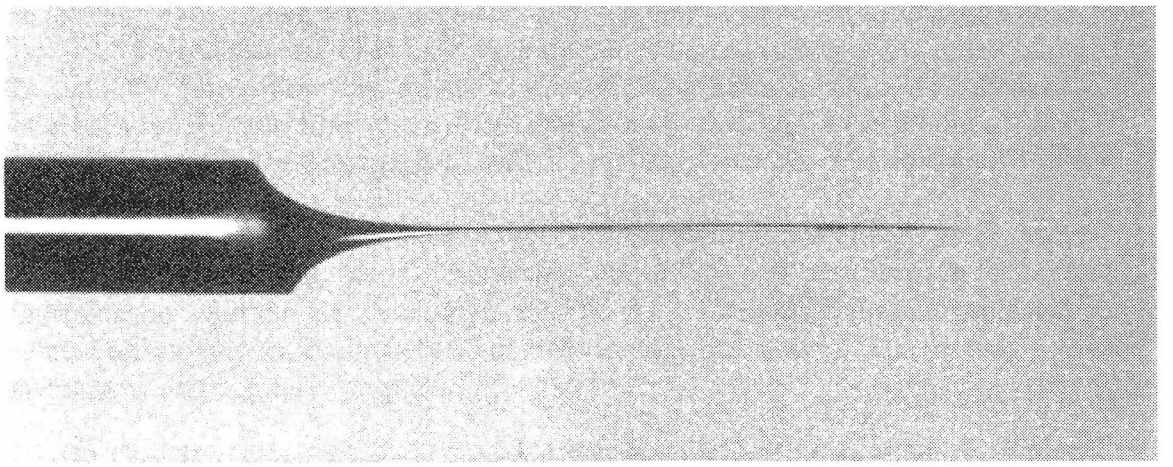

Figure 12: Optical micrograph of a 145 μm core chalcogenide fiber etched at reduced temperature (5° C). Scale bar = 150 μm.

Reduced temperatures increase the viscosity of the piranha solution, thus making convection slower. In the second experiment, etching was performed in the normal apparatus, but with fairly rapid stirring of the piranha solution. Stirring essentially equalizes the concentration of H_2O_2 and dissolved chalcogenide throughout the piranha solution (see Figure 13).

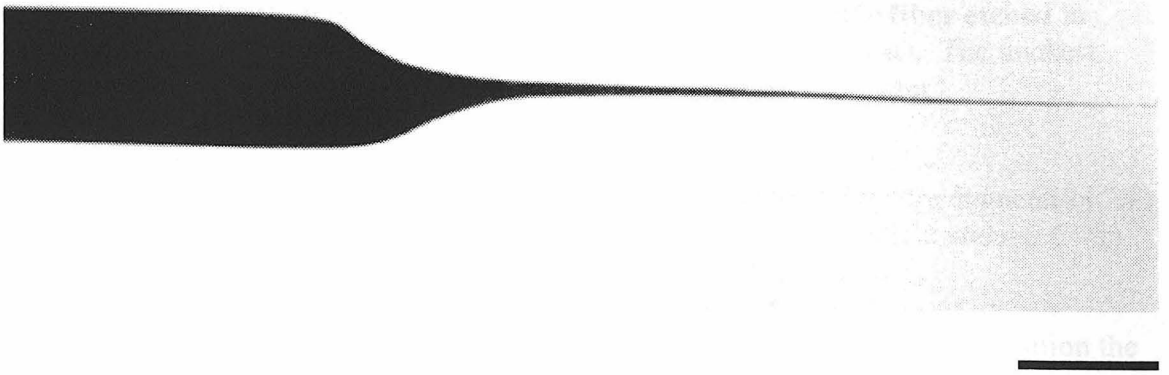

Figure 13: Optical micrograph of a 145 μm core chalcogenide fiber etched in stirred pihrana solution. Scale bar = 150 μm.

In the third experiment, a glass capillary (i.d. ~ 1.5 mm) was used instead of a glass vial (i.d. ~ 2.5 cm). Since the fiber itself took up a substantial portion of the interior space in the capillary, convection was seriously impeded (results not shown). In all three cases, long, high aspect-ratio fiber tips without evidence of "necking" were produced. It is more difficult to judge "completion" with these fibers, since there is no "falloff" event.

From our hypothesis, we would also expect that the neck should always point straight down from the meniscus. To test this prediction, etching was performed in the normal apparatus, but with the glass vial tilted at ~60°. As predicted, the tip thus produced pointed off-axis by approximately 60 degrees (results not shown). The tip was, however, asymmetric and not very sharp.

E. IR Radiation Throughput Measurements

For transmission measurements chalcogenide glass fibers with a 250 μm core were used. A two step etching procedure has been used to ensure the straight taper and sharp taper angle. At the first step, the long (about 1 mm) concave taper has been achieved during about 30 min. of etching, then the fiber was inserted an additional 0.5 mm into the etching solution and etched another 1-2 min. until the straight taper of about 20° (half angle) has been achieved. The resulting shape of the etched tip is shown in Figure 14 with optical original magnification x200.

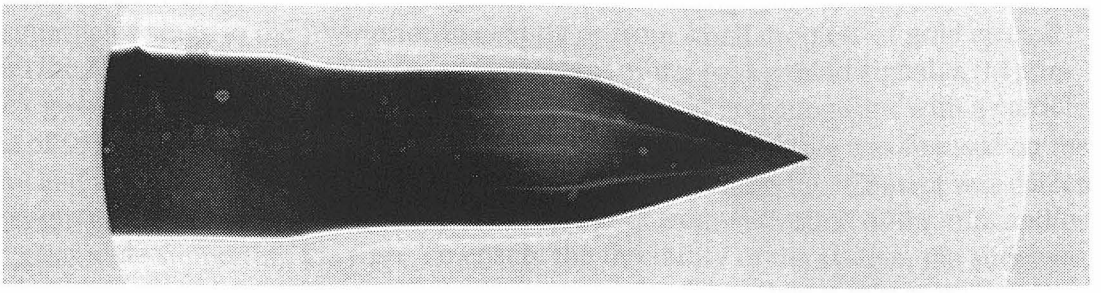

Figure 14: Optical micrograph of a 250 μm core chalcogenide fiber etched in pihrana solution utilizing two-step procedure (described in text). The thickest portion of the fiber in this picture corresponds to initial core diameter.

The thickest portion of the fiber in this picture corresponds to initial core diameter of 250 microns. The second step of etching is clearly seen on this photograph at about 0.6 mm from the tip.

The etched fiber was coated with a 190 nm layer of gold. During the gold deposition the fiber was rotated around its axis oriented at about 45° to the direction towards the source, with the tip pointing towards the evaporation boat. Such a coating geometry should result in complete opacity of the tapered tip.

The coated fiber was fixed in a micromanipulator on an inverted microscope (Zeiss, Axiovert 35) with the tip pointing down, towards the objective. For detection of the IR radiation a Cassegrain objective was used (N.A. 0.65, Ealing Electrooptics Inc., Holliston, MA). The collimator lens was removed to ensure transmission of the IR radiation. A MCT detector (Kolmar Technologies Inc., Conyers, GA) was used for detection of the IR radiation collected by the objective and reflected towards the epi-illumination port. The reflector slider contained two reflector slides - one with gold coating for full reflection of the measured IR light, and the other - an uncoated glass slide - for observation of the fiber tip with epi-illumination. A T-shaped adapter was used at the rear port of the microscope to accommodate both the illumination lamp and the MCT detector.

The radiation of the Free Electron Laser (FEL) was focused on the input end of a ~1m long fiber. Macropulses of about 3 ms duration and repetition rate of 10 Hz were applied at the wavelength of 6.01 μm with the average power of 2.5 mW. A small portion of the FEL beam has been reflected to the reference detector for monitoring the input beam intensity, and the signal received through the fiber was ratioed to the reference signal to ensure the signal stability at various input energies.

The fiber tip was positioned in focus of the objective (the tip was observed through the microscope with x20, x40, and x100 refractive objectives under epi-illumination) and the IR signal was detected using the reflective objective. The non-zero signal at this point

indicated a leak of the radiation through the holes in coating. Such holes may result from dust particles stuck to the fiber prior to coating or from small droplets of gold ejected from the evaporation boat. After the measurement of the background signal, a 0.1 mm thick glass slide was positioned under the fiber tip. A thin polishing film with a particle size of 0.05 μm was attached to the slide. The microscope objective was focused on the film, and the fiber was carefully brought into contact with the film. Contact was detected by slight movement of the film out of focus resulting from deflection of the film and/or the glass slide supporting the film. To ensure the flexibility of the system, the slide was held only at one side providing a long cantilever under the polishing film and the film was attached to the slide at one end providing some free space between the film and the glass under the tip. The film was scanned in x and y directions over a few microns, then the tip was withdrawn from contact, and the slide with polishing film was moved aside.

The resulting flat aperture was observed through the x100 objective and its dimensions measured with resolution of about 0.5 μm. Then the IR signal transmitted through the tip was measured using the reflective objective. The polishing procedure and corresponding transmission measurements were repeated until the taper was completely removed. The background was subtracted and the data normalized to 1.0 for an aperture equal in width to the fiber (i.e., no taper). The curve of throughput as a function of the aperture area is shown in Figure 15.

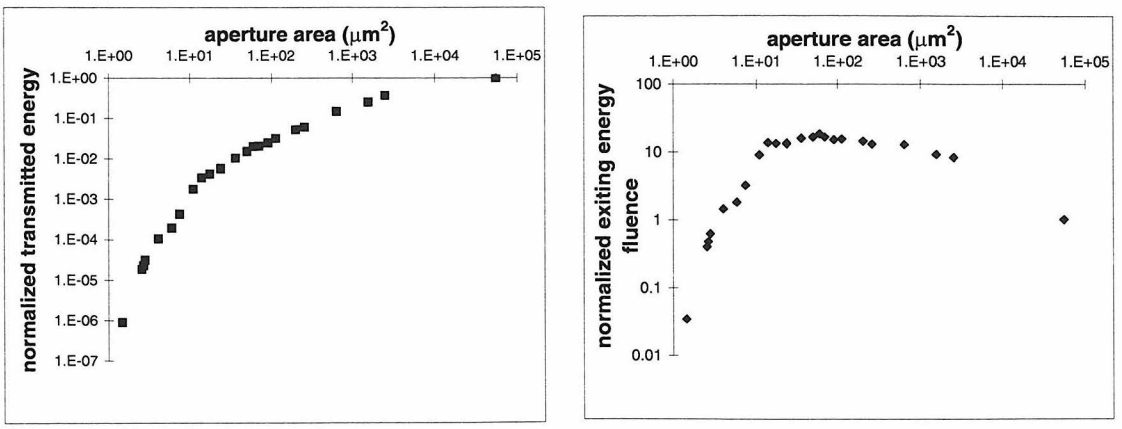

a. **b.**

Figure 15: IR radiation transmission at D=6.01 μm through an etched gold coated fiber as a function of exit aperture area. a: normalized transmission, **b:** normalized transmitted power fluence at the surface of exit aperture.

We used the aperture area instead of diameter due to the fact that the aperture was not round and the elliptical axis ratio varied with the distance from the tip. In Figure 15b the power fluence (i.e., power per unit area) at the tip exit is depicted as a function of the tip size (this curve is a result of division of transmitted power (shown in Figure 15a) by corresponding aperture area). As can be seen on this graph, the power fluence grows at the beginning of the taper up to about 15 times the input fluence due to the light

concentration, and remains constant up to the aperture size of about 10 μm^2, which correspond to about $(\lambda/2)^2$; this behavior is typical for macroscopic tapered fibers. At smaller apertures the power fluence drops due to exponential attenuation of the light intensity in the waveguide below the cut-off diameter[17]. The throughput becomes lower than 10^{-4} at the aperture size below about 4 μm^2, which corresponds to the round aperture diameter of about $\lambda/3$. By comparison, pulled fiber probes with a $\lambda/3$ aperture typically[18] have a throughput of $< 10^{-6}$.

The described results indicate higher throughput of etched fiber probes as compared to pulled probes. Demonstrated characteristics of etched probes make it possible to substitute an Optical Parametric Oscillator (OPO) laser as a light source. As OPO lasers are far more common and much less costly than FELs (~250k$ vs 1M$ + shielded facility cost), this would make NSIM a vastly more accessible technique.

Another potential use of etched IR fiber probes is for high-spatial-resolution temperature measurements, such as those required in semiconductor device diagnostics. Tapered IR-transparent fibers are also used as attenuated total reflectance (ATR) "cells" in FTIR spectroscopy[19]. Chemical etching, as opposed to hot-filament-pulling, may also be a useful way to fabricate probes for this application.

V. Conclusion

We have demonstrated methods to remove the coating and cladding from chalcogenide infrared transmitting fibers, as well as a simple chemical method to etch the fibers to a point with submicron radius of curvature. Chemical etching is simpler and more reproducible than heat pulling infrared fibers. The tips produced also have a much shorter taper length; this makes them more robust and also improves throughput by minimizing the distance that light must travel in a subwavelength aperture.

The chemical etching mechanism has been shown to be convective control of tip etching. Laminar flow down the fiber causes the least saturated (most reactive) etching solution to enter the flow stream primarily just below the meniscus. The presence of a protective solvent overlayer serves to keep the meniscus flat, regularizing the laminar flow down the fiber. Reducing the effects of convection (by reducing temperature or stirring) produces isotropic etching and reduces tip sharpness dramatically.

[1] Harootunian, A., Betzig, E., Isaacson, M., Lewis, A. (1986). Superresolution Fluorescence Near-Field Scanning Optical Microscopy. *Appl. Phys. Lett.* **49,** 674

[2] Betzig, E., Trautman, J., Harris, T., Weiner, J. and Kostelak, R. (1991). Breaking the Diffraction Barrier – Optical Microscopy on a Nanometric Scale. *Science* **251**, 1468.

[3] Courjon, D., Baineier, C. (1994). Near-field Microscopy and Near-field Optics. *Reports on Progress in Physics* **57 (10)**, 989

[4] Kopelman, R., Tan, W.H. (1994). Near-field Microscopy, Spectroscopy, and Chemical Sensors. *Applied Spectroscopy Reviews* **29**, 39

[5] Betzig, E., Trautman, J.K. (1992). Near-field Optics – Microscopy, Spectroscopy, and Surface Modification Beyond the Diffraction Limit. *Science* **257**, 189

[6] Trautman, J.K., Macklin, J.J., Brus, L.E., Betzig, E. (1994). Near-field Spectroscopy of Single Molecules at Room Temperature. *Nature* **369**, 40

[7] Assuming cutoff at 50 dB/km, or 20 dB/m.

[8] Valaskovic, G.A., Holton, M., Morrison, G.H. (1995). Parameter Control, Characterization, and Optimization in the Fabrication of Optical Fiber Near-field Probes. *Appl. Opt.* **34**:1215

[9] Massey, G.A., Davis, J.A., Katnik, S.M., Omon, E. (1985). Subwavelength Resolution Far-Infrared Microscopy*Applied Optics* **24**(10), 1498

[10] Nakano T., Kawata, S. (1993). Infrared Evanescent-field Microscope using CO_2 Laser for Reflectance Measurement. *Optik* **94**(4), 159

[11] Lahrech, A., Bachelot, R., Gleyzes, P., Boccara, A.C. (1996). Infrared Reflection-mode Near-field Microscopy Using an Aperatureless Probe with a Resolution of Lambda/600. *Optics Letters* **21**(17), 1315

[12] Piednoir, A., Licoppe, C., Creuzet, F. (1996). Imaging and Local Infrared Spectroscopy with a Near-field Optical Microscope. *Optics Communications* **129** (5-6), 414

[13] Hong, M.K., Erramilli, S., Huie, P., James, G., Jeung, A. (1996). *SPIE* **2863**, 54

[14] Zeisel, D., Dutoit, B., Deckert, V., Roth, T., Zenobi, R. (1997). Optical Spectroscopy and Laser Desorption on a Nanometer Scale. *Anal. Chem.* **69** (4), 749

[15] Zeisel, D., Dutoit, B., Deckert, V., Roth, T., Zenobi, R. (1997). Optical Spectroscopy and Laser Desorption on a Nanometer Scale. *Anal. Chem.* **69** (4), 749

[16] S. Erramilli and M. Hong, personal communication

[17] For example: page 207 in Corle, T.R., Kino, G.S. Confocal Scanning Optical Microscopy and Related Imaging Systems, Academic Press, San Diego 1996.

[18] Personal communication, Daniel Palanker, Stanford Free Electron Laser Facility.

[19] Ertan-lamontagne, M.C., Lowry, S.R., Seitz, W.R., Tomellini, S.A. (1995). Polymer-coated Tapered Cylindrical ATR Elements for Sensitive Detection of Organic Solutes in Water. *Applied Spectroscopy* **49** (8), 1170

CHAPTER SIX

Mounting Carbon Nanotubes on SPM probes

This chapter describes a method for mounting carbon nanotubes on AFM tips. The method was developed by the Smalley group at Rice University and learned by the author. Nanotubes are "dotted" on acrylic adhesive tape to disperse them for mounting. Micromanipulators and dark-field optical microscopy are used to attach a small quantity of adhesive to the AFM tip. The adhesive is then used to capture a single nanotube. The tube structure is analyzed in an AFM instrument and the tubes are electroshortened to a useful length. Nanotube tips are relatively easy to make, give resolution equal to or slightly better than commercially available AFM tips, and (most importantly) are exceptionally durable.

I. Introduction

In 1985, Kroto and Smalley discovered a 60-carbon allotrope of carbon, and correctly identified its structure as the I_h-symmetrical buckminsterfullerene (Figure 1), igniting an entirely new field of research.

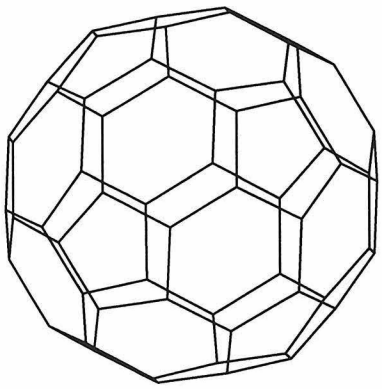

Figure 1: C_{60}, Buckminsterfullerene

In 1991, experiments with an arc-discharge evaporation apparatus used to produce C_{60} led Iijima[1] to the discovery of another carbon allotrope: multiwalled carbon nanotubes, consisting of concentric tubes of graphite a few nanometers to a few tens of nanometers in diameter. Soon thereafter, Iijima and Ichihashi[2] developed a method to produce single-walled carbon nanotubes, with a 1 nanometer diameter.

Figure 2: left, idealized multiwalled nanotube structure; right, a singlewalled tube.

The high aspect ratio, small end radius of curvature, and high strength of these carbon nanotubes made them perfect candidates for use as AFM and STM tips. All that was missing was a way to attach them to a more macroscopic object.

In November 1996, the Smalley group at Rice University published a method for mounting multiwalled carbon nanotubes on AFM probes[3],[4]. Perceiving the value of this technique for making derivatized probes, the author traveled to Houston in March 1997 to learn the technique.

This chapter describes the process of mounting, shortening, and testing the nanotubes as learned at Rice, as well as adaptations made to the technique at Caltech. The goal is to illuminate the subsequent chapters, which describe efforts to create a derivatized, mounted nanotube probe.

II. Experimental

A. Nanotube production

Closed and opened multiwalled nanotubes were produced in the Smalley lab at Rice University. Closed multiwalled nanotubes (cMWNT) are produced in a DC arc apparatus under an inert atmosphere[5]. As grown, the material consists of multiwalled nanotubes, fullerene onions, and amorphous carbon, and forms a dense black mass. This material can be oxidized in dry air (750° C) until 98% of the mass is removed. This process removes most of the fullerene onions, amorphous carbon, and fullerene end-caps on the tubes. The result is a fluffy mass of opened multiwalled nanotubes (oMWNT), occupying the same volume as the original mass but with far lower density.

B. Taping the Boule

Mounting a nanotube on an AFM tip requires that the tubes be separated from each other and project out into space. This is accomplished by "taping the boule". Essentially, a

pair of XYZ translators are used to "dot" the fluffy mass of multiwalled nanotubes (the boule[6]) on a piece of tape (see Figure 3), while viewing the operation with a dark-field optical microscope.

In our case the microscope is a Nikon Diaphot with epi-fluorescence attachments. The objective used is 10x (Nikon, Ph 1, 0.25 NA) and used in conjunction with a modified condensor to provide dark-field capability at long working distances. An additional 10x magnification (in the eyepiece turret) is used to increase the visual image size. Replacing the commercial sample stage is a home-built stage with two XYZ micrometer translation stages mounted on it. Each XYZ stage has a rotating "arm" with a banana plug socket, in which the various jigs used here are mounted, as shown in Figure 4.

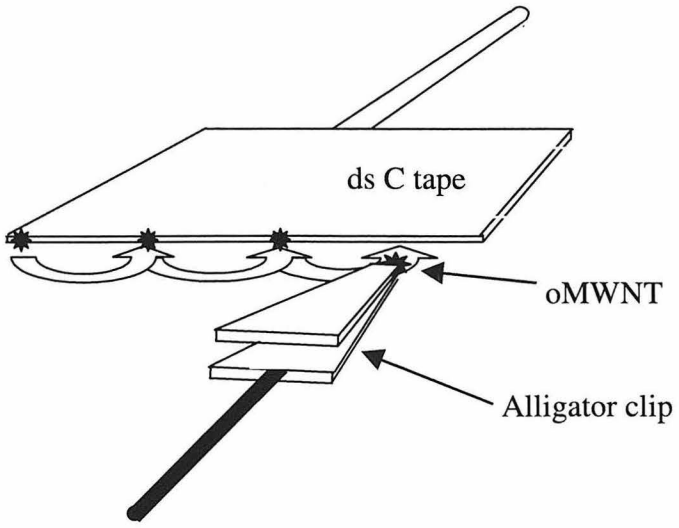

Figure 3: Taping the Boule

Figure 4: photograph of the microscope with XYZ stages

To tape the boule, one XYZ stage is used to hold a piece of doubled-over carbon conductive tape (Electron Microscopy Sciences 77816), and the other holds the boule itself. A corner of the boule is touched to the tape edge and withdrawn, leaving a thicket of nanotubes on the tape. The tape is then translated, leaving a space free of nanotubes, and the process is repeated.

C. Mounting the tubes

The next step is to mount a tube on the AFM tip. Essentially, the AFM tip is dipped in adhesive and a nanotube is captured with the adhesive.

It is easiest to use AFM probes with stiff cantilevers, such as those used for tapping mode imaging; cantilevers with lower spring constants (such as most contact mode cantilevers) can be captured by the adhesive and break. In our case, we used Digital Instruments FESP tips (spring constant 1-5 N/m, resonance frequency 74-99 kHz). The tips are sputtered with a thin layer of gold (~20 nm) to make the adhesive stick better.

The boule is replaced with a jig holding the AFM tip so that the wall of the pyramid on which the tube is to be mounted is approximately perpendicular to the tape surface:

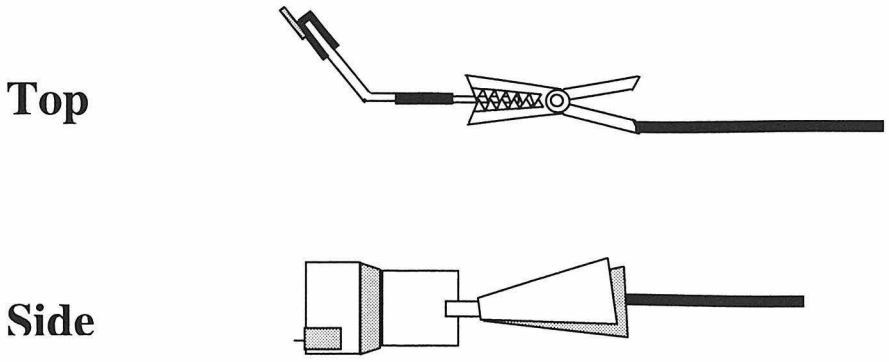

Figure 5: Diagram of Tip Holder

The AFM tip is translated, "dipped" in the tape adhesive on a space empty of nanotubes, and withdrawn. If done properly, the "string" of adhesive formed by the adhesive between the tape and the AFM tip will break in the middle, making certain that there is adhesive on the probe (Figures 6b,c).

Now the goal is to mount a desirable nanotube. The ideal probe (for tapping mode AFM) is one with a nanotube bundle attached to the AFM tip and projecting a few microns beyond it, with a single tube sticking out a few tenths of a micron further than the others. Nanotube bundles can be distinguished from single tubes in dark field microscopy; bundles are brighter and appear unevenly illuminated, whereas single tubes are dim and appear isotropically illuminated. In the microscope, the ideal candidate bundle is one that appears to be hanging isolated in space; this is a bundle at the end of a single tube (Figure 6d). The side of the AFM tip is brought in contact with the bundle and withdrawn, bringing the bundle (and hopefully the single tube) with it (Figures 6d-f).

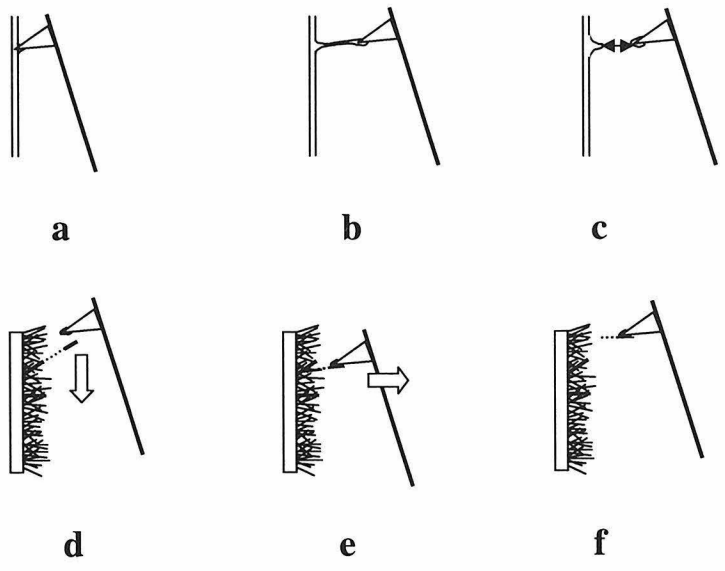

Figure 6: The Mounting Process

D. AFM Analysis and Electroshortening

Next is the analysis of the attached bundle and electroshortening. The length of bundle and tube can be measured with the tapping mode AFM, and application of a voltage between the tip and the substrate can etch the tubes until they are the correct length.

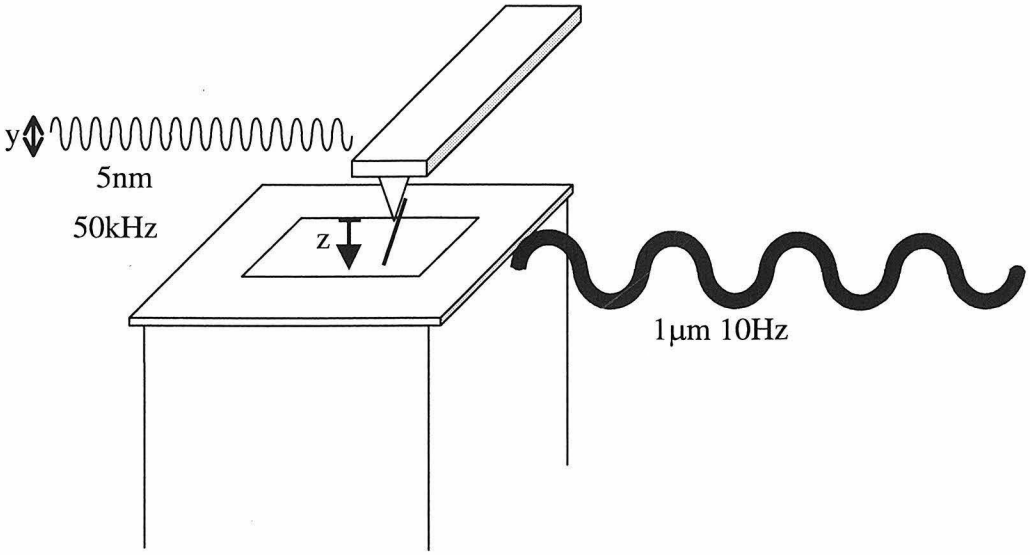

Figure 7: Schematic of the Testing Motion

The AFM probe is resonated at its resonance frequency and its oscillation amplitude (nominally ~5 nm) monitored. The substrate – a Niobium AFM resolution tester[7] – is then moved up and down (nominally 1 μm) at a much slower frequency (~10 Hz), and the oscillation amplitude of the cantilever is observed *as a function of substrate position.*

These motions are easily executed on a Nanoscope AFM[8] by using "Force Calibration" mode. Empirically, the oscillation amplitude as a function of substrate position shows the nature of the attached nanotube / bundle. Single tubes and bundles each have a distinct signature:

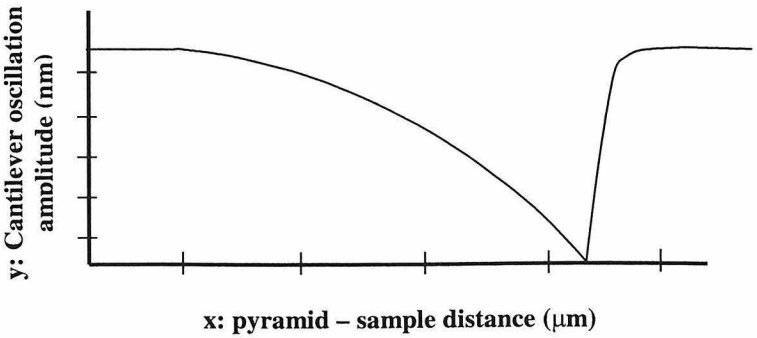

Figure 8a: Schematic Single Tube Signature

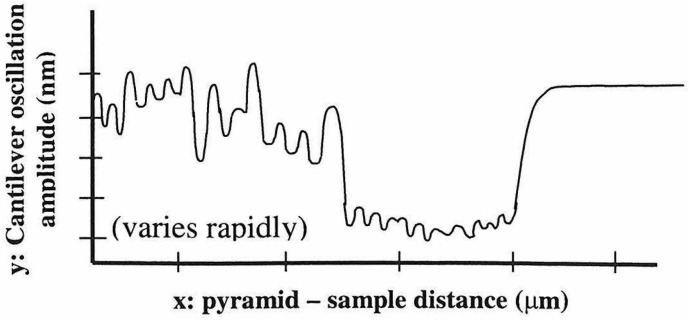

Figure 8b: Schematic Bundle Signature

The section of the nanotube that is being examined can be altered by changing the "zero" position of the substrate. The pyramid of the AFM tip can be found by simultaneous observation of the AFM deflection signal; when the pyramid begins to hit the substrate, the cantilever will deflect upwards:

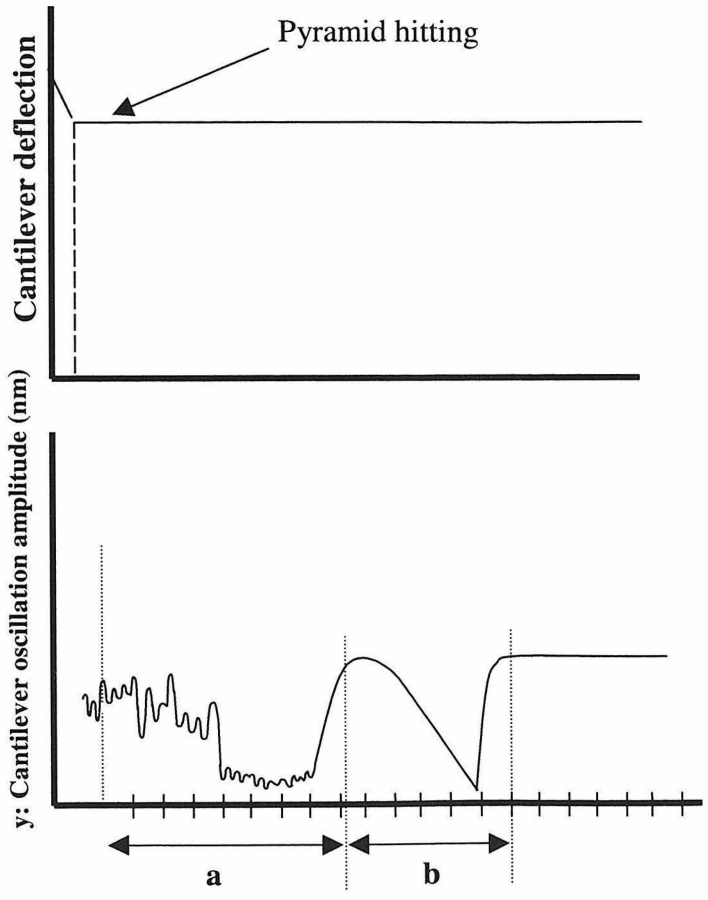

Figure 9: Schematic Single Tube on Bundle as Pyramid Signature

This signal, for instance, shows a bundle of length [a] projecting off the pyramid, with a single tube of length [b] projecting from the bundle.

It is important to understand the implications of these curves. The cantilever oscillation remains at its nominal value until the attached nanotube begins to touch the surface. As a single tube begins to touch the surface, it damps the cantilever oscillation completely. As the cantilever comes closer to the surface, the nanotube begins to "kink", and it absorbs less of the oscillation driving energy. Ultimately the oscillation recovers to almost its nominal initial value, as shown in Figure 8a. With a bundle, after the initial damping of the cantilever oscillation, the recovery of the oscillation amplitude with decreasing distance to the surface is not smooth (see Figure 8b). The bundle is kinking, but since there are many tubes the behavior is more variable; full recovery to the pre-contact amplitude does not occur. As the cantilever is brought closer to the surface, the pyramid eventually comes in contact with the surface. At this point, the cantilever oscillation amplitude decreases abruptly to zero and does not recover, and the cantilever deflects from contact with the surface. Note that at this point the entire nanotube is smashing into the surface 10 times per second without damage.

It is unlikely to have the ideal bundle-and-single-tube described in the last section. Much more common is a bundle with a long single tube projecting off the AFM tip (or a bundle without any projecting single tube). The next phase of preparation is to electrically etch ("electroshorten") the nanotube /bundle down to the correct length. A power supply is set up to charge the tip to (up to) 20 V with the sample grounded. The substrate position is adjusted until the oscillating nanotube is missing the substrate by ~50 nm, and the voltage is increased until the oscillation amplitude increases, and then further until the increased amplitude disappears. This process etches the nanotube by ~30 to several hundred nm.

The resolution of tips produced by this process can be evaluated by using the nanotube tip to image the Nb resolution tester. The features on the resolution tester are small, so the image is effectively many images of the end of the AFM tip. The size of the smallest bumps observed in the image is a good rough approximation to the size of the tip. Nanotube tips produced by this method are approximately as sharp as good commercially available AFM tips. Unlike commercially available tips, however, the nanotube probes maintain their sharpness rather than being blunted by contact with the surface.

III. Results and Discussion

The tips so produced can be examined in the TEM. Figures 10 and 11 show two tips with their attached nanotubes produced by the author while learning the technique at Rice University.

Figure 10: Mounted Carbon Nanotube Tip #1. In **a**, the tip is just barely visible as a proturbance beyond the Si pyramid (arrow). In **b**, we see a length of single tube extending beyond a bundle. **c**. is a closeup of the tip end. The tube appears ~15 nm wide, and gave resolution of ~10 nm on the resolution tester.

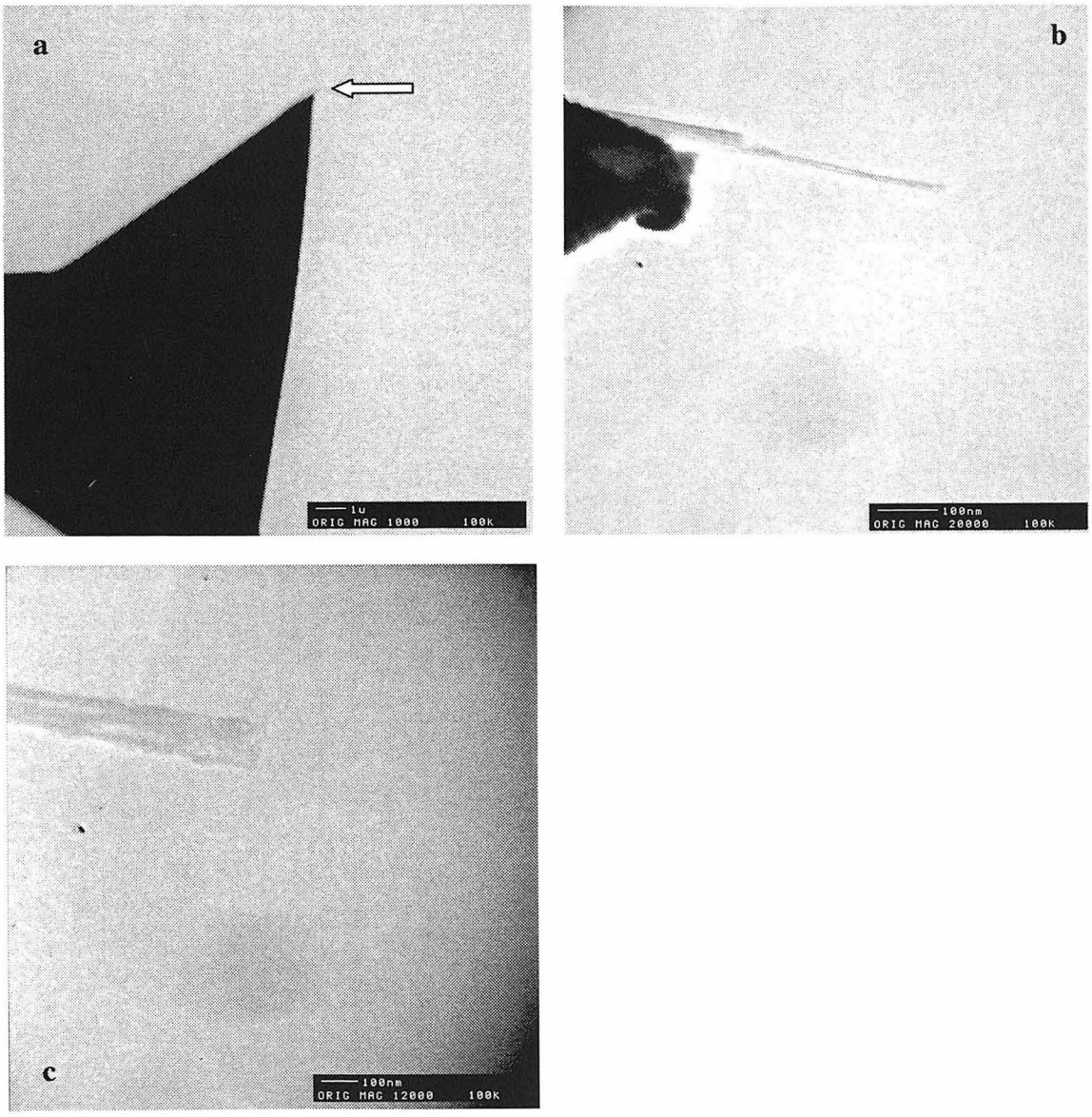

Figure 11: Mounted Carbon Nanotube Tip #2. This tip illustrates the durability of nanotubes vs. Si tips. **a**, the first ~250 nm of the Si tip is smashed flat from impacting the substrate surface in force cal mode (arrow). **b,c**, the nanotube is unharmed.

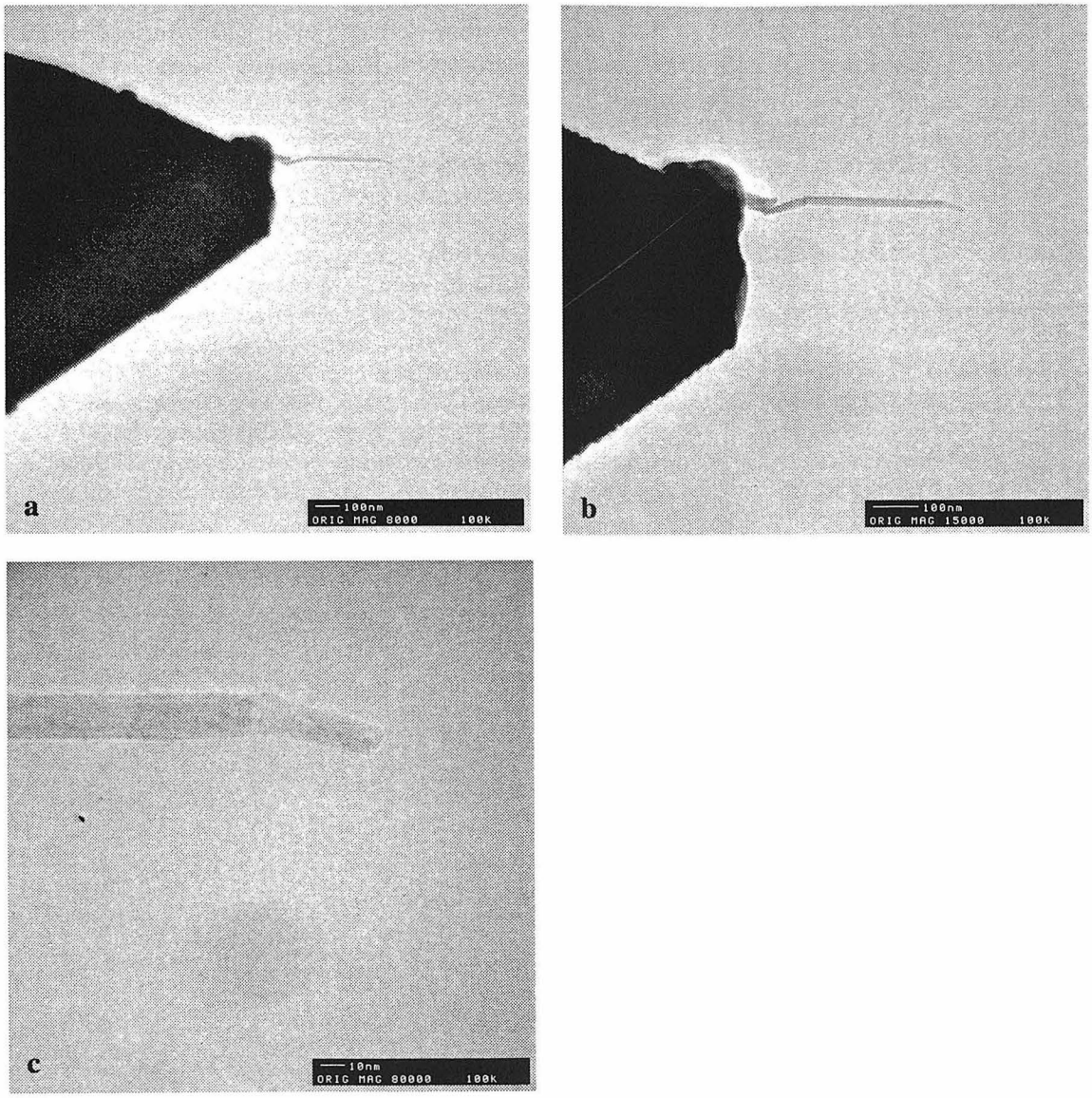

IV. Conclusion

The mounting protocol developed by the Smalley group functions well. Mounting carbon nanotubes on AFM tips is relatively easy. Electroshortening the tubes is more time-consuming and more prone to failure (~33% yield). Mounted nanotube tips are extremely durable, especially in comparison with conventional silicon tips.

---

[1] Iijima, S., (1991). Helical Microtubules of Graphitic Carbon. *Nature*, **354**: (6348) 56-58, Nov, 7.

[2] Iijima, S., Ichihashi, T., (1993). Single-shell Carbon Nanotubes of 1nm Diameter. *Nature*, **363**: (6430) 603-605 JUN 17 1993

[3] Dai, H.J., Hafner, J.H., Rinzler, A.G., Colbert, D.T., Smalley, R.E., (19960. Nanotubes as Nanoprobes in Scanning Probe Microscopy. *Nature*, **384**: (6605) 147-150 NOV 14 1996

[4] The canonical reference for this technique as developed at Rice is a web page authored by Jason Hafner: http://cnst.rice.edu/mount.html

[5] Colbert, D.T., Zhang, J., McClure, S.M., Nikolaev, P., Chen, Z., Hafner, J.H, Owens, D.W., Kotula, P.G., Carter, C.B., Weaver, J.H., Rinzler, A.G. and Smalley, R.E. , (1994). "Growth and sintering of fullerene nanotubes," *Science*, B, pp. 1218-1222.

[6] A "boule" properly refers only to a grown single-crystal mass (i.e. the silicon single-crystal boule from which silicon wafers are sliced); the Smalley group has adopted the name for the fluffy mass of oMWNT.

[7] "Nioprobe", General Micro, Canada, generalmicro@ccinet.ab.ca

[8] Digital Instruments, Santa Barbara, CA; www.di.com

CHAPTER SEVEN
Bulk Chemistry of Carbon Nanotubes

This chapter describes the development of a protocol to derivatize carbon nanotubes. Model substrates and then nanotubes were biotinylated and labeled with avidin conjugates; avidin-gold conjugates were examined with TEM to obtain qualitative results, and fluorescent avidin conjugates were employed for quantitation. Since only small quantities of nanotubes were available, fluorescence quantitation was performed by ratioing the fluorescence to the absorbance of the nanotube samples. Carboxylic acid groups on oxidation-opened multiwalled carbon nanotubes were successfully biotinylated with a biotin hydrazide in a reaction employing carbodiimide and NHS. Direct attachment of fluorophores to nanotubes was also demonstrated.

The appendix to this chapter describes novel nanotube manipulation techniques developed in the process of doing this chemistry. Methods are described for fluorescent staining of nanotubes, for creating stable nanotube suspensions, for removing the amorphous carbon layer without oxidation, and for removing the nanotubes from solution without collapse to a solid mass.

I. Introduction

A. Methodology

The goal of the nanotube experiments was to attach a single molecule to the end of a mounted nanotube. Bulk experiments were chosen as a method to derivatize many nanotubes simultaneously, in order to collect data faster than would be possible with mounted nanotubes. Development of a derivatization protocol also required a method to measure the success of the derivatization. Two methods suggested themselves. The first method was direct attachment of a molecular tag to the nanotubes. The second method was to biotinylate the nanotubes and add avidin to which a molecular tag was attached.

Direct attachment of a molecular tag was potentially problematic, in that attaching a new substrate might require reworking the attachment chemistry. The second method – biotinylation followed by the addition of tagged Avidin – was more flexible. Biotin – also known as vitamin H - is a small molecule which is bound with extraordinary affinity[1] ($K_d = 1.3 \times 10^{-15}$) by a protein known as Avidin.

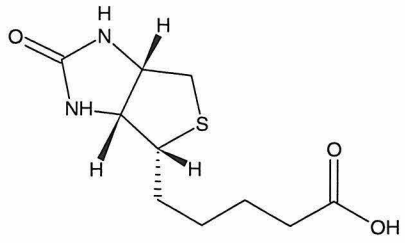

Figure 1: Molecular structure of biotin

Avidin is a ~70kD protein capable of binding 4 biotin molecules. The avidin-biotin link is the strongest known non-covalent interaction. Since its discovery it has become widely used in molecular biology[2], and reagents for Avidin-Biotin chemistry are now relatively commonplace. Avidin is available in several different variants (with different isoelectric points, for instance), and with several different types of tags attached – in particular, fluorophores and tiny gold balls (4 nm to hundred of nm). Fluorescent-labeled avidin is used in optical microscopy, whereas the gold balls coated with Avidin are used in electron microscopy.

Biotinylation reagents are also available. Most biotinylation reagents are designed to label nucleophilic chemical groups (i.e., amines), but biotin hydrazide was also available, making it possible to label carboxylic acid groups.

Fluorescent labeling and gold ball labeling each have advantages and disadvantages. Fluorescence detection is relatively easy and gives good quantification, but has the disadvantage that fluorescence can be strongly affected by the molecular environment, including pH, steric crowding, and proximity to other fluorophores or conductors. Gold balls have the advantage of being unambiguous and environmentally insensitive (they are either present or not), but the disadvantage that they require imaging to detect. Collecting statistically significant amounts of data requires collection of many TEM images. Biotinylation and labeling with a fluorescein conjugate of Avidin and with an Avidin-gold ball conjugate were the workhorse techniques for the nanotube bulk derivatization discussed here. TEM analysis was used as a qualitative tool; fluorescence was employed for quantitation.

B. Chemical Strategy

Carbon nanotubes are essentially graphite tubes – either of a single closed sheet[3] (single walled nanotubes, SWNT), or of multiple tubes arranged one-inside-the-other in a "Russian doll" fashion[4] (multiwalled nanotubes, MWNT). The basal plane of graphite is essentially inert. However, the *ends* of nanotubes may be derivatized[5,6].

1. Fullerene Reactivity

A native nanotube is closed at both ends with a cap of carbon. This cap may come in different shapes. For SWNT, the cap is essentially a fullerene structure – i.e., half of a

C_{60} or C_{70} molecule. For MWNT, the cap structure will vary from tube to tube. However, in order for the cap to be closed, geometry requires that it *must* contain a minimum of 6 pentagons[7]. The presence of a pentagon in a graphitic sheet creates strain and increases reactivity. Fullerenes are well known[8] to undergo addition reactions with nucleophiles at such sites, as shown in Figure 2:

Figure 2: Nucleophilic addition to C60

The end cap of a SWNT should react like a fullerene; the end cap of a MWNT should have a similar (although perhaps lesser) reactivity where its curvature is high.

2. Carbon Oxide Reactivity

Oxidation-opened MWNT (oMWNT) display a different target. Oxidation destroys the end caps preferentially, leaving an open-ended graphitic tube[9]. Depending on the conditions and mechanism of oxidation[10], several different partially-oxidized forms of carbon may be present at the edge. See Figure 3.

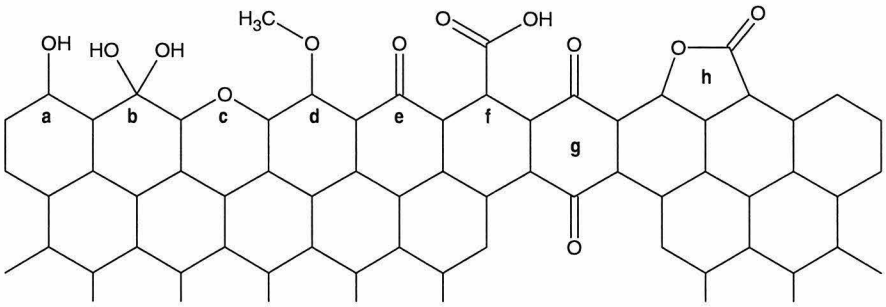

Figure 3: Species present on the edge of oxidized graphite. a: hydroxyl, **b:** vicinal hydroxyl, **c:** bridging oxygen (ether), **d:** methoxy, **e:** carbonyl, **f:** carboxylic acid, **g:** quinone, **h:** lactone.

Of these, the easiest to derivatize is the carboxylic acid group, which may be activated with a carbodiimide and then attacked by a nucleophile[11], as shown in Figure 4:

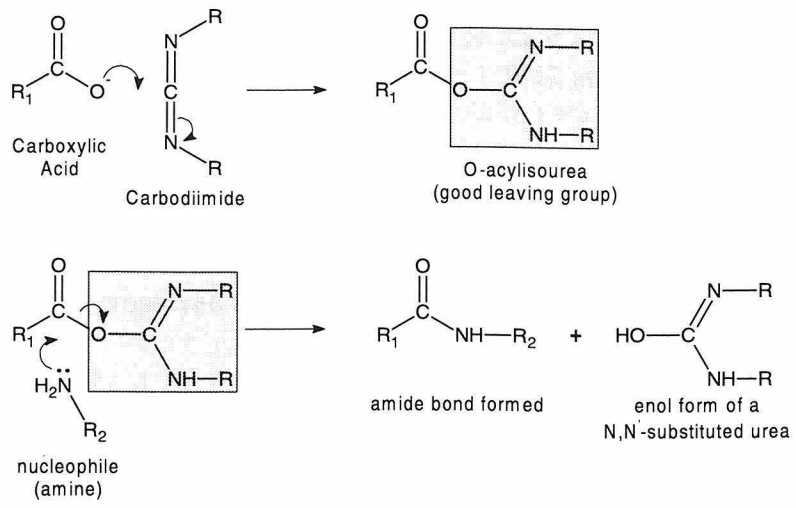

Figure 4: Basic mechanism of carbodiimide activation and nucleophilic attack

These two pathways constitute the core of the chemistry applied to carbon nanotubes in this laboratory. The closed end-cap pathway benefits from literature on the topic of fullerene chemistry. The carboxylic-acid pathway benefits from the literature on carbon chemistry (i.e., graphite, charcoal, and carbon black) as well as the more extensive (although perhaps less applicable) literature on attaching things to COOH groups on molecules and hydrophilic polymers.

II. Experimental

A. Carbon Nanotubes

Single-walled, multi-walled, and opened multi-walled nanotubes were the gift of the Richard Smalley group at Rice University. Single-walled tubes (SWNT) were prepared by pulsed laser vaporization of a metal/carbon target in a furnace at 1100°C[12]. This method produces a 'felt' of material, consisting of 40-50 vol% of single-wall nanotubes, with the remainder being amorphous carbon and graphitic carbon fragments.

Closed multiwalled nanotubes (cMWNT) are produced in a DC arc apparatus under an inert atmosphere[13]. As grown, the material consists of multiwalled nanotubes, fullerene onions, and amorphous carbon, and forms a dense black mass. This material can be oxidized in air (750°C) until 98% of the mass is removed. This process removes most of the fullerene onions, amorphous carbon, and fullerene end-caps on the tubes. The result is a fluffy mass of opened multiwalled nanotubes (oMWNT).

Some nanotubes used here were purified by liquid-phase oxidation as described by Hiura[14]. Briefly, cMWNT were mechanically crushed and then suspended in 1N H_2SO_4 with sonication. The suspension was heated to 130°C, and an equivalent volume of 10% $KMnO_4$ in H_2SO_4 was added dropwise. The solution was refluxed for 5 hours and washed extensively with concentrated HCl and pure water to remove MnO_2.

B. Basic Bulk Derivatization Method

The basic method employed to treat nanotubes (single- or multi-walled) is the following:

1. Suspend
2. Add reagent(s)
3. Incubate with rotation,
4. Wash (x4)
   a. Centrifuge
   b. Decant
   c. Resuspend

Suspension is typically accomplished with a few pulses of ultrasound in solution. Surprisingly, nanotubes are easier to suspend (and form a more stable suspension) in aqueous solution than in any organic solvent tested. Suspensions of nanotubes typically fall out of solution with a "half-life" on the order of several hours. Rotation is employed to keep the tubes suspended during reaction.

Separating the excess reagent from the nanotubes is difficult. Conventional separation techniques employed by organic chemists (i.e., chromatography) cannot be used due to the large size of the nanotubes. Membrane filtration also fails, because the tubes invariably stick to the membranes. Large quantities of tubes were not available to circumvent this problem. The most effective technique is to centrifuge to pull the tubes out of suspension, carefully decant the solution, and resuspend by mechanical agitation. Even careful decanting leaves approximately 1% of the original solution behind, so multiple cycles of washing are required to reduce reactant concentration to an acceptable level.

All experiments were done in glass vials, as nanotubes stick irreversibly to plastic containers (i.e., microcentrifuge tubes).

C. TEM Sample Prep

Optimal TEM sample preparation for carbon nanotubes is to allow the nanotubes to settle on a holey carbon covered TEM grid. A holey carbon membrane is prepared by arc evaporation of carbon rod anodes onto a freshly cleaved mica substrate, giving a carbon layer ~300 A thick. A section of this mica is then immersed in water, leaving the carbon membrane floating on the surface of the water. TEM grids are immersed in the water and then removed from the water through the carbon membrane, coating the top surface of

the grid with holey carbon. The grids are used promptly to avoid deposition of contaminants from the air.

10 μL of nanotube suspension is placed on top of the grid, and incubated for several hours in a humid environment (to avoid evaporation). The tubes settle on the holey carbon membrane during this time. The solution is wicked away from the side with a piece of filter paper, and the grid is placed on a piece of filter paper and allowed to dry for one hour.

III. Results and Discussion

A. Testing N Attack on C60:

Before discovering that the closed MWNT have a relatively thick layer of amorphous carbon, experiments were performed to test the attachment of molecules to the fullerene end-caps. The model target compound in these experiments was C_{60} itself, in order to make use of solution-phase analytical tools (i.e., NMR, MS). Fullerenes are known to be attacked by nucleophiles. Most biotinylation reagents are designed to *be attacked* by nucleophiles (i.e., they possess a good leaving group); one exception was the biotin hydrazides (structure shown in Figure 5):

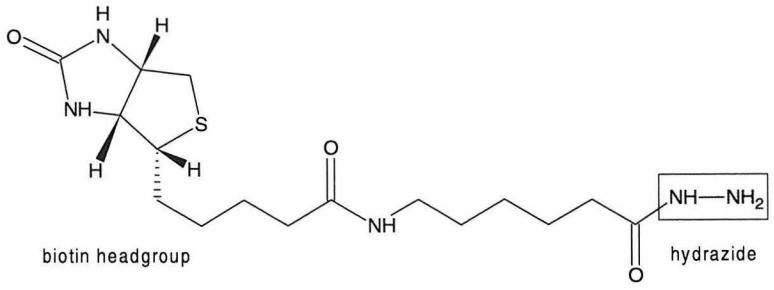

Figure 5: Biotin LC hydrazide

Hydrazides are close relatives of the amines, which are known[15] to add to C_{60}. There is reasonably good evidence for the mechanism of amine addition shown in Figure 6.

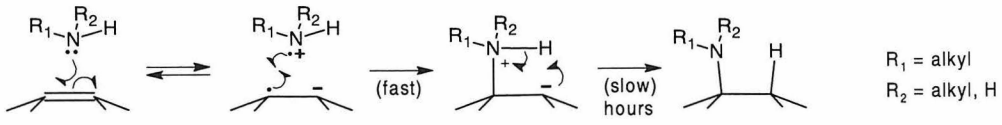

Figure 6: Mechanism of amine addition to C_{60}

However, hydrazides are less basic than amines[16] (at least in water):

$H_2N\text{-}NH_2 + H_2O \rightarrow H_2N\text{-}NH_3^+ + OH^-$ $\quad K = 8.5 \times 10^{-7}$
$NH_3 + H_2O \rightarrow NH_4^+ + OH^-$ $\quad K = 1.8 \times 10^{-5}$

When considering the same element (i.e., two nitrogen bases), nucleophilicity correlates well with basicity, so we expect hydrazides to be worse nucleophiles than amines. The reactivity of hydrazides and amines were tested with simple compounds. 2.6 mg of C_{60} was rotated with methylamine, dimethylamine, methyl hydrazide, and 1,1 dimethyl hydrazide (each 2.0 **M** in tetrahydrofuran) respectively. All four compounds were found to form addition products, as evidenced by the formation of a red / chestnut-brown colored product (characteristic of formation of the amine adduct[17]), disappearance of solid C_{60} (which is completely insoluble[18] in THF), mass spectrometry and NMR spectra. t-butyl amine and t-butyl hydrazine are also found to form adducts with C_{60}, based on similar evidence.

Unfortunately, cMWNT as prepared in the DC arc apparatus have a relatively thick coating of amorphous carbon. Since the method for removing this amorphous carbon layer without destroying the fullerene end-cap had not yet been discovered (see Chapter 7 Appendix), this line of inquiry was abandoned.

B. COOH Biotinylation - Model Substrates

After some initial nanotube experiments, an early version of the derivatization protocol was tested on two model substrates: agarose beads chemically modified to contain COOH groups, and native graphite. Both of these substrates are easier to handle than nanotubes because they do not form stable suspensions (and can therefore be separated from the derivatization solutions easily).

Biotinylation Protocol I:

1. Suspend substrate in MES buffer by sonication.
2. Add 25 μL biotin-LC-hydrazide solution. Mix.
3. Add 12.5 μL EDC solution. Mix.
4. Rotate for ≥ 2 hours (typically overnight).
5. Centrifuge and remove supernatant.
6. Wash (add 1 mL MH_2O, agitate, centrifuge, remove supernatant) x 2.

MES buffer: 0.1 **M** MES (2-N-Morpholinoethanesulfonic acid) pH 5.5.

Biotin-LC-hydrazide solution: 50 m**M** biotin-LC-hydrazide (biotinamidocaproyl hydrazide) in DMSO, prepared fresh.

EDC solution: 100 mg/mL EDC (1-(3-dimethylaminopropyl)-3-ethyl carbodiimide) in 0.1 **M** MES buffer, prepared fresh.

25 μL COOH beaded agarose solution (6-aminohexanoic acid, immobilized on 4% beaded agarose; Sigma) was diluted to 1 mL, biotinylated by the protocol described above, washed with PBS buffer (pH 7.2), and labeled with the addition of 5 μL of 1mg/mL SA-FITC (Strepatividin-fluorescein conjugate, Pierce) followed by rotation for 1 hour. The beads were thoroughly washed with PBS buffer and examined under a fluorescence microscope. Fully biotinylated beads showed fluorescence that was smooth, even, and strong. The no-EDC-control showed lesser fluorescence, the no-BH-control showed still less, and the no-EDC-no-BH control showed no detectable fluorescence at all.

Graphite (1.0 mg, Aldrich) was also biotinylated and labeled according to the protocol above (with overnight rotation in the biotinylation step). Fluorescence microscopy and absorbance measurements show significant nonspecific binding of SA-TRITC to the unmodified graphite surface. Subsequent experiments showed that this nonspecific binding was partially eliminated by the action of EDC and BH on the graphite. Post-treatment (after biotinylation) with bovine serum albumin (BSA) nearly completely eliminated nonspecific binding.

Once the non-specific-binding problem was solved, examination of graphite particles with fluorescence microscopy revealed that fluorescence was not homogenous across the surface of the particles, instead being confined to "hot spots" of much smaller spatial extent. Similar inhomogeneity has been previously observed on a fluorescently-labeled graphite electrode[19]. If either EDC or BH is omitted in the biotinylation reaction, the hotspots failed to appear.

C. COOH biotinylation – Nanotubes

1. Derivatization

Armed with the information gained from fluorescence-labeling of the model substrates and information gleaned from the literature, we proceeded on to biotinylate and label nanotubes. One small but important modification was the addition of N-hydroxysuccinimide (NHS) to the reaction mixture:

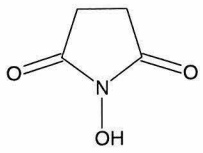

Figure 7: Molecular structure of NHS

NHS has been found[20] to improve the yield of carbodiimide-mediated amine-COOH coupling reactions. NHS reacts with carboxyl-containing compounds to give aminoacyl esters under gentle conditions. This can occur with either the native carboxyl group or with the O-acylisourea derivative (from carbodiimide activation), as shown in Figure 8:

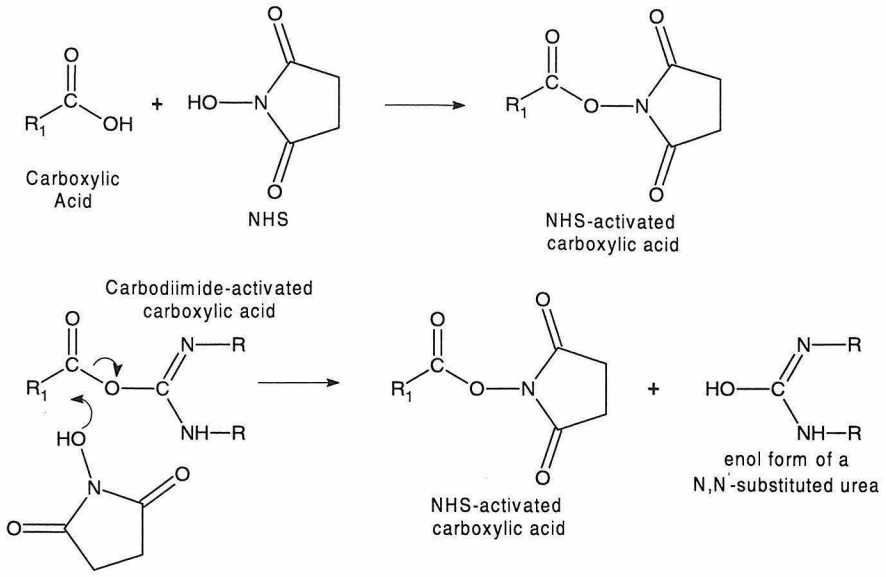

Figure 8: COOH activation by NHS

In either case, the NHS group is (like the carbodiimide addition product) a good leaving group, so the molecule is still activated towards nucleophilic attack, as shown in Figure 9:

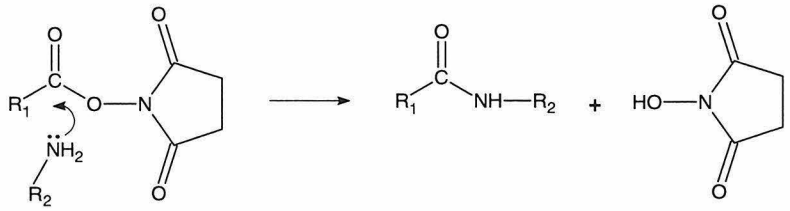

Figure 9: NH2 attack on NHS ester

The mechanism by which this increases yield is not completely clear, but is probably due to the increased hydrolytic stability of the NHS ester versus the O-acylurea[21]. As our results below demonstrate, NHS does increase the number of COOH groups successfully derivatized.

Biotinylation Protocol II:

1. Suspend substrate in MES buffer by sonication.
2. Add 25 μL EDC solution. Mix. Wait 5 minutes.
3. Add 25 μL NHS solution.
4. Add 50 μL biotin-LC-hydrazide solution. Mix.
5. Rotate overnight.
6. Centrifuge and remove supernatant.
7. Wash (add 1 mL MH_2O, agitate, centrifuge, remove supernatant) x 2.

MES buffer: 0.1 **M** MES (2-N-Morpholinoethanesulfonic acid) pH 5.5.

EDC solution: 100 mg/mL EDC in 0.1 **M** MES buffer, prepared fresh.

NHS solution: 4 mg/mL N-hydroxysuccinimide in 0.1 **M** MES buffer, prepared fresh.

Biotin-LC-hydrazide solution: 50 m**M** biotin-LC-hydrazide in DMSO, prepared fresh.

2. Quantitation

Fluorescence on the model substrates was assessed qualitatively in a fluorescence microscope – a technique that was feasible because of the large particle size of the model substrates. In order to *quantify* fluorescence intensity of fluorophores attached to the nanotubes, a better measurement technique was necessary. In addition to a quantitative measure of fluorescence, quantification of the amount of tubes was also necessary. Especially with oMWNT and KMWNT, the quantities utilized are far too small to be weighed accurately. (For oMWNT, a "tweezer pinch" – approximately 0.05 mg based on volume and a density 0.02x that of cMWNT – is suspended in 1 mL to make a stock solution. A typical experiment uses ~50 μL of this stock solution, giving a weight approximately 2.5 μg.) After biotinylation and labeling, tubes were filtered through glass filter paper (GF/A glass microfiber filters, 1.6 μm pores, Whatman) and washed with PBS buffer. Fluorescence was measured with Fluorscan III, a prototype commercial confocal fluoresence scanner[22]. Non-specifically bound SA-TRITC was subtracted using the local background on each glass filter paper. The amount of nanotubes was measured by using an optical densitometer (IS-1000 Digital Imaging System, Alpha Innotech Co.) to quantify the dark nanotubes against the white filter paper. The specific fluorescence is defined as

$$S.F. = \frac{(\text{avg fluorescence - local background})(\text{pixels})}{(\text{Optical density - blank optical density})(\text{fluorescence gain})}$$

Figure 10 shows the specific fluorescence measurements for closed (cMWNT) and oxygen-opened (oMWNT). For each type of tube, tubes biotinylated according to Biotinylation Protocol II (with and without NHS), were compared with un-biotinylated tubes.

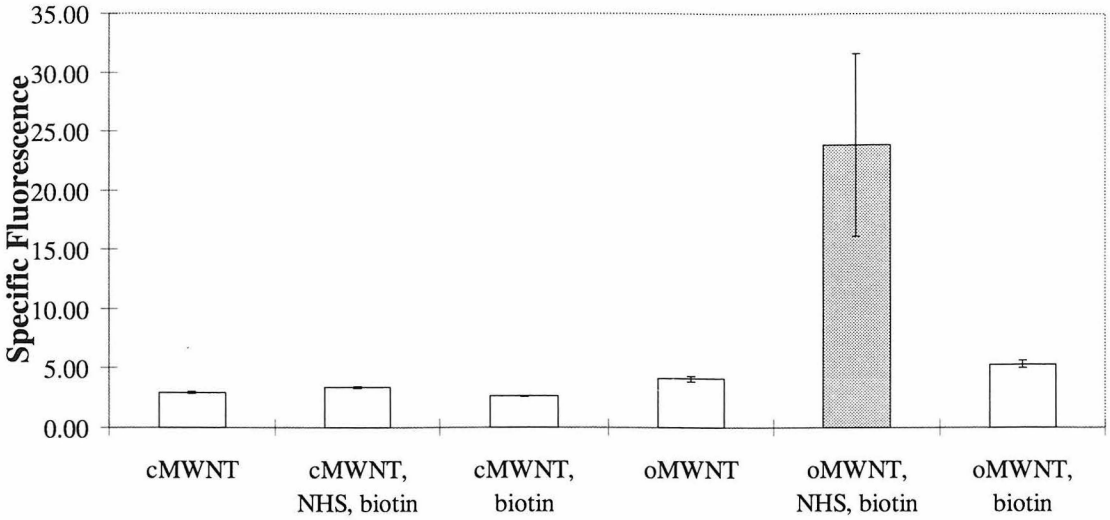

Figure 10: Biotinylation and fluorescent labeling of nanotubes

It is clear from this data that nanotubes are labeled differently depending on their preparation, with oMWNT > cMWNT. It is also apparent that nanotubes biotinylated with both BH and NHS are more brightly labeled than those derivatized with BH alone, which are in turn more brightly labeled than the no-BH control.

D. Direct Fluorescence Labeling of Nanotubes

Several experiments were performed with direct fluorescence labeling of nanotubes. In order to test for actual addition of nucleophile to COOH groups, three fluorophores were employed: 4'-(aminomethyl)fluorescein·HCl (AMF), fluorescein thiosemicarbazide (FTSC), and fluorescein isothiocyanate (FITC).

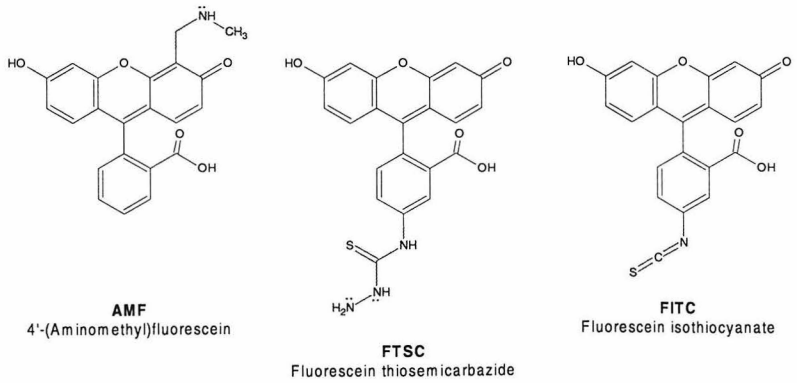

Figure 11: Structures of AMF, FTSC, FITC

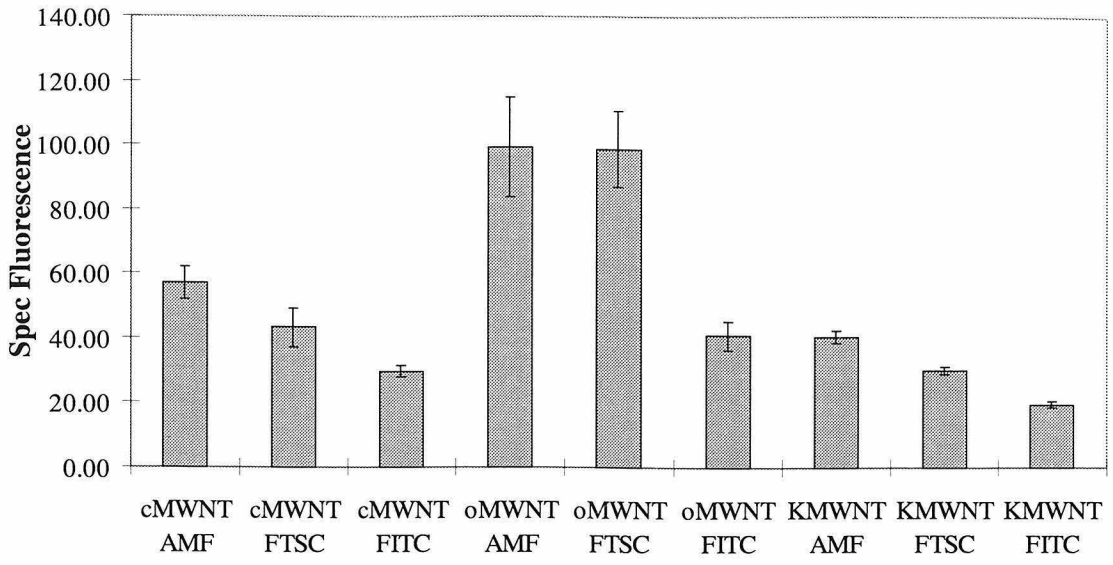

Figure 12: Direct fluorescence labeling of nanotubes

AMF possesses a secondary amine, FTSC has a rough analog of a hydrazide, and FITC has no nucleophilic functionality.

Standard amounts of cMWNT, oMWNT, and KMWNT in MH_2O were activated with EDC and NHS in dimethyl formamide (125 μL of 20 mg/mL EDC; 25 μL 4.0 mg/mL NHS). Each solution is q.s.ed to 1 mL with DMF, and rotated for 15 hours. The samples are then washed once with DMF, once with PBS buffer, filtered through glass filter paper, washed with PBS buffer, and analyzed with the fluorescence scanner and optical densitometer as described earlier.

Figure 12 shows the results for closed (cMWNT), oxygen-opened (oMWNT), and $KMnO_4/H_2SO_4$-opened (KMWNT) nanotubes treated with AMF, FTSC, and FITC.

Clearly, the more nucleophilic fluorophores produce more strongly fluorescent nanotubes: AMF > FTSC > FITC. oMWNT are also clearly more strongly labeled than cMWNT and KMWNT. All these results are consistent with the data obtained through biotinylation and labeling with SA-FITC.

IV. Conclusion

MWNT opened by oxidation clearly have functional groups – most likely carboxylic acids - that can be derivatized. These groups can be activated with carbodiimide and NHS, and form bonds with hydrazides and amines. Nanotubes were successfully biotinylated and labeled with avidin conjugates. Direct attachment of fluorophores to nanotubes was also demonstrated, and was dependent on the presence of a nucleophilic

group on the fluorophore. Fluorescence was successfully quantified by ratioing the fluorescence to the absorbance of the nanotube samples.

In Chapter 6, techniques for mounting carbon nanotubes on SPM probes were described. In this chapter, chemistry for derivatizing the nanotubes was developed. These two chapters laid the groundwork for derivatization of mounted nanotubes – Chapter 8.

---

[1] Green, N.M. (1963a). Avidin. 1. The use of [^{14}C]biotin for kinetic studies and for assay. *Biochemical Journal* **89**, 585-591

[2] For an overview, see Avidin-Biotin Chemistry: A Handbook, M.D. Savage, G. Mattson, S. Desai, G.W. Nielander, S. Margensen, E.J. Conklin, Pierce Chemical Co. 1994.

[3] Iijima, S., Ichihashi, T. (1993). Single-shell Carbon Nanotubes of 1nm Diameter. *Nature*, **363**: (6430) 603-605

[4] Iijima, S. (1991). Helical Microtubules of Graphitic Carbon. *Nature*, **354**: (6348) 56-58

[5] Obviously, references 5 and 6 appeared after I had completed this work.
Wong, S.S., Joselevich, E., Woolley, A.T., Cheung, C.L., Lieber, C.M. (1998). Covalently Functionalized Nanotubes as Nanometre-sized Probes in Chemistry and Biology. *Nature*, **394**: (6688) 52-55

[6] Wong, S.S., Woolley, A.T., Joselevich, E., Cheung, C.L., Lieber, C.M., (1998). Covalently-Functionalized Single-walled Carbon Nanotube Probe Tips for Chemical Force Microscopy. *J. of the Amer. Chem Soc.*, **120**: (33) 8557-8558

[7] Euler's theorem, which says that for the closure of a spherical network of n hexagons, 12 pentagons are required, except for n=1.

[8] Hirsch, A. (1994). The Chemistry of the Fullerenes, Georg Thieme Verlag, Stuttgart, 1994, Chapter 3.

[9] Seshadri, R., Govindaraj, A., Aiyer, H.N., Sen, R., Subbanna, G.N., Raju, A.R., Rao, C.N.R. (1994). Investigations of Carbon Nanotubes. *Current Science*, **66**: (11) 839-847

[10] Kinoshita, K., (1998). Carbon – Electrochemical and Physiochemical Properties. Wiley, New York, 1988.

[11] Organic Chemistry (2nd ed.) G. M. Loudon. The Benjamin/Cummings Publishing Co, Menlo Park, CA

[12] Rinzler, A.G., Liu, J., Dai, H., Nikolaev, P., Huffman, C.B., Rodriguez-Macias, F.J., Boul, P.J., Lu, A.H., Heymann, D., Colbert, D.T., Lee, R.S., Fischer, J.E., Rao, A.M., Eklund, P.C., Smalley R.E. (1998). Large Scale Purification of Single Wall Carbon Nanotubes: Process, Product and Characterization, *Applied Physics A*, **67**, 29-37

[13] Colbert, D.T., Zhang, J., McClure, S.M., Nikolaev, P., Chen, Z., Hafner, J.H., Owens, D.W., Kotula, P.G., Carter, C.B., Weaver, J.H., Rinzler A.G., Smalley, R.E. (1994). Growth and Sintering of Fullerene Nanotubes, *Science,* **266**, 1218-1222

[14] Hiura, H., Ebbsen, T.W., Tanigaki, K., (1995). Opening and the Purification of Carbon Nanotubes in High Yields. *Advanced Materials*, **7**: (3) 275-276

[15] Wudl, F., Hirsch, A., Khemani, K.C., Suzuki, T., Allemand, P.M., Koch, A., Eckert, H., Srdanov, H.G., Webb, H., (1992). In: Fullerene: Synthesis, Properties, and Chemistry of Large Carbon Clusters; G.S. Hammond, V.J. Kuck, Eds.; *American Chemical Society Symposium Series,* **481**; 1992; p161.

[16] Chemistry of the Elements, Greenwood, N.N., Earnshaw, A. (1984), Pergammon Press, Oxford, 1984, p493

[17] Ibid Wudl

[18] Ruoff, R.S., Tse, D.S., Maljotra, R., Lorents, D.C. (1993). Colubility of C-60 in a Variety of Solvents. *J. of Phys. Chemistry.* **97**: (13) 3379-3383

[19] Pantano, P., Kuhr, W.G. (1991). Characterization of the Chemical Architecture of Carbon-fiber Microelectrodes 1: Carboxylates. *Anal. Chem.* **63**: (14) 1413-1418

[20] Staros, J.V., Wright, R.W., Swingle, D.M. (1986). Enhancement bu Hydroxysulfosuccinimide of Water-soluble Carbodiimide-mediated Coupling Reactions. *Anal. Biochem.* **156**: (1) 220-222

[21] Sehgal, D., Vijay, I.K. (1994). A Method for the High-effeiciency of Water-soluble Carbodiimide-mediated Amidation. *Anal. Biochem.* **218**: (1) 87-91

[22] Combion, Inc. – since acquired by Incyte Pharmaceuticals. See Chapter 4 for instrumental details.

CHAPTER SEVEN
Appendix

I. Nanotube Staining

Visualization of carbon nanotubes is possible with electron microscopy. Visualization of *isolated* carbon nanotubes is also possible with an optical microscope (as described in Chapter 6). Darkfield microscopy is capable of detecting the light scattered by the nanotubes, although it lacks the resolution required to resolve individual tubes. However, darkfield microscopy has not been shown to be capable of resolving individual tubes in solution. Since solution techniques are essential for chemical manipulation of nanotubes, a technique for visualizing nanotubes in solution is quite valuable.

We demonstrate here that fluorescent staining of carbon nanotubes is a very promising technique for visualization in aqueous solution.

Suspensions of cMWNT, oMWNT, KMWNT, and SWNT in TE buffer containing 10 m**M** NaCl were stained with YOYO (by addition of 10 μL 1m**M** YOYO, 1% β-mercaptoethanol in TE buffer with 10 m**M** NaCl) and allowed to incubate for 1.5 hours. 7.5 μL of the suspension was examined on an epi-fluorescence microscope (IX50, Olympus) with a 100 W Hg lamp, a YOYO filter set (Chroma), a 60x PlanApo 1.4 NA oil immersion objective (Olympus), and a cooled CCD camera (SBIG ST7I). Mobile bright specks were observed by eye in all cases. The control (identical preparation without nanotubes) showed no mobile specks.

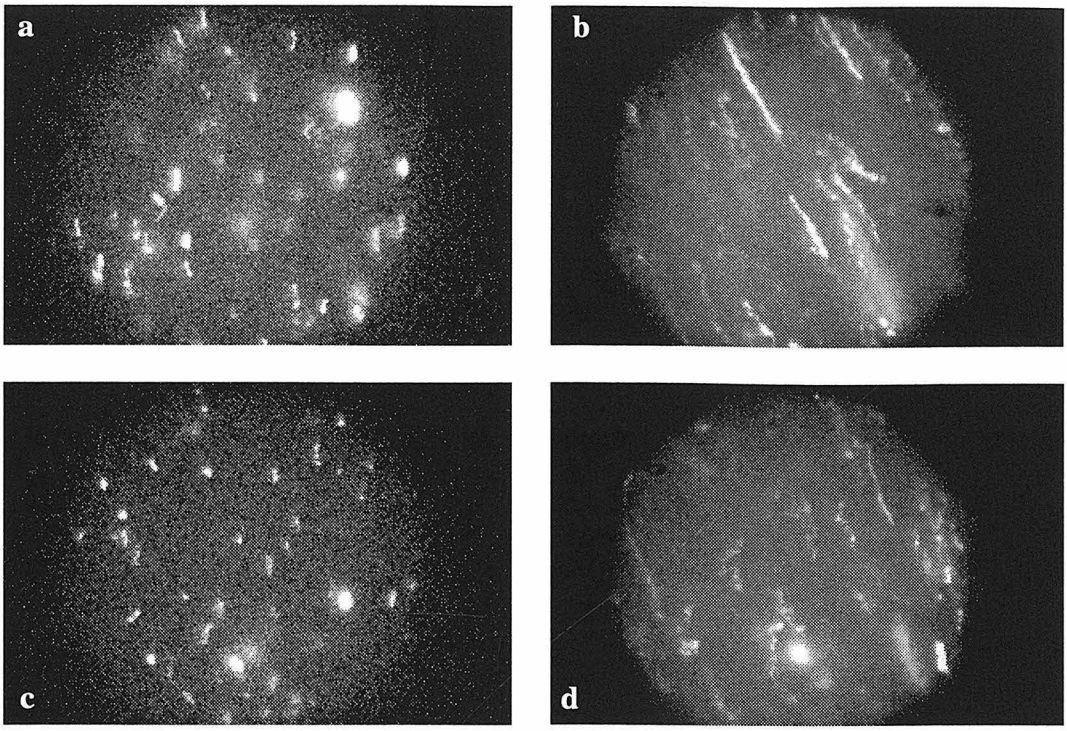

Figure 1: SWNT suspension stained with YOYO

Figure 1 shows images of the SWNT suspension taken with different exposure times. Longer exposure times show significantly longer "tracks" than short exposures, demonstrating that the particles are mobile in the suspension.

Figure 2 shows images taken of the cMWNT, oMWNT, and KMWNT suspensions, showing fluorescent staining of different types of nanotubes.

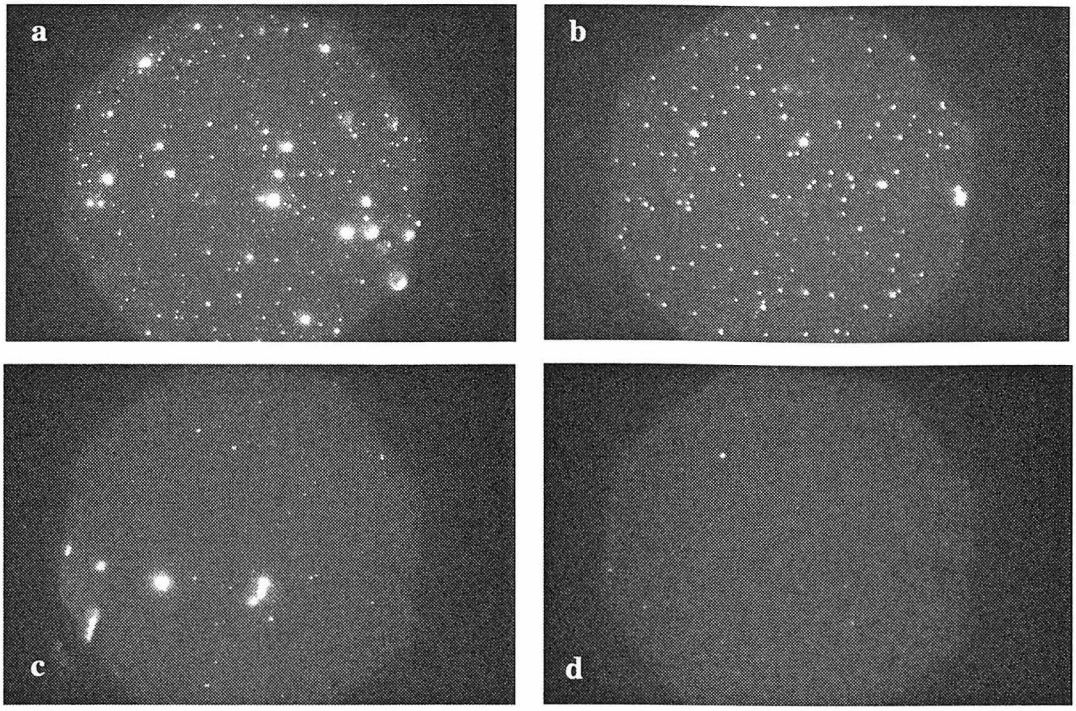

Figure 2: c,o,K MWNTs, stained with YOYO

Examination by eye shows that the nanotubes tendency to stay in suspension decreases in the order SWNT > oMWNT > KMWNT > cMWNT. This is probably due to the (relatively) low molecular weight of SWNT and the higher hydrophilicity of oMWNT and KMWNT than cMWNT.

II. Suspension and Cleaning

A. Surfactant Suspension

As mentioned previously, nanotubes can be suspended in water for several hours with a few pulses of ultrasound. Increasing the stability of the suspension may be accomplished with the addition of surfactant.

0.7 mg of cMWNT was suspended in 1 mL aqueous solutions of 1% Triton X-100, 1% sodium dodecyl sulfate (SDS), 1% mellitic acid, and MH20 with 10 minutes of sonication. The nanotubes do not form a stable suspension with the mellitic acid solution. This is consistent with the presence of acidic surface oxides (e.g., COOH), which would be ionized at pH ~7 ($-COO^-$) but undisassociated (and therefore less hydrophilic) at low pH. Long-time observation showed some precipitation from solution, but a significant fraction remains suspended. The stability of tubes in suspension decreases in the order.

Triton X-100 > SDS > MH_2O >> mellitic acid.

These results were extended to other types of nanotubes as well. cMWNT, oMWNT, and SWNT were suspended in 1 mL aqueous solutions of 1% Triton X-100, 1% sodium dodecyl sulfate, and 1 mL MH_2O, respectively, as described above. Four days after the initial suspension, some settling is present in all samples. However, a significant fraction of tubes remain suspended in the Triton X-100 and SDS samples **more than a year later**. The tubes demonstrate a stability in surfactant suspension according to the order

oMWNT > cMWNT ≅ SWNT.

Consistent with the strong stability of surfactant suspensions, it proved difficult to sediment the tubes even with a centrifuge. Centrifugation at 1700 G for 45 minutes (or 3000 G for 10 minutes) yields only partial sedimentation. Experimentally, reduction of the surfactant concentration (by addition of more water) and persistent centrifugation are necessary to sediment the tubes enough to decant the overlying solution.

B. Surfactant Cleaning

It was serendipitously discovered during the course of these experiments that closed nanotubes suspended in surfactant solutions were cleaner than tubes suspended without surfactant. cMWNT prepared as described above with 1% SDS solution or 1% Triton X-100 solution were washed thoroughly with MH_2O (4 cycles) and examined with the transmission electron microscope. Figure 3A shows images of the cMWNT suspended without surfactant. A coating of amorphous carbon is clearly visible. Figure 3B and 3C shows cMWNT with SDS and Triton X-100. SDS clearly reduces the thickness of the amorphous carbon layer; Triton X-100 seems to completely remove it.

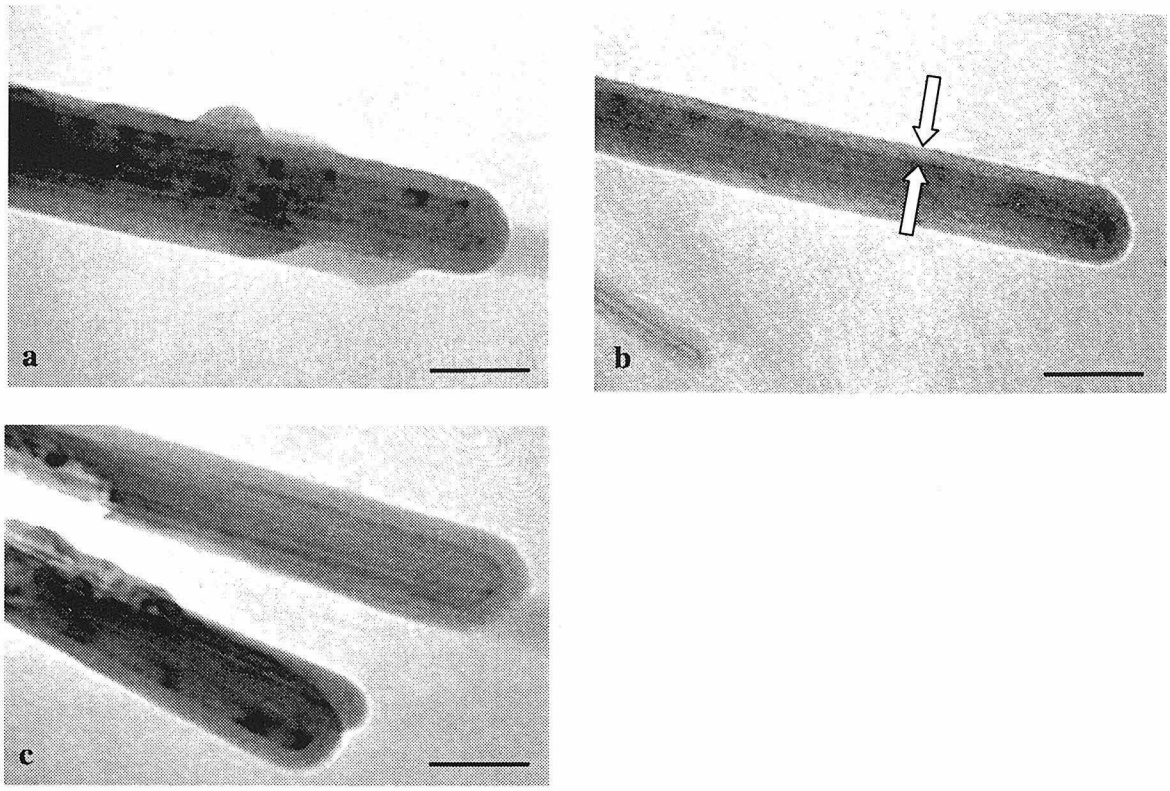

Figure 3A: cMWNT suspended without surfactant

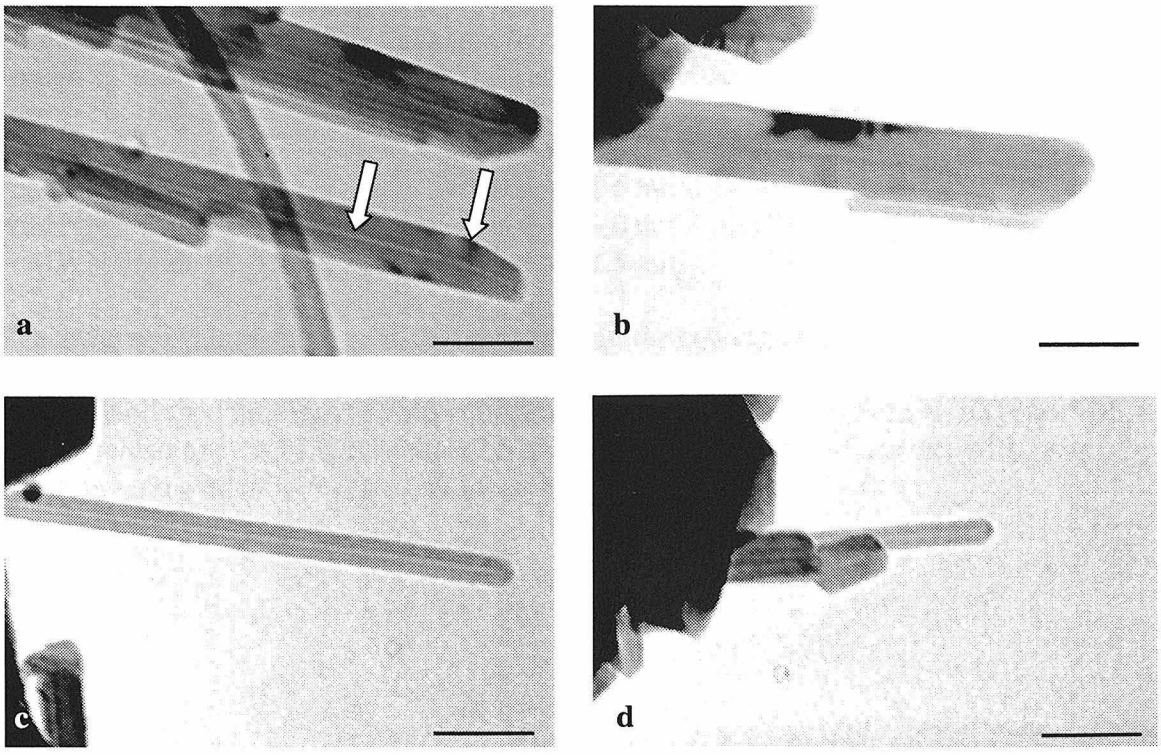

Figure 3B: cMWNT suspended with SDS

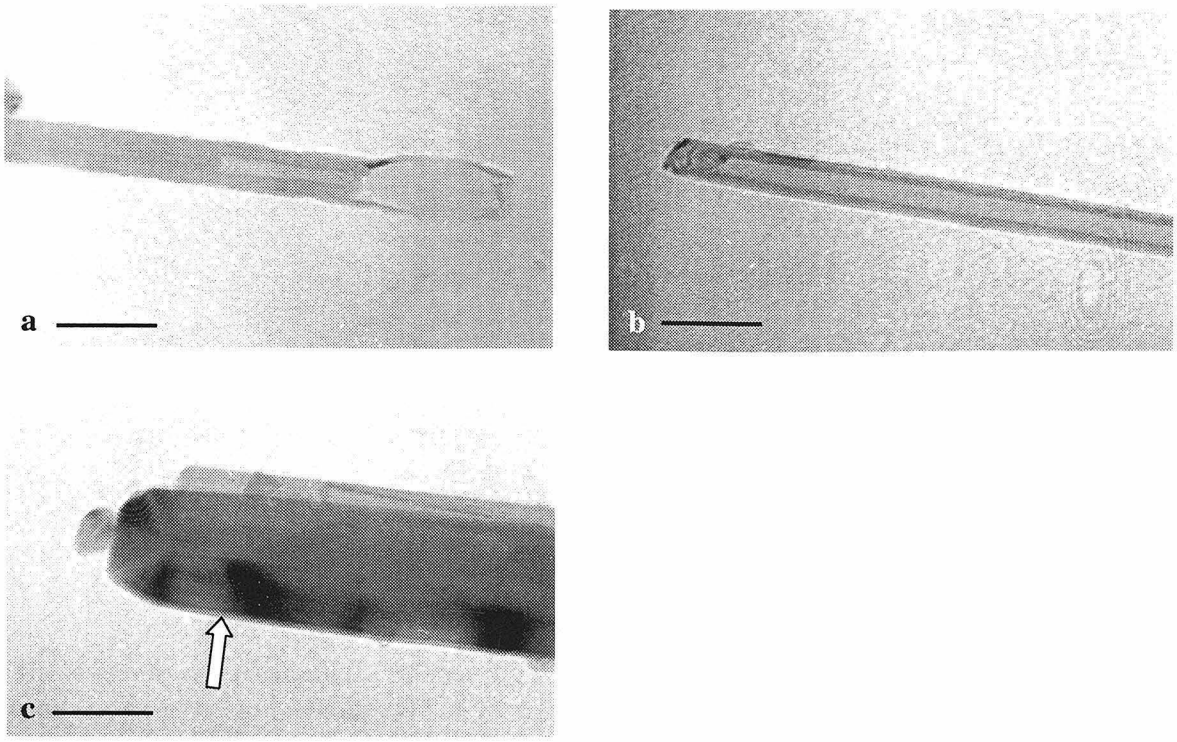

Figure 3c: cMWNT suspended with Triton X-100

Measurement of the coating thickness over a large number of TEM photos taken at high magnification (150,000 and 200,000x) shows that the average coating thickness layers are

cMWNT:	9.4 +/- 1.6 nm
cMWNT with 1% SDS:	1.4 +/- 3.0 nm.
cMWNT with 1% Triton X-100:	1.3 +/- 2.5 nm.

The average values show a ~7-fold reduction in the coating thickness. The uncertainties are estimates based primarily on the limitations of microscope focus and measurement error (uncleaned tubes), or run-to-run variation (cleaned tubes). Triton X-100 and SDS each yielded one set of tubes with ~2.5 nm coating thickness, and another with *zero* coating – no evidence was present for *any amorphous carbon at all.*

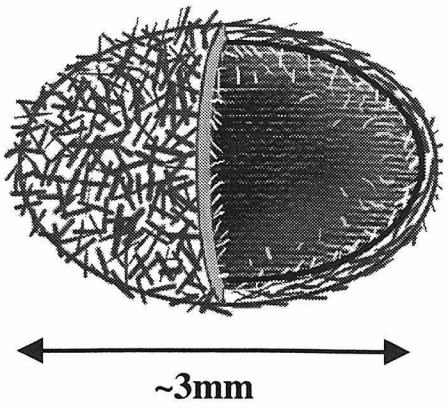

Figure 4: Nanotube "pellet"

These results are particularly interesting when one considers that no other method exists for removing the amorphous carbon from nanotubes without destroying the nanotube end-caps (opening the tubes). All the cleaning methods referred to in the literature utilize oxidation, which opens the tubes as well as removing the amorphous carbon.

C. Nanotube De-suspension

One of the problems of solution-phase chemical treatment of nanotubes is the difficulty of mounting single tubes afterwards. Bringing tubes into aqueous suspension is relatively easy, especially with surfactant. Upon drying of the water, the tubes clump together in a condensed mass. The surface tension of the water is sufficient to pull the tubes together, and the water-air interface collects the nanotubes as it recedes. The condensed mass cannot be used to mount single nanotubes, as the tubes are not separated enough to be taped and mounted (see Chapter 6).

This problem can be almost completely avoided by removing the solvent by lyophilization. An aqueous suspension of tubes in a microcentrifuge tube was vortexed, immediately flash-frozen in liquid nitrogen, and then placed under vacuum for several hours in a lyophilizer. This treatment yields a "hollow pellet" of nanotubes – essentially a capsule constructed from a loose web of nanotubes:

Figures 5a, b, c ,d show the result of this process as applied to a suspension of cMWNT.

Figure 5a-d: Pictures of cMNWT hollow pellet. Pellet (left) removed from microfuge tube w/tweezers, stuck on C ds tape, and "dotted" on another piece of C ds tape (right) perpendicular to the first.

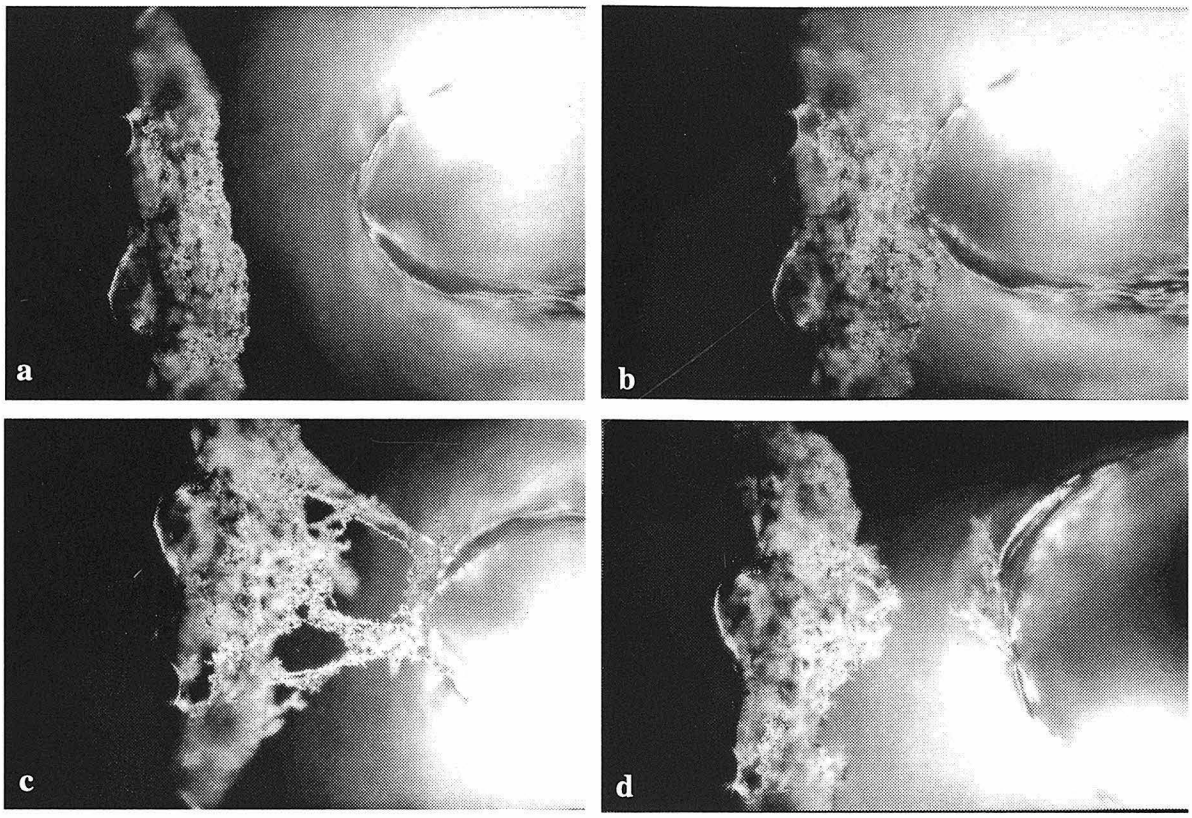

Although the tubes are probably not dispersed as well as air-oxidized nanotubes (oMWNT), one must remember that our starting material is completely undispersed solid block of cMWNT. As far as the author is aware, this is the only method for freeing closed multi-walled nanotubes from each other.

CHAPTER EIGHT
Chemistry on Mounted Nanotubes

This chapter describes the derivatization and labeling of carbon nanotubes mounted on SPM tips. Nanotubes were mounted by the method described in Chapter 6. Etched tungsten tips were used instead of AFM probes. This allowed more rapid mounting of carbon nanotubes and made analysis of the results easier. Nanotube tips were biotinylated through their carboxylic acid groups, using the protocol described in Chapter 7, and labeled with avidin-gold conjugates. Mounted tubes were examined with TEM. Although the yield of this process is low, nanotube end-labeling was definitely observed.

I. Introduction

In Chapter 6, a method to mount carbon nanotubes on SPM probes was described. In Chapter 7, a protocol for biotinylation of carboxylic acid groups present on opened nanotubes was described. Armed with methods for mounting, biotinylating, and labeling nanotubes, the final challenge was to combine these methods to biotinylate and label a single mounted nanotube.

II. Experimental

A. Multiplex Mounting of Carbon Nanotubes

Chapter 6 discussed the procedure by which carbon nanotubes are mounted on AFM tips. For doing chemistry on mounted nanotubes, tubes were mounted on electrochemically sharpened tungsten wire tips – essentially, STM probes. There were several reasons for this. First was the cost issue: tapping mode Si tips purchased from Digital Instruments cost approximately $40 per tip, whereas W wire was already available in the lab ($0). It was anticipated that many samples would be needed, so using AFM tips would have been quite costly.

Mounted nanotubes on AFM tips would also have been less useful than at Rice University. The Topometrix Discoverer prototype AFM present in our laboratory was

not capable of tapping mode operation. A Nanoscope III AFM available in the chemistry department (Lewis group / Beckman Institute Surface Analytical Facility) had tapping mode, but did not have the accessory required to make it capable of electroshortening mounted nanotubes. It was unclear if electroshortening could be performed without damage to the instrument.

Analysis of AFM-tip-mounted nanotubes also presented technical problems. A custom holder is required for examination of AFM tips with a transmission electron microscope[1]; unfortunately the sole TEM capable of accepting the existing holder at Caltech was out of commission. Using AFM-tip-mounted nanotubes would thus have been expensive, would have required modifying at least one AFM to electroshorten the tubes, and it would have required machining a new type of tip holder to analyze the tips by TEM.

Mounting the nanotubes on tungsten tips, on the other hand, provided some advantages. Unlike AFM-tip mounting, which can be done only one at a time, a simple holder, shown in Figure 1, allows mounting nanotubes on up to 5 W tips at one sitting.

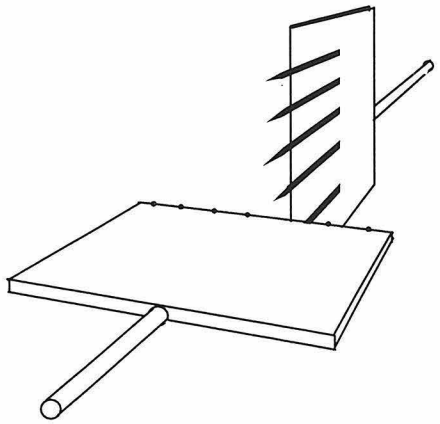

Figure 1: Multiplexing nanotube mounting apparatus. The taped nanotubes are on the holder in the foreground. 5 tungsten tips are held with another piece of double-sided carbon tape by the second holder (background).

Tungsten tips were produced by electrochemical etching in basic solution, loosely following the literature[2]. Briefly, a droplet of a 1 **M** solution of KOH is captured in a wire loop approximately 4 mm diameter, and a piece of tungsten wire is inserted through the loop. 10V are applied with the loop positive, and etching is allowed to proceed until the bottom piece of the wire falls free. This method produces two tips for each etch – one pointing up, one pointing down. Both tips were employed for mounting nanotubes with equivalent results.

B. Mounted Nanotube Liquid Treatment

1. Apparatus

Mounted nanotubes were treated with liquid using the simple apparatus shown in Figure 2, allowing up to six mounted tubes to be treated in the same solution simultaneously. Note that this apparatus should be capable of handling either STM- or AFM-tip mounted nanotubes.

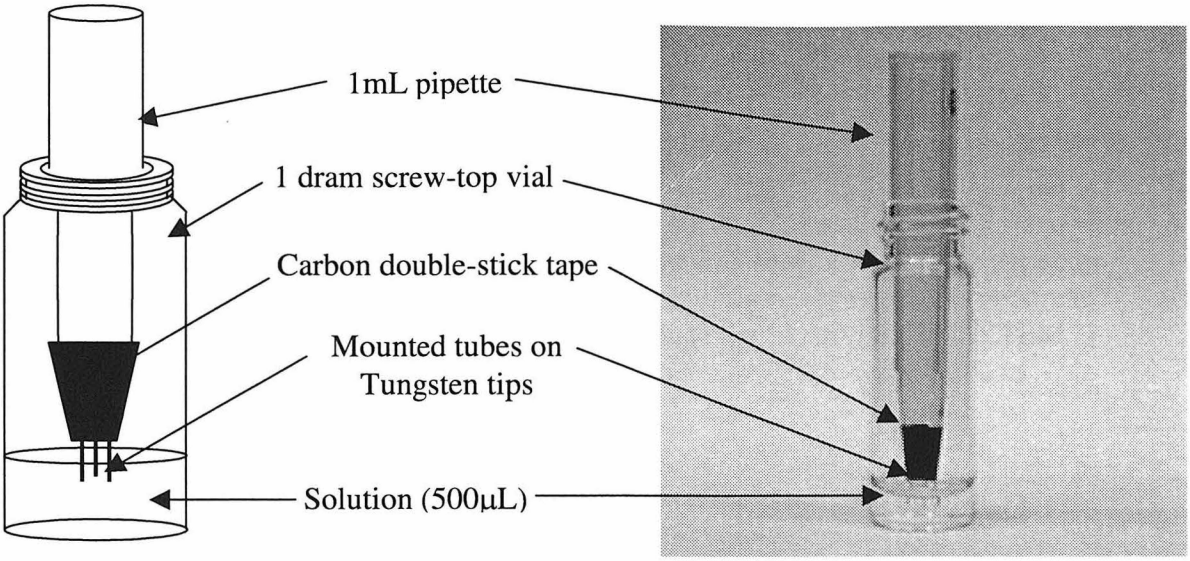

Figure 2: Apparatus for mounted nanotube liquid treatment

2. Hydrodynamic and Surface Forces:

As mentioned earlier (Chapter 7 Appendix, "Nanotube de-suspension"), a liquid interface can exert significant force on nanotubes. Two forces on nanotubes are of concern in liquid treatment: surface tension and viscous forces. The surface tension effect arises from the fact that the interfacial energy (J/m^2) between carbon nanotubes and water is high. Insertion of a carbon nanotube into water requires expanding the interface, which requires energy and therefore requires application of a force, as shown in Figure 3. This force resists the insertion of the nanotube, and can be enough to buckle the nanotube. Viscous forces arise from the drag of water moving past a nanotube.

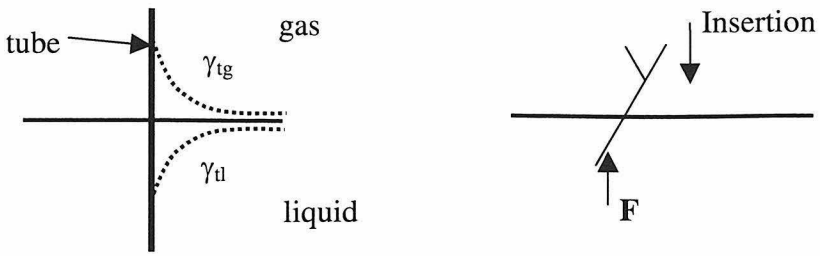

Figure 3: Insertion force

Insertion and viscous forces are important: the tube survival rate of the liquid treatments required for derivatization is approximately 50% (varying from 20% to 75% depending on the batch), and the author has noticed a negative correlation between the apparent length of the nanotube during mounting and the chance that it survives to the TEM analysis stage.

C. Chemistry

The possibility of damaging mounted nanotubes with repeated immersion and removal from solution required minor modification of the biotinylation protocol. The EDC, NHS, and biotin additions were compressed into one solution. An acid soak prior to derivatization was also added, in an attempt to increase the yield of biotinylation by making sure that all surface oxides capable of being converted to COOH groups were converted.

Informed by the literature[3], we also tried two new biotinylation reagents: biotinamidopentylamine (BPA), and biotin-LC-PEO-amine (BLCA), shown in Figure 4:

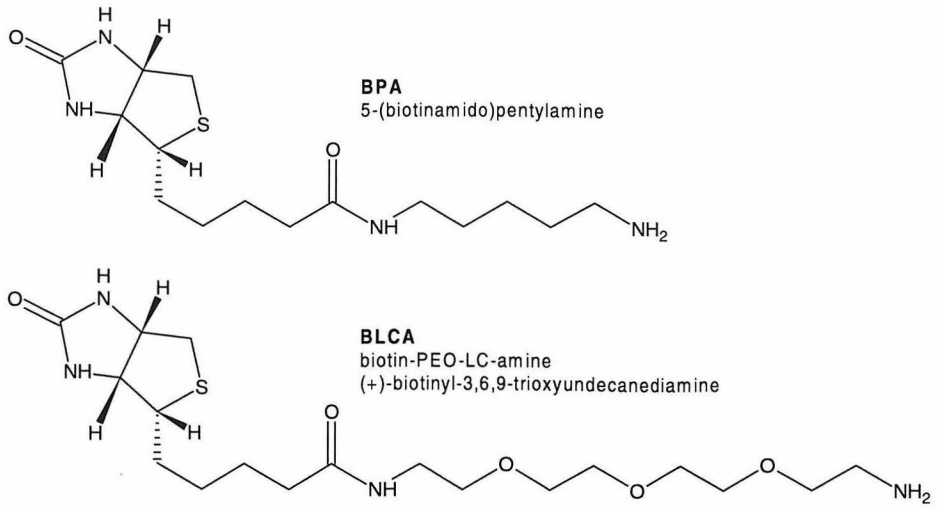

Figure 4: Molecular structures of BPA and BLCA

Mounted Nanotube Biotinylation Protocol:

1. Mount nanotubes
2. Soak in 1 N H_2SO_4 1 hour
3. Soak in MH_2O 30 minutes
4. Soak in NHS/EDC/Biotin solution
5. Incubate overnight
6. Soak in MH_2O 1 hour
7. Incubate in Au-SA solution 6 hours
8. Soak in MH_2O 1 hour

MES buffer: 0.1 **M** MES (2-N-Morpholinoethanesulfonic acid) pH 5.5.

EDC solution: 100 mg/mL EDC (1-(3-dimethylaminopropyl)-3-ethyl carbodiimide) in 0.1 **M** MES buffer, prepared fresh.

NHS solution: 4 mg/mL NHS (N-hydroxysuccinimide) in 0.1 **M** MES buffer, prepared fresh.

BH solution: 50 m**M** biotin-LC-hydrazide (biotinamidocaproyl hydrazide) in DMSO, prepared fresh.

BPA solution: 20 m**M** BPA (5-(biotinamido)pentylamine) in 0.1 **M** MES buffer, prepared fresh.

BLCA solution: 50 m**M** biotin-LC-PEO-amine ((+)-biotinyl-3,6,9-trioxyundecaneamine) in 0.1 **M** MES buffer, prepared fresh.

NHS/EDC/Biotin solution: Mix 25 μL EDC solution, 25 μL NHS solution, 50 μL biotin solution. Q.s. to 1 mL with MES buffer.

Au-SA solution: 50 μg/mL gold-streptavidin conjugate in PBS buffer (4nm Au colloid, Pierce).

D. TEM Examination

Derivatized nanotubes mounted on tungsten tips were examined with the transmission electron microscope using a standard TEM grid sample holder with minor modifications. The tungsten probes were mounted on a TEM slot grid with silver paint, taking care to keep the probe tip from hitting the surface.
The TEM sample holder is modified by machining a groove from the grid nest back towards the shaft of the holder; the tungsten wire is thus held in place and level during imaging.

III. Results and Discussion

After several batches of mounted tubes, we obtained the desired evidence of derivatization of mounted tubes.

Figures 5a-c show a nanotube mounted on a tungsten tip, derivatized with the protocol described above using BPA. At the highest resolution (1,850,000 X), the size of the gold balls can clearly be seen. The average size is approximately 3.2 nm, slightly smaller than the nominal 4 nm claimed by the manufacturer. The structure of the tube can also be seen. The round circular shape appears to be a hole through the side of the nanotube. The author has observed that gold balls seem to preferentially attach near etched parts of the tubes; this is consistent with attachment through COOH groups. The coating present on the tube may be glycerol from the streptavidin-gold colloid solution.

Figures 6a-c shows a mounted nanotube derivatized using BLCA. Gold balls are clearly attached, although the coating is present here as well.

Figures 7-9 show controls. Since yield of labeled tubes was relatively low, pictures of *un*labeled single tubes are not very meaningful. Pictures of bulk samples (containing many tubes) are more informative. The author had a bias towards taking pictures of gold balls; in general, if balls were not present, no pictures were taken. Many fields of view were examined and found to be empty of gold balls. Note that although a few gold balls are present in these images, the vast majority of the tubes have no gold colloid attached.

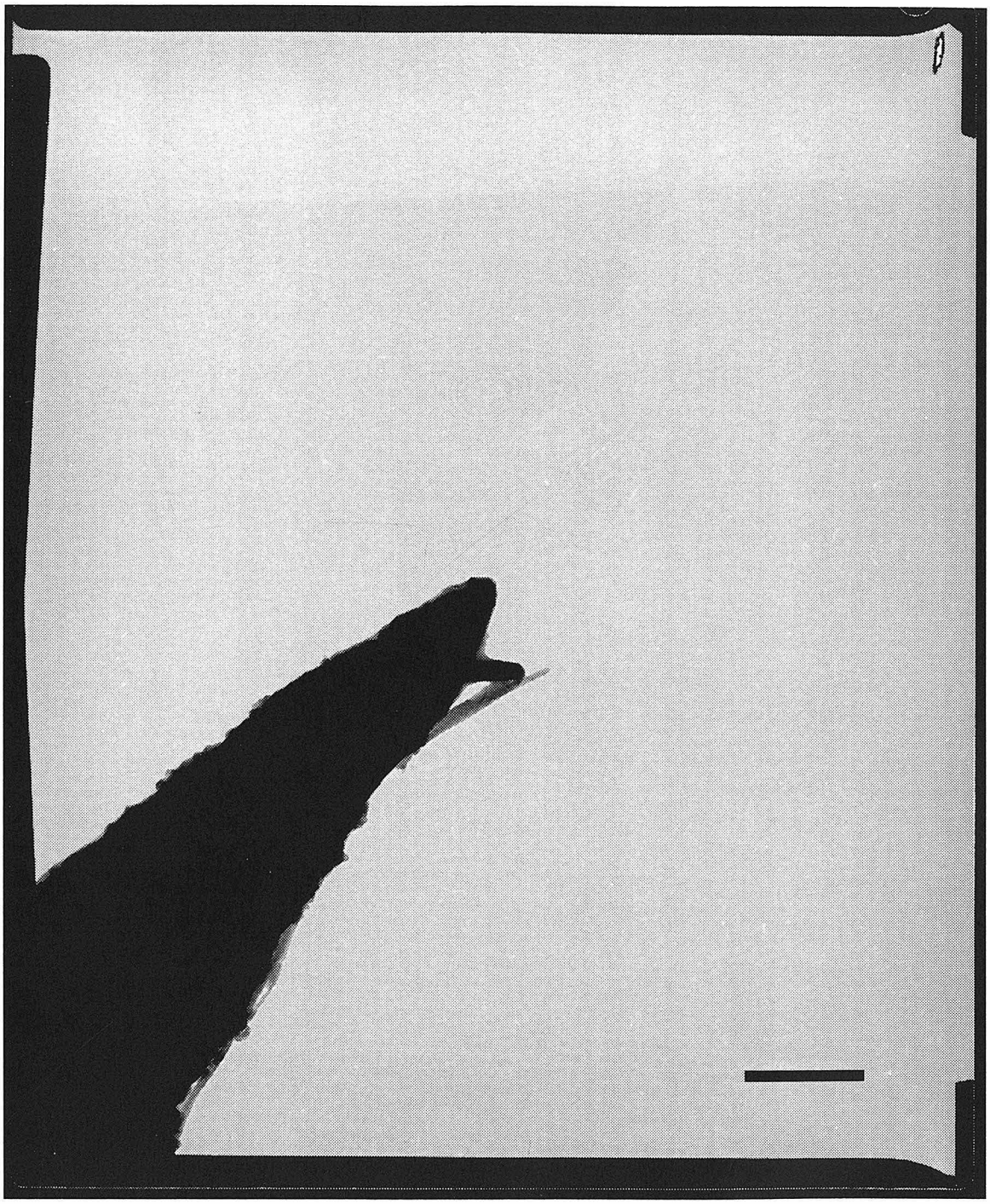

Figure 5a: Mounted tube derivatized with BPA. 18,500 X. The scale bar is 1 μm long. The tube projects from a "knee" of some kind. The visible tube is approximately 1 micron long, but appears to run down the lower right edge of the tungsten tip.

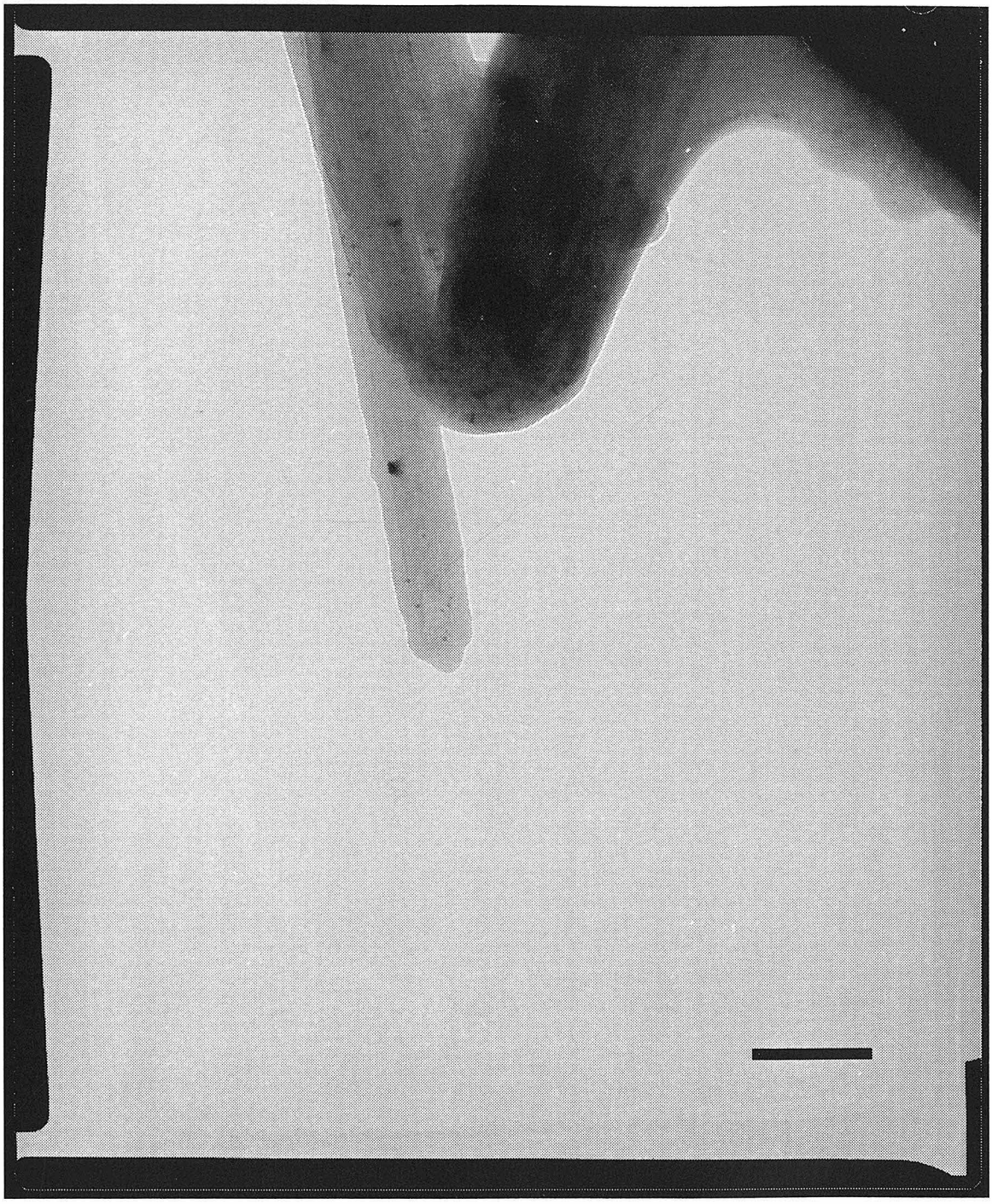

Figure 5b: Mounted tube derivatized with BPA. 185,000 X. The scale bar is 100 nm long. The "knee" appears to be a bundle of nanotubes. Gold balls are visible as small dark specks near the end of the tube.

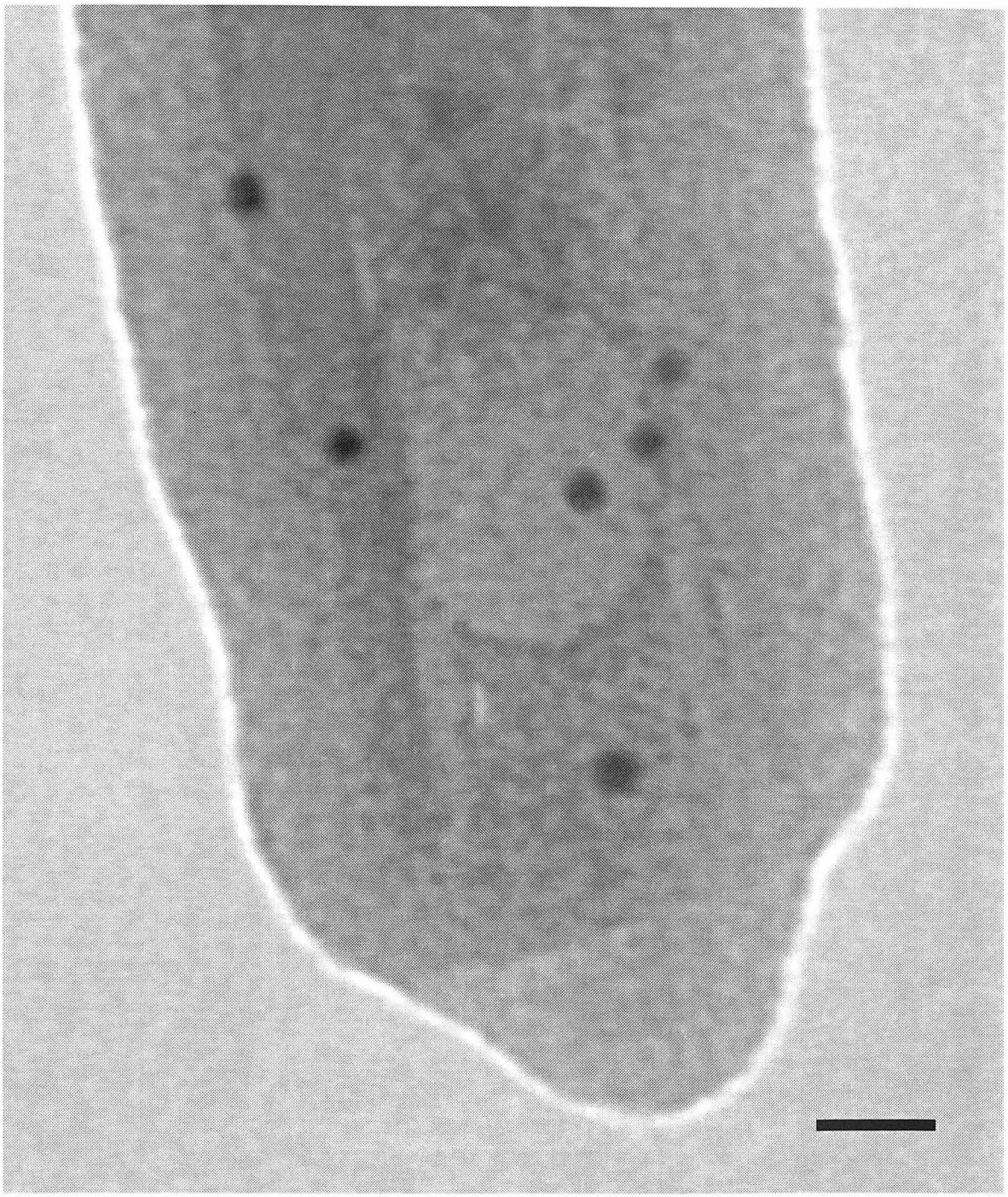

Figure 5c: Mounted tube derivatized with BPA. 1,850,000 X. The scale bar is 10 nm long. The gold balls are clearly seen. A coating is visible on the nanotube.

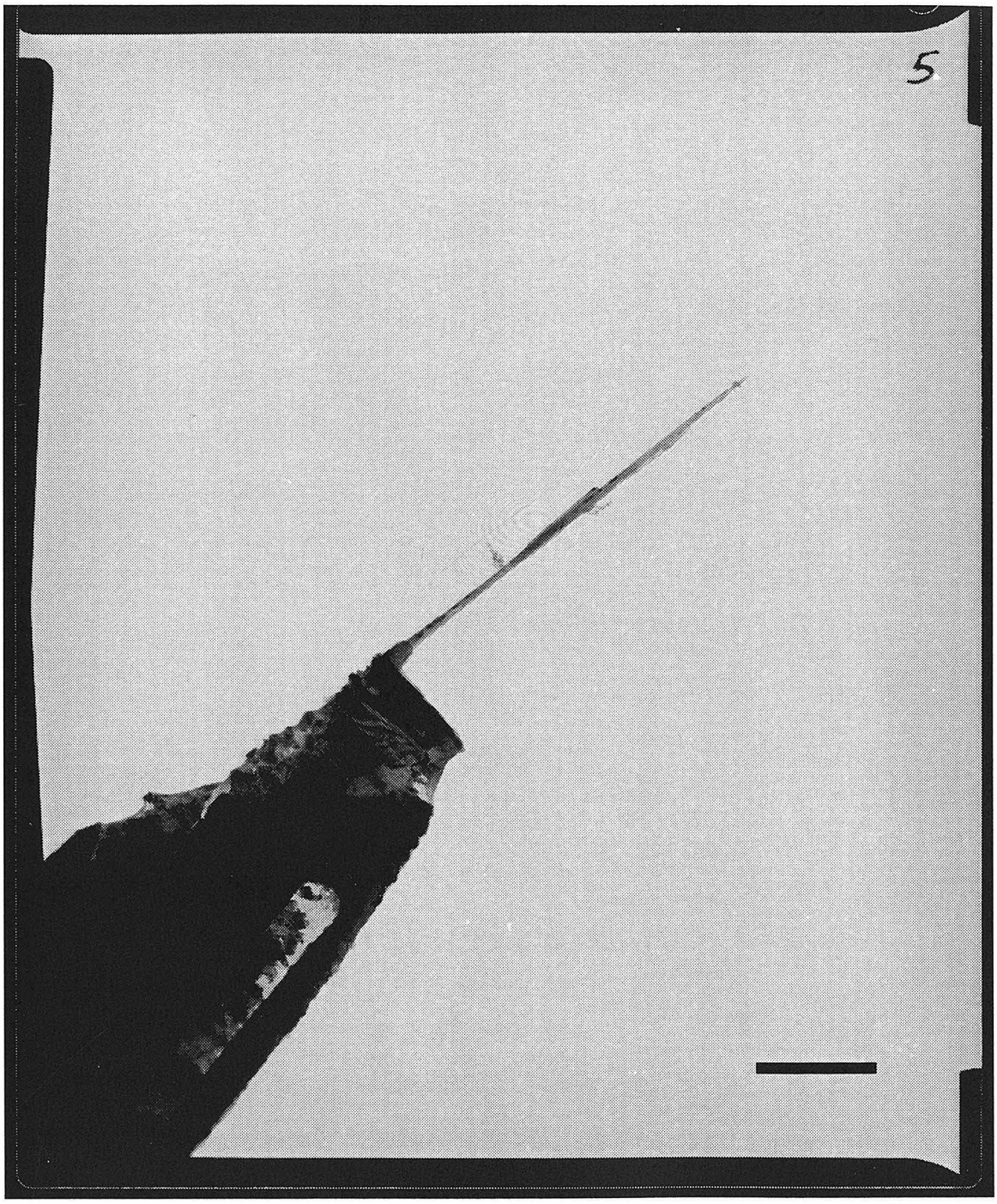

Figure 6a: Mounted tube derivatized with BLCA. 18,500 X. The scale bar is 1 μm long. The tube appears to be ~3 microns long.

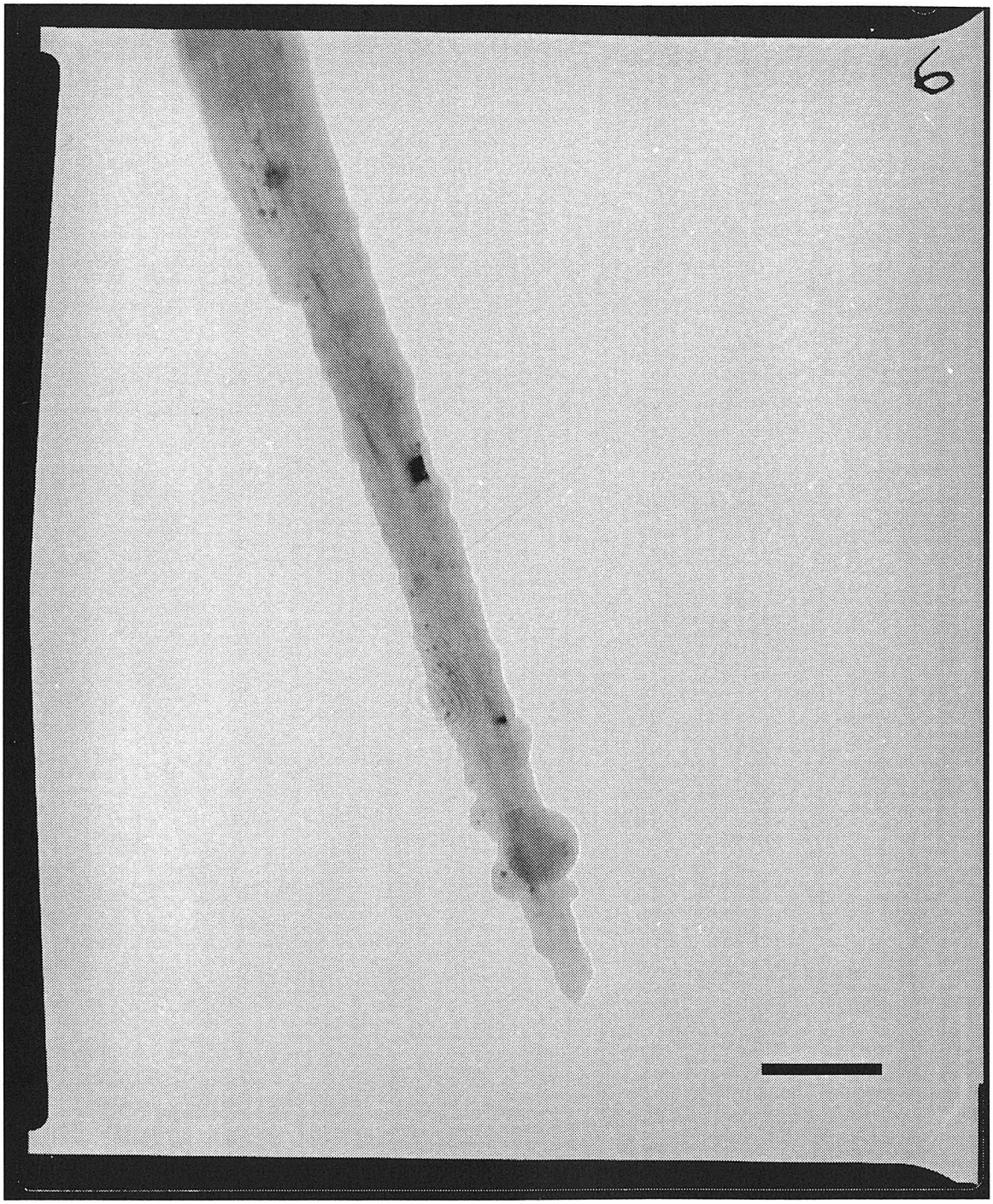

Figure 6b: Mounted tube derivatized with BLCA. 185,000 X. The scale bar is 100 nm long. Attached gold balls are visible just to the lower left of the picture center.

Figure 6c: Mounted tube derivatized with BLCA. 1,850,000 X. The scale bar is 10 nm long. Gold balls are visible on the surface of the nanotube. The "ripples" are an interference pattern from the process used to scan the negatives into digital form.

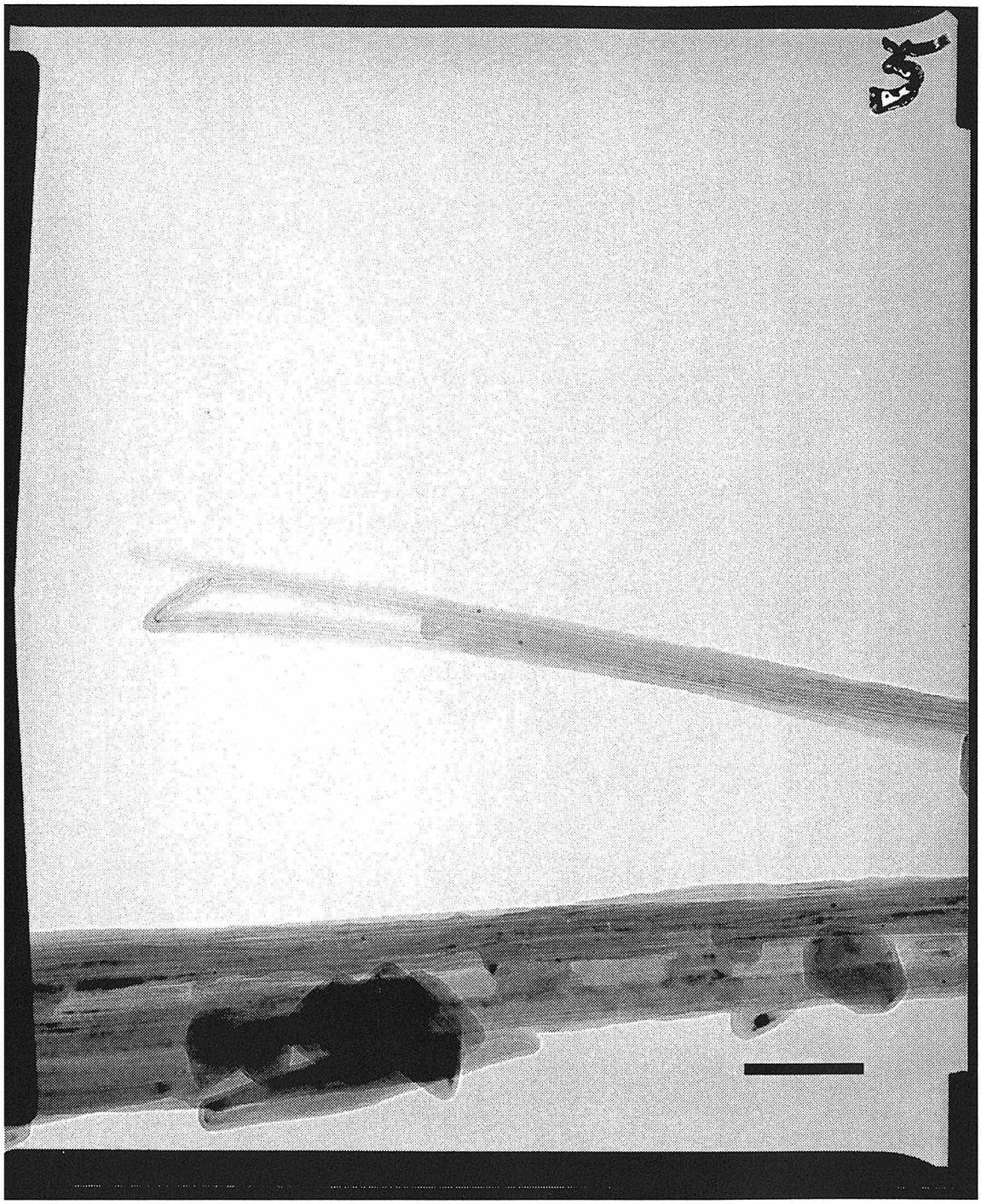

Figure 7a: Control. Bulk oMWNT sample, derivatized with biotin, omitting EDC. 185,000 X. The scale bar is 100 nm. A few Au balls evident, but quite rare.

Figure 7b: Control sample prepared identically to 7a. 280,000 X. Again, gold balls are very rare. The scale bar is 100 nm.

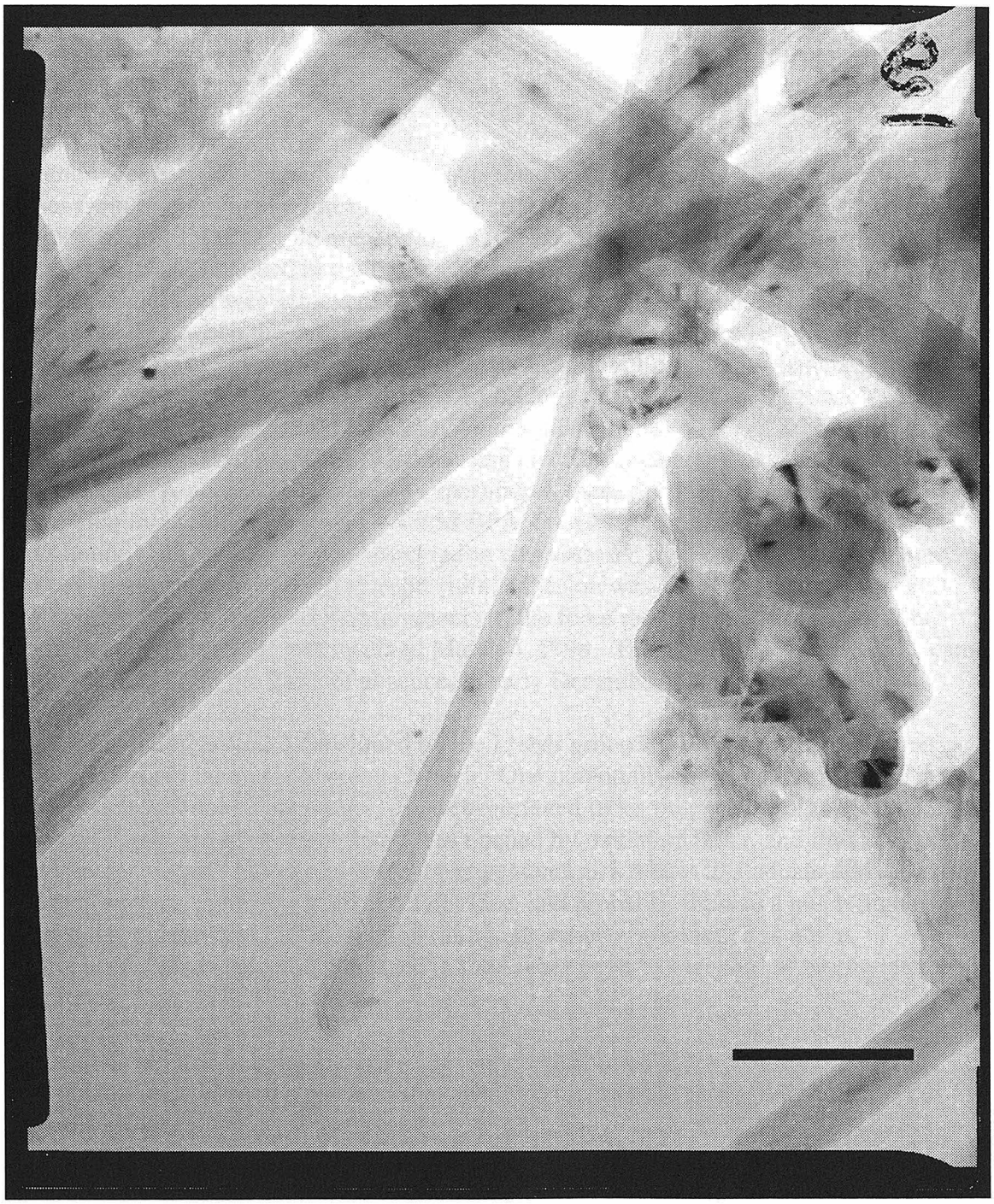

Figure 7c: Control. 280,000 X. Another bulk oMWNT control sample, derivatized with EDC but omitting biotin. Again, a few Au balls are present, but they are very rare. The scale bar is 100 nm.

IV. Conclusion

Mounting, derivatization, and TEM analysis are time-consuming. The combination of losses from hydrodynamic forces (~50%), derivatization failures, and sample handling attrition during TEM sample preparation (~10%) meant that *statistical* numbers of samples were not obtained in the time available. There is little doubt that biotinylation of mounted nanotubes was achieved; the fact is, however, that the yield is relatively low. During the time when the author was on leave of absence (1/1/98 – 10/30/98), the Lieber group published a paper in Nature: **Covalently functionalized nanotubes as nanometre-sized probes in chemistry and biology**, S. S. Wong, E. Joselevich, A.T. Woolley, C.L. Cheung and C.M. Lieber. *Nature*, **394**: (6688) 52-55. Carbon nanotubes were mounted on tapping-mode AFM tips and electroshortened by the method described in Chapter 6. Among other (simpler) experiments, these tips were biotinylated by immersion in a solution containing 5 mM BPA, 50 mM EDC, and 0.1 M MES at pH 6.0 for 2 hours. The success of the biotinylation was assessed by measuring the adhesion force with a surface coated with streptavidin; adhesion was quantized in units of ~200 pN, consistent with previous measurements of the force required to break the avidin-biotin bond[4]. This paper was received March 4, 1998. The author's positive results came after returning from his leave of absence, in early December 1998.

The biotinylation protocol developed by the Lieber group is virtually identical to that developed in our laboratory here at Caltech. One potentially significant difference is the use of electroshortened nanotubes. Electroshortened tubes may have a higher number of carboxylic acid groups present than tubes opened by oxidation in air, and thus may be easier to derivatize. The use of force measurements as a means to evaluate derivatization and map surface chemistry is an excellent idea, and probably allowed a much higher sample throughput than TEM imaging (although, strictly speaking, it is not as informative). One issue not addressed in the Lieber paper is the yield of biotinylated nanotubes.

While disappointed at being beaten to the punch, the author takes pleasure in having independently developed a protocol that achieved his primary goal – derivatization of carbon nanotubes.

---

[1] DeRose, J.A., Revel, J.P. (1997). Examination of Atomic (scanning) Force Microscopy Probe Tips with the Transmission Electron Microscope. *Microscopy and Analysis;* **3**: (3) 203-213

[2] Fotino, M., (1993). Tip Sharpening by Normal and Reverse Electrochemical Etching. *Review of Scientific Instruments*, **64**: (1) 159-167

[3] Wong, S.S., Joselevich, E., Woolley, A.T., Cheung, C.L., Lieber, C.M. (1998). Covalently Functionalized Nanotubes as Nanometre-sized Probes in Chemistry and Biology. *Nature*, **394**: (6688) 52-55

[4] Lee, G.U., Kidwell, D.A., Colton, R.J. (1994). Sensing Discrete Streptavidin Biotin Interactions with Atomic-force Microscopy. *Langmuir*, **10**: (2) 354-357

Appendix A

Photoresist Durability

Durability of AZ photoresist

Condition:	Effect:
50:50 HCl/MeOH, 20 min RT	No damage
50:50 HCl/MeOH, 20 min warm	Destroyed
[H_2SO_4], 20 min:	No damage
[H_2SO_4], Hot:	PR film lifts off
H_2O	No Damage
H_2O, 5 min boiling	Physically destroyed
Sonication, 10 min	Destroyed
[NH_3] gas, RT	Cracking and crazing
[$SOCl_2$]	Instantly destroyed
[aminoethanol]	Quickly destroyed
[butylamine]	Quickly destroyed
Toluene, 15 min	No damage
C8-SH 2mM in Octane	No damage
C2-SH 0.5% in Octane	No damage
HO-C_3-SH 2mM in Octane	Destroyed
[TMS]	Very slight dissolution
[APTS] 10 min	Destroyed
APTS 2% in tol, 20 min	No dissolution
APTS 2% in tol. 60 min	Embrittlement, some damage
Acetone	Complete removal
Ethanol	Effectively destroyed
Developer (aqueous base)	
- room light stored	Complete removal
- NH3 100C 15 min	Removes in ~1 min
- NH3 100C 60 min	Partial removal after 10 min

Appendix B

Absorbance-Surface Density Calculation

Conversion of absorbance to molecular surface density

Absorbance measurements obey Beer's Law, normally written

$$A = \varepsilon bc,$$

where b is the path length in cm, c is the concentration in mol/L, and ε is the molar absorptivity, with units of $cm^{-1}mol^{-1}L$. Since we have a flat surface rather than a solution, we need to recast ε in units appropriate to the situation:

$$[\varepsilon] = cm^{-1}mol^{-1}L\ (1000\ cm^3/L)$$

$$= 10^3\ mol^{-1}cm^2\ (1m/100\ cm)^2$$

$$= 10^{-1}\ mol^{-1}m^2\ (1\ mol / 6.02 \times 10^{23}\ molecules)$$

$$= 1.66 \times 10^{-25}\ m^2/molecule$$

m^2/molecule is a cross-section, so we write the absorption cross-section σ_a in terms of ε:

$$\sigma_a = (1.66 \times 10^{-25})\varepsilon\ m^2/molecule$$

where ε is in $cm^{-1}mol^{-1}L$. Now we can rewrite Beer's law as

$$A = \sigma_a\sigma$$

where sigma is the surface density of molecules in molecules/m^2. For fluorescein, the molecule used here, ε = 72,000 $cm^{-1}mol^{-1}L$, so σ_a is clearly

$$\sigma_a = 1.2 \times 10^{-20} \text{ m}^2/\text{molecule}.$$

We see that an absorbance A=1 gives

$$A = \sigma_a \sigma$$

$$\sigma = 1/\sigma_a$$

$$= 8.33 \times 10^{19} \text{ molecules/m}^2$$

$$= 83.3 \text{ molecules/nm}^2.$$

The same result can be obtained by a more intuitive consideration. Consider a 1 cm^3 cube of solution at a concentration of 1 **M**. By Beer's Law, $A=\varepsilon bc = |\varepsilon|$. In this cube, the total amount of solute is (1 **M**)(.001 L) = 10^{-3} mol. Let us now perform a thought experiment, where the solute is compressed into only half the cube. We see that the path length is irrelevant as long as the total amount of solute present to absorb the beam remains the same. The absorbance is the same even if all the molecules "settle" uniformly on the side of the cube where the light enters. If that were to occur, the surface density would then be 10^{-3} mol/cm^2 = 10 mol/m^2 = 6.02 x 10^{24} molecules/m^2. 1 part in [Epsilon] of this would give an absorbance of 1, so we would have 6.02 x 10^{24} / 72,000 = 8.3 x 10^{19} molecules/m^2, in accordance with the result obtained above.

One correction must be applied to this result: absorbances measured here pass through *both* sides of a glass slide. Further, the glass slides were held at a slight angle to the incident light, increasing the effective surface density. Thus, we must divide our measured absorbances by 2.17 before converting to molecules per unit area.

Appendix C

US Patent 5,824,470

Method of Preparing Probes for Sensing and Manipulating Microscopic Environments and Structures

US005824470A

United States Patent [19]

Baldeschwieler et al.

[11] **Patent Number: 5,824,470**

[45] **Date of Patent: Oct. 20, 1998**

[54] **METHOD OF PREPARING PROBES FOR SENSING AND MANIPULATING MICROSCOPIC ENVIRONMENTS AND STRUCTURES**

[75] Inventors: **John D. Baldeschwieler**, Pasadena, Calif.; **David Randall Baselt**, Alexandria, Va.; **Marc A. Unger**; **Stephen D. O'Connor**, both of Pasadena, Calif.

[73] Assignee: **California Institute of Technology**, Pasadena, Calif.

[21] Appl. No.: **453,958**

[22] Filed: **May 30, 1995**

[51] **Int. Cl.**[6] **C12Q 1/68**; G01N 33/53; G01N 21/00; C01B 25/00

[52] **U.S. Cl.** **435/6**; 435/7.1; 435/7.2; 422/57; 204/157.45; 204/157.6

[58] **Field of Search** 435/6, 7.1, 7.2; 204/157.45, 157.6; 422/57

[56] **References Cited**

U.S. PATENT DOCUMENTS

5,063,081	11/1991	Cozzette et al.	427/2
5,242,541	9/1993	Bayer et al.	156/653
5,250,473	10/1993	Smits	437/238
5,363,697	11/1994	Nakagawa	73/105
5,495,109	2/1996	Lyndsay et al.	250/306

OTHER PUBLICATIONS

Lee et al. (1994) Langmuir 10:354–357.
Frisbie et al. (1994) Science 265:2071–2074.
Lee et al. (1994) Science 266:771–773.

Primary Examiner—Ardin H. Marschel
Assistant Examiner—Jezia Riley
Attorney, Agent, or Firm—Swanson & Bratschun LLC

[57] **ABSTRACT**

Probes for sensing and manipulating microscopic environments and structures, their method of preparation and methods of use are disclosed.

5 Claims, 5 Drawing Sheets

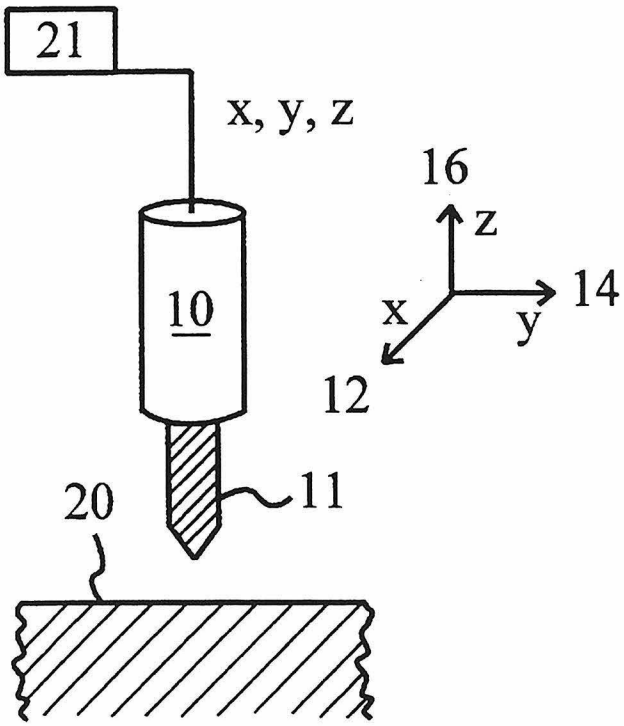

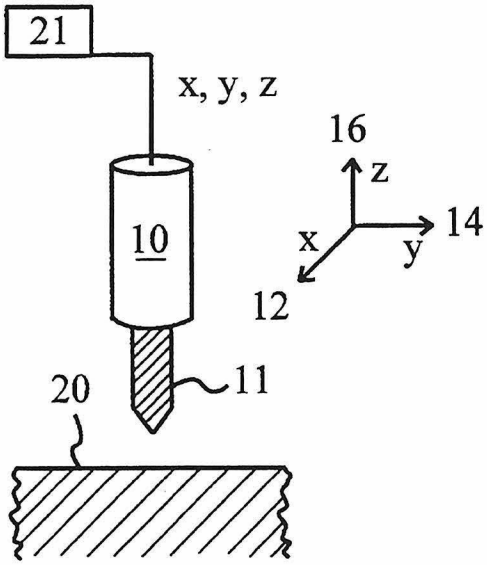

FIG. 1A

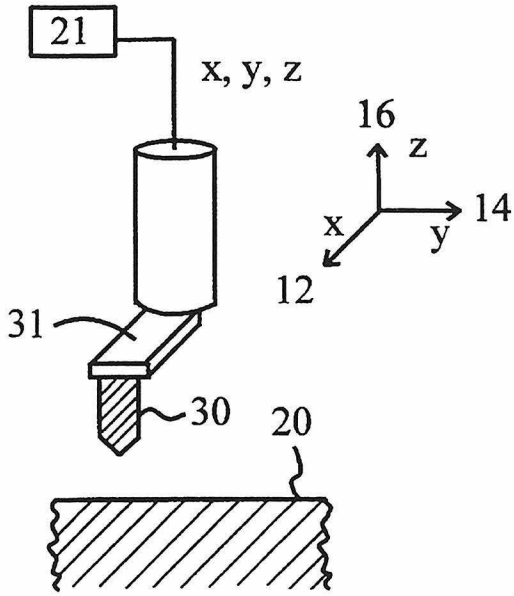

FIG. 1B

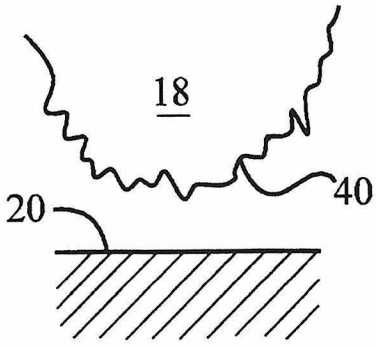

FIG. 1C

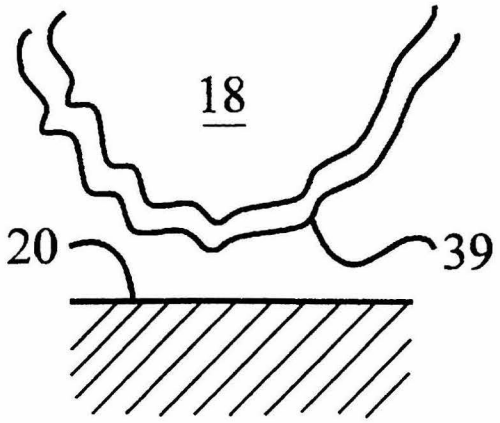

FIG. 2A

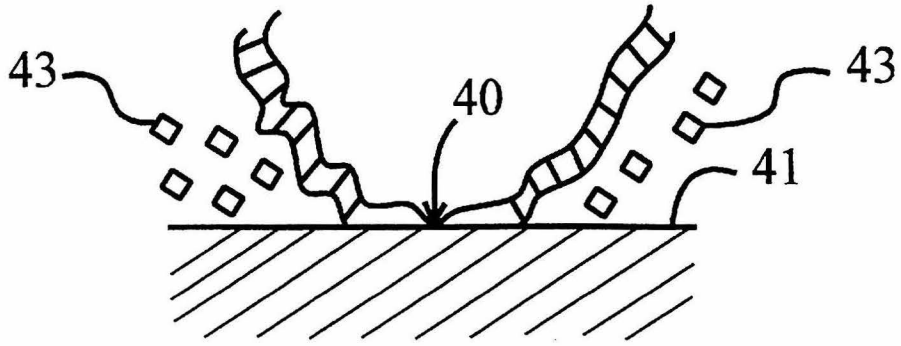

FIG. 2B

FIG. 3

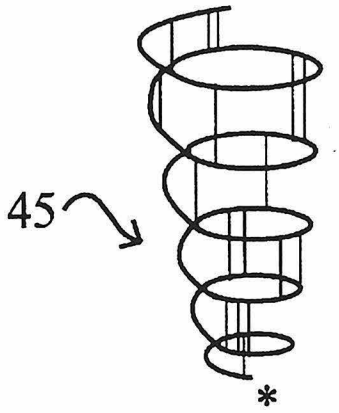

FIG. 4

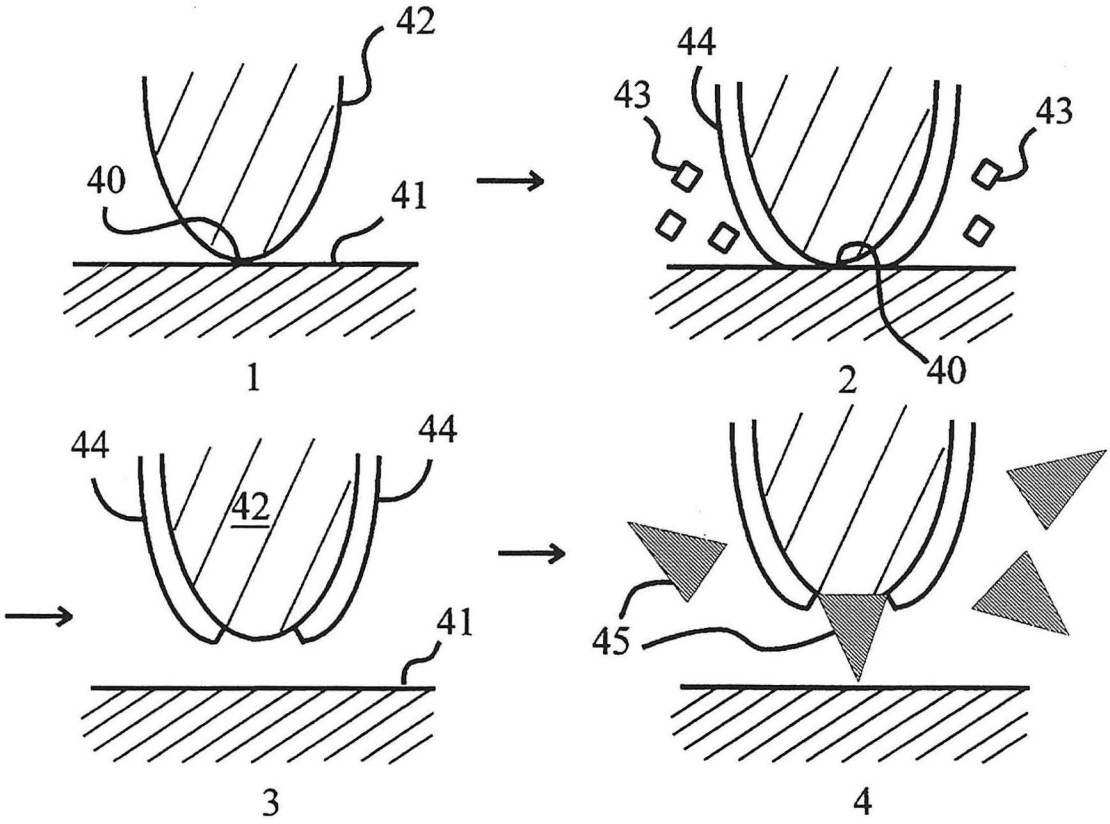

FIG. 5

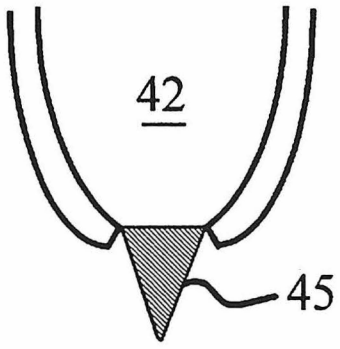

FIG. 6

METHOD OF PREPARING PROBES FOR SENSING AND MANIPULATING MICROSCOPIC ENVIRONMENTS AND STRUCTURES

FIELD OF THE INVENTION

The present invention relates generally to probes for sensing and manipulating microscopic environments and objects, and more particularly to a chemically functionalized scanning probe tip.

BACKGROUND OF THE INVENTION

Information about the microscopic three dimensional topography of a surface may be obtained by scanning probe microscopy (SPM) techniques providing atomic or near-atomic resolution. The principal scanning probe microscopes are the scanning tunneling microscope (STM) and the atomic force microscope (AFM), both of which achieve the microcharacterization of materials by the use of a fine scanning probe tip. The force or current between the sample atoms and the atoms of the tip is a highly nonlinear function of their relative distance. For surfaces that are nearly atomically flat, the force or current between the sample and the tip is usually dominated by a single atom of the tip that happens to extend slightly more than the others. This property allows imaging of the flat surface with atomic resolution.

The STM operates on electric principles and therefore requires both a conducting tip and a conducting sample. When the tip is positioned within a few atomic diameters of the sample and a bias voltage is applied, a small tunneling current flows between tip and sample. The tip may then be moved laterally with a piezoelectric translator to scan a surface while a computer-controlled feedback mechanism adjusts the height of the tip to maintain a constant current (constant-current mode), or the tip may be moved across the surface at a constant height while monitoring the current (constant-height mode). A surface image may be generated by plotting the tip height or current change versus the lateral position of the tip.

Atomic force microscopy relies upon atomic interactions between the tip and the sample, and has more versatility in that it requires neither a conducting tip nor a conducting sample. In atomic force microscopy, the surface of a sample is scanned by a sharp tip held at the end of an elastic member, such as a wire or cantilever beam, attached at its other end to a transducer. The force between the tip and the sample due to interaction of their electron clouds deforms the elastic member and, if the member is vibrated by the transducer, changes its resonance frequency and amplitude of oscillation. The deformation or vibration is monitored using electron tunneling (using an STM), or laser interferometry, or with an optical lever, and the resulting signal may be used to drive the transducer in a feedback loop. In this manner, the surface topography of the sample may be characterized. The sensitivity of the AFM technique is such that it is also possible to measure the chemical interactions between chemical groups on the probe surface and chemical groups on the sample surface. Thus, it is possible to obtain a chemical interaction image of the sample, which yields information about the chemical nature of the sample surface.

Other scanning probe microscopes, such as magnetic force microscopes and electrostatic force microscopes operate on analogous principles to provide microscopic surface images.

At present, most tips have a tapered shape ending with a rounded surface having a radius of curvature of 5 nm or more. Previously used materials for tips include silicon, silicon nitride, diamond, graphite, transition metal carbides and refractory metals. Such tips may be obtained by one or a combination of methods including cleaving or single crystals, chemical or electrochemical etching, and surface reactions such as anomalous dry oxidation of silicon followed by etching. The radius of curvature and the angle of taper of the tip limit the resolution of imaging of steep or low-radius-of-curvature surface features in the scanning probe microscopes known heretofore, and prevent imaging such features with atomic resolution.

Previous attempts to reduce tip size for improved resolution have focussed on electrochemical etching of traditional tip materials, particularly silicon and tungsten. U.S. Pat. No. 5,242,541, for example, provides a method for producing single-crystal silicon tips with radii of 2 to 5 nm by a masking and etching process. The formation of tungsten tips having radii of curvature as small as 1 to 5 nm by reverse electrochemical etching has also been disclosed (Fontino (1993) Rev. Scientific Instruments 64:159–167). However, etching produces tips with irregular shapes, only some of which are suitable for microscopy. In order to maximize production quality and the resolution of the images obtained by the scanning probes there is still a need for scanning probe tips having regular, predictable shapes, smaller radii of curvature and greater angle of taper than currently available.

There have been few attempts to modify the chemical nature of the probe surface. The non-covalent derivatization of a silicon nitride probe tip by avidin and biotin has been demonstrated. Semi-covalent derivatization of a silicon nitride cantilever by self-assembly of thiols on a sputtered gold surface has also been disclosed. Non-covalent attachment, however, is not sufficient, because the interaction forces between attached molecule and sample are of a comparable strength, and may detach the molecules from the probe surface. The strength of the gold-thiol bond appears nearly sufficient, but the thick layer of gold used reduces the resolution of the probe microscopy technique. Thus, there is a need for a technique which can reliably and stably functionalize probe surfaces.

Heretofore, scanning probe microscopes have been useful for sensing atomic environments. However, the present invention is advantageous in that probes are provided for functions beyond the imaging of microscopic surfaces. For example, tips are provided by the present invention with specific functional moieties to target and/or interact with biological molecules in vivo, or to assist in nano-chemistry, lithography, or nanofabrication techniques.

Accordingly, an object of the present invention is to provide a method of preparing a probe tip functionalized with chemical moieties.

It is another object of the present invention to provide a method of preparing a probe tip suitable for scanning probe microscopy comprising a single macromolecule attached at its apex.

It is a further object of the present invention to provide methods of stiffening appropriate macromolecules, preparing a probe tip to receive a single macromolecule and securing a single macromolecule to a probe tip.

It is a further object of the present invention to provide a method of preparing a probe tip functionalized with a manipulative agent or agents.

It is yet another object of the present invention to provide a method of sensing a microscopic environment using probes prepared by the method described herein.

It is yet another object of the present invention to provide a method of manipulating a microscopic environment, object, or structure using probes prepared by the method described herein.

Additional objects and advantages of the invention will be set forth in the description which follows, and in part will be obvious from the description, or may be learned by the practice of the invention. The objects and advantages of the invention may be realized and obtained by means of the instrumentalities and combinations particularly pointed out in the claims.

SUMMARY OF THE INVENTION

The present invention is directed to methods and apparatus for a probe for sensing and/or manipulating a microscopic environment or structure. For sensing and manipulation techniques that require a probe tip which is entirely functionalized with a specific chemical moiety, the probe tip is prepared using covalent derivatization.

For sensing and manipulation techniques which require attachment of a single macromolecule, the method of preparing the probe comprises the step of protecting an area at the tip of a probe from a passivating agent, where the area is suitable for covalent linkage thereto of a single macromolecule. Preferably, this area is in the range of about 10,000 $Å^2$ to 3 $Å^2$. The tip is then contacted with a passivating agent so that its unprotected portion is passivated. The unpassivated area is then deprotected and one end (the proximal end) of a single macromolecule is covalently attached to the unpassivated area.

For SPM with improved tip radius and aspect ratio, the attached macromolecule preferably has a substantially cylindrical or conical shape and an outer diameter at its distal (unattached) end of about 2 to 50 Å. The probe prepared according to the invention may be used to determine surface topography, or as a chemical or biochemical tool to detect or manipulate molecules or other microscopic substrates.

BRIEF DESCRIPTION OF THE DRAWINGS

The accompanying drawings, which are incorporated in and constitute a part of the specification, schematically illustrate a preferred embodiment of the invention, and together with the general description given above and the detailed description of the preferred embodiment given below, serve to explain the principles of the invention.

FIG. **1A** is a schematic representation of a scanning probe microscope showing the configuration of the piezoelectric tube, tip and sample used for Scanning Tunneling Microscopy.

FIG. **1B** is a schematic representation of a scanning probe microscope showing the configuration of the piezoelectric tube, cantilever, tip and sample used for Scanning Force Microscopy.

FIG. **1C** is an enlarged view of the apex of a typical scanning probe tip **18** known in the art.

FIG. **2A** is an enlarged view of the apex of a scanning probe tip, completely functionalized according to the present invention.

FIG. **2B** is an enlarged view of the apex of a scanning probe tip, passivated except for a small area of the apex, as described in the present invention.

FIG. **3** is a schematic representation of a linker molecule according to the present invention.

FIG. **4** is a schematic representation of a single, rigid macromolecule according to the present invention.

FIG. **5** is a schematic representation of the attachment of a single macromolecule to a scanning probe tip according to the present invention.

FIG. **6** is a schematic representation of a fully assembled scanning probe tip according to the present invention.

DESCRIPTION OF THE PREFERRED EMBODIMENTS

The present invention is directed to a modified scanning probe tip, methods of preparation and methods of use thereof. The invention will be described, in part, in terms of preferred embodiments, as illustrated in the accompanying FIGS.

Referring to FIG. **1A**, a piezoelectric tube **10** of a scanning probe microscope equipped with a conventional tip **11**, is shown. The tube may be extended in the x **12**, y **14** and z **16** directions to support and control the scanning probe tip **11** as it scans over the substrate **20**, under control of the computer **21**.

In FIG. **1B**, the tip **30** is at the end of a cantilever **31**, by which the force on the tip may be measured. The tip **30** may be composed of silicon, silicon nitride, diamond, graphite, transitional metal carbides or refractory metals and sharpened by one or a combination of methods including cleaving of single crystals, chemical or electrochemical etching, ion milling, and surface reactions such as anomalous dry oxidation of silicon followed by etching. The cantilever may be composed of silicon, silicon nitride, diamond, or metal.

FIG. **1C** shows an expanded view of the apex **40** of a typical scanning probe tip **18** known in the art. The shape and sharpness of the tip is highly dependent upon the manner in which the tip is prepared.

Functionalization of the scanning probe

Functionalization, as used herein, means the modification of a surface to terminate it with a specific chemical moiety. Depending on the functionalization method, the target moiety may be rigidly determined or freely chosen. If the target moiety may be freely chosen, it will be referred to herein as "Y".

The following are schematic representations (I, II, III, and IV) of the functionalization of the scanning probe tip according to the present invention. In these schemes D represents the reactive group on the substrate; A, B and X are other reactive groups used to form intermediates and Y is the target moiety, the specific chemical moiety which terminates the probe. In schemes II, III and IV, linker molecules are used, typified by the molecule of FIG. **3**.

I. 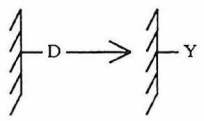

(single step)

-continued

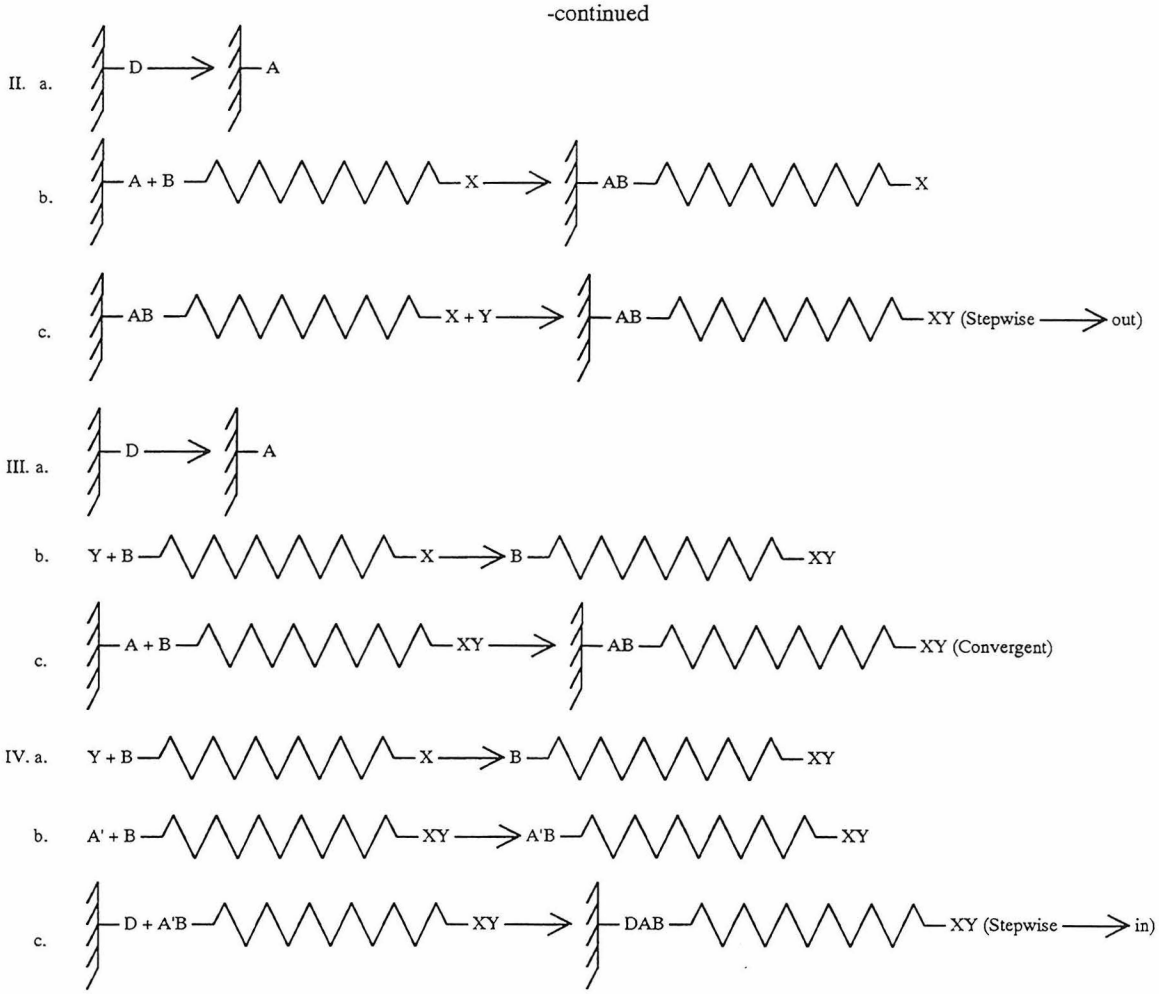

Scheme I shows a direct functionalization from the native reactive moiety on the surface of the probe by conversion in single step to the desired Y moiety. This will be referred to as a "single step" functionalization.

Scheme II is a multi-step conversion from the native probe surface moiety to an intermediate functional group "A" which is, in turn, reacted with a linker terminated at its distal end with a functional group "X". The group "X" is then reacted with the "Y" functional group to form the desired terminus. This will be referred to as a "stepwise out" functionalization.

Scheme III is a multi-step conversion whereby the native functional group of the probe is converted to intermediate function group "A". In a separate step the desired functional terminus "Y" is attached to the end of a linker. The proximal end of the linker containing functional group "B" is then reacted with the surface functional group "A" to attach the linker to the surface. This will be referred to as a "convergent functionalization."

Scheme IV shows the separate synthesis of a functionalizing reagent and its attachment to the probe surface. The functionalizing reagent is synthesized with proximal group A', which directly reacts with surface functional group O, and distal group Y.

The two preferred materials used for the scanning force microscopy probe are silicon nitride (Si_3N_4) and silicon (Si). Both of these materials develop a layer of silicon dioxide (SiO_2) on exposure to atmospheric oxygen. Silicon dioxide is terminated with silanol groups Si-OH, approximately 1–10 groups/nm^2. Table 1 shows the reactions of the silanol groups, indicating their target moieties.

TABLE 1

Silanol Reactions		
$\geq Si-OH + CH_3Li$	$\longrightarrow$	$\geq Si-O-Li + CH_4$
$\geq Si-OH + ROH$	$\rightleftharpoons$	$\geq Si-OR + H_2O$

TABLE 1-continued

Silanol Reactions

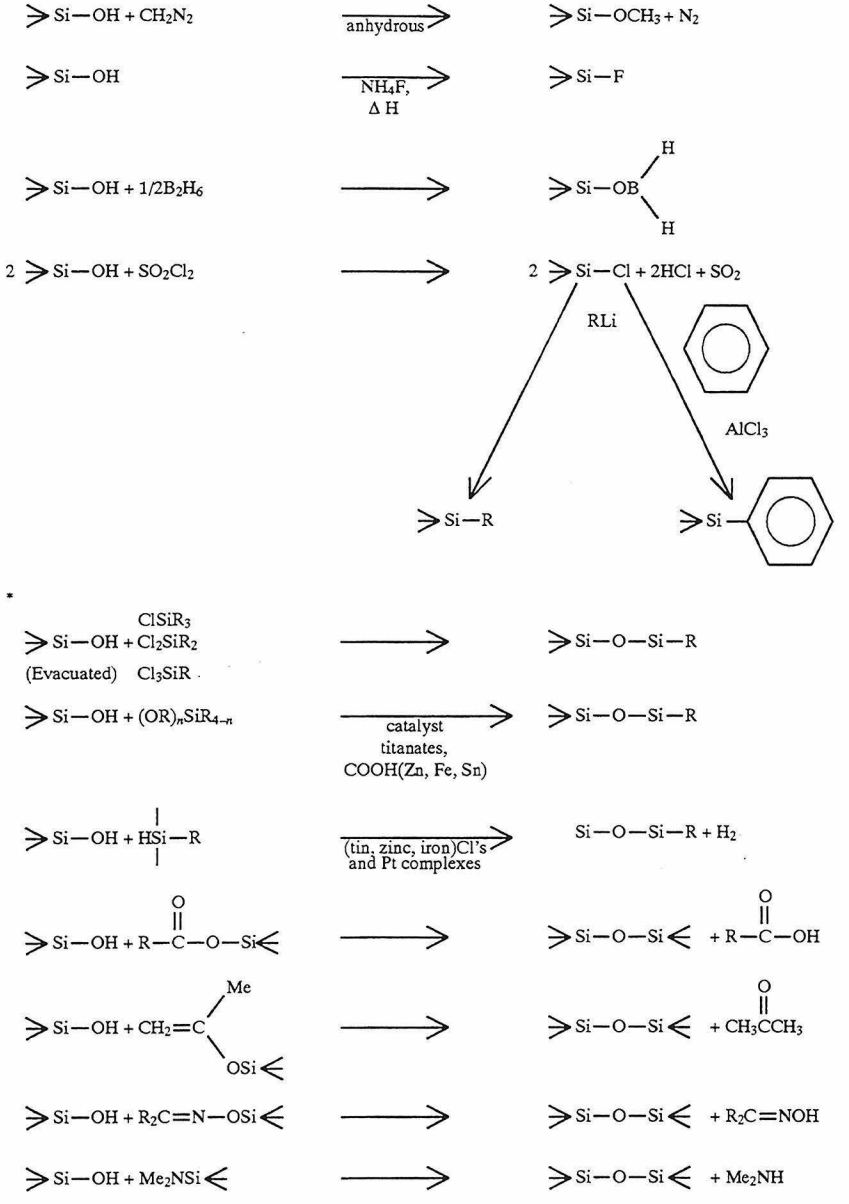

All reactions from * down may be used to attach a more or less arbitrary Y group, assuming the proper synthesis of the derivatizing agent (containing Y).

The entire tip may be functionalized to produce a tip as shown in FIG. **2**A. The tip **18** is entirely functionalized with layer **39**.

The tip may also be functionalized by evaporation of a layer of gold onto the tip surface, followed by treatment with Y-alkyl-thiols, which self-assemble to form a bound Au—S—R—Y monolayer (R=alkyl) on the gold surface. Normally, a Si or Si_3N_4 surface is first coated with chromium in order to enhance the adhesion of the gold layer.

Diamond surfaces may be functionalized with fluorine by treatment with fluorocarbons.

Materials used for scanning tunneling microscopy probes must be conductive, and are therefore generally metals or (doped) semiconductors.

Gold and silver may be functionalized by Y-alkyl-thiols, which self-assemble to form a bound Au—S—R—Y monolayer (R=alkyl) on the gold surface.

Aluminum may be functionalized by Y-alkyl phosphates of the class $N(RPO)(OH_2)_nY_{3-n}$. (R=alkyl, n=1-2).

Platinum may be functionalized by treatment with molecules containing an olefinic moiety, i.e. by alkene-Y.

Titanium dioxide (TiO_2), tin dioxide (SnO_2), and ruthenium dioxide (RuO_2) have an oxide coat which allows them to be silanized analogously to SiO_2. The surfaces of platinum and gold may be prepared by electrochemical means to have an oxide coat within similar reactivity. In general, any substance with a surface terminated with hydroxyl (—OH) groups may be silanized in like fashion.

EXAMPLE 1

Stepwise-out Functionalization

A silicon scanning probe is functionalized with single-stranded DNA as follows: The surface of the silicon probe is derivatized by immersion in a 2% solution of aminopropyltriethoxysilane (APTS) in anhydrous toluene for 1 hour, yielding an amino (—NH_2) group covalently bound to the surface. 10 m g disuccinimidyl suberate (DSS) is dissolved in 600 μL DMSO. A solution of 21 μL aminopentanol in 5.4 mL of 1×PBS buffer is prepared, and the DSS solution is added to it. The resulting solution is stirred for 10 minutes. The probe is added to this solution, and the solution is stirred for 10 minutes. The result is a surface of —OH groups at the end of long spacer arms. This is the starting point for conventional automated solid-phase DNA synthesis. We have replaced the glass beads, which are normally the substrate, with the scanning probe. The scanning probe chip fits easily within a standard DNA synthesis fritted filter chamber.

The functionalization proceeds stepwise, starting from the probe surface and working out, as shown by the following scheme:

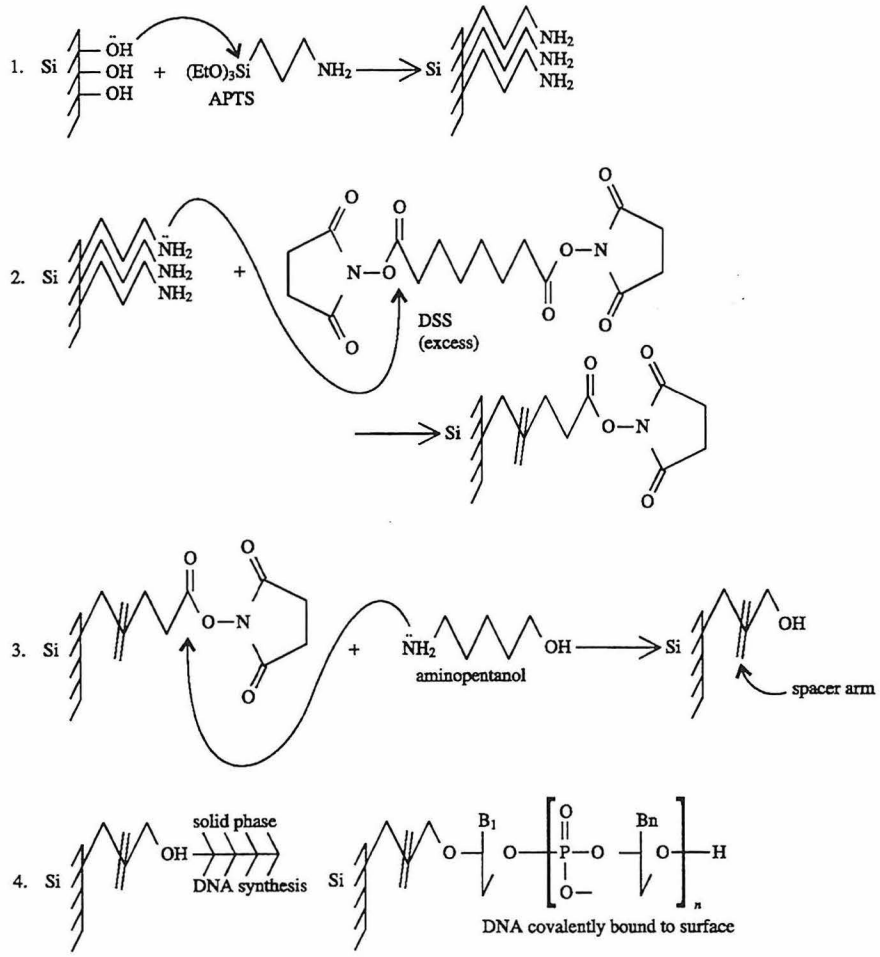

EXAMPLE 2

Convergent Functionalization

A silicon nitride scanning probe is functionalized with a peptide epitope sequence as follows: A thin (30 Å) layer of chromium is evaporated onto the probe, followed by a thin (100 Å) layer of gold. A peptide epitope sequence (for instance, enkephalin, Tyr-Gly-Gly-Phe (SEQ ID NO:1), or human endorphin, Tyr-Gly-Gly-Phe-Met-Thr-Ser-Glu-Lys-Ser-Gln-Thr-Pro-Leu-Val-Thr-Leu-Phe-Lys-Asn-Ala-Ile-Ile-Lys-Asn-Ala-Tyr-Lys-Lys-Gly-Glu (SEQ ID NO:2)) is synthesized using solid-phase Merrifield synthesis such that all amino-containing side chains are protected. The peptide is released from its solid phase support, and treated with a 5 mM solution of Traut's Reagent (2-iminothiolane.HCl), which converts the amino-terminus of the protein to a sulfhydryl terminus. The probe is then added to a 3% solution of this sulfhydryl-derivatized epitope in ethanol and the solution is stirred for 3 hours. The derivatized epitope self-assembles on the gold-coated probe. Finally, the protecting groups on the side-chain amino groups are removed.

As shown in the following scheme both the surface and the target moiety are modified separately, and the two are

brought together to create the functionalized surface. This is a convergent synthesis.

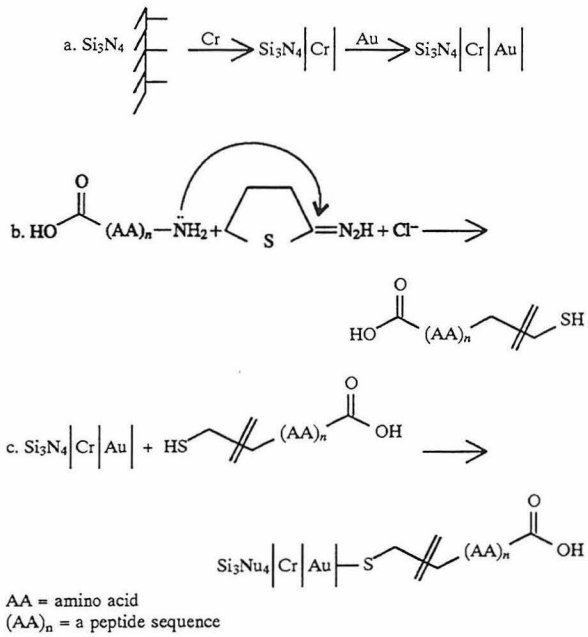

AA = amino acid
$(AA)_n$ = a peptide sequence

EXAMPLE 3

Conduction Through Covalent Bonds

A platinum scanning probe is functionalized with an electroactive reagent (for instance, allylhydroquinone) as follows: the Pt probe is cleaned of organic contaminants by heating in a methane-oxygen flame for 10 minutes with repeated quenching in perchloric acid. Final cleaning is achieved by applying a cyclic potential (2 mV/s, from 0.4 V to 1.3 V, then to −0.4 V and finally to 0.4 V vs NaCe) in 1M HCO_4. The probe is then immersed for 5 minutes in a 10 mM solution of the electroactive reagent in pure water.

This functionalized moiety can be oxidized and reduced by application of a potential to the scanning probe, showing that the covalent bonds connecting it to the platinum probe are electrically conductive.

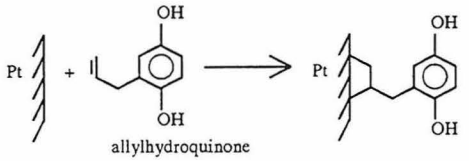

allylhydroquinone

Passivation of the scanning probe

Passivation, as used herein, means the protection by way of a layer on or by chemical, optical, or electric treatment of a substrate surface to isolate the substrate from electrical and chemical conditions in the environment.

Functionalization to a chemically unreactive moiety is one way to implement passivation. Therefore, for tips of silicon and silicon nitride, passivation methods useful in the present invention include treatment with diazomethane, fluorination, chlorination followed by alkylation or arylation, silanization to alkyl groups, hydrosilylation to alkyl groups, or treatment with acloxy-, enoxy-, oxime-, alkoxy-, or alkylamine-organosilanes.

Other means of applying passivation layers include low pressure chemical vapor deposition (LPCVD), as described in U.S. Pat. No. 5,250,473, thermal oxidation, and direct oxidation of the substrate by exposure to oxidizing agents.

EXAMPLE 4

Passivation By Methyl-Functionalization

The surface of a silicon scanning probe may be passivated with methyl groups as follows: the probe is immersed in a 2% solution of trimethylchlorosilane (TMCS) in dry benzene for 1 hour.

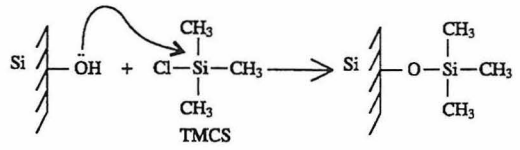

EXAMPLE 5

Passivation by Alkyl-Functionalization

The surface of a platinum scanning probe may be passivated by alkyl-functionalization as follows: the probe is cleaned as described in Example 3, and then functionalized by immersion in a 10 mM solution of 1-octene for 5 minutes.

Tip-Alpex Functionalization.

The ability to attach a single macromolecule to, or specifically functionalize a small area of, the apex of an SPM tip depends on the ability to physically differentiate the apex from the remainder of the tip, and to cause chemical change based on that differentiation. Since the area is desired to be on the order of molecular dimensions, the physical effects used must be very short-range, capable of affecting one area while leaving another, relatively few atomic distances away, unchanged. There are many ways to do this, including employing steric control, evanescent waves, electron tunneling, or lithographic techniques.

Apex differentiation may constitute either activation toward, or protection from, chemical change.

Methods based on apex activation have three steps:

1. Activation of a small area at the apex of the scanning probe toward functionalization.
2. Functionalization of said area with a desired moiety according to the present invention.
3. Passivation of the non-activated area of said tip according to theneresent invention (if necessary).

Methods based on apex protection have four steps:

1. Protection of a small area at the apex of the scanning probe tip from passivation.
2. Passivation of the unprotected area of said probe tip according to the present invention.
3. Deprotection of the protected area at the apex of said tip.
4. Functionalization of said area with a desired moiety.

Differentiation by Steric Control

Steric interactions (inter-atomic repulsion at short distances) are extremely short range. This type of interaction can be used to block a reagent from the apex of an SPM tip, or to confine a reagent to the apex.

Referring to FIG. **5**, the protection (1) of a small area **40** at the apex of the scanning probe tip **42** may be accomplished by bringing the small area into close proximity with a substrate surface **41**, (2) such that the molecules **43** of the passivating agent are sterically impeded from contact with the small area **40** at the apex of the tip. Passivation layer **44** is formed at other unprotected areas. This can be seen in more detail in FIG. **2**B. As an example, if the passivating agent comprises molecules of effective maximum diameter of 20 Å, the apex may be located next to the surface such that the space therebetween is much less than 20 Å. Deprotection (3) is accomplished by simply withdrawing the probe tip **42** from the substrate **41**. Functionalization (4) can then proceed using the specialized molecules **45** designed to attach at the unpassivated tip. A typical rigid molecule **45** is shown in FIG. **4**.

Differentiate by Applied Potential

Application of an electrical potential between a sharp tip and a substrate creates highly nonhomogeneous electric fields which are extremely intense near the apex of the tip. Magnetic fields at sharp tips are similarly nonhomogeneous and intense at the tip apex. Thus, these fields can be used to guide ions or electrons onto a small area at the apex, to selectively functionalize or passivate the tip. The strong fields may also activate or deactivate chemical groups toward a particular reaction pathway.

Differentiate with Lithographic Techniques

Lithographic techniques to differentiate the tip from other surfaces on the probe depend on lateral, differentiation (along the surface of the probe), rather than vertical differentiation as implied in the evanescent wave and electron tunneling techniques.

Differentiate with an Evanescent Wave

The intensity of an evanescent wave at a flat surface falls off exponentially with distance. A more complicated optical field is created at an aperture smaller than the wavelength of light, with an intensity that may fall off even faster than the evanescent wave at a flat surface. This exponential falloff can be used to differentiate an area at the apex from the remainder of the tip. Since intensity of an evanescent wave decreases exponentially with distance, the probability of reaction of a photoactive group on the probe surface also decreases exponentially with distance from the surface.

Differentiate by Electron Tunneling

The probability of electron tunneling also falls off exponentially with distance. Electro-active (redox) groups on the apex can thus be differentiated by proximity to the substrate. Electron transfer between the electrode and redox-active groups on the probe surface can lead to oxidation or reduction of the redox-active groups. Since electron transfer occurs by quantum-mechanical tunneling, the probability of electron transfer decreases exponentially with distance.

The number of electrons that tunnel may also be controlled by controlling the applied potential and the number of electrons available at the tunneling site.

After the passivation procedure, the small unpassivated area remaining at the apex of the tip is preferably in the range of about 10,000 Å to 3 $Å^2$. It will be realized that the size of area may vary and is controlled by the shape of the tip, and the proximity to and local topography of the substrate surface, or the masking process. However, a small unpassivated area at the substrate tip enhances the probability of attachment thereto of only one macromolecule.

The macromolecule will be attached to the substrate probe tip material in a manner which restricts motion with respect to the substrate. Thus, preferably, there should be a plurality of sites of attachment.

EXAMPLE 6

Apex Assembly of a Single Enzyme Molecule Tip

The apex of a silicon nitride scanning probe may be functionalized with a single molecule of an enzyme (for instance Horseradish Peroxidase, molecule weight 44,000) as follows: A silicon nitride probe is mounted in a SPM liquid cell. The apex of a silicon nitride scanning probe is brought into close proximity with a graphite surface, as described above. The unprotected surface is then passivated by filling the liquid cell with a 2% solution of TMCS in anhydrous toluene and allowing reaction for 1 hour. At the end of this period, the probe tip is withdrawn from the surface and the apex is derivatized by filling the liquid cell with a 2% solution of APTS in anhydrous toluene and allowing reaction for 1 hour. This yields an apex derivatized covalently with amino groups. The probe is then removed from the liquid cell, and the remaining reaction steps are carried out as for functionalization of an entire scanning probe. A solution of 100 mg DSS/1 mL DMSO is prepared, and the scanning probe is stirred in it for 10 minutes. The resulting groups are highly reactive toward amino groups. The probe is removed from the DSS/DMSO solution, rinsed with DMSO to remove excess DSS, and placed in a solution of 3% enzyme in ethanol, where it is allowed to react for 1 hour. Finally, the probe is washed with ethanol and distilled water to remove excess enzyme.

As can be seen from the scheme, the functionalization proceeds stepwise, starting from the probe surface and working out.

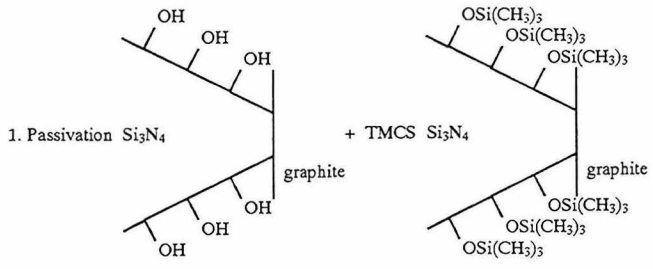

-continued

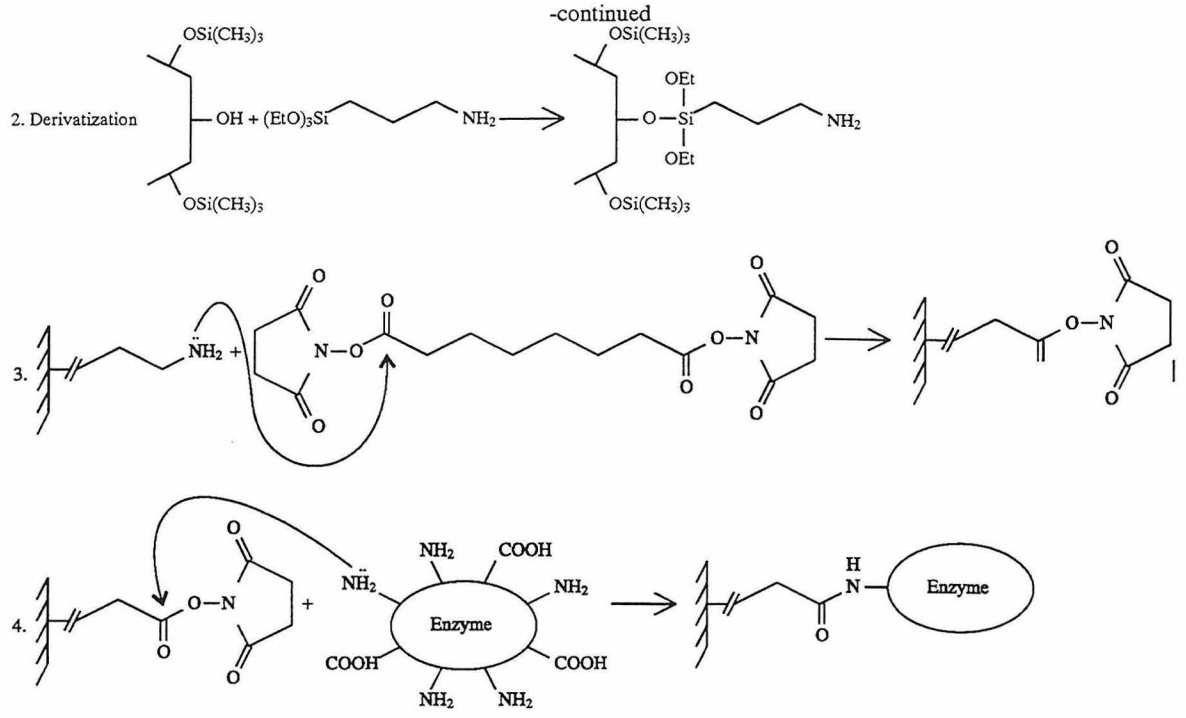

EXAMPLE 7

Apex Assembly of a Polypeptide Nanotubule Tip

A silicon nitride probe is protected with TMCS and its apex derivatized with APTS as described in Example 6. The cyclic polypeptide cyclo[-(D-Leu-Glu-D-Leu-Glu)$_2$] (SEQ ID NO:3) is prepared by the method of Ghadiri et al. (1993) Nature 366:324). Aggregation of this polypeptide is stabilized axially by hydrogen bonds between backbone units and potentially by Van der Waals interactions between the isoleucine side groups. In contrast to the polypeptide of Ghadiri et al., however, lateral association is discouraged, both because of the steric bulk of the isoleucine side groups and because no amino side chains are present to form hydrogen bonds. Self-assembly occurs as pH is reduced.

A single polypeptide nanotube is anchored to the amino apex covalently as follows: a 10 mM solution 1-ethyl-3-(3-dimethylaminopropyl)-carbodiimide hydrochloride (EDC) in aqueous buffer at pH 7 is prepared. 1% by weight of polypeptide is added. The EDC activates the carboxylic acid groups of the glutamic acid side chains for attack by amino groups. After dissolution of the peptide, the probe chip is added and allowed to react for 1 hour. The amino groups on the apex form amide bonds with a polypeptide, anchoring it to the surface. The probe is washed with aqueous buffer solution at pH 9 to remove excess peptide, and then immersed in a fresh solution of 1% polypeptide at pH 7. The pH of the solution is gradually lowered by addition of dilute HCl to allow the polypeptide nanotubule to self-assemble.

As may be seen from the scheme, both the surface and the target are modified separately and then brought together to create the functionalized apex. This is a convergent synthesis.

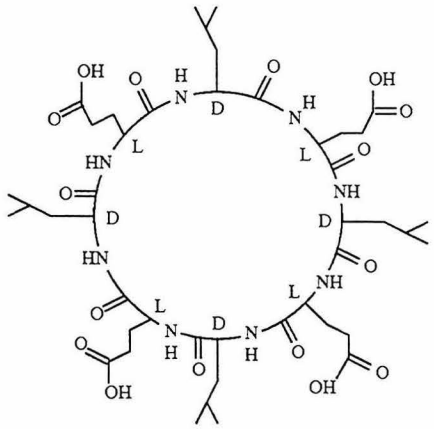

-continued

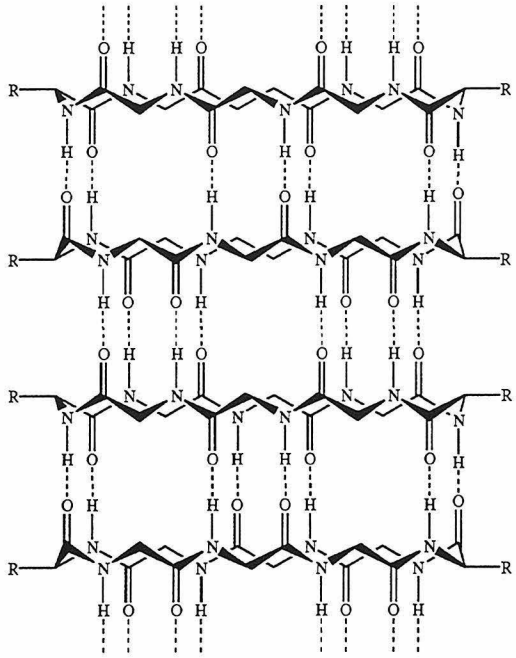

Adapted from Nature, V366, p. 324

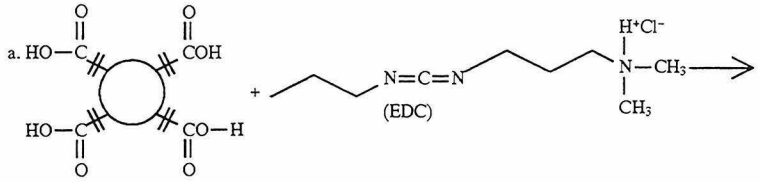

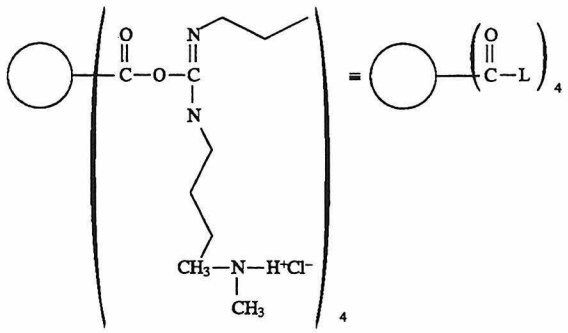

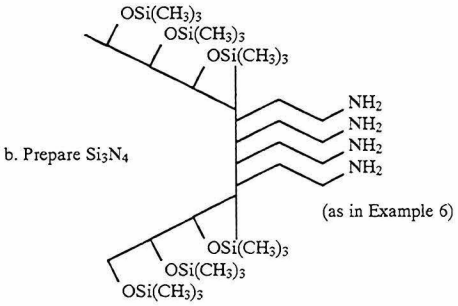

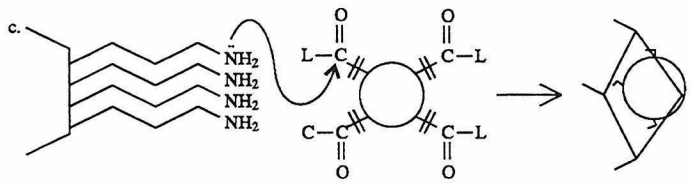

-continued

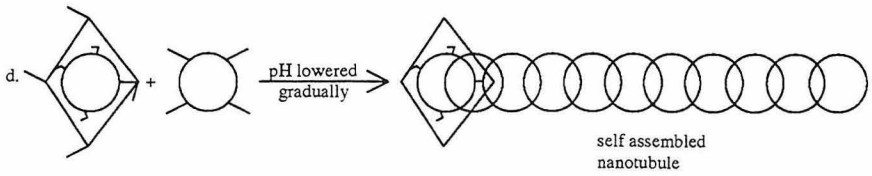

EXAMPLE 8

Apex Assembly of a DNA Double Helix on a Pt Probe

The apex of a platinum scanning probe may be functionalized with a DNA double helix as follows: the probe is cleaned as described in Example 3, and then mounted in an SPM liquid cell. The apex of the probe is brought into close proximity to a mica substrate, as described above. The unprotected surface is then passivated by filling the liquid cell with a 10 mM solution of 1-pentane in anhydrous pentane and allowing reaction for 5 minutes. The liquid cell is flushed with anhydrous pentane, followed by acetonitrile and pure water and then filled with a 10 mM solution of the vinyl-derivatized double helix (prepared as described below) in water. The probe is withdrawn from the surface and allowed to react for 10 minutes, after which the liquid cell is flushed with pure water.

The 2-aminobutyl-1,3-propanediol (ABPD) structure shown in the following scheme replaces a normal DNA base in a strand of DNA. The DMT-protected phosphoramidite based on the ABPD structure (SBPD-PA) is a perfect chemical replacement for a DMT-protected nucleotide phosphoramidite in automated solid-phase synthesis of DNA; it undergoes the same addition, deprotection, capping, and chain extension reactions. The amino-terminated "side chain" of ABPD-PA can also be derivatized, and this is how the DNA double helix will be attached.

A 100 mM solution of ABPD-PA in anhydrous acetonitrile is prepared. To this is added an equal amount of 1M 1-vinyl-2-pyrrolidionone (VPD) in acetonitrile, and the reaction is allowed to proceed for 30 minutes. This terminates the side chain of ABPD-PA with a vinyl group (ABPD-PA-V). The reaction mixture is purified by column chromatography and the ABPD-PA-V fraction is retained.

The desired sequence of DNA and its complement are synthesized by automated solid-phase synthesis. On one strand, additional 3' and 3'+1 residues are inserted; these are ABPD-PA-V. On the complementary strand, additional 5'–1 and 5' residues are added; these are also ABPD-PA-V. This yields a DNA double-helix with four double bonds capable of covalent bond formation with the surface. The complementary strands are hybridized together.

As can be seen from the scheme, the derivatized DNA double-helix is created entirely separately from the surface, and then attached as a final step. The functionalization proceeds stepwise, starting with the ABPD-PA and working in.

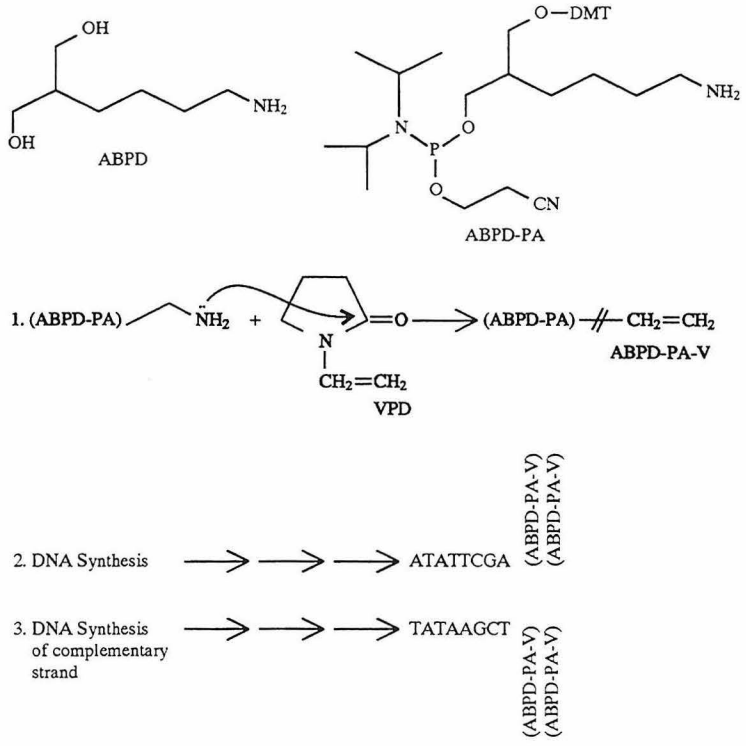

-continued

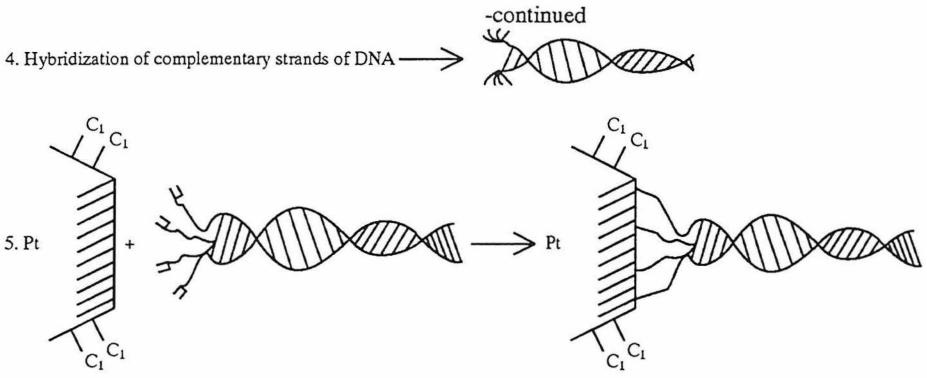

EXAMPLE 9

Differentiation by Steric Control by blocking a passivation reagent from reaching the apex

The following steric control methods can be used to constrain a masking agent to the apex.

1. Touch tip apex down on the surface, flow in passivation solution, rinse, retract.

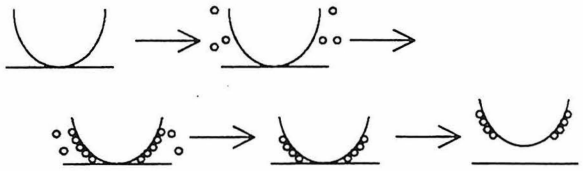

2. Alternatively, touch tip apex down on surface through a drop of passivation solution. Typically, the slow chemical kinetics of passivation prevent apex passivation.

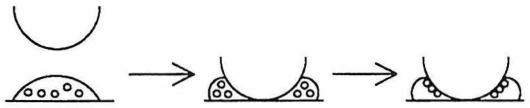

3. Alternatively, touch tip apex on surface through an electroactivatable passivation solution; then
electroactivate the solution with an external electrode,
or
electroactivate with the tip as an electrode, or
electroactivate with the substrate as an electrode.

4. Alternatively, touch tip apex down through a heat-activatable passivation solution. Then
heat solution from the tip, or
heat solution from the substrate, or
heat with an external probe, or
heat with a laser.

4a. Alternatively, touch tip apex down through a light-activatable passivation solution, then, light from tip, substrate, probe, laser etc.

5. Alternatively, touch tip apex down, then electrochemically passivate the tip. Note that this is different than 3. In 3, some species, A, in solution is activated to an activated species A* which can then passivate the surface. In 5, a surface bound species S is oxidized or reduced on the surface of the tip in such a fashion that it can be oxidized or reduced only in the presence of another species present in solution. In 3, A* is blocked from reaching the apex whereas in 5 a necessary solution reagent NN is blocked from reaching S* on the surface.

6. Alternatively touch down the tip apex, then light-passivate tip (same principle as in 5).

7. Alternatively touch down the tip apex, then heat-passivate tip (same principle as in 5).

EXAMPLE 10

Differentiation by steric control to constrain an activation agent to the apex

1. Touch down tip into an aperture filled with an activation reagent/functionalization reagent:

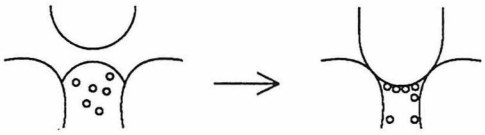

The activation/functionalization reagent may be electroactivated, photoactivated, or heat-activated.

2. In a solution containing electroactivatable reagent, touch down on an aperture where electroactivation, photoactivation or heat activation may selectively occur.

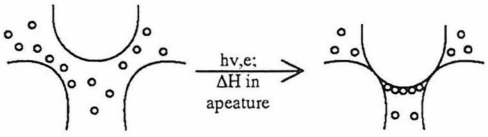

3. Town down on a catalytic surface (for example, to reduce —No_2 groups to —NH_2 groups with Pd).

4. Touch down on a surface which chemically reacts with groups on the apex to activate or functionalize the apex.

EXAMPLE 11

Differentiation by steric control to constrain a masking agent to the apex

1. Touch down on a surface to transfer a temporary masking agent to the apex.

EXAMPLE 12

Differentiation by (Evanescent) Photon Control

To photoactivate a reaction (i.e., cause a photochemical change) with light at the apex, one takes advantage of the exponential distance dependence of evanescent waves.

1. Touch tip down at a surface where a wave is undergoing total internal reflection.

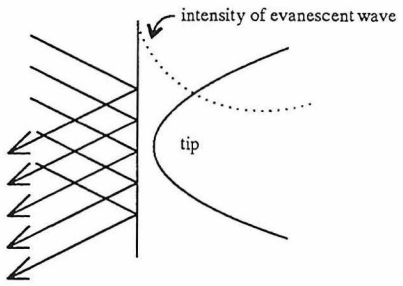

2. Alternatively, touch tip down at an aperture smaller than the wavelength of light.

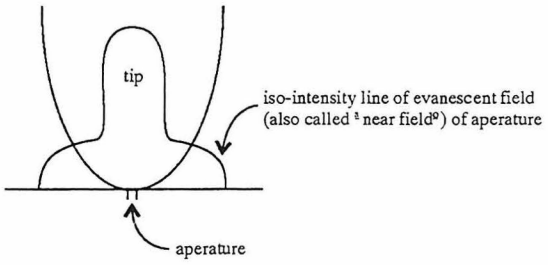

3. Alternatively, the near-field light of a pulled-optical-fiber near-field scanning optical microscope tip (NSOM tip) may be used to photochemically alter the apex of the tip.

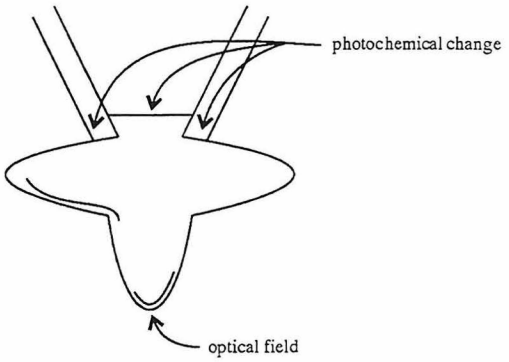

EXAMPLE 13

Differentiation by non-evanescent photon control

1. A tip is brought close to the surface and irradiated with light of high intensity, having a wavelength too long to cause the desired photoreaction. Second harmonic generation at the tip-sample interface will double the frequency (half wave-length) of some of the light. This frequency-doubled light can cause photochemical change which the original light could not, due to higher energy per photon.

2. Alternatively, bring the tip down to a point source of light of the required wavelength to activate

a frequency-"upping" molecule, or

an electroactivatable luminescent molecule

EXAMPLE 14

Differentiation by (Tunneling) Electron Control

Specificity of an electrochemical change to the apex comes about through exponential distance dependence of tunneling probability of electrons. For specificity one should limit the number of e^- transferred in an electrochemical cell. Therefore, a limited electron source/drain (a "limited e^- sink") for this purpose can be provided as follows.

1–6. Either electroactivate groups on apex, with an unlimited e^- sink or source, limited e^- sink or source or null sink or source, or electroprotect the substrate connected to an unlimited e^- sink or source, limited e^- sink or source or null sink or source.

7. Connect to sink/source as in 1–6 above, but with the tip in contact, instead of in the tunneling region.

8. Connect to sink/source as in 1–7, but with electron-transfer chemical groups on the substrate.

9. Connect to sink/source as in **8**, where the electron-transfer groups are spatially limited.

10. Contact sink where the applied voltage is varied with time.

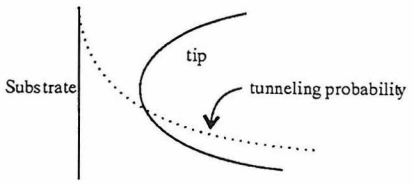

EXAMPLE 15

Limited electron sinks/sources

The following sinks/sources are all drawn with e^- transferred from substrate to tip, but the extension to e^- transfer from tip to sample is apparent.

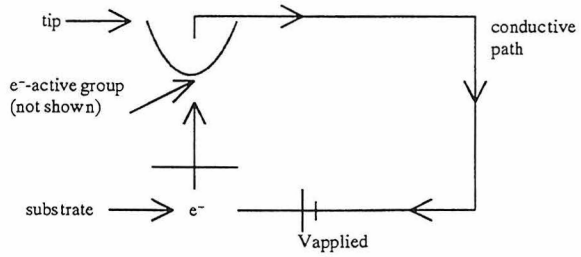

Unlimited Sink
Complete circuit.

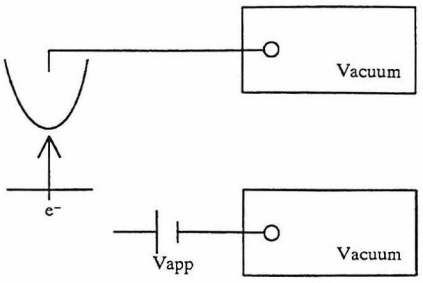

Null sink. Each e^- transferred sets up an opposing field.

-continued

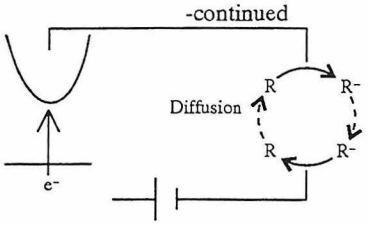

Limited e^- sink. Can control the number of e^- by limiting the time of contact, since diffusion is slow.

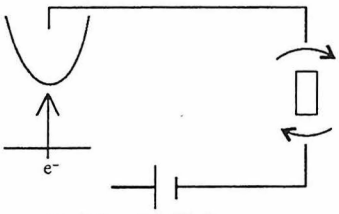

Limited e^- sink. Limit limits the number of e amount of A can be limit dilute quantity.

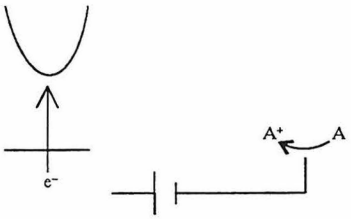

Limited e^- sink. As A is converted to A^+, the concentration of A decreases, the concentration of A^+ increases and the reverse voltage builds up. By controlling the concentration of A, one should be able to control the number of electrons

EXAMPLE 16

Differentiation by Applied Fields

An applied field is utilized to single out the apex. These are essentially static fields which are not extremely-fast-oscillating fields like an electromagnetic wave (light):

1. A chemical change is induced by field ionization at the apex.
2. A chemical change is induced by high field intensity. For example, if the high field lowers the energy of the transition state of a chemical reaction, ionization is not necessary.
3. As 1., but assisted with applied light or heat.
4. As 2., but assisted with applied light or heat.
5. Chemical change is induced by ion or e^- collision, where the ions or e^- are guided to the apex by an applied field.
6. Ionize the apex with a field, then guide ions to apex.

EXAMPLE 17

Differentiation by Lithographic Techniques

1. A (negative) resist is applied, the apex exposed with light or e^-, and unexposed resist is removed. The tip is passivated, the exposed apex resist is removed, and the exposed surface is functionalized.

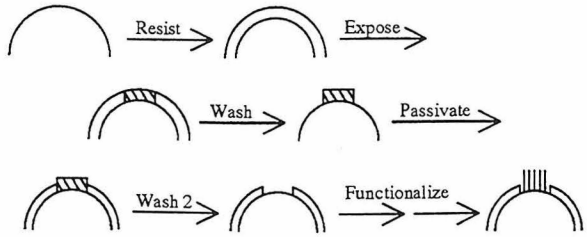

2. A (negative) resist is applied, patterned with light or e^-, and the unexposed resist is removed. The exposed apex surface is functionalized, and the exposed resist is removed.

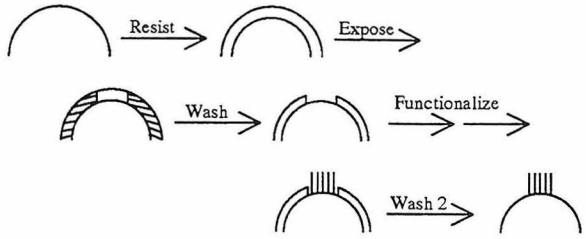

3. Alternatively, proceed as 1, but with a positive resist and expose the tip except for the apex.
4. Alternatively, proceed as 2, but with a positive resist and expose the tip except for the apex.
5. Alternatively, proceed as 2 and 3, but with a negative resist of electro- or photo-sensitive molecules which on exposure react to leave the exposed area derivatizable.
6. Alternatively, functionalize entire tip with photo- or electrosensitive target molecule. Irradiate all areas except for apex to remove the target molecule from all sites except the apex.

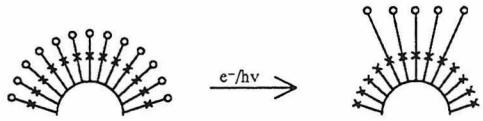

Tip macromolecule

Referring to FIG. **6**, the macromolecule **45** needs to be sufficiently rigid after attachment to the tip **42** in order to avoid undesired displacement which is not under control of the computer-controlled mechanism for moving the tip. Hence, complex molecules which are cross-linked, folded or otherwise restricted in degrees of freedom around covalent bonds are required. Such molecules include, but are not limited to, single-wall carbon nanotubes, deoxyribonucleic acid (DNA) double helices, polymeric nanotubes composed of sugar molecules, cyclic peptide nanotubes, proteins, and synthetically constructed macromolecular structures. Nanotubes are molecular structures stacked or coiled to form tubular shapes. Protein structures may be locked by cross-linking or by inserting metal atoms to chelate internal groups.

Single-wall carbon nanotubes having typical diameters of 0.2 to 3 nm may be prepared according to the methods described in Iijima (1993) Nature 363:603 and Bethune (1993) Nature 363:605. These nanotubes are believed to be significantly stiffer than coiled proteins or DNA.

Since a DNA helix fragment is a rigid, electronically coupled aromatic column of stacked base pairs within a sugar phosphate backbone about 2 nm thick which can efficiently promote electron-transfer reactions over distances of more than 40 Å, such helices are useful as probe tips according to the invention.

Polyrotaxane nanotubes, prepared by polymerizing α-cyclodextrin sugar units (see Harada (1993) Nature 364:516) are also useful in the practice of the invention. These tubes have internal and external diameters of about 0.5 and 1.5 nm, respectively. Since cyclodextrins bind organic substrates in aqueous media and the tubes have about the same internal diameter as native biological tubular structures, aside from being useful as a sensing probe, they are useful as extremely selective filters and catalysts for reactions taking place inside the cavity.

Another class of molecules that may be used according to the practice of the invention is cyclic peptide or protein nanotubes having internal diameters of about 0.8 nm (Ghadiri et al. (1993) Nature 366:324). Peptides and proteins may be rigidified with metal atoms, such as copper, which chelate with functional groups internal to the structure. Furthermore, by selecting and/or modifying the amino acid constituents, protein tubes may be prepared to achieve a desired internal diameter or to place reactive moieties at the tip in order to perform particular functions.

The macromolecules, particularly proteins and sugars which have pendant functional groups, can be cross-linked to impart stiffness to the structure. Cross-linking may be accomplished by known methods as disclosed, for example, by Mattson et al. (1993) Molec. Biol. Reports 17:167–183.

Accordingly, the present invention provides a scanning probe tip capable of specific molecular interactions with a substrate. The tip is useful for sensing and analyzing microscopic structures and environments by means of the interactions between the tip moieties and the substrate.

In addition to improving scanning probe microscopy, the functionalized tip of the present invention is useful as a molecular biological or chemical tool. For example, a probe functionalized with a DNA molecule bearing a specific code sequence may be used to selectively detect, manipulate or remove specific DNA fragments in a complex mixture of biological molecules, either in vitro or in vivo. Detection, in this application, may be achieved by monitoring conformational or other changes in the tip molecule caused by binding to its substrate, or by chemical means upon removal of the tip from the mixture, or by means of the force exerted on the tip when it is moved away from the location of the complementary DNA on the substrate.

Similarly, a probe may be functionalized with a protein macromolecule with an epitope sequence at its tip. Such a probe may then be used, in vitro or in vivo to detect, select or manipulate antigenic materials in mixtures.

Referring to FIG. **6**, the completed tip comprises a single, rigid macromolecule **45** rigidly attached to a small area of the apex of a scanning probe tip **42**.

Accordingly, the present invention provides a scanning probe tip having a smaller radius of curvature, greater angle of taper and a more reproducible shape than the tips previously available. This tip is useful for sensing microscopic environments since the macromolecular tip is able to penetrate or sense finer indentations in a substrate surface than prior tips.

A probe modified according to the present invention may also be used as a tool in nanofabrication techniques, in molecular chemistry or biochemical catalysis. With the appropriate functional group attached, a probe may be used to add or remove a chemical moiety in a precise location on a molecular structure. Alternatively, a probe may act as a catalyst in chemical or biochemical reactions by precise positioning of a specific functional group in the reaction environment, or by providing the reaction environment itself, for instance, the cavity of a tubular macromolecular tip.

The present invention has been described, in part, in terms of preferred embodiments. The invention, however, is not limited to the embodiments depicted and described. Rather the scope of the invention is defined by the appended claims.

SEQUENCE LISTING

(1) GENERAL INFORMATION:

(i i i) NUMBER OF SEQUENCES: 3

(2) INFORMATION FOR SEQ ID NO:1:

(i) SEQUENCE CHARACTERISTICS:
(A) LENGTH: 4 amino acid residues
(B) TYPE: amino acids
(C) STRANDEDNESS: single
(D) TOPOLOGY: linear

(x i) SEQUENCE DESCRIPTION: SEQ ID NO:1:

Tyr Gly Gly Phe

(2) INFORMATION FOR SEQ ID NO:2:

(i) SEQUENCE CHARACTERISTICS:
(A) LENGTH: 31 amino acid residues
(B) TYPE: amino acids
(C) STRANDEDNESS: single
(D) TOPOLOGY: linear

(x i) SEQUENCE DESCRIPTION: SEQ ID NO:2:

-continued

```
Tyr Gly Gly Phe Met Thr Ser Glu Lys Ser Gln Thr Pro Leu
                5                  10

Val Thr Leu Phe Lys Asn Ala Ile Ile Lys Asn Ala Tyr Lys
 15                 20                  25

Lys Gly Glu
      30
```

(2) INFORMATION FOR SEQ ID NO:3:

(i) SEQUENCE CHARACTERISTICS:
(A) LENGTH: 8 amino acid residues
(B) TYPE: amino acid
(C) STRANDEDNESS: single
(D) TOPOLOGY: linear

(i x) FEATURE:
(D) OTHER INFORMATION: Leu at positions 1, 3, 5 and 7 are D- leucine

(i x) FEATURE:
(D) OTHER INFORMATION: This peptide is a cyclic compound

(x i) SEQUENCE DESCRIPTION: SEQ ID NO:3:

```
Leu Glu Leu Glu Leu Glu Leu Glu
                5
```

What is claimed is:

1. A method of preparing a probe for sensing or manipulating a microscopic environment or structure comprising the steps of:

(a) protecting a small area at the tip of the probe, wherein said area of protection is in the range of about 10,000 $Å^2$ to 3 $Å^2$;

(b) passivating the unprotected area of said probe tip;

(c) deprotecting the protected area of said probe tip; and

(d) functionalizing the deprotected area at the tip of said probe with a desired moiety.

2. A method of preparing a probe for sensing or manipulating a microscopic environment or structure comprising the steps of:

(a) activating a small area at the tip of the probe towards functionalization;

(b) functionalizing said area with a desired moiety, comprising a single, rigid macromolecule that has an outer distal diameter in the range of about 2 Å to about 50 Å; and

(c) passivating the non-activated area of said tip (if necessary).

3. The method according to claim **2** wherein said single, rigid macromolecule is selected from the group consisting of a carbon nanotube and a polyrotaxane.

4. A method of preparing a probe for sensing or manipulating a microscopic environment or structure comprising the steps of:

(a) protecting a small area at the tip of the probe;

(b) passivating the unprotected area of said probe tip;

(c) deprotecting the protected area of said probe tip; and

(d) functionalizing the deprotected area at the tip of said probe with a desired moiety comprising a single, rigid macromolecule that has an outer distal diameter in the range of about 2 Å to about 50 Å.

5. The method according to claim **4** wherein said single, rigid macromolecule is selected from the group consisting of a carbon nanotube and a polyrotaxane.

* * * * *

Appendix D

US Patent Application 08/960,034

Chemical Etching of Fiber Probe

PATENT
ATTORNEY DOCKET NO. 06618/122001

CHEMICAL ETCHING OF FIBER PROBE

FIELD OF THE INVENTION

The invention relates to chemical etching of fibers, and more specifically to chemical etching of infrared fibers to form an optical probe.

BACKGROUND OF THE INVENTION

An end of a piece of optical fiber can be shaped into a cone or tapered section. The tip of the cone or tapered section forms a small optical aperture for transmitting light. This can be used as an optical probe in a "near-field" configuration in which light is coupled between two elements separated by a spacing less than one wavelength of the light. In the near-field configuration, the "far-field" approximation to the propagation behaviors of electromagnetic waves is no longer valid. One result of such near-field optical configuration is a spatial resolution higher than what is permissible by the far-field diffraction limit in optical sensing.

Near-field scanning optical microscopy ("NSOM") explores the above property of the near-field optical sensing to achieve a spatial resolution of down to about one fiftieth of a wavelength. This compares favorably to the far-field diffraction limit which is approximately one half of a wavelength.

A near-field scanning optical microscope can be implemented with an optical fiber probe. As with almost all scanned probe techniques, the performance of a near-field scanning optical microscope is significantly determined by the quality of the optical probe. One challenge in achieving such a high resolution is construction of a probe with an aperture of the size of the desired feature size.

FIG. 1 shows a typical structure of a fiber probe 100 which includes a fiber body 106, a cone or tapered

section 104, and a tip aperture with a tip apex 102. To resolve a feature much smaller than one wavelength, the size of the tip aperture should be about the feature size. Several other parameters may also affect the performance of a fiber probe, such as transmission wavelength range, mechanical properties of the probe material, and the geometry of the tapered section 104 of the probe.

For a given fiber material, the quality of the probe is largely determined by the tip aperture and the geometry of the tapered section. In general, the tip aperture should be as small as possible since it determines the minimum resolvable feature size. One parameter for characterizing the size of the tip aperture is the radius of curvature of the tip apex 102. A smaller radius of the tip curvature can resolve smaller features and produces higher resolution.

Light coupling efficiency or light throughput is another measure of the performance of a fiber probe. The surface quality of the tip apex 102 and the geometry of the tapered section 104 can affect the light coupling efficiency. In particular, the length of the tapered section 104 should be small in order to increase the light coupling efficiency of the probe. This is at least in part due to the cross-section of the tapered section 104 decreasing from the fiber body 106 to the tip apex 102 to a diameter smaller than the wavelength. A longer tapered region 104 requires radiation to propagate a
longer distance within a confined dimension smaller than its wavelength. This reduces the light energy transmitted through the region. Thus, a short taper section 104 and a large cone angle Θ are desirable. One method of making fiber probes is mechanical pulling.

A fiber is first heated by a laser beam or a filament to a soft state at an elevated temperature and subsequently is pulled to form a tapered section and a tip. The tapered section of a probe may be coated with metal except for an aperture at the tip apex.

Another method of making fiber probes is by chemically etching the fiber material by using an active chemical etchant solution. Chemical etching is advantageous over the mechanical pulling in that higher light coupling efficiency can be achieved. Zeisel *et al.* has shown that chemically etched optical fiber probes have light throughput of about 100 - 1000 times greater than mechanically pulled fiber probes. Zeisel *et al.*, Applied Physics Letters, Vol. 68(18), p. 2491 (1996). It is recognized that chemically etched fiber probes usually have shorter tapered region, smoother tip surface, and smaller radius of tip apex curvature than mechanically pulled probes.

One etching approach involves full immersion of a mechanically cleaved fiber end into a hydrofluoric acid solution. This method usually produces a sharp tip and a long tapered section (*e.g.* 10 mm long for a silica fiber of 125 μm in diameter). However, such a probe can be mechanically fragile. See, for example, Radojewski *et al.*, International Journal of Electronics, Vol. 76(5), pp. 973-980 (1994).

An alternative etching approach uses a layer of protection liquid on top of the etchant liquid to automatically terminate the etching process. See, for example, U.S. Patent No.4,469,554 to Turner, and Hoffmann *et al.*, "Comparison of mechanically drawn and protection layer chemically etched optic fiber tips", Ultramicroscopy 61, pp. 165-170 (1995). According to this method, a portion of a fiber is immersed in the etchant liquid. The tip formation takes place at the interface of the etching liquid and

the protection liquid layer. The etching process is self-terminated as the fiber portion immersed in the etching liquid is etched away to form a tip within the protection layer and the etching liquid breaks away from the fiber tip.

Many NSOM instruments operate in the optical spectral range from about 375 nm to about 850 nm. Fiber probes are usually made of quartz glass (SiO_2) fibers. A near-field scanning infrared microscope ("NSIM"), operating in the infrared region from submicron to about 10 μm, is an advantageous extrapolation of the NSOM technique for several reasons. For example, not all molecules have absorption bands in the visible region but almost every molecule has absorption bands in the IR region.

Therefore, NSIM instruments can be used to detect more molecular species than NSOM. Also, IR absorption bands provide direct information about the presence and nature of chemical bonds in the observed spectral region. Hence, NSIM can be a useful tool in many applications.

One suitable set of compounds for IR-transmitting fibers is the chalcogenides. Chalcogenide fibers have good chemical stability and are less brittle than the other families of compounds for IR fibers

Like optical fibers, they are also glasses and can be heat-pulled with a capillary puller in a fashion similar to pulling regular optical fibers. However, heat-pulling of chalcogenide fibers is much more difficult than heat-pulling of glass fibers (*e.g.*, SiO_2). Moreover, the throughput of heat-pulled fibers is low. For example, Hong *et al.* report low light throughput in a range of

about 10^{-4} to about 10^{-6} in heat-pulled IR fibers (Proceedings of SPIE 2863, pp. 54, 1996). This probably is in part due to a long tapered section of several mm as shown in a micrograph of FIG. 2 which was produced by using a scanning electron microscope.

SUMMARY OF THE INVENTION

The present disclosure describes a two-phase chemical etching process and system for shaping optical fibers. One embodiment of the two-phase etching system comprises a lower-phase aqueous oxidizing etchant and an upper-phase protective solvent overlayer. The oxidizing etchant is chemically reactive while the protective solvent is substantially inert. Preferably, the etchant and the protective solvent are substantially immiscible with respect to each other and the density of the protective solvent is less than that of the etchant. The etchant and the solvent are preferably chosen so that the meniscus of the etchant formed at the interface of the two liquid phases surrounding the submerged portion of a material to be etched is substantially flat. Convective flows within the aqueous etchant surrounding the immersed material are preferably maintained.

In operation, one end of a fiber is immersed in the etchant which is preferably unstirred. The immersed portion is etched to form an initial "neck" at a location within the etchant near the meniscus and eventually the portion below the neck falls off, thus forming a tip within the etchant.

For etching chalcogenide glass fibers operating in the IR range, a mixture of oxidizing acid and hydrogen peroxide may be used as the etchant solution. According to one embodiment, piranha solution, *i.e.*, an approximately 7:3 mixture by volume of concentrated sulfuric acid and hydrogen peroxide of 30% water solution, may be used with various organic compounds as

the protective solvent. Suitable protective solvents include but are not limited to, tetramethylpentadecane (TMPD), polydimethylsiloxane (PDMS) and CCl_4.

Chalcogenide IR fibers can be processed using two-phase etching to from a sub-micron tip apex. First, the polymer coating of a fiber is removed. Next, the fiber cladding is stripped. Finally, the chalcogenide fiber core is etched to a sharp point by using a two-phase etching system. The resulting fibers have a taper length on the order of the core diameter and terminate with a sub-micron radius of tip curvature.

One advantage of the two-phase etching is the short tapered section and smooth and small tip apex of the etched fibers. Another advantage is that the geometry and quality of the etched probes are consistent and controllable.

These and other features and advantages will become more apparent in light of the following detailed description, including the accompanying drawings and the appended claims.

BRIEF DESCRIPTION OF THE DRAWINGS

FIG. 1 is a diagram showing the structure of a typical optical fiber probe.

FIG. 2 is a micrograph of a heat-pulled chalcogenide fiber produced by a scanning electron microscope (scale bar = 1 mm).

FIG. 3 is a schematic diagram of a two-phase etching system in accordance with the invention.

FIGs. 4A, 4B, and 4C are schematic diagrams showing the two-phase etching mechanism under convective control.

FIG. 5 is an optical micrograph of a fiber with a core diameter of 145 μm which was removed from the etching solution before the falloff point (scale bar = 150 μm).

FIG. 6 is a SEM micrograph of a 145 μm diameter core chalcogenide fiber etched by the two-phase etching process of the invention (scale bar = 100 μm).

FIG. 7 is a SEM micrograph showing a further magnified image (scale bar = 1 μm) of the apex of the tip shown in FIG. 6.

FIG. 8 is a SEM micrograph of a clad 250 μm diameter core chalcogenide fiber etched by the two-phase etching process of the invention (scale bar = 500 μm).

FIG. 9 is a magnified SEM image of the tip shown in FIG. 8 (scale bar = 250 μm).

FIG. 10 is a further magnified SEM image of the tip shown in FIG. 8 (scale bar = 1 μm)

FIGs. 11A, 11B, 11C, and 11D are schematic diagrams illustrating the two-phase etching mechanism under conditions of isotropic etching, in which the dotted lines qualitatively indicate rates of etching, or the new profile of the tip after a discrete time-interval.

FIG. 12 is an optical micrograph of a 145 μm core chalcogenide fiber etched at a reduced temperature of about 5°C (scale bar = 150 μm).

FIG. 13 is an optical micrograph of a 145 μm core chalcogenide fiber etched in stirred piranha solution at the room temperature (scale bar = 150 μm).

FIGs. 14A, 14B, and 14C show optical micrographs of asymmetrical and corrugated tips that are etched without protective solvent overlayers (scale bar = 150 μm).

DESCRIPTION OF THE INVENTION

The present disclosure involves a two-phase etching system to etch an optical fiber to form a fiber probe with a small tip apex, short tapered section and a large cone angle. It should be understood that etching optical fibers is described as an example and should not be construed as a limitation of the invention.

FIG. 3 shows a two-phase etching system 300 according to one embodiment of the invention. A container 310 has a lower phase 320 which is an aqueous etchant and an upper phase 330 which is an overlayer of a protective solvent. An end of an optical fiber 340 held by a fiber holder 350 is immersed in the liquids 320 and 330. The etchant 320 is chemically reactive to the fiber 340 while the protective solvent 330 is substantially inert to the fiber 340. The etchant 320 and the protective solvent 330 are substantially immiscible with respect to each other and form an interface on the top surface 360 of the etchant 320. In addition, the density of the protective solvent 330 is less than that of the etchant 320 so that the protective solvent 330 remains on top of the etchant 320 in the container 310.

The physical properties of the etchant 320 and the protective solvent 330, such as density, viscosity, and surface tension, can be chosen relative to each other so that the meniscus formed on the top surface 360 of the etchant 320 surrounding the optical fiber 340 is substantially flat. When the meniscus is flat, the interfacial energy of the interface between the material 340 and the etchant 320 due to the surface tension is approximately equal to the interfacial energy of the interface between the material 340 and the protective solvent 330.

The dimension of the container 310 is sufficiently larger than the cross-section of the fiber 340 so that a convective flow within the aqueous etchant 320 near

the submerged portion of the fiber 340a can be maintained. For typical fibers of several hundred microns in diameter, the thickness of the convective flow layer may be on the order of millimeters. Furthermore, the volume of the container 310 is sufficiently large to hold enough fresh etchant 320 to completely dissolve the inserted portion 340a of the fiber 340.

In operation, one end of the fiber 340 is immersed in the etchant 320. FIG. 4A shows the system at the beginning of etching. Preferably, the etchant 320 should not be stirred. The immersed portion 340a is etched to form a "neck" 410 at a location within the etchant 320 near the meniscus (FIG. 4B). As etching continues, the neck 410 is etched away faster than the rest of the submerged portion 340a which eventually falls off. This is illustrated in FIG. 4C. A tapered tip 420 is thus formed on the fiber 340. The fiber 340 is then withdrawn from the etchant and washed. Finally, the etched tip may be dried by gently blowing a gas (e.g., air or nitrogen) along the cylindrical axis towards the tip.

Chalcogenide glass fibers may be etched with the two-phase etching system 300 by using a mixture of oxidizing acid and hydrogen peroxide as the etchant solution. For example, a piranha solution with a 7:3 mixture by volume of concentrated sulfuric acid (e.g., H_2SO_4) and hydrogen peroxide of 30% water solution may be used. Various organic compounds may serve as the protective solvent, including but not limited to, tetramethylpentadecane (TMPD), polydimethylsiloxane (PDMS) and CCl_4. Preferably, TMPD may be used in combination with piranha solution to achieve an improved long-term stability of the etchant system.

One aspect of the invention is etching an IR-transmitting optical fiber probe and in particular etching chalcogenide fibers. Chalcogenide fiber probes etched the two-phase system 300 usually taper to a sharp point with a radius of curvature of less than about 150 nm at the tip apex over a length of approximately one fiber diameter along the fiber axis. Examples of etching chalcogenide fiber probes and methods of removing polyamide plastic coatings and SSe cladding on the fibers are described below. Testing results suggest that an approximate 100-fold increase in light throughput over conventionally pulled-fiber probes has been achieved. This is consistent with the reduction in the length of the tapered section by the two-phase etching system of the invention.

In the following examples, chalcogenide fibers manufactured by Amorphous Materials, Inc.(3130 Benton, Garland, TX 75042) were used. Both thin (unclad, but plastic coated) and thick (clad and plastic coated) fibers were used in etching fiber probes. The chalcogenide core is made of an As-Se-Te glass. The cladding is primarily SSe. Both types of fiber are Plate # 94-131-8, Run # 71395.

Thin fibers have a core diameter of about 0.0058 inch (about 145 μm) and a polyamide coating 0.0009 inch (about 22.5 μm) thick (for a total fiber diameter of .0076 inch (about 190 μm)).

Thick fibers have a core diameter of .010 inch (about 250 μm), S-Se cladding 0.004 inch (about 100 μm) thick, and a polyamide coating 0.003 inch (about 75 μm) thick for a total fiber diameter of 0.024 inch (about 600 μm).

An optical microscope with an epi-fluorescence/reflectance microscopy attachment was used to inspect the fibers. The polyamide coating is slightly fluorescent under illumination of blue or green light, making it easy to determine the presence

of the polyamide coating. Microscopy of the probes under both backlighting and reflected light is used to determine the shape of the fiber.

The probe tip can be inspected by using a scanning electron microscope. Since chalcogenides are semiconductors, sputtering the tips with gold is therefore not strictly necessary, although gold or other metallic coatings may be used to improve image clarity at very high magnifications.

REMOVAL OF POLYAMIDE COATING

The polyamide coating can be removed by repeatedly immersing the coated fiber in stirred solvent for several minutes (*e.g.*, 1-2 minutes) at room-temperature and wiping with a laboratory tissue or the like. A number of solvents may be used for this purpose, including but not limited to, 4-chloro-1-butanol, methanol, and acetone. The surface of properly stripped fibers appears smooth when wiped with a laboratory tissue or the like. If not all the polymer has been removed, higher friction can be noticed.

REMOVAL OF CLADDING

If a fiber is clad, the fiber cladding should be removed before etching. One commonly used cladding is SSe. The cladding can be removed by first soaking the polyamide-stripped fiber in a NaOH solution with a concentration of 0.1 M at the room temperature for approximately 18 hours

Higher concentrations may be used to reduce the soaking time. At the end of this time, the portion of the fiber immersed in the NaOH solution generally has lost its reflective sheen. The treated portion of the cladding then can be removed from the core by, for example, wiping gently with a laboratory tissue or the like.

If the fiber is removed from the NaOH solution too soon before the fiber loses its reflective sheen, the cladding may be difficult to remove or could not be completely removed by wiping. In this case, the fiber may be safely put back in the NaOH solution. If the fiber is left too long in the NaOH solution (*e.g.*, longer than 24 hours in the 0.1M NaOH solution), the NaOH may slowly start etching the chalcogenide core.

ETCHING OF CHALCOGENIDE CORE

Once the core has been exposed, etching can be performed by using the two-phase etching system 300 of FIG. 3. A protection layer of tetramethylpentadecane (TMPD) and an etchant of piranha solution are used. The protective solvent overlayer was about 1 to 2 mm thick. The protective solvent serves to keep the meniscus substantially flat at the fiber-etchant interface.

The chalcogenide fiber is immersed in the etching system. At room temperature and without stirring, the fiber usually forms a "neck" at a location approximately one fiber diameter down from the solvent-piranha meniscus. FIG. 5 shows a pronounced neck 510 formed on a fiber core 500 before the neck is etched through. Ultimately, the neck 510 will be completely etched through, and the lower piece 520 will fall off. This is referred to as the "falloff" point.

The etching time for reaching "falloff" depends on the age of the piranha solution, its temperature, and the thickness of the chalcogenide core 500. As a guideline, with freshly made piranha at room temperature, and a 145 μm core, etching takes about 15 minutes. With 2-month old piranha (stored at about 5°C) and a 250 μm core, etching takes approximately 50 minutes at the room temperature.

> Approximately 30 seconds after the "falloff", the fiber is withdrawn from the etchant and washed in gently stirred methanol at the room temperature. Next, the

tip is gently blown dry with N_2 blowing along the fiber axis towards the tip, rather than from the side.

FIGs. 6 and 7 respectively show micrographs of an etched unclad 145 μm fiber by using a scanning electron microscope (SEM). The corrugations and the structure on the underside of the tip are believed to be due to the thin layer of gold applied for SEM imaging. FIGs. 8, 9, and 10 are SEM micrographs of different scales showing an etched, clad fiber with a 250 μm core. In FIG. 8, removal of the clad and etching of the core are visible and the "blob" at the top is silver paint applied to provide a conductive path to ground for SEM imaging.
The above processing method resulted in sharp tips with a taper length on the order of the core diameter and a radius of curvature of the tip apex generally less than about 150 nm. In general, the tips are concave-conical in shape and have a smooth tip apex.

CHALCOGENIDE CORE ETCHING MECHANISM

It is a belief of the inventors that the unique tip formation produced by the two-phase etching is in part caused by a convective flow in the etchant. The etching mechanism may be explained with the following hypothetical convection flow model.

ferring to FIGs. 4A-4C, as the etching agent dissolves the mersed portion 340a of the fiber core 340, the solution nsity of the etchant increases in the proximity of the ber surface. Thus, the etching solution near the fiber rface is more dense than the rest of the solution and ows down along the fiber due to gravity. This forms a nvective flow 430 which is substantially laminar under ese conditions. As the dense solution flows down along e fiber 340a, more etchant solution will move in to take s place. Since there is a fluid layer moving parallel to

the surface of the fiber 340a everywhere except the location close to the meniscus where the fiber 340 enters the etchant 320, new etchant solution enters the convection pattern primarily at the meniscus, as illustrated in FIGs. 4A-4C.

Therefore, the etchant solution contacting the fiber 340 at the meniscus contains a higher concentration of H_2O_2 and acid and less dissolved chalcogenide. As a result, the fiber section at or near the meniscus is etched faster than other fiber section immersed in the etchant 320 to produce the observed "necking" effect. Eventually the "neck" is completely dissolved away, and the fiber below the neck falls off.

According to the above convective control hypothesis, if the effects of convection are reduced relative to diffusion and reaction, more isotropic etching would be expected. FIGs. 11A, 11B, 11C and 11D illustrate such isotropic etching wherein no necking effect occurs. Three different experiments were performed to test this prediction. In the first experiment, etching was performed in the normal two-phase etching apparatus as shown in FIG. 3, but at a temperature below the room temperature. Reduction in temperature increases the viscosity of the piranha solution and decreases the flow speed of the convective flow. FIG. 12 is an optical micrograph of a 145 μm chalcogenide fiber etched at 5°C which is below the room temperature of about 25°C. No necking effect was present at 5°C while a pronounced neck is formed when the temperature is at the room temperature as shown by FIG. 6.

In a second experiment, etching was performed in the normal two-phase etching apparatus of FIG. 3 at the room temperature, but with fairly rapid stirring of the piranha solution. Stirring essentially equalizes the concentration of etchant and the dissolved chalcogenide throughout the piranha solution. Thus stirring substantially eliminates the convective flow. The

etched profile of a fiber core is shown in FIG. 14 by an optical micrograph of a 145 μm chalcogenide fiber. Again, no necking effect is observed in contrast to the etched profile of FIG. 6 in which the etchant is unstirred.

In the third experiment, a glass capillary with an inner diameter of about 1.5 mm was used instead of a glass vial of an inner diameter of about 2.5 cm. Since the fiber itself took up a substantial portion of the interior space in the capillary, convection was seriously impeded. A long, high aspect-ratio fiber tip without evidence of "necking" was produced.

The above three experiments demonstrate that convection contributes to the desirable necking effect for achieving a short taper section with a wide cone angle. When the convection is impeded, the etching profile becomes more isotropic and may cause diminishing of the necking effect so that it is more difficult to judge "completion" under such circumstance, since there is no "falloff" event.

The protective solvent overlayer serves to make tip shape more smooth and reproducible. Fibers etched without solvent overlayers are typically asymmetric and lack the smooth concave conical shape of fibers etched with solvent overlayers. FIGs. 14A, 14B and 14C show optical micrographs of several fiber tips etched without protective solvent overlayers. Further experimentation by the inventors indicated that the meniscus of piranha solution at an inserted fiber curves up if a solvent overlayer is not used, whereas with a properly-selected solvent overlayer the meniscus of the piranha solution at the fiber is essentially flat. This meniscus curvature is believed to disrupt the convection pattern responsible for producing smooth, concave-conical tips.

In addition, it is contemplated that the etched neck should point straight down from the meniscus. To test this prediction, etching was performed in the normal apparatus, but with the glass vial tilted at about 60° with respect to the vertical direction. As predicted, the tip thus produced pointed off-axis by approximately 60°. The tip was, however, asymmetric and not very sharp.
The two-phase etching process and system in accordance with the invention can be used to produce optical fiber probes with sharp and smooth tips and short transitional tapered section. Such etched probes can be used to resolve smaller feature size and to achieve a throughput several orders of magnitude higher than conventional IR fiber probes including the mechanically pulled counterparts. Thus the fiber probes produced in accordance with the invention may improve various near-field sensing systems and open up new applications.

For example, the use of pulled IR fiber probes in conventional NSIM systems has required intense sources of IR light such as expensive and bulky Free Electron Laser (FEL) due to the low throughput of conventional IR fiber probes. Therefore, IR fiber probes etched in accordance with the present invention may enable an NSIM system to use other less powerful IR sources to substitute the FELs. An optical parametric oscillator (OPO) laser, for example, may be used as the IR light source in a NSIM system. OPO lasers are far more common and much less costly (e.g., about 250K dollars) than FELs (e.g., about one million dollars plus shielded facility cost). This would make NSIM a much more accessible technique.

Etched IR fiber probes according to the invention may be used for high-spatial-resolution temperature measurements, such as those required in semiconductor device diagnostics. The present invention may also be used to make tapered IR-transparent fibers for attenuated total reflectance (ATR) "cells" in FTIR

spectroscopy, see, Ertan-lamontagne *et al.*, Applied Spectroscopy, Vol. 49(8), pp. 1170 (1995).

Although the present invention has been described in detail with reference to a preferred embodiment and a few examples, one ordinarily skilled in the art to which this invention pertains will appreciate that various modifications and enhancements may be possible without departing from the spirits and scope that are encompassed by the following claims.

What is claimed is:

1. A method of etching a fiber, comprising:
providing an etchant solution which is chemically reactive to the fiber and has a first interfacial energy with respect to the fiber;
forming a layer of a protective solvent that is chemically inert to the fiber on top of said etchant solution, said protective solvent having a density smaller than said etchant solution and having a second interfacial energy with respect to the fiber, wherein said first interfacial energy is substantially equal to said second interfacial energy;
immersing a portion of the fiber in said etchant solution and said protective solvent; and
maintaining convective flows surrounding said immersed portion within said etchant solution so that said immersed portion is broken away by etching to form a tapered tip within said etchant solution.

2. A method as in claim 1, wherein said etchant solution includes a mixture of an oxidizing acid and a hydrogen peroxide.

3. (Amended) A method as in claim 1, wherein said protective solvent is a solution having a chemical material selected from a group consisting of tetramethylpentadecane (TMPD), polydimethylsiloxane (PDMS), [or] and CCl_4[, which are operable to etch chalcogenide fibers].

4. A method as in claim 2, wherein said etchant solution is an approximately 7:3 mixture by volume of concentrated sulfuric acid and a hydrogen peroxide of 30% water solution.

5. (Amended) A method as in claim 1, [further comprising] wherein the immersing step comprises holding the fiber in said etchant solution and said protective solvent in a substantially vertical orientation [direction].

6. A method of etching a fiber, comprising:
providing an etchant solution which is chemically reactive to the fiber;
forming a layer of a protective solvent that is chemically inert to the fiber on top of said etchant solution and having a density smaller than said etchant solution,
selecting said etchant solution and said protective solvent to have predetermined densities and viscosity coefficients to form a substantially flat meniscus on the interface between said etchant solution and protective solvent around the fiber when immersed;
immersing a portion of the fiber in said etchant solution and said protective solvent; and
maintaining convective flows surrounding said immersed portion within said etchant solution so that said immersed portion is broken away by etching to form a tapered tip within said etchant solution.

7. A method as in claim 6, wherein said etchant solution includes a mixture of an oxidizing acid and a hydrogen peroxide.

8. (Amended) A method as in claim 6, wherein said protective solvent is a solution having a chemical material selected from a group consisting of tetramethylpentadecane (TMPD), polydimethylsiloxane (PDMS), [or] and CCl_4[, which are operable to etch chalcogenide fibers].

9. A method as in claim 7, wherein said etchant solution is an approximately 7:3 mixture by volume of concentrated sulfuric acid and a hydrogen peroxide of 30% water solution.

. (Amended) A method as in claim 6, [further comprising] erein the immersing step comprises holding the fiber in

said etchant solution and said protective solvent in a substantially vertical orientation [direction].

11. A method of forming a chalcogenide fiber probe by chemical etching, comprising:
processing a fiber having a chalcogenide fiber core to expose the fiber core at one end;
providing an etchant solution which is chemically reactive to said fiber core and has a first interfacial energy with respect to said fiber core;
forming a layer of a protective solvent chemically inert to said fiber core on top of said etchant solution, said protective solvent having a density smaller than said etchant solution and a second interfacial energy with respect to said fiber core, wherein said first interfacial energy is substantially equal to said second interfacial energy;
immersing said fiber core in said etchant solution and said protective solvent; and
maintaining convective flows surrounding said immersed fiber core within said etchant solution so that a portion of said fiber core is broken away by etching at a location below interface between said protective solvent and etchant to form a tapered probe tip within said etchant solution.

12. A method as in claim 11, wherein the step of processing the fiber to expose the fiber core comprises removing polymer coating and fiber cladding outside the fiber core.

13. A method as in claim 12, wherein said polymer coating is removed by immersing the fiber in 4-chloro-1-butanol, methanol, or acetone.

14. A method as in claim 12, wherein said fiber cladding is SSe which is removed by immersing the clad fiber in a NaOH solution after said polymer coating is removed.

15. A method as in claim 11, wherein said etchant solution includes a mixture of an oxidizing acid and a hydrogen peroxide.

16. (Amended) A method as in claim 11, wherein said protective solvent is a solution having a chemical material selected from a group consisting of tetramethylpentadecane (TMPD), polydimethylsiloxane (PDMS), [or] and CCl_4[, which are operable to etch chalcogenide fibers].

17. A method as in claim 15, wherein said etchant solution is an approximately 7:3 mixture by volume of concentrated sulfuric acid and a hydrogen peroxide of 30% water solution.

18. (Amended) A method as in claim 11, [further comprising] wherein the immersing step comprises holding the fiber in said etchant solution and said protective solvent in a substantially vertical orientation [direction].

19. A method as in claim 11, further comprising:
removing the fiber from said etchant solution and said protective solvent after an immersed portion of said fiber core falls off from the fiber; and
washing the fiber with a cleansing solution to remove residual of the etchant solution from the fiber.

20. A fiber etching device, comprising:
a container;
an etchant solution filled in a bottom portion of said container and chemically reactive to an optical fiber material; and
a protective solvent chemically inert to the fiber material and having a density smaller than said etchant solution, said protective solvent formed a protective layer on top of said etchant solution,

wherein said etchant solution and said protective solvent have predetermined densities and viscosity coefficients to form a substantially flat meniscus on the interface between said etchant solution and protective solvent around the fiber material which has a portion immersed in said etchant solution and said protective solvent, and said container is configured to maintain convective flows surrounding the immersed portion within said etchant solution.

21. A device as in claim 20, wherein said etchant solution includes a mixture of an oxidizing acid and a hydrogen peroxide.

22. A device as in claim 20, wherein said protective solvent is a solution having tetramethylpentadecane (TMPD), polydimethylsiloxane (PDMS), or CCl_4, which are operable to etch chalcogenide fibers.

23. (New) A method as in claim 1, wherein the fiber comprises a chalcogenide glass.

24. (New) A method as in claim 6, wherein the fiber comprises a chalcogenide glass.

ABSTRACT

A two-phase etching system having an etchant solution and an overlayer of a protective solvent. The physical properties of the etchant solution and the protective solvent are matched to form a substantially flat meniscus on the top surface of the etchant solution around a fiber immersed in the protective solvent and the etchant solution. Convective flows within the etchant solution are maintained in order to form a smooth and sharp fiber probe with a small tip apex.

3708.LJ1

Appendix E

Marc's Rules of Research

Major Rules – 1/11/99

1. **Don't do an experiment hastily unless you don't mind doing it over.**
2. **If you really knew what you were doing, it wouldn't be research.**
3. **First step in trying to solve a problem: If you don't have a clue, call someone who does.**
4. **If it's taking too long, you're doing it wrong.**
5. **Don't bother doing experiments carefully until you have an assay that works to evaluate the results.**
6. **Measuring noise takes n^2 time.**
7. **The time required to draw conclusions is n^2 in the number of different experiments.**

There are several criteria for being included on this list.

First, a rule must have a "kernel of wit" – a non-obvious interpretation, a play on a more normal boring suggestion, or an interesting association from another field – so that I can *remember* it. Rules aren't any good if you can't remember them.

Second, they have to have proven reproducibility – that is, I have to run across a circumstance where the rule is applicable multiple times.

Third, I have to have experienced negative consequences at least once because I broke the rule. (Some of these are multiple winners on that score!)